STUDY OF HINDERED INTERNAL ROTATION IN SOME SUBSTITUTED AMIDES BY NUCLEAR MAGNETIC RESONANCE SPECTROSCOPY

Thesis for the Degree of Ph. D.
MICHIGAN STATE UNIVERSITY

James Calvin Woodbrey

1960

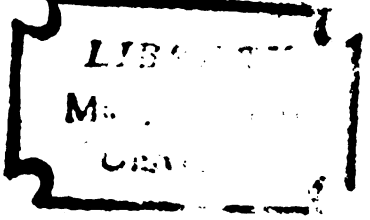

MICHIGAN STATE UNIVERSITY
OF AGRICULTURE AND APPLIED SCIENCE
DEPARTMENT OF CHEMISTRY
EAST LANSING, MICHIGAN

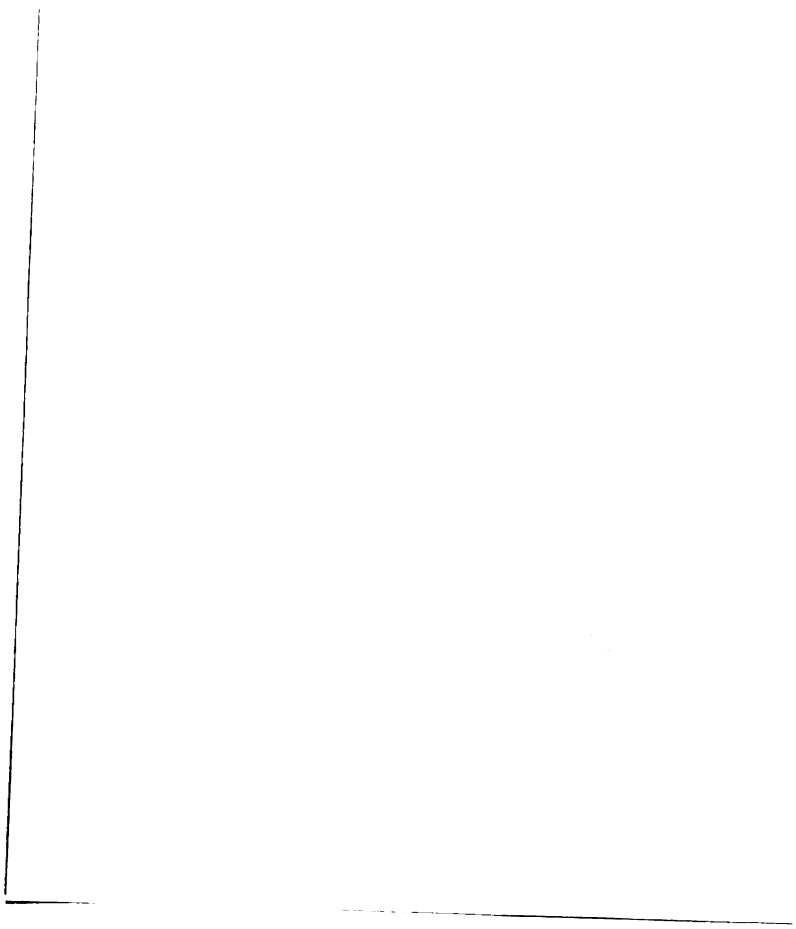

STUDY OF HINDERED INTERNAL ROTATION IN SOME SUBSTITUTED AMIDES BY NUCLEAR MAGNETIC RESONANCE SPECTROSCOPY

By

James Calvin Woodbrey

A THESIS

Submitted to the School for Advanced Graduate Studies
of Michigan State University in partial
fulfillment of the requirements
for the degree of

DOCTOR OF PHILOSOPHY

Department of Chemistry

1960

In Memoriam

MARJORIE MABELLE HEWES

ACKNOWLEDGMENTS

It is with sincere appreciation that I acknowledge the counsel of Professor M. T. Rogers under whose direction this investigation was conducted.

I also wish to express my gratitude to Doctor P. T. Narasimham for many informative discussions during the early phases of this research; to Mr. Forrest Hood for fabricating the glassware; to the Union Carbide Corporation for a fellowship, and to the National Science Foundation for grants subsidizing part of this research.

To Connie, my wife, who patiently gave encouragement and self sacrifice in order that I might complete this phase of my education, I offer my everlasting appreciation.

****

VITA

James Clavin Woodbrey
candidate for the degree of
Doctor of Philosophy

Dissertation: Study of Hindered Internal Rotation in Some Substituted Amides by Nuclear Magnetic Resonance Spectroscopy

Outline of Studies

Major: Physical Chemistry
Minor: Physics and Organic Chemistry

Biographical:

Born, October 16, 1934, Sebago Lake, Maine
Undergraduate Studies: B. S., Chemistry, The University of Maine, Orono, Maine, 1956.

Professional Affiliations: American Chemical Society
The Society of Sigma Xi
Tau Beta Pi
Sigma Pi Sigma

STUDY OF HINDERED INTERNAL ROTATION IN SOME SUBSTITUTED AMIDES BY NUCLEAR MAGNETIC RESONANCE SPECTROSCOPY

By

James Calvin Woodbrey

AN ABSTRACT

Submitted to the School for Advanced Graduate Studies
of Michigan State University in partial
fulfillment of the requirements
for the degree of

DOCTOR OF PHILOSOPHY

Department of Chemistry

1960

Approved _____

ABSTRACT

A Varian high-resolution nuclear magnetic resonance spectrometer was used for observing proton and fluorine magnetic resonance spectra of several symmetrically N, N-disubstituted amides over a wide range of temperatures. Apparatus for controlling sample temperatures at high or low values was constructed. Also, coils for electrically shimming the applied magnetic field were constructed. The use of these coils was essential to the observation of high-resolution fluorine magnetic resonance spectra at the applied radio-frequency 60.000 mcs.

Theoretical methods for relating the rate of internal rotation about the central C-N bond of the substituted amides to various components of resonance line shapes were considered. Three of these methods were applied experimentally to the study of the phenomenon of hindered internal rotation. Of the three methods used, only one was well adapted to the study of hindered internal rotation about the central C-N bond of the symmetrically N, N-disubstituted amides used in this work. This method relates the ratio of maximum to central minimum absorption intensities of a symmetrical resonance doublet to the rate of internal rotation. The energy barrier and frequency factor, for each internal rotation studied, were calculated from the experimental temperature dependence of the rate of internal rotation. The experimental errors were much lower than those previously reported for similar studies.

The phenomenon of hindered internal rotation about the central C-N bond of the following pure liquid amides was studied: N, N-dimethylformamide; N, N-dimethylacetamide; N, N-dimethylpropionamide;

N, N-dimethyltrichloroacetamide; N, N-dimethyltrifluoroacetamide; N, N-dimethylacrylamide; and N, N-dimethylcarbamyl chloride. The internal rotation about the C-N bond of N, N-dimethylbenzamide was studied for a solution of the amide in dibromomethane. Similar studies were made for a solution of N, N-dibenzylacetamide in dibromomethane, and for a solution of this amide in carbon tetrachloride.

The apparent rates of internal rotation about the central C-N bond of ethyl-N, N-dimethylcarbamate, and about the central C-N bond of methyl-N, N-bis-(trifluoromethyl)-carbamate, were too fast to be detected, even at quite low temperatures. In addition, the presence of hindered internal rotation about the central C-N bond of N, N-bis-(trifluoromethyl)-trifluoroacetamide could not be detected.

The origin of the barrier to internal rotation about the C-N bond of the amide group is attributed to the existence of partial C=N bond character, which arises from resonance between valence bond structures. Some possible explanations for the exceptionally high barrier observed for N, N-dimethylformamide are the following: a small amount of intermolecular association of the pure liquid, the nonexistence of contributing resonance structures that would suppress the partial double bond character of the central C-N bond, and the possibility of the barriers for all the other amides being suppressed by transition states which involve excited electronic states. The low-barrier compounds were compared with N, N-dimethylacetamide. The values of the energy barriers for these compounds were explained in terms of contributing resonance structures which suppress the double bond character of the central C-N bond.

For most of the internal rotations studied, the experimental frequency factors were from about 10^5 to 10^7 $sec.^{-1}$ These low values were attributed to low transmission coefficients.

The phenomenon of hindered internal rotation about the central C-N bond of N, N-dimethylpropionamide was studied for several solutions of the amide in dibromomethane and in carbon tetrachloride. The concentration dependence of the barrier to internal rotation for the amide in dibromomethane solutions suggests the possible existence of a specific solvent-solute interaction. When the amide was diluted with carbon tetrachloride, the barrier was observed to decrease markedly. This decrease is attributed to the dissociation of the slightly associated pure liquid amide upon dilution. Similar effects were observed for solutions of N, N-dimethylcarbamyl chloride in dibromomethane and in carbon tetrachloride.

The apparent very rapid internal rotations about the central C-N bond of ethyl-N, N-dimethylcarbamate, and about the central C-N bond of methyl-N, N-bis-(trifluoromethyl)-carbamate, are attributed to a low energy barrier for the internal rotations. These compounds have important resonance structures which tend to suppress the double bond character of the central C-N bond.

TABLE OF CONTENTS

TABLE OF CONTENTS - Continued

LIST OF TABLES

LIST OF TABLES - Continued

LIST OF TABLES - Continued

LIST OF FIGURES

LIST OF FIGURES - Continued

FIGURE Page

LIST OF FIGURES - Continued

FIGURE Page

LIST OF FIGURES - Continued

LIST OF FIGURES - Continued

INTRODUCTION

The investigation of hindered internal molecular rotations has been a subject of interest for about thirty years. Among the numerous physical methods adaptable to the study of this phenomenon are infrared, Raman, microwave, and nuclear magnetic resonance (NMR)* spectroscopy and electron diffraction, dipole moment, and thermodynamic measurements (1, 2, 3).

When internal molecular rotations are the cause of cis-trans or other types of conformational isomerism, frequently one may use NMR to determine the molecular ratios of isomers. The thermodynamic energies of isomerization may then be calculated from the temperature dependence of such ratios. In some cases, NMR may be used to measure the temperature dependence of the rates of internal molecular rotations. Then the energy barriers (more precisely, the experimental activation energies) and the frequency factors for the hindered internal rotations may be calculated with the use of the classical Arrhenius-type rate equation (4).

One of the earlier adaptations of high-resolution NMR spectroscopy to the study of hindered internal molecular rotations was made by Gutowsky and Holm (5, 6). These authors developed a high-resolution proton magnetic resonance (PMR) technique for determining the energy barriers and frequency factors for hindered internal rotation about the central C-N bond in the two compounds N, N-dimethylformamide and N, N-dimethylacetamide. Their values for the energy barriers in these two compounds were reported to contain errors as large as 43 per cent. Also, the relative magnitudes of their values for the energy barriers in these two compounds appeared to be in error. Since this fairly

---

*To conserve space, this and other similarly designated abbreviations will be used throughout the remainder of the thesis.

early investigation, NMR instrumentation and techniques have been improved tremendously.

Therefore, the research reported in this thesis consists of the following: (1) re-examination and comparison of some of the high-resolution NMR theory and techniques for obtaining energy barriers and frequency factors for hindered internal molecular rotations; (2) re-examination of the phenomenon of hindered internal rotation about the central C-N bond in each of the two pure liquids N, N-dimethylformamide and N, N-dimethylacetamide; (3) extension of the study of this phenomenon to a series of several other symmetrically N, N-disubstituted amides; and (4) extension of the study of the phenomenon to two of the amides dissolved in the solvents carbon tetrachloride and dibromomethane.

The historical and theoretical backgrounds for the problem just outlined are given in the following two sections. The remaining sections consist of a description of the experimental methods, a statement of the results, a discussion of the results, and a summary.

HISTORICAL REVIEW

Pauling postulated that the C-N bond of amides should possess considerable double bond character arising from resonance between the structures A and B shown in Figure 1 (7).

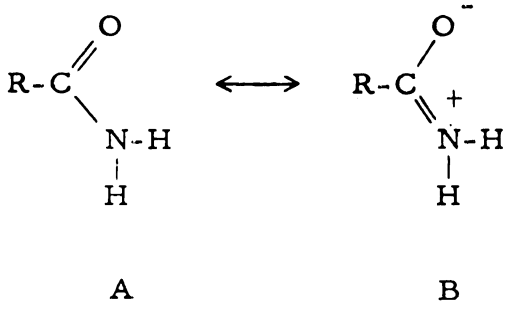

A B

Figure 1. Resonance formulae for amides.

He empirically estimated the resonance energy to be about 21 kcal./mole^{-1}, and the basicity constant for the amide group to be of the order of 10^{-20}. Such a high resonance energy suggests restricted (or partially restricted) rotation about the C-N bond, whereas the small basicity constant merely confirms the fact that most amides fail to form stable salts.

Because N-methylacetamide is the simplest peptide molecule, a great number of investigations have dealt with physical and chemical properties of this and similar molecules (references 8 through 15 and many others). Mizushima and collaborators have used dielectric measurements and Raman, infrared, and ultraviolet spectroscopy to interpret the structure N-methylacetamide (16). They estimated the resonance energy for this molecule to be about 16 kcal./mole. Their measurements provided evidence that nearly all the molecules exist in the trans configuration over the temperature range: ca. 25-95°C. Also, the data indicated that intermolecular hydrogen bonding causes

considerable chain-like association of the trans amide in carbon tetrachloride solution. Mizushima has also shown that hindered internal rotation about the C-N bond in amides is an important consideration in theories pertaining to the structure of protein molecules (17).

Cannon has made extensive infrared absorption measurements for a number of amides in carbon tetrachloride/chloroform and carbon tetrachloride/anhydrous hydrogen chloride solutions (18). When diluted with carbon tetrachloride, the N-H absorption band for N-ethylacetamide shifted to higher frequencies. This shift was attributed to depolymerization upon dilution. From the infrared spectra of N-ethylacetamide in the mixed solvents, it was concluded that this amide is much less associated in chloroform than in carbon tetrachloride solutions. When N, N-diethylacetamide and N, N-dimethylacetamide were diluted with various mixtures of carbon tetrachloride and chloroform, frequency shifts for the C=O absorption band were observed for both dilution and changes in solvent. These changes were attributed to changes in the dielectric constant of the solution; association due to hydrogen bonding being assumed negligible for these compounds. The infrared spectra of N-ethylacetamide in solutions of carbon tetrachloride plus anhydrous hydrogen chloride indicated that protonation of this amide occurs at the nitrogen atom: $CH_3CONH_2C_2H_5^+$. Finally, Cannon concluded that the C=O group of secondary amides readily forms hydrogen bonds with proton donating molecules, whereas the N-H group is inert (somewhat doubtful), neither donating nor accepting a proton for hydrogen bond formation.

The question as to whether amides preferentially protonate at the oxygen atom or at the nitrogen atom has been the subject of several investigations. From infrared absorption measurements of crystalline urea nitrate, Davies and Hopkins have concluded that urea preferentially protonates at the nitrogen atom: $H_2NCONH_3^+$ (19). Based upon similar

spectral measurements in the infrared and ultraviolet regions, Spinner has concluded that the salts of urea, thiourea, and acetamide are also preferentially protonated at the nitrogen atom: $H_2NCONH_3^+$, $H_2NCSNH_3^+$, and $CH_3CONH_3^+$ (20). However, Goldfarb, et al., have interpreted their ultraviolet spectral measurements on several amides in sulfuric acid solutions as evidence for preferential protonation at the oxygen atom: $HOCRNHR^+ \longleftrightarrow HOCRNHR^+$ (21).

Fraenkel and Niemann have observed the NMR spectra of several N-substituted amides in acidic solutions, from which they concluded that amides preferentially protonate at the oxygen atom (22). Berger, Loewenstein, and Meiboom have studied the protolysis kinetics of N-methylacetamide in aqueous solutions using a high-resolution PMR technique (23). They found the protolysis reaction to be both acid and base catalyzed, the reaction rate being proportional to the amide concentration and the hydrogen ion concentration. The data indicated that protonation at the oxygen atom is preferred, but that an equilibrium exists between N- and O- protonated ions. Also, they found that acidification of N, N-dimethylacetamide reduced the energy barrier to internal rotation about the central C-N bond to the extent that "free rotation" occurs (obviously, the authors mean free rotation on the NMR time scale--their spectrometer frequency was 31.65 mcs.). These workers attributed this reduction in the energy barrier to the minor N-protonation, thus leading to destruction of the partial $\bar{O}\text{-}C\text{=}\overset{+}{N}$ character. Takeda and Stejskal have confirmed the PMR studies of the protolysis kinetics of N, N-dimethylacetamide, and they have extended the work to the investigation of the similar protolysis kinetics of N, N-dimethylformamide (24). In these protolysis studies, the kinetic equation of major importance may be written as

$$RCONHCH_3 + (H_3O)^+ \underset{k_2A}{\overset{k_1A}{\rightleftharpoons}} (RCOHNHCH_3)^+ + H_2O, \qquad (1)$$

where the reported equilibrium values of k_{1A} are as follows: 380 ± 40 sec.$^{-1}$M^{-1} at 23 ± 2°C. (23) and 200 ± 70 sec.$^{-1}$M^{-1} at 25°C. (24) for N-methylacetamide and 10 ± 3 sec.$^{-1}$M^{-1} at 25°C. for N-methylformamide (24).

Spinner has recently made an unsuccessful attempt to explain the apparent contradiction between infrared spectral results which have been interpreted as evidence for preferential protonation of amides at the nitrogen atom (18, 19, 20), and NMR data that have shown that preferential protonation takes place at the oxygen atom (22, 23, 24). As Spinner pointed out, the internal rotation about the C-N bond in acetammonium type ions (e.g. $CH_3C\overset{+}{O}NH_3$) is not "free." Rather, such internal rotations are probably hindered by energy barriers of about one to three kcal./mole (i.e., energy barriers of about the same magnitudes as those inhibiting internal rotations of methyl groups). However, the frequencies of internal rotations (or torsional oscillations) with such small energy barriers are too great to be detected by existing NMR techniques. Spinner has suggested that the NMR doublet observed for the N-methyl group of N-methylacetamide in highly acidic solutions, $[(CH_3CONHCH_3)H]^+$, is due to chemical nonequivalence of the protons on the N-methyl group, resulting from hindered internal rotations about the C-N-C bonds. This suggestion is <u>not</u> correct. Chemical non-equivalence of the type suggested by Spinner would lead to an unsymmetrical 2:1 doublet. Such a doublet is not observed. Indeed, the observed symmetrical doublet has been shown to be the result of spin-spin coupling and not chemical shift differences (23).

Corey and collaborators have determined the structure of the amide group in a number of peptides and related substances (26). Their results, based on several X-ray structure determinations, are shown in Figure 2. In this structure, the value of the O=C-N bond angle is about the same as the tetrahedral value 125°16'. The central C-N bond

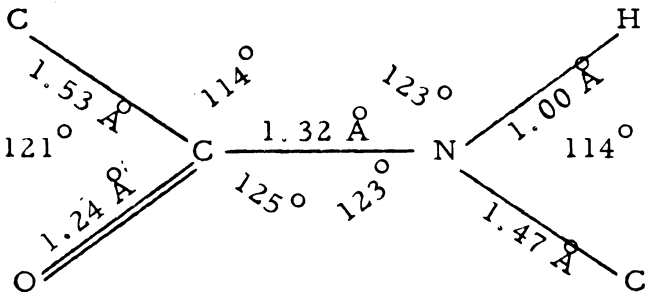

Figure 2. Structural formula for the amide group in peptides and related substances.

distance, 1.32 Å, is 0.13 Å shorter than the normal C-N bond distance. This is evidence for about 40 per cent contribution of the resonance structure analogous to B of Figure 1 (27).

Kurland and Wilson have reported the structure and dipole moment of formamide, as determined by microwave spectroscopy (28, 29). They found this molecule to be planar, thus proving that the resonance structure analogous to B of Figure 1 is a major contributor to the normal state of the molecule. The structure and dipole moment of formamide are diagramed in Figure 3. As expected, the C-N bond distance is appreciably shorter than the normal C-N bond distance. This confirms the

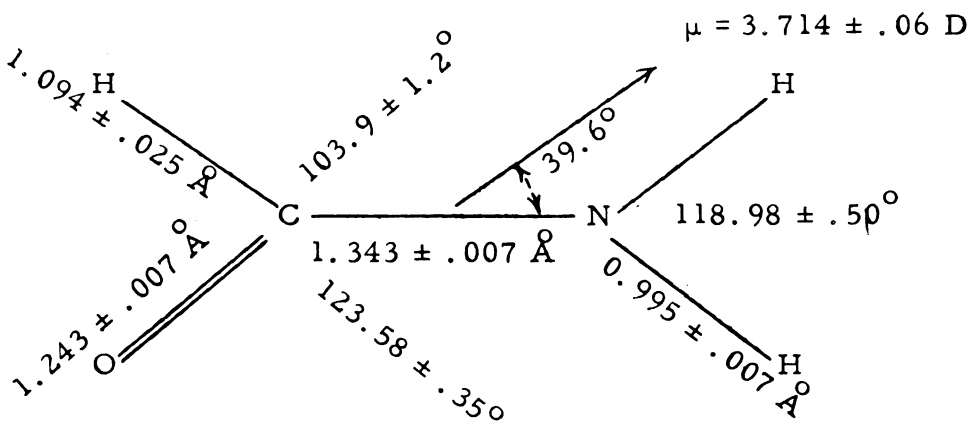

Figure 3. Structural formula and dipole moment for formamide.

existence of considerable $\bar{O}\text{-}C{=}\overset{+}{N}$ bond character. Pauling has suggested that in addition to the normally expected $\bar{O}\text{-}C{=}\overset{+}{N}$ contribution, the C-N bond in amides might have some contribution of multiple bonds involving the p orbitals normal to the plane of the group (30).

Electric moments and dielectric constants have been measured for numerous primary and N-substituted amides. These data are tabulated in Table I. From the electric moments of several halogen-substituted benzamides, Bates and Hobbs have shown that the amide group moment is oriented at an angle of about 70° to the C-C bond between the aromatic ring carbon atom and the carbon atom of the amide group (31).

Using high-resolution PMR at the spectrometer frequencies ν_0, 30 and 40 mcs., Phillips proved that the doublet PMR structure for N, N-dimethylformamide and N, N-dimethylacetamide was due to the chemical nonequivalence of the protons of the two N-methyl groups (39). This confirmed unequivocally the existence of highly hindered internal rotation about the central C-N bond in these amides. Also, he found evidence that the compounds N-methylformamide and N-methylacetamide exist in only one configuration.

The PMR studies by Phillips were confirmed later by Gutowsky and Holm (5, 6). Using PMR at the spectrometer frequency 17.735 mcs., they also observed that when N, N-dimethylformamide and N, N-dimethylacetamide were heated, the two N-methyl resonances coalesced to a single line. This coalescence was attributed to thermal enhancement of the internal rotation about the central C-N bond. They related the temperature dependence of the internal chemical shift between the two N-methyl resonance lines to the rate of the internal rotation. From the experimental temperature dependencies of these chemical shifts for N, N-dimethylformamide and N, N-dimethylacetamide, they were able to estimate the following: energy barriers E_a, frequency factors A, the temperatures at which the chemical shifts coalesced to zero

TABLE I

ELECTRIC MOMENTS AND DIELECTRIC CONSTANTS FOR SOME PRIMARY AND N-SUBSTITUTED AMIDES

Compound	μ, D, from benzene	Ref.	μ, D, from dioxane	Ref.	Dielectric Constant, ε					Ref.
					15°C.	20°C.	25°C.	30°C.	35°C.	
$HCONH_2$	3.37	(31)	3.22	(32)	113.4-0.4 (t - 15), t in °C.					(35)
			3.86	(31)						
			3.71*	(29)						
$HCONHCH_3$					200.1	190.5	182.4	174.3	167.1	(36)
$HCON(CH_3)_2$					38.42	37.65	36.71	35.87	35.05	(36)
CH_3CONH_2	3.44	(31)	3.6	(33)						
			3.90	(31)						
			3.92	(34, 37)						
$CH_3CONHCH_3$			4.39	(16)					169.7	(36)
$CH_3CONHC_2H_5$			3.87	(34)						
$CH_3CON(CH_3)_2$			3.79	(34)	40.9	38.93	37.78	36.81	35.83	(36)
$CH_3CON(C_2H_5)_2$	3.80	(34)	3.72	(34)			55.0			(18)
$C_2H_5CONH_2$	3.30	(31)	3.85	(31)						
$C_2H_5CONHCH_3$					188.1	179.8	172.2	164.3	156.7	(36)
n-$C_3H_7CONH_2$	3.48	(31)	3.86	(31)						
n-$C_3H_7CONHC_2H_5$	3.87	(38)								
$(CH_3)_2CHCONH_2$	3.46	(31)	3.88	(31)						
$C_6H_5CONH_2$	3.65	(31)	3.6	(33)						
			3.84	(31)						
m-$ClC_6H_4CONH_2$	3.64	(31)	3.67	(31)						
p-$ClC_6H_4CONH_2$	3.38	(31)	3.73	(31)						
m-$BrC_6H_4CONH_2$	3.40	(31)	3.66	(31)						
p-$BrC_6H_4CONH_2$	3.16	(31)	3.68	(31)						
$(CONH_2)_2$			9	(31)						
$CH_2(CONH_2)_2$			3.5	(31)						
$C_2H_5OCONHCH_3$					25.3	24.3	23.5	22.7	21.9	(36)

*Gas-phase microwave determination.

(the NMR coalescence temperatures) T_c, and the free energies of activation $\Delta F^{\dagger}$ for the hindered internal rotation about the central C-N bond. From the PMR spectrum of N, N-dimethylformamide at the spectrometer frequency 30 mcs., Phillips, et al., later estimated T_c and $\Delta F^{\dagger}$ for this compound (40). The reported values are tabulated in Table II.

By analogy with N, N-dimethylformamide, the protons bonded to nitrogen in formamide itself might be expected to be chemically non-equivalent. Due to the quadrupole broadening by N^{14}, the normal proton spectrum of formamide is of no help in providing such information. However, the nonequivalence of these protons is revealed by the proton spectrum observed when the nuclear resonance of N^{14} is saturated by the application of a strong radiofrequency field at the N^{14} resonance frequency (42).

Magnetic resonance spectra of nuclei other than hydrogen have given little information pertaining to the structures of amides. Lauterbur has observed the NMR spectrum (ν_0 = 8.5 mcs.) due to the one per cent natural abundance of C^{13} isotope in the compound N, N-dimethylformamide, $H^{A}C^{A}ON(C^{B}H_3^{B})_2$ (43). The chemical shifts, relative to $CH_3C^{13}O_2H$, are δ_A = 14 ± 1ppm and δ_B = 143 ± 1 ppm. The spin-spin coupling constants are $J_{H^AC^A}$ = 198 ± 5 cps and $J_{H^BC^B}$ = 139 ± 5 cps. Holder and Klein have found the N^{14} chemical shift in acetamide to be 244 ppm (relative to NO_3^-) (44).

TABLE II

SUMMARY OF SOME EARLY NMR RESULTS FOR THE HINDERED INTERNAL ROTATION IN N, N-DIMETHYLFORMAMIDE (DMF) AND N, N-DIMETHYLACETAMIDE (DMA)

Compound	E_a, kcal./mole	A, sec^{-1}.	ν_0, mcs.	T_c °K.	$\Delta F^{\dagger}_{T_c}$ kcal./mole	Reference
DMF	7 ± 3	10^3 to 10^7	17.735	372	22	(5, 6)
DMF			30	453	24	(40)
DMF	ca. 20		40			(41)
DMA	12 ± 2	10^7 to 10^{10}	17.735	325	19	(5, 6)

THEORETICAL BACKGROUND

The magnetic induction $\underset{\sim}{B}$ and magnetic field $\underset{\sim}{H}$ are related classically by

$$\underset{\sim}{B} = \underset{\sim}{H} + 4\pi \underset{\sim}{M} \tag{2}$$

where $\underset{\sim}{M}$ is the intensity of magnetization or magnetic moment per unit volume. The magnetic field and magnetization are connected by the equation

$$\underset{\sim}{M} = \chi_v \underset{\sim}{H}; \tag{3}$$

χ_v is called the volume magnetic susceptibility and depends upon the nature of the material. The volume susceptibility is a scalar for non-ferromagnetic isotropic materials and a tensor of rank two for anisotropic materials. Substances for which χ_v is positive are said to be paramagnetic. The induced magnetization is then parallel to the applied magnetic field. When χ_v is negative the substance is said to be diamagnetic, and the induced magnetization is then antiparallel to the applied field. Paramagnetism usually occurs when the substance has unpaired electron spins associated with it. All substances have some diamagnetism arising from interaction of paired electrons with the applied field (45). The total susceptibility of a paramagnetic material is positive because the electron spin and/or orbital contribution more than compensates for the diamagnetic term.

Since strong applied magnetic fields are used in observing magnetic resonance of nuclei, it is pertinent to show that thermodynamic properties and kinetic activation energies will not deviate markedly from their values in a normal environment. Consider a substance of volume diamagnetic susceptibility χ_v in an applied magnetic field H. The interaction energy per mole is given by $M \chi_v H^2/2d$, where M and d

are the molecular weight and density respectively. Typical values of M χ_v/d and H of 10^{-4} and 10^4 gauss respectively correspond to an energy of 5,000 ergs/mole. At room temperature the thermal energy RT is about 2.5×10^{10} ergs/mole, so the magnetic field has a negligible effect on thermodynamic properties. For paramagnetic substances, where the magnitude of χ_v may be larger, the effect of the magnetic field is still negligible except at very low temperatures. Similar arguments show that the effect of strong magnetic fields upon kinetic activation energies is negligible.

To explain some of the details of optical atomic spectra, Pauli postulated that nuclei may possess angular momenta and associated magnetic moments (46). This postulate has since been confirmed for many of the atomic isotopes. According to the general principles of quantum mechanics, the maximum measurable component of the angular momentum of any system must be an intergral or half-intergral multiple of $h/2\pi$, where h is Planck's constant. If I is chosen as the maximum measurable component of the angular momentum of a nucleus, then I is the nuclear spin quantum number. The nucleus will have 2I + 1 distinct states in which the component of angular momentum along any given direction will have the values I, I-1, $\cdots$ -I+1, -I. It is found that the magnetic moment vector for a nucleus is always collinear with the angular momentum vector when $I \neq 0$, and that the magnetic moment is zero when I = 0 (47).

A uniform static magnetic field H_0 separates the energies of the various spin states of nuclei of spin I = 1/2, 1, 3/2, $\cdots$ by an amount $\mu H_0/IkT$ (48); μ is the maximum component of the nuclear magnetic moment, k is the Boltzmann constant, and T is the absolute temperature. For an assembly of nuclei in thermal equilibrium at temperature T, the lower states will be more populated. The relative populations are given by the Boltzmann factor $\exp[(2I+1)m\mu H_0/IkT]$, or to sufficient accuracy

$$\frac{1}{2I+1}\left(1 - \frac{m\mu H_0}{IkT}\right), \qquad (4)$$

where the nuclear magnetic quantum number m takes on the 2I+1 values I, I-1, $\cdots$-I+1, -I.

The unequal distribution of spins among their possible spin states gives rise to a resultant macroscopic magnetic moment in the direction of the applied field $\underset{\sim}{H}_0$. This susceptibility is paramagnetic and temperature dependent. It is exactly analogous to the paramagnetic susceptibility of unpaired electron spins. The average value of the component of the nuclear magnetic moment parallel to the applied static magnetic field is expressed as

$$\bar{\mu} = \sum_{m=-I}^{I} \frac{1}{2I+1} \left(1 - \frac{m\mu H_0}{IkT} \right) \frac{m\mu}{I} . \qquad (5)$$

For N nuclei per unit volume, the volume nuclear magnetic susceptibility is

$$\chi_0 = \frac{N\bar{\mu}}{H_0} = \frac{(I+1)\, N\mu^2}{3IkT} . \qquad (6)$$

The rate at which the nuclear spins approach their equilibrium distribution among states may be an important factor in determining the nature of an NMR absorption line. For nuclei of spin I = 1/2, the rate equation is

$$n - n_{eq.} = (n - n_{eq.})_0 \exp(-t/T_1). \qquad (7)$$

The quantity n is the excess number of nuclei per unit volume in the lower state at time t, $n_{eq.}$ is the excess number at equilibrium, the subscript zero denotes any arbitrary time t, and the time constant T_1 is called the spin-lattice relaxation time. Here, the definition of T_1 may be expressed as

$$T_1 = \frac{1}{2W} = \frac{1}{W_{- \longrightarrow +} + W_{+ \longrightarrow -}} \qquad (8)$$

where W is the mean of the two probabilities for transitions upward $W_{- \longrightarrow +}$ and downward $W_{+ \longrightarrow -}$. The value of T_1 is a measure of the difference between the excess population and its equilibrium value, and it varies with the type of nucleus and its environment. For this reason T_1 measures the extent of spin-lattice interactions. Here, the lattice is considered as any degree of freedom that may give rise to local fluctuating magnetic fields; some examples are electron spins, electron orbital motions, and fluctuating electric fields arising from nuclear electric quadrupole moments. Liquids of low viscosity tend to have small values of T_1, about 10^{-2} to 10^2 seconds; solids may have T_1 as large as several days; and paramagnetic substances may have values of T_1 as small as 10^{-4} seconds.

The quantum-mechanical treatment of NMR absorption predicts extremely sharp absorption lines. This arises from the use of the Dirac δ function in calculating transition probabilities. In reality, the absorption lines are broadened because of various factors. Therefore, in the quantum-mechanical formulation, an arbitrary line-shape function $g(\nu)$ is introduced to account for the line broadening. The form of $g(\nu)$ is such that it is proportional to the absorption intensity at any frequency ν. In addition, it is usually convenient to normalize $g(\nu)$; i.e.,

$$\int_0^\infty g(\nu)\, d\nu = 1. \tag{9}$$

There are about six factors which may cause broadening of NMR absorption lines; these are spin-lattice relaxation, magnetic dipole interactions, electric quadrupole moments, applied field inhomogeneity, and spontaneous emission.

Because of the possibility of spontaneous emission, the line width of any spectroscopic transition may have a lower limit determined by

the finite lifetime of the upper state (49). For the case of nuclear spin transitions this possible cause of line broadening was shown to be negligible compared to the broadening due to other factors (50).

The finite lifetimes of both states are of more importance, since other atomic and molecular degrees of freedom may induce transitions between them. This is the always-present spin-lattice relaxation mentioned earlier. The broadening caused by this type of relaxation is estimated from the uncertainty principle to be of the order $1/T_1$. Although spin-lattice relaxation may occur by many mechanisms, frequently the most important is that of direct interaction of neighboring dipoles. This interaction depends upon the dipole-dipole distances and their relative orientations so that energy may be transferred to the spin system from translational and rotational degrees of freedom.

In some highly viscous liquids and in solids, where nuclei stay in similar relative positions for a long enough time, interactions of magnetic dipoles lead to greater line broadening than given by the spin-lattice relaxation time. In such cases, it is necessary to treat nuclei as being in all the local magnetic fields of neighboring dipoles. When broadening due to spin-lattice relaxation is minor compared to direct dipole-dipole interactions, another characteristic time constant T_2 is usually defined. The convenient definition of T_2 is in terms of the line-shape function $g(\nu)$:

$$T_2 \equiv \tfrac{1}{2} \left[g(\nu) \right]_{\max.} \quad . \tag{10}$$

Here the factor 1/2 is introduced to make this definition of T_2 consistent with that of Bloch's definition to be mentioned later. Because the interaction of nuclear magnetic dipoles is the predominant cause of line broadening in many solids, T_2 is often called the spin-spin relaxation time. When molecules rotate and tumble rapidly, as in fluids of low viscosity, the local magnetic fields become averaged and only

spin-lattice relaxation remains. In these cases T_1 and T_2 are equivalent, or very nearly so, and only one time constant need be employed.

Line broadening may be increased by the presence of nuclei of spin $I > 1/2$. These nuclei may have electric quadrupole moments which interact with fluctuating electric field gradients. As mentioned earlier, this is another spin-lattice relaxation mechanism.

The widths of absorption lines due to nuclei in fluids of low viscosity are frequently determined by inhomogeneities in the applied static magnetic field H_0 over the volume of the sample. This is an instrumental limitation and really leads to the superposition of absorptions due to molecules in different regions of the sample.

Consideration of the classical equation of motion for a magnetic dipole in a magnetic field reveals much information about the nature of resonance absorption. The nuclear magnet experiences a torque $\underset{\sim}{\mu} \wedge \underset{\sim}{H}$, which by Newtonian mechanics must equal the rate of change of angular momentum $\dot{\underset{\sim}{I}}$. The nuclear magnetic moment and the angular momentum are collinear. Their ratio is defined by the scalar γ, called the magnetogyric or gyromagnetic ratio. The classical equation of motion may then be written as

$$\dot{\underset{\sim}{I}} = \frac{\underset{\sim}{\mu}}{\gamma} = \underset{\sim}{\mu} \wedge \underset{\sim}{H}. \tag{11}$$

Equation (11) represents the precession of the magnetic dipole $\underset{\sim}{\mu}$ about the field $\underset{\sim}{H}$ with angular frequency $\underset{\sim}{\omega}$, where

$$\underset{\sim}{\omega} = - \gamma \underset{\sim}{H} \tag{12}$$

The angular frequency of nuclear precession is called the Larmor angular or precessional frequency. For an applied field of several kilogauss, most nuclei have a Larmor angular frequency of the order

of a few megacycles per second, or in the radio frequency (RF) range. If the total applied field is a constant $\underset{\sim}{H}_0$, then in a coordinate system rotating with the Larmor angular frequency—$\gamma\underset{\sim}{H}_0$ the magnetic moment $\underset{\sim}{\mu}$ is stationary. That is, in the rotating frame, the effect of the applied field $\underset{\sim}{H}_0$ is reduced to zero. In addition to $\underset{\sim}{H}_0$, consider the application of a field of constant magnitude H_1, which is rotating about and perpendicular to the direction of $\underset{\sim}{H}_0$. If the angular frequency of $\underset{\sim}{H}_1$ is different from that of the Larmor angular frequency, then $\underset{\sim}{H}_1$ will be rotating in the rotating frame. The applied rotating field $\underset{\sim}{H}_1$ exerts a torque $\underset{\sim}{\mu} \wedge \underset{\sim}{H}_1$ on the nuclear dipole, tending to turn its moment to the plane perpendicular to $\underset{\sim}{H}_0$. When $\underset{\sim}{H}_1$ is moving in the rotating frame, the torque $\underset{\sim}{\mu} \wedge \underset{\sim}{H}_1$ varies rapidly, and the result will be a slight wobbling perturbation of the steady precessional motion of the dipole $\underset{\sim}{\mu}$. When $\underset{\sim}{H}_1$ is stationary in the rotating frame, that is, when $\underset{\sim}{H}_1$ is rotating with the Larmor precessional frequency, then it acts as a stationary field and the torque $\underset{\sim}{\mu} \wedge \underset{\sim}{H}_1$, remaining in the same direction for a long time, will affect large oscillations in the angle between $\underset{\sim}{\mu}$ and $\underset{\sim}{H}_0$. When the angular frequency of $\underset{\sim}{H}_1$ is varied through the Larmor angular frequency, the oscillations will be largest at the Larmor frequency and will show themselves as a resonance phenomenon. A similar resonance will occur if $\underset{\sim}{H}_1$ is in a fixed direction but varies sinusoidally in magnitude with a frequency in the vicinity of the Larmor value. Such a variation can be resolved into two fields rotating with equal angular frequencies in opposite directions, the phases being appropriate. The component rotating in the direction opposite to the Larmor precessional frequency will have very little effect on the resonance.

In his original formulation of the behavior of nuclear magnetic moments in variable magnetic fields, Bloch used a set of phenomenological equations for the variation of the components of the total nuclear magnetic moment per unit volume (51). These important equations are the bases for the discussion of the time dependent phenomena to be considered later.

Summing equation (11) over unit volume, one may write

$$\dot{\underset{\sim}{M}} = \gamma \underset{\sim}{M} \wedge \underset{\sim}{H}, \qquad (13)$$

where $\underset{\sim}{M}$ is the macroscopic moment in unit volume. Equation (12) does not allow for the relaxation effects already mentioned, so it must be modified by addition of appropriate damping terms. The component M_z approaches an equilibrium value, which is the product of the volume susceptibility, equation (6), and the field $H_z = H_0$. The rate of approach to equilibrium is governed by the spin-lattice relaxation time according to the equation

$$\dot{M}_z = - \frac{M_z - M_0}{T_1} . \qquad (14)$$

Because T_1 is the time-constant determining relaxation of the magnetization in the direction parallel to the large static magnetic field H_0, it is called the longitudinal relaxation time.

The solution of equation (13) shows that the component of $\underset{\sim}{M}$ perpendicular to H_0 rotates about the z-axis with the Larmor angular frequency. However, because of fluctuations and relaxation effects, the individual nuclei will get out of phase, and the components M_x and M_y will decay to zero. Similar to the longitudinal relaxation, Bloch assumed this transverse relaxation to be an exponential decay with the characteristic time-constant T_2. The equations of relaxation for the x and y-components are then

$$\dot{M}_x = - M_x/T_2, \qquad (15)$$

$$\dot{M}_y = - M_y/T_2. \qquad (16)$$

The time constant T_2 is called the transverse relaxation time.

The complete equations of motion for the magnetization vector in unit volume are obtained by adding the right-hand sides of equations (14), (15) and (16) to that of equation (13). In the NMR experiment, the vector $\underset{\sim}{H}$ of equation (13) takes on the components

$$\begin{aligned} H_x &= H_1 \cos \omega t \\ H_y &= -H_1 \sin \omega t \\ H_z &= H_0 \quad . \end{aligned} \tag{17}$$

Thus the complete Bloch equations are

$$\dot{M}_x = \gamma (M_y H_0 + M_z H_1 \sin \omega t) - \frac{M_x}{T_2} \tag{18}$$

$$\dot{M}_y = \gamma (M_z H_1 \cos \omega t - M_x H_0) - \frac{M_z}{T_2} \tag{19}$$

$$\dot{M}_z = \gamma (-M_x H_1 \sin \omega t - M_y H_1 \cos \omega t) - \frac{M_z - M_0}{T_1} \; . \tag{20}$$

In substances of high viscosity the locations (not directions) of nuclear spins may remain essentially fixed for long times. The spin-lattice relaxation time T_1 is then very large, and M_z changes only slowly. If the range of local fields due to neighboring nuclei is δ H, the nuclei will be precessing at angular frequencies which cover the range $\gamma (\delta H)$. As a result, individual nuclei will get out of phase in a time $1/\gamma(\delta H)$ and the amplitude of M_x or M_y will decay in a time $T_2 \approx 1 / \gamma(\delta H)$. Under the above conditions the decay of M_x and M_y will be very rapid while that of M_z will be very slow. Herein the reason for the two time constants T_1 and T_2 is explained. The equivalence of the constant T_2, as introduced by Bloch, to that defined earlier will become apparent with the final solutions of the Bloch phenomenological equations (18), (19), and (20).

In fluids of low viscosity where molecular motions are rapid, the local magnetic fields due to neighboring nuclei become averaged to a very narrow range of values. In this case T_1 and T_2 are essentially the same, and in the absence of any paramagnetic materials the nuclear resonance lines are very narrow. This permits the resolution of very closely spaced resonance lines. The whole field of high-resolution NMR spectroscopy falls into this last mentioned class, and only systems belonging to this class are of interest in this present work. At this point, it is worth noting that the nonequivalence of T_1 and T_2 in liquids may frequently be used to measure the rate of molecular tumbling, self diffusion or intermolecular exchange of nuclei.

In order to obtain quantitative relationships between the shape of an NMR signal and the values of the relaxation times T_1 and T_2, it is desirable to solve the Bloch equations. These equations, (18), (19) and (20), are simplified by transforming to a set of coordinates rotating with frequency-ω about the z-axis. The new components of $\underset{\sim}{M}$, $\mathcal{U}$ and $\mathcal{V}$, are called the in-phase and out-of-phase components respectively of the RF magnetization M_{rf}. Since all the components of M in the new frame are orthogonal, the RF magnetization is conveniently written as the complex number

$$M_{rf} = \mathcal{U} + i\mathcal{V} \tag{21}$$

The transformations from the rotating frame to the Cartesian frame are

$$M_x = \mathcal{U} \cos \omega t - \mathcal{V} \sin \omega t \tag{22}$$

$$M_y = -\mathcal{U} \sin \omega t - \mathcal{V} \cos \omega t, \tag{23}$$

and the inverse transformations are

$$\mathcal{U} = M_x \cos \omega t - M_y \sin \omega t \tag{24}$$

$$\mathcal{V} = -M_x \sin \omega t - M_y \cos \omega t \, . \tag{25}$$

The Bloch equations in the new rotating frame are then written as

$$\dot{\mathcal{U}} + \frac{\mathcal{U}}{T_2} + \Delta \omega = O \tag{26}$$

$$\dot{\mathcal{V}} + \frac{\mathcal{V}}{T_2} - \mathcal{U} \Delta \omega + \omega_1 M_z = O \tag{27}$$

$$\dot{M}_z + \frac{M_z - M_0}{T_1} - \mathcal{V} \omega_1 = O \, , \tag{28}$$

where $\Delta \omega = \omega_0 - \omega = \gamma H_0 - \omega$ and $\omega_1 = \gamma H_1$. Equations (26), (27) and (28) are a set of coupled linear differential equations with constant coefficients and are readily solved. The steady-state solutions of these equations are obtained by setting $\dot{\mathcal{U}}$, $\dot{\mathcal{V}}$ and $\dot{M}_z$ all equal to zero. The steady-state solutions are

$$\mathcal{U} = M_0 \frac{\omega_1 T_2^2 \Delta \omega}{1 + T_2^2 \Delta \omega^2 + \omega_1^2 T_1 T_2} \tag{29}$$

$$\mathcal{V} = - M_0 \frac{\omega_1 T_2}{1 + T_2^2 \Delta \omega^2 + \omega_1^2 T_1 T_2} \tag{30}$$

$$M_z = M_0 \frac{1 + T_2^2 \Delta \omega^2}{1 + T_2^2 \Delta \omega^2 + \omega_1^2 T_1 T_2} \tag{31}$$

The rate of absorption of energy per unit volume is given by $-M_x \dot{H}_x$, which is proportional to $\mathcal{V}$, the out-of-phase component of the RF magnetization vector. Under conditions of "slow-passage," e.g., when the field H_0 is varied slowly through resonance at constant ω so that $\dot{\mathcal{U}} \cong \dot{\mathcal{V}} \cong \dot{M}_z \cong O$, the rate of absorption of energy is proportional to $\mathcal{V}$ of equation (30). If the magnitude of the oscillating field is small so that

$$\gamma^2 H_1^2 T_1 T_2 \ll 1 \, , \tag{32}$$

then the rate of absorption of energy becomes proportional to

$$\frac{2\,T_2}{1 + T_2^2\,\Delta\omega^2} \quad , \tag{33}$$

which gives the form of the line-shape function $g(\nu)$,

$$g(\nu) = \frac{2\,T_2}{1 + 4\,\pi^2\,T_2^2\,(\nu_0 - \nu)^2} \quad . \tag{34}$$

Function (33) describes a Lorentzian or damped oscillator curve. Its peak value is given by

$$[g(\nu)]_{max.} = 2\,T_2 \, , \tag{35}$$

which is identical with the earlier definition of T_2; see equation (10).

Returning to equation (30), one notes that at the resonant frequency, the denominator becomes $1 + \omega_1^2 T_1 T_2$. This quantity is called the saturation factor. When it becomes greater than unity, the resonance is said to be saturated, or partially so, and the line shape is no longer correctly approximated by equation (34).

Under suitable experimental conditions, it is possible to observe u, the in-phase component of the RF magnetization vector. This is known as the dispersion mode and under conditions of "slow-passage," the line shape function is proportional to equation (29). When saturation is negligible, i.e. when $\gamma_1^2 H_1^2 T_1 T_2 << 1$, the dispersion mode line shape function is

$$\frac{\nu_0 - \nu}{1 + 4\,\pi^2 T_2^2\,(\nu_0 - \nu)^2} \quad . \tag{36}$$

The forms of the absorption and dispersion modes, under conditions of "slow-passage" and negligible saturation, are shown in Figure 4.

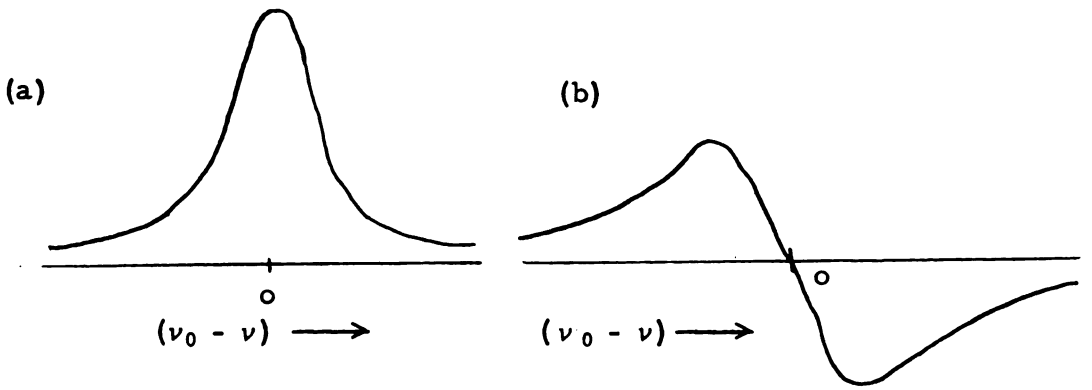

Figure 4. Representation of unsaturated and "slow-passage" NMR line shapes for: (a) the absorption υ-mode and (b) the dispersion $\mathcal{U}$ -mode.

From equations (34) and (35) it can easily be shown that the width of the absorption υ -mode curve is $1/\pi\ T_2$ at one-half maximum intensity. The value $1/\pi T_2$ is called the natural line width, since it is the line width in the absence of "fast passage," saturation, chemical exchange and other complicating factors. Similarly, the natural line width for the dispersion mode, the width from minimum to maximum, is $1/\pi \sqrt{3}\ T_2$.

In the above, only the features of a single isolated NMR line have been considered. When a spectrum has multiple resonance lines, the form of each line may frequently be represented by the Bloch equations, and under conditions of "slow-passage" and negligible saturation, by the Lorentzian curve. The Bloch equations, as discussed above, do not correctly represent the form of a spectral line when overlapped with another spectral line. Overlap, i.e. when the separation between lines is of the same order of magnitude as the natural line widths, is very common.

The most important parameters derivable from high-resolution NMR spectra are obtained from experimentally measured frequency

separations and relative intensities. These two measured quantities are influenced, especially in regions of overlap, by the shapes of individual resonance lines. The theoretical background for resonance line shapes enables one to apply corrections to the apparent measured values of frequency separations and relative intensities. Of more importance in this present work is the influence of time-dependent processes upon the parameters determining resonance line shapes. Before consideration of this problem, it seems beneficial to discuss briefly the two most important causes for multiple line high-resolution NMR spectra. These are chemical shift and electron coupled nuclear spin-spin interactions.

As mentioned earlier, nuclear dipole-dipole and quadrupole moment interactions cause extensive broadening of resonance lines. The effect of these two types of interactions upon the nature of the resonance spectrum depend upon the environment of the nuclei under observation. The existence of either of these two types of interactions usually causes such extensive broadening that resolution of closely spaced lines becomes impossible. In the realm of high-resolution NMR spectroscopy, another environmental effect becomes extremely important. This effect is called the chemical shift, and its cause is magnetic shielding of nuclei by electrons. An atom or molecule acquires a diamagnetic moment when placed in a strong magnetic field. The moment results from the induction of orbital motions of the electrons. These electron motions constitute magnetically effective currents within the molecule or atoms which also act on the nuclei. These induced currents are proportional to the applied field H_0, so the secondary field will also be proportional to H_0. The local magnetic field at the position of the nucleus will be given by

$$H_{local} = H_0 (1 - \sigma), \qquad (37)$$

where σ is called the screening constant.

Electron screening brings the nuclear Zeeman levels closer together so that the energy (resonance frequency) for a transition between states will be lower than for an unscreened nucleus. If the experiment is performed by varying H_0 through resonance at constant frequency, the applied field necessary for resonance of a screened nucleus will be larger than that needed for an unscreened nucleus if, as is normally the case, the screen constant σ is positive.

Because the distribution of electrons in molecules may vary markedly with the nature of the chemical bonds, it is not surprising that strong applied magnetic fields cause differences in the electron screening of chemically different nuclei of the same species. The result of these differences in screening is that nuclei of a common species but of chemically different groups will resonate at the various applied fields that are characteristic of each individual chemical group. The field separation of two such resonance peaks is referred to as the chemical shift. The closely related "Knight shift" in metals was first observed in 1949 (52), and chemical shifts for N^{14}, F^{19}, and H^1 nuclei were first observed by Proctor and Yu (53), Dickinson (54), and Linström (55) and Thomas (56) respectively. Since these early observations, many theoretical considerations have been made concerning the nature of electron screening of nuclei. An excellent review of these works is given in Chapter 7 of reference 48.

Chemical shift separations may be expressed either in units of magnetic field or in frequency units. The two systems of units are readily converted by use of the Larmor resonance condition, equation (12). From this and equation (37) it is apparent that the chemical shift is proportional to the applied field. Reported values of chemical shift separations must necessarily be accompanied by the values of the applied fields or resonant frequencies used in their measurements. Therefore, it is convenient to express chemical shifts in terms of the dimensionless unit defined by

$$\delta = \frac{H - H_r}{H_r} \quad , \tag{38}$$

where H is the resonance field of the signal being measured at a fixed frequency and H_r is the corresponding value for a second resonance signal. The separation of resonance signals is usually most easily measured in frequency units by the well-known side-band technique (57), or the "Wiggle-beat" method (58, 59, 60). The chemical shift is then easily expressed as

$$\delta = \frac{\nu - \nu_r}{\nu_r} \quad , \tag{39}$$

where ν is the resonant frequency of the signal being measured and ν_r is the corresponding value for a reference signal. Usually ν_r is very nearly equal to the spectrometer frequency. Since both these frequencies are usually very much greater than $\nu - \nu_r$, equation (39) may be rewritten as

$$\delta = \frac{\nu - \nu_r}{\nu_0} \quad . \tag{40}$$

In this present work, the symbol δ will be reserved for the purpose of expressing chemical shifts with respect to some stated reference signal in units of ppm, i.e., values of δ will be calculated by use of equation (40). For convenience, however, the symbols $\delta\nu$ and $\delta\omega$ will be used to express the frequency separations of chemically shifted resonance lines in units of cps and radians per second respectively. The appropriate values of ν_0 and ω_0 will necessarily accompany all reported values of $\delta\nu$ and $\delta\omega$ respectively.

In early NMR experiments on liquids it was found that many substances show more resonance lines than required by simple considerations of the number of chemically nonequivalent nuclei (61,62, 63). Many molecules gave symmetrical doublets, triplets, quartets, etc., and the frequency separations of the multiplet components were found to be

independent of the applied field H_0. On the basis of these early experiments, Gutowsky, McCall, and Slichter (64) and Hahn and Maxwell (65) proposed that the multiplets arise from the indirect interaction of neighboring nuclear spins. They proposed that the energy of this type of interaction was proportional to the "dot" product $\underset{\sim}{I}_i \cdot \underset{\sim}{I}_j$, where $\underset{\sim}{I}_i$ and $\underset{\sim}{I}_j$ are the nuclear spin vectors of the two magnetically active but chemically different nuclei i and j respectively. The constant of proportionality, $J_{ij} = J_{ji}$, is called the nuclear spin-spin coupling constant and is usually given in the energy units of Planck's constant; i.e., in units of cps. In some special cases, spin-spin coupling may occur between chemically equivalent nuclei. The independence of spin-spin coupling of the applied field may be qualitatively understood with the assumption that the magnetic fields responsible for the interaction arise within the molecule itself.

A simple example of spin-spin coupling is provided by the molecule acetaldehyde, in which there are three chemically equivalent protons A, each of spin $I = 1/2$, and one other chemically different proton B of spin $I = 1/2$. The multiplet of the resonance of the three protons A will arise only from spin-spin interaction with proton B. Interaction with C^{12} or O^{16} each of $I = 0$ is impossible, and any interaction with the one per cent natural abundance of C^{13} of $I = 1/2$ is of such low intensity that it may be neglected in the present consideration. Therefore, the resonance of the three A protons is a symmetrical doublet because the B proton has two spin states. Similarly, proton B will "see" all the possible spins states of three A protons. The energy of the proton B transition will depend only on the sum of the spin components of the three A protons ΣI_{Az}. Since $I_{Az} = \pm 1/2$, this sum can take the values $3/2$, $1/2$, $-1/2$, $-3/2$. Therefore, the proton B signal is split into a symmetrical quartet with relative intensities 1:3:3:1.

For the case of a set of n_i chemically equivalent nuclei of type i interacting with n_j chemically equivalent nuclei of type j such that $J_{ij}/ | \nu_i - \nu_j | << 1$, the j signal has $2 n_i I_i + 1$ components and the i signal has $2 n_j I_j + 1$ components. The relative intensities of the components within each symmetrical multiplet will be given by the corresponding binomial coefficients. These simple rules are probably always valid when nuclei of different elements interact; for in such cases the "chemical shifts" are much larger than the largest values of J yet measured. However, for the case of interaction of nuclei of a common species, there are countless examples of the situation in which the chemical shift and coupling constant are of the same order of magnitude. In situations of this type, the simple rules given above are no longer valid. When the chemical shift and corresponding coupling constant are of the same order of magnitude, the transition frequencies and relative intensities no longer fall into any simple regular pattern. Indeed, the number of observable transitions may be much greater than that predicted by the above simple rules.

The nature of spin-spin coupling has been theoretically investigated by several authors. All but the most recent of these works are discussed in Chapter 8 of reference 48. Also, the general analysis of most of the easier spin systems, having coupling constants comparable in magnitude to the corresponding chemical shifts, is discussed in Chapter 6 of reference 48.

NMR spectra that are complicated by spin-spin interactions frequently may be simplified by the method of double irradiation, which was originally demonstrated by Bloch (66). The method consists of the saturation of one chemical group of nuclei while observing the NMR spectrum of another group of nuclei. This experiment is applicable only when the ratio of the chemical shift to the corresponding spin-spin coupling constant is very large. The saturation of one group leads to very fast

transitions between the possible states of nuclei in that group, so that the nuclei in the group become effectively decoupled from the nuclei in the other group being observed. The theory of double irradiation, also called spin decoupling, has been given by Bloom and Shoolery (67), and some very good experimental examples have been given by Anderson (68).

From the previous discussion, it is apparent that the shapes of all NMR signals are influenced to some extent by the motions of nuclei or "lattice" of the material under observation. These effects provide methods for studying a large number of rate processes in the solid, liquid, and gas phases. The first theoretical and experimental analysis of such an effect was given by Bloembergen, Purcell, and Pound (50). They proved that "lattice" motions were an important mechanism for spin-lattice relaxation and for narrowing NMR absorption lines. Their treatment is well adapted to the study of rates of certain types of "lattice" motions in solids and viscous liquids. In these cases, the occurrence of rate processes may cause narrowing of resonance lines which are otherwise broadened by direct nuclear dipole-dipole interactions. The work of Bloembergen, Purcell and Pound is only one example of the large number of broad-line NMR investigations of rate processes. The narrowing observed in these broad-line NMR works are, in principle, the same as the observed effects of rate processes upon the narrow lines encountered in the high-resolution NMR spectra of liquids and gases. However, because of the obvious basic differences between the characteristics of these two types of spectra, the observed effects of rates processes manifest themselves in quite different ways. As a result, the mathematical methods for relating rates of kinetic processes to line-shape parameters are also different. Only high-resolution spectra of some non-paramagnetic liquids are encountered in the work reported in this thesis. Therefore, the theory discussed in the remainder of this section is usually best adapted to high-resolution type spectra.

If a magnetically active nucleus ($I \neq 0$) kinetically experiences different magnetic environments separated by resonance frequencies $\Delta\nu$, the resolution of the NMR signals for that nucleus at each magnetic environment is possible only if the lifetime τ of the nucleus at each environment is greater than $\sim 1/2\ \pi\ \Delta\nu$. This is a statement of the uncertainty principle, from which it is apparent that kinetic processes may cause coalescence of multiple line spectra. The first quantitative formulation of such coalescence was given by Gutowsky, McCall, and Slichter (69). They derived equations which quantitatively related the coalescence of spin-spin coupling multiplets to the rates of random fluctuations in the spin coordinates of the coupled nuclei. These equations served as an argument for the nonexistence of F^{19}-P^{31} spin-spin coupling in some fluorinated phosphorus compounds. Although these authors did not use their equations for any actual calculations of rates, their theory was the basis for many later applications (references 5, 6, 12, 13, 40, 70 through 81, and others).

According to Gutowsky and collaborators (69, 70, 5, 6), two NMR lines A and B may be considered as arising from: (a) two magnetically different sites A and B having X - NMR positions differing by a frequency $\delta\omega$ or (b) the spin-spin interaction of the X nuclei with one other chemically nonequivalent nucleus Y of spin $I = \frac{1}{2}$, where $J_{XY} = \delta\omega$. Here, X represents the nuclei being observed. The molecule N, N-dimethylacetamide is an example of case (a) above. The protons of the two N-methyl groups constitute the X nuclei, the protons of one of these methyl groups (say cis = A) is chemically nonequivalent to the other N-methyl group (trans = B). The trimethylammonium ion is an example of case (b) above. Here, the protons of the three methyl groups constitute the X nuclei. The magnetic resonance of these protons is split into two lines A and B by the equivalent spin-spin coupling of all X nuclei with a Y nucleus of spin $I = \frac{1}{2}$, the $\overset{+}{N}$ - H proton. In making the definitions

described above, one must keep the facts in mind--that spin-spin coupling constants J are field invarient, whereas chemical shifts $\delta\omega$ are proportional to the applied static magnetic field.

Choosing the average field H_0 of the resonance lines A and B as a reference, the line shapes for these lines may be represented by the Bloch equations (26, 27 and 28). The resonance frequency for one X resonance line, say A, may be taken as $\gamma H_0 + \delta\omega/2$. The other X resonance line B will then be at $\gamma H_0 - \frac{\delta\omega}{2}$. Thus, for line A, equations (26), (27), and (28) must have all values of $\Delta\omega$ replaced by $\Delta\omega + \frac{\delta\omega}{2}$, and for line B, all values of $\Delta\omega$ must be replaced by $\Delta\omega - \frac{\delta\omega}{2}$. This modification of the Bloch equations is equivalent to adding descrete quantum states (the descrete values $\pm \frac{\delta\omega}{2}$) to classical equations of motion. Such a treatment provides a simple way of taking into account the spin-spin coupling or chemical shift differences responsible for the existence of the two resonance lines. If magnetically different sites cause chemical shift differences among the X nuclei, then any additional multiplicity in the resonance arising from spin-spin coupling among the X nuclei at these sites may, in principle, be taken into account.

If the magnitude H_1 of the applied radiofrequency (RF) magnetic field is small, so that

$$\gamma^2 H_1^2 T_{1A} T_{2A} << 1 >> \gamma^2 H_1^2 T_{1B} T_{2B} , \qquad (41)$$

then saturation of the resonance lines A and B due to X nuclei is negligible. If, in addition, the experimental conditions are those of "slow-passage," then from equation (31) it is apparent that

$$M_z = M_0 . \qquad (42)$$

Using equations (26), (27) and (28) with the modifications described above, and using the notation of equation (21), the equations of motion for the

RF magnetizations of the X nuclei, M_A and M_B, may be written as

$$\dot{M}_A + \left[\frac{1}{T_2} - i \left(\Delta\omega + \frac{\delta\omega}{2}\right)\right] M_A = -i\,\omega_1 M_0 \quad , \tag{43a}$$

$$\dot{M}_B + \left[\frac{1}{T_2} - i \left(\Delta\omega - \frac{\delta\omega}{2}\right)\right] M_B = -i\,\omega_1 M_0 \quad , \tag{43b}$$

respectively. In equations (43a and b) it is assumed the natural line width of A, $1/\pi\, T_{2A}$, is equal to that of line B, $1/\pi\, T_{2B}$; or

$$T_{2A} = T_{2B} = T_2. \tag{44}$$

This restriction will not be made in a later simplified treatment.

Applying the Laplace transformation to equation (43a), the transformation of variables being (a) the time t to time s and (b) the RF magnetization M_A to m_A, one obtains

$$m_{A(s)} = -\frac{i\omega_1 M_0}{s(s+a_A)} + \frac{M_A(0^+)}{s + a_A} \quad . \tag{45}$$

In this last equation, $M_A(0^+)$ is the RF magnetization of X nuclei for line A at the arbitrary time t equal to zero, and a_A is defined for convenience as

$$a_A = \frac{1}{T_2} - i \left(\Delta\omega + \frac{\delta\omega}{2}\right). \tag{46a}$$

Also, for convenience, a_B is defined as

$$a_B = \frac{1}{T_2} - i \left(\Delta\omega - \frac{\delta\omega}{2}\right). \tag{46b}$$

A solution of equation (43a) may be obtained from the inverse Laplace transformation of equation (45). This solution is given by the theory of residues as

$$M_{A(t)} = \left[\frac{-i\omega_1 M_0}{s + a_A} e^{st}\right]_{s \to 0} + \left[\frac{-i\omega_1 M_0}{s} e^{st}\right]_{s \to -a_A} + \left[M_{A(0^+)} e^{st}\right]_{s \to -a_A}$$

$$= \frac{-i\omega_1 M_0}{A} (1 - e^{-a_A t}) + M_{A(0^+)} e^{-a_A t} . \qquad (47)$$

A similar solution in $M_{B(0^+)}$ and a_B may be obtained for $M_{B(t)}$.

Now consider three cases in which effective random exchange of nuclei will tend to remove the degeneracy causing the existence of the two resonance lines A and B. One case is that of effective random exchange of X nuclei between two chemically different sites A and B. A second case is that of effective random exchange of a Y nucleus ($I = 1/2$) between two (or more) environments with X-Y spin-spin coupling occurring in only one of the environments available to Y. A third case is that of effective random exchange of X nuclei between two (or more) environments with X-Y spin-spin coupling ($I_Y = 1/2$) occurring in only one of the environments available to X, namely, the environment being observed. In all three cases, the nuclei causing the twofold degeneracy (the two resonance lines A and B) experience effective random fluctuations in their spin coordinates. Therefore, although the three cases are chemically and/or physically different, they are mathematically equivalent in that the same equations may be applied in all three cases. To conserve space, the remaining derivations will be discussed in terms of the nomenclature of the first case mentioned above (i.e., in terms of effective random exchange of X nuclei between the two chemically different sites A and B).

Suppose now that some kinetic process effectively causes random exchange of X nuclei between sites A and B, and consider the effect of such a process upon the appropriate simultaneous solutions of equation (47) and the similar one for $M_{B(t)}$. Assume the kinetic process may be represented by

$$\dot{N}_A^* = -k_A N_A^* \quad \text{and} \quad \dot{N}_B^* = -k_B N_B^*, \tag{48}$$

where N_A^* and N_B^* are the number of labelled X nuclei at sites A and B at time t, respectively. Since the kinetic process is one of exchange, the following useful equations may be written.

$$k_A p_A = k_B p_B \tag{49}$$

$$\tau_A = \frac{1}{k_A} = \frac{\tau}{p_B} \quad \text{and} \quad \tau_B = \frac{1}{k_B} = \frac{\tau}{p_A} \tag{50}$$

In these latter equations, p_A and p_B are the fractions of X nuclei at sites A and B at time t, respectively, k_A and k_B are the specific first-order rate constants for the equilibrium exchange of X nuclei between sites A and B, τ_A and τ_B are the mean lifetimes of X nuclei at sites A and B, respectively, and τ is defined for convenience as

$$\tau = \frac{\tau_A \tau_B}{\tau_A + \tau_B} . \tag{51}$$

The probability that a given X nucleus will have stayed at site A a time between t and t + dt is given by the exponential factor $\tau_A^{-1} \exp(-t/\tau_A)dt$. The value of M_A for those X nuclei with M_A equal to $M_A(0^+)$ at time t equal to zero, when averaged over the exchange, is given by

$$\begin{aligned} \langle M_A \rangle &= \int_0^\infty \tau_A^{-1} \exp(-t/\tau_A) M_A(t)dt \\ &= \frac{M_A(0^+)}{1 + a_A \tau_A} - \frac{i\omega_1 M_0 \tau_A}{1 + a_A \tau_A} . \end{aligned} \tag{52}$$

A similar equation in $M_B(0^+)$, a_B, and τ_B may be obtained for $\langle M_B \rangle$.

Thus far, only X nuclei with given values of $M_A(0^+)$ and $M_B(0^+)$ have been considered. Since different X nuclei may have different values

of $M_A(0^+)$ and $M_B(0^+)$, it is necessary to average equation (51) and the similar one for $< M_B >$ over all possible "initial states" $M_A(0^+)$ and $M_B(0^+)$. To obtain these averages, it is assumed that the RF magnetization M, summed over all X nuclei, is not affected by the kinetic process. Such an assumption imposes the boundary condition that the average value of $M_A(0^+)$ must equal the average value of M_B at the time of an exchange of an X nucleus between sites A and B. Since the exchange is random, i.e., an event is as likely at any one time as at any other time, the average value of M_B at the time of an exchange must be equal to the value of M_B at any time t, namely $< \bar{M}_B >$. Therefore, the following equations may be written,

$$M_A(0^+) = < \bar{M}_B > \text{ and } < \bar{M}_A > = M_B(0^+) \tag{53}$$

Substituting equations (53) into equation (52) and into the similar one for $< M_B >$, and simultaneously solving the two resulting equations, leads to the following relationships.

$$< \bar{M}_A > = -i\omega_1 M_0 \frac{\tau_B + (1 + a_B \tau_B)\tau_A}{(1 + a_B \tau_B)(1 + a_A \tau_A) - 1} \tag{54a}$$

$$< \bar{M}_B > = -i\omega_1 M_0 \frac{\tau_A + (1 + a_A \tau_A)\tau_B}{(1 + a_A \tau_A)(1 + a_B \tau_B) - 1} \tag{54b}$$

The RF magnetization M, summed over all X nuclei and averaged over the exchange and "initial states," is given by the weighted sum:

$$M = p_A < \bar{M}_A > + p_B < \bar{M}_B > . \tag{55}$$

Using equations (50), (54a) and (54b), equation (55) may be written in the form:

$$M = -i\omega_1 M_0 \quad \frac{(\tau_A + \tau_B) + \tau_A \tau_B (\alpha_A p_B + \alpha_B p_A)}{(1 + \alpha_A \tau_A)(1 + \alpha_B \tau_B) - 1} \qquad (56)$$

Equation (56) is the same as equations (3) and (18) of references (5) and (67), respectively. This equation expresses the total RF magnetization for all X nuclei as a function of the rate constants for an effective random kinetic exchange of X nuclei between two sites A and B. The RF magnetization is a complex number. The real part of M gives the dispersion mode shape function u in terms of the rate constants, and the imaginary part of M gives the absorption mode shape function v in terms of the rate constants. In principle, equation (56) is only applicable to a doublet-type resonance structure having a common natural line width for each line. The importance of this restriction will be considered later.

Although the method described above provides an illustrative background for the calculation of more complex line-shape functions in terms of rate constants, an easier method has been formulated by McConnell (82). His formulation will now be applied to the "two-site" problem solved above. In the following treatment of the problem the restriction of equation (44), that $T_{2A} = T_{2B}$, will be removed and the final solution will be that for the more generalized "two-site" problem. Also, certain approximations that were implicit in the earlier solution of the problem will be pointed out.

The Bloch equations (26), (27), and (28) are modified to the following:

$$\dot{u}_A + \Delta\omega_A v_A = -\frac{u_A}{\tau_{2A}} + \frac{u_B}{\tau_B} \qquad (57)$$

$$\dot{u}_B + \Delta\omega_B v_B = -\frac{u_B}{\tau_{2B}} + \frac{u_A}{\tau_A} \qquad (58)$$

$$\dot{v}_A - \Delta\omega_A u_A = -\frac{v_A}{\tau_{2A}} + \frac{v_B}{\tau_B} - \omega_1 M_{zA} \tag{59}$$

$$\dot{v}_B - \Delta\omega_B u_B = -\frac{v_B}{\tau_{2B}} + \frac{v_A}{\tau_A} - \omega_1 M_{zB} \tag{60}$$

$$\dot{M}_{zA} - \omega_1 v_A = \frac{M_{0A}}{T_{1A}} - \frac{M_{zA}}{\tau_{1A}} + \frac{M_{zB}}{\tau_B} \tag{61}$$

$$\dot{M}_{zB} - \omega_1 v_B = \frac{M_{0B}}{T_{1B}} - \frac{M_{zB}}{\tau_{1B}} + \frac{M_{zA}}{\tau_A} , \tag{62}$$

where

$$\frac{1}{\tau_{1A}} = \frac{1}{T_{1A}} + \frac{1}{\tau_A} , \tag{63}$$

$$\frac{1}{\tau_{2A}} = \frac{1}{T_{2A}} + \frac{1}{\tau_A} , \tag{64}$$

similarly for τ_{1B} and τ_{2B}, and

$$\Delta\omega_A = \omega_A - \omega , \tag{65}$$

$$\Delta\omega_B = \omega_B - \omega . \tag{66}$$

In the last two equations, ω_A and ω_B are the resonance frequencies for X nuclei at sites A and B, respectively, and ω is the angular frequency of the applied RF field. All other symbols in equations (57) through (62) are the same as before. The Bloch equations, as just modified, are written to obey the kinetic equations (48) through (51) used in the earlier treatment. The reasoning behind the above modification can be seen by comparing equations (57) and (64) with equation (26). Equation (57)

differs from equation (26) by the addition of two terms, $-\mathcal{U}_A/\tau_A$ and $\mathcal{U}_B/\tau_B$, to the right hand side. The first term, $-\mathcal{U}_A/\tau_A$, accounts for the transfer of $\mathcal{U}$ magnetization out of site A to site B. The second term accounts for the transfer of $\mathcal{U}$ magnetization from site B to site A. The same type of modification leads to equations (58) through (62).

The Bloch equations resulting from the type of modification just described require approximations not imposed on the ordinary Bloch equations. It must be assumed that any magnetic environment of X nuclei other than A and B (e.g. an "activated complex"), is short lived so as to produce no change in the magnetization components as the X nuclei are effectively exchanged between A and B. Also, it is required that T_{1A}, T_{2A}, T_{1B}, and T_{2B} be independent of τ_A and τ_B. This last requirement is most easily realized when $\tau_A > (T_{1A}, T_{2B}, T_{1B}, T_{2B}) < \tau_B$; i.e., when the X nuclear relaxations are of high frequency compared to τ_A^{-1} and/or τ_B^{-1}. In addition, the relaxations of the X nuclear magnetizations at site A must be independent, except for the kinetic exchange effects, of those at site B. It should be noted that all the above restrictions are implied for the solution of the "two-site" problem described earlier. Even with all the above restrictions, equations (57) through (62), along with obvious extensions to multiple-site systems and to multiple resonance experiments, may be used to study a large number of kinetic problems.

Although the set of coupled differential equations (57) through (62) may be applied to the important case of kinetic processes as observed by "rapid-passage" transient experiments (83), the easiest problems to solve are those for the case of "slow-passage," so that

$$\dot{\mathcal{U}}_A \cong \dot{\mathcal{U}}_B \cong \dot{\mathcal{V}}_A \cong \dot{\mathcal{V}}_B = \dot{M}_{z_A} = \dot{M}_{z_B} = 0. \qquad (67)$$

In this case, equations (57) through (62) become a complete set of ordinary simultaneous linear equations in six unknowns. In many cases of interest these equations may easily be solved in closed form, and they can always be solved numerically in the most general case. With negligible saturation the total z magnetization M_z becomes unaffected by kinetic processes, i.e.,

$$M_z = M_{zA} + M_{zB} = M_0 = M_{0A} + M_{0B} = \frac{M_{0A}}{p_A} = \frac{M_{0B}}{p_B} . \qquad (68)$$

The RF magnetization, summed over all X nuclei, is written as

$$M = \mathcal{U} + i\mathcal{V} = M_A + M_B = \mathcal{U}_A + i\mathcal{V}_A + \mathcal{U}_B + i\mathcal{V}_B. \qquad (69)$$

Equations (50), 63), (64), (68), (69) and (57) through (60) are then easily transformed to

$$M = -i\omega_1 M_0 \frac{\tau_A + \tau_B + \tau_A \tau_B (p_B \beta_A + p_A \beta_B)}{(1 + \tau_A \beta_A)(1 + \tau_B \beta_B) - 1} , \qquad (70)$$

where β_A and β_B are defined for convenience as

$$\beta_A = \frac{1}{T_{2A}} - i\Delta\omega_A, \qquad \beta_B = \frac{1}{T_{2B}} - i\Delta\omega_B. \qquad (71)$$

Equations (56) and (70) are equivalent except for the restriction of equation (44) being implied in the former case.

Choosing the average resonance frequency γH_0 of ω_A and ω_B as a reference, then $\Delta\omega_A$ and $\Delta\omega_B$ may be written as

$$\Delta\omega_A = \Delta\omega + \frac{\delta\omega}{2} , \quad \Delta\omega_B = \Delta\omega - \frac{\delta\omega}{2} , \qquad (72)$$

respectively, where $\delta\omega$ is equal to $\omega_A - \omega_B$. Upon rationalizing equation (70), the real part gives the dispersion $\mathcal{U}$-mode shape function in terms of the rate constants, and the imaginary part gives the absorption $\mathcal{V}$-mode

shape function in terms of the rate constants. These functions may be written as

$$\mathcal{U} = \frac{-\omega_1 M_0 \left\{ QP - \left[1 + \gamma \left(\frac{P_B}{T_{2A}} + \frac{P_A}{T_{2B}} \right) \right] R \right\}}{P^2 + R^2} , \tag{73}$$

$$\mathcal{V} = \frac{-\omega_1 M_0 \left\{ P \left[1 + \gamma \left(\frac{P_B}{T_{2A}} + \frac{P_A}{T_{2B}} \right) \right] + QR \right\}}{P^2 + R^2} \tag{74}$$

The quantities P, Q, R, and S are defined for convenience as

$$P = \gamma \left[\frac{1}{T_{2A} T_{2B}} - \Delta\omega^2 + \left(\frac{\delta\omega}{2} \right)^2 \right] + \frac{P_B}{T_{2B}} + \frac{P_A}{T_{2A}} = S - \gamma \Delta\omega^2, \tag{75}$$

$$Q = \gamma \left[\Delta\omega - \frac{\delta\omega}{2} (P_A - P_B) \right] , \tag{76}$$

$$R = \Delta\omega \left[1 + \gamma \left(\frac{1}{T_{2A}} + \frac{1}{T_{2B}} \right) \right] + \frac{\gamma \, \delta\omega}{2} \left(\frac{1}{T_{2B}} - \frac{1}{T_{2A}} \right) + \frac{\delta\omega}{2} (P_A - P_B) . \tag{77}$$

For practical applications of equations (73) and (74), the parameters $\delta\omega$, T_{2A}, T_{2B}, P_A, and P_B must be known. A family of line shapes, corresponding to a set of rate constants, may then be generated by calculating $\mathcal{U}$ and/or $\mathcal{V}$ over the desired range of values for $\Delta\omega$. The experimental rate constants may then be taken as those values giving a calculated line-shape function best matching the experimental line shape. Such a method is obviously very time-consuming, and it is seldom applied to high-resolution type spectra. More direct methods of evaluating the rate constants consist in relating the rate constants to measurable components of the line-shape functions. The following are some of the more useful

components: frequency separations of absorption maxima, frequency separations of dispersion intensity nulls, ratios of maximum to central minimum absorption intensities, widths of one-half maximum intensity for absorption lines, and frequency separations of maximum and minimum dispersion intensities. The equations for some of these components, as they pertain to the "two-site" problem, will now be derived.

In equation (74), $\delta\omega$ is the frequency separation, in the absence of any kinetic processes, between the resonance absorptions for **X** nuclei at sites **A** and B. In equation (73), $\delta\omega$ is the same value when measured as the frequency separation between dispersion intensity nulls. In both cases, the line shape functions depend upon the frequency scale $\Delta\omega$, which was arbitrarily taken as zero for the frequency $(\omega_A + \omega_B)/2$. At this time only the more useful absorption $\mathcal{V}$ -mode, equation (74), will be considered. The values of $2\Delta\omega$ for which $\mathcal{V}$ of equation (74) is maximized will give the observed frequency separation $\delta\omega_e$ in terms of the rate constants. The values of $\Delta\omega$ corresponding to maxima and minima in $\mathcal{V}$ are given by the solutions of the equation obtained when the derivative $d\mathcal{V}(\Delta\omega)/d(\Delta\omega)$ is set equal to zero, or since $P^2 + R^2 \neq \pm\infty$ and $\omega_1 M_0 \neq 0$,

$$0 = (P^2 + R^2)\frac{d}{d(\Delta\omega)}\left[\frac{\mathcal{V}(P^2+R^2)}{-\omega_1 M_0}\right] - \left[\frac{\mathcal{V}(P^2+R^2)}{-\omega_1 M_0}\right]\frac{d}{d(\Delta\omega)}(P^2+R^2)$$

$$= 2\tau^2 A\,\Delta\omega^5 + 3\tau^2 B\,\Delta\omega^4 + 4\tau^2 C\,\Delta\omega^3 + (BD-AE)\Delta\omega^2 + 2(CD-AF)\Delta\omega + (CE - BF), \qquad (78)$$

where

$$A = \tau^2\left(\frac{P_A}{T_{2A}} + \frac{P_B}{T_{2B}}\right), \qquad (79)$$

$$B = \tau^2\,\delta\omega\left(\frac{P_B}{T_{2B}} - \frac{P_A}{T_{2A}}\right), \qquad (80)$$

$$C = \tau\left(\frac{\delta\omega}{2}\right)^2 \left[1 - (p_A - p_B)^2 + \frac{A}{\tau}\right] + \frac{\tau}{T_{2A}T_{2B}} \left[1 + p_A^2 + p_B^2 + \tau\left(\frac{p_B}{T_{2A}} + \frac{p_A}{T_{2B}}\right)\right] + \tau p_A p_B \left(\frac{1}{T_{2A}^2} + \frac{1}{T_{2B}^2}\right) + \frac{A}{\tau^2}, \quad (81)$$

$$D = \left[1 + \tau\left(\frac{1}{T_{2A}} + \frac{1}{T_{2B}}\right)\right]^2 - 2\tau S, \quad (82)$$

$$E = \delta\omega\,(D + 2\tau S)^{\frac{1}{2}} \left[p_A - p_B + \tau\left(\frac{1}{T_{2B}} - \frac{1}{T_{2A}}\right)\right], \quad (83)$$

$$F = S^2 + \frac{E^2}{4}\,(D + 2\tau S)^{-1}. \quad (84)$$

Equation (78) should always have a solution in each limit $\Delta\omega \longrightarrow \pm\infty$. These solutions correspond to minima in the absorption intensity at the "wings" of the τ-mode shape function. When $\tau \longrightarrow 0$ (i.e., for very rapid exchange) equation (74) has only one maximum. From equation (78), the frequency position of this maximum is given by

$$\Delta\omega = \frac{\delta\omega}{2}\,(p_B - p_A). \quad (85)$$

Therefore, for very fast exchange, the **X** nuclear resonance is coalesced to one line, and equation (78) has two imaginary solutions.

When $\tau \longrightarrow \infty$ it is important to note that, in general, equation (78) does not have solutions at $\pm\frac{\delta\omega}{2}$. Because the natural line widths, $\sim 1/T_{2A}$ and $\sim 1/T_{2B}$, may be comparable in magnitude to $\delta\omega$, the observed separation $\delta\omega_e = 2\Delta\omega$ in the absence of exchange may be less than the true value $\delta\omega$. Indeed, if T_{2A} and T_{2B} are small enough, then resolution of the two resonance lines is both experimentally and theoretically impossible. This phenomenon results from the overlap of resonance lines. Correction for this effect is made conveniently by letting $2\Delta\omega = \delta\omega_e \longrightarrow 2\Delta\omega_\infty = \delta\omega_\infty$ as $\tau \longrightarrow \infty$ in equation (78).

The result may be written as

$$2\left(\frac{P_B}{T_{2B}} - \frac{P_A}{T_{2A}}\right)\left(\frac{\delta\omega}{2}\right)^5 + 6\Delta\omega_\infty\left(\frac{P_A}{T_{2A}} + \frac{P_B}{T_{2B}}\right)\left(\frac{\delta\omega}{2}\right)^4 +$$

$$2\left\{\left(\frac{P_B}{T_{2B}} - \frac{P_A}{T_{2A}}\right)\left[2\Delta\omega_\infty^2 + \frac{2}{T_{2A}T_{2B}} + \left(\frac{1}{T_{2B}} - \frac{1}{T_{2A}}\right)^2\right] -\right.$$

$$\left.\left(\frac{P_A}{T_{2A}} + \frac{P_B}{T_{2B}}\right)\left(\frac{1}{T_{2B}^2} - \frac{1}{T_{2A}^2}\right)\right\}\left(\frac{\delta\omega}{2}\right)^3 +$$

$$4\Delta\omega_\infty\left\{\frac{1}{T_{2A}T_{2B}}\left(\frac{P_B}{T_{2A}} + \frac{P_A}{T_{2B}}\right) - \Delta\omega_\infty^2\left(\frac{P_A}{T_{2A}} + \frac{P_B}{T_{2B}}\right)\right\}\left(\frac{\delta\omega}{2}\right)^2 +$$

$$2\left\{\left(\frac{P_A}{T_{2A}} - \frac{P_B}{T_{2B}}\right)\left[3\Delta\omega_\infty^4 - \frac{2\Delta\omega_\infty^4}{T_{2A}T_{2B}} - \frac{1}{T_{2A}^2T_{2B}^2} + \left(\frac{1}{T_{2A}} + \frac{1}{T_{2B}}\right)^2\Delta\omega_\infty^2\right] +\right.$$

$$\left.\frac{1}{T_{2A}T_{2B}}\left(\frac{P_B}{T_{2A}} + \frac{P_A}{T_{2B}}\right)\left(\frac{1}{T_{2A}^2} - \frac{1}{T_{2B}^2}\right)\right\}\left(\frac{\delta\omega}{2}\right) +$$

$$\Delta\omega_\infty\left\{\frac{2}{T_{2A}T_{2B}}\left(\frac{P_B}{T_{2A}} + \frac{P_A}{T_{2B}}\right)\left[\frac{2}{T_{2A}T_{2B}} - 2\Delta\omega_\infty^2 - \left(\frac{1}{T_{2A}} + \frac{1}{T_{2B}}\right)^2\right] +\right.$$

$$\left.\left(\frac{P_A}{T_{2A}} + \frac{P_B}{T_{2B}}\right)\left[\frac{2}{T_{2A}^2T_{2B}^2} - 2\Delta\omega_\infty^4 + \left(\frac{1}{T_{2B}^2} - \frac{1}{T_{2A}^2}\right)\right]\right\} = 0. \quad (86)$$

Equation (86) may be used to correct for the overlap of any two Lorenztian line shapes.

In some systems, the overlap effect is negligible and the restriction that

$$\frac{1}{T_{2A}} << \delta\omega >> \frac{1}{T_{2B}} \quad (87)$$

may be imposed on equation (78) (i.e., all terms in $\frac{1}{T_{2A}}$ and/or $\frac{1}{T_{2B}}$ may be neglected). Such a restriction enables one to write equation (78) as

$$2\tau^2\Delta\omega^3 + [\,1 - 2\tau^2(\frac{\delta\omega^2}{2}]\,\Delta\omega + (p_A - p_B)\,\frac{\delta\omega}{2} = 0 \qquad (88)$$

or

$$\tau = \sqrt{\frac{2\,[\,\delta\omega_e + \delta\omega\,(p_A - p_B)]}{\delta\omega_e\,(\delta\omega^2 - \delta\omega_e^2)}} \quad . \qquad (89)$$

When $p_A = p_B$, $\tau_A = \tau_B = 2\tau$, the restriction of equation (44) may often be a valid one. Imposing these restrictions enables one to write equation (78) as

$$\frac{\tau^4}{T_2}\,\Delta\omega^5 + 2\tau^2 s\,(1 + \frac{\tau}{T_2})\,\Delta\omega^3 + \Big[(1 + \frac{\tau}{T_2})\,(1 + \frac{2\tau}{T_2})^2 - \tau\, s\,(2 + \frac{3\tau}{T_2})\Big]\, s\,\Delta\omega = 0, \qquad (90)$$

and equation (86) as

$$(\frac{\delta\omega}{\delta\omega_\infty}) = \pm\frac{1}{\sqrt{3}}\left\{2\left[\frac{16}{(T_2\delta\omega_\infty)^4} + \frac{4}{(T_2\delta\omega_\infty)^2} + 1\right]^{\frac{1}{2}} + 1 - \frac{4}{(T_2\delta\omega_\infty)^2}\right\}^{\frac{1}{2}} , \qquad (91)$$

where s in equation (90), derived from S of equation (75), may be written as

$$s = \frac{1}{T_2} + \frac{\tau}{T_2^2} + \tau(\frac{\delta\omega}{2})^2 \quad . \qquad (92)$$

Equations (90) and (91) are the same as equations (5) and (8) respectively of Gutowsky and Holm (5), who derived them from equation (56). Equation (90) always has one solution at $\Delta\omega = 0$. This solution corresponds

to a maximum in $\mathcal{V}$ for small τ (i.e., fast exchange) and a minimum in $\mathcal{V}$ for large τ (i.e., slow exchange). The other four solutions of equation (90) are given by

$$\Delta\omega = \pm\left[-s\left(\frac{1}{\tau} + \frac{T_2}{\tau^2}\right) \pm s^{\frac{1}{2}}\left(\frac{\delta\omega}{2}\right)^2\left(\frac{T_2}{\tau^3} + \frac{4\,T_2}{\tau^2} + \frac{4}{\tau}\right)^{\frac{1}{2}}\right]^{\frac{1}{2}}. \quad (93)$$

There should always be a solution in each limit $\Delta\omega \longrightarrow \pm\infty$; these correspond to the "wings" of the absorption lines. When the exchange is slow, the remaining two solutions give the maxima in the absorption mode. These two solutions are imaginary when the exchange is fast.

Since the dispersion $\mathcal{U}$ -mode is <u>similar</u> in appearance to the derivative of the absorption $\mathcal{V}$-mode, the position of a resonance dispersion line is taken as that of zero intensity dispersion. For the "two-site" exchange problem the frequency separation of these dispersion intensity nulls in terms of the rate constants may easily be found by setting $\mathcal{U}$ of equation (73) equal to zero. When the restrictions $p_A = p_B$ ($\tau_A = \tau_B = 2\tau$) and that of equation (44) are imposed, the above procedure yields the following equation.

$$\tau^2\Delta\omega^3 + \left\{\frac{\tau}{T_2}\left[2 + \frac{\tau}{T_2}\right] - \tau^2\left(\frac{\delta\omega}{2}\right)^2 + 1\right\}\Delta\omega = 0 \quad (94)$$

The solution at $\Delta\omega = 0$ corresponds to the frequency position of the central minimum absorption for slow exchange, and to the position of the coalesced dispersion line for the case of fast exchange. For this last case the remaining two solutions of equation (94) are imaginary. The two non-zero solutions of equation (94) may be written as

$$\delta\omega_e = 2\Delta\omega = \pm 2\delta\omega\sqrt{\frac{1}{4} - \frac{1}{\delta\omega^2}\left[\frac{1}{T_2^2} + \frac{2}{\tau T_2} + \frac{1}{\tau^2}\right]}. \quad (95)$$

The equation for overlap corrections is obtained by letting $2\Delta\omega = \delta\omega_e \longrightarrow 2\Delta\omega_\infty = \delta\omega_\infty$ as $\tau \longrightarrow \infty$ in equation (95). The result

may be written as

$$\left(\frac{\delta\omega}{\delta\omega_\infty} \right) = \pm \sqrt{1 + \frac{4}{\delta\omega_\infty^2 T_2^2}} \quad . \tag{96}$$

These overlap corrections for the dispersion mode may be very much larger than for the absorption mode. The large difference in these overlap effects is apparent from the plots of equations (92) and (96) shown in Figure 5.

When overlap effects are negligible, imposing the restriction of inequality (87) upon equation (93) yields the following simple relationships between the separation of absorption maxima and the rate constants:

$$\left(\frac{\delta\omega_e}{\delta\omega}\right) = \left(\frac{2\,\Delta\omega}{\delta\omega}\right) = \pm\sqrt{1 - \frac{2}{\tau^2\delta\omega^2}} \quad \text{if } \tau\delta\omega > \sqrt{2}$$

$$\delta\omega_e = 2\Delta\omega = 0 \qquad \text{if } \tau\delta\omega \leq \sqrt{2} \tag{97}$$

This result is the same as equations (6) and (60) of references (5) and (84), respectively.

Imposing the restriction of inequality (87) on equation (95) gives a similar simple relationship between the separation of dispersion lines and the rate constants.

$$\left(\frac{\delta\omega_e}{\delta\omega}\right) = \left(\frac{2\,\Delta\omega}{\delta\omega}\right) = \pm\sqrt{1 - \frac{4}{\tau^2\delta\omega^2}} \quad \text{if} \quad \tau\delta\omega > 2$$

$$\delta\omega_e = 0 \qquad \text{if} \quad \tau\delta\omega \leq 2 \tag{98}$$

The ratio r of maximum to central minimum intensities for the absorption $\mathcal{V}$-mode may easily be related to the rate constants in the region of intermediate rates of exchange. For the "two-site" problem having negligible overlap and each line of common intensity, the $\mathcal{V}$-mode

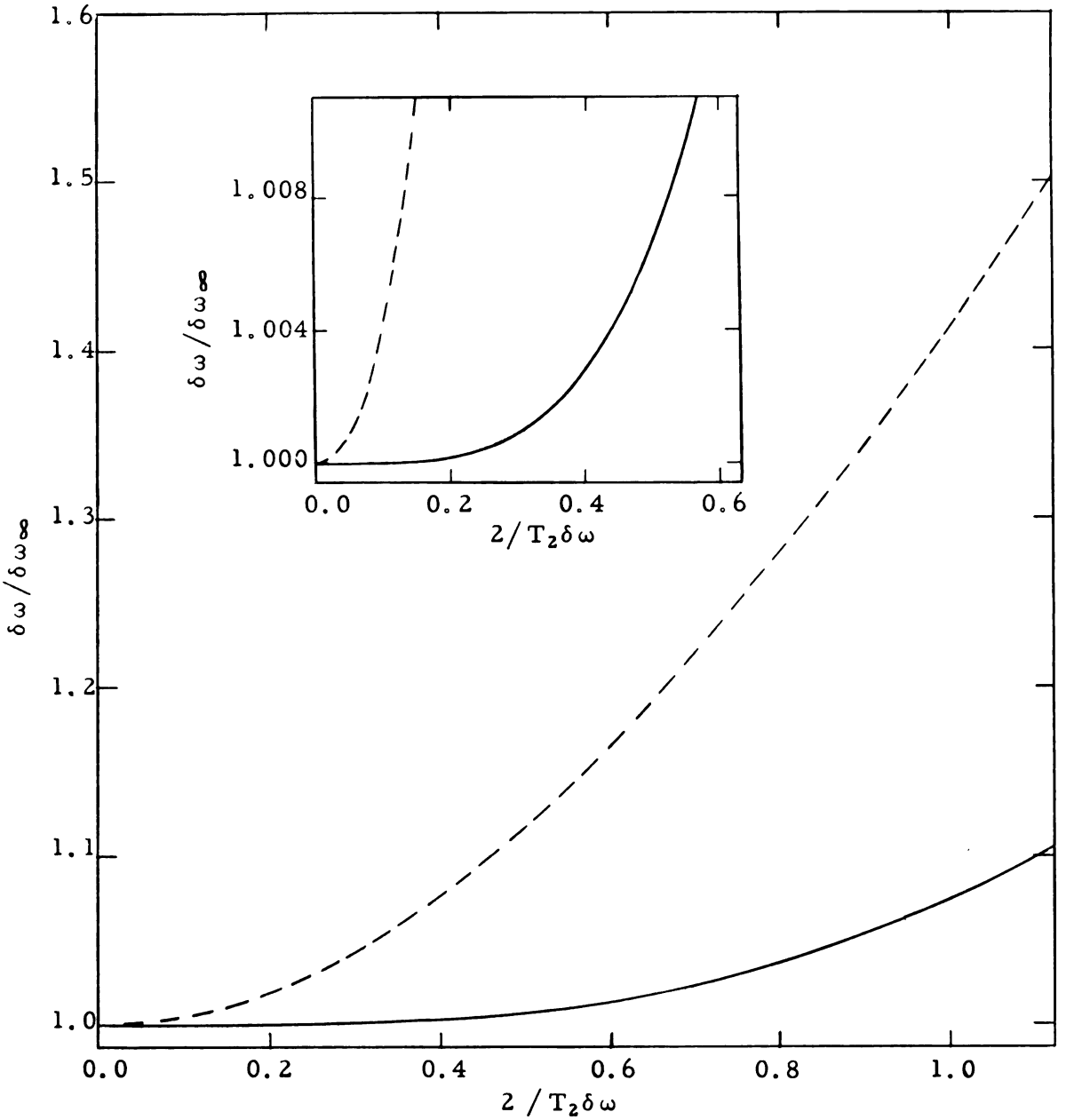

Figure 5. The effect of overlap of two equally intense resonance lines on their apparent separation, as a function of line width $2/T_2$. The observed separation is $\delta\omega_\infty$ and the separation corrected for overlap is $\delta\omega$. Absorption $\mathcal{V}$-mode: solid curves, dispersion $\mathcal{U}$-mode: dashed curves.

shape function is easily obtained from equation (74) by imposing the restriction that $p_A = p_B$ and that equation (87) be valid. The result, written in frequency units of cps, may be written as

$$\mathcal{V} \propto \frac{\tau \delta\nu^2 / 4}{4\pi^2 \left(\frac{\tau \delta\nu^2}{4} - \tau \Delta\nu^2\right) + \Delta\nu} . \qquad (99)$$

For this particular case, the frequency positions of the maxima and minima in $\mathcal{V}$ are given by equations (97) and (90), respectively. These frequency positions may be expressed by

$$\Delta\nu_{max.} = \frac{\delta\nu}{2} \sqrt{1 - \frac{1}{2\pi^2 \tau^2 \delta\nu^2}} \quad \text{if} \quad \tau\delta\nu > \sqrt{2} / 2\pi \qquad (100a)$$

$$\Delta\nu_{min.} = 0 \text{ if } \tau\delta\nu > \sqrt{2} / 2\pi \qquad (100b)$$

From equations (99, 100a and b), the values of $\mathcal{V}_{max.}$ and $\mathcal{V}_{min.}$ may be written as

$$\mathcal{V}_{max.} \propto \frac{\tau^3 \delta\nu^2}{\tau^2 \delta\nu^2 - 1/4\pi^2} \qquad (101)$$

and

$$\mathcal{V}_{min.} \propto 1 / \pi^2 \tau \delta\nu^2 \qquad (102)$$

respectively. The rate constants, in terms of $r = \mathcal{V}_{max} / \mathcal{V}_{min.}$, may be written as

$$\tau\delta\nu = \frac{\pm\sqrt{2}}{2\pi} \cdot \left[r \pm (r^2 - r)^{\frac{1}{2}} \right]^{\frac{1}{2}} . \qquad (103)$$

For the case in which $p_A = p_B$, the rate constants $k_A = k_B$ are equal to $1/2\tau$. In this case, the rate constants are most easily evaluated in terms of the quantity $\tau\delta\nu$. Since $\delta\nu$ is a constant for a given system, the classical Arrhenius-type rate equation (4) may be written as

$$\log_{10} (\tau \delta \nu) = \log_{10} (\frac{\delta \nu}{2 A}) + \frac{E_a}{2.303 RT} , \qquad (104)$$

where R is the molar gas constant, A is the frequency factor for the kinetic process, and E_a is the energy barrier (more precisely, the experimental activation energy) inhibiting the kinetic process. From the value of $\delta \nu$ and the temperature dependence of $\tau \delta \nu$, the quantities A and E_a are conveniently evaluated from the intercept and slope, respectively, of the straight line plot of $\log_{10} (\tau \delta \nu)$ versus $1/T$. Assuming the validity of the absolute rate equation (85), the free energy of activation $\Delta F^{\dagger}$ for the kinetic process may be calculated from

$$\Delta F^{\dagger} = 2.303 RT \log_{10} (\frac{2 \tau kT}{h}) . \qquad (105)$$

Grunwald, Loewenstein and Meiboom have observed the effect of direct chemical exchange upon the absorption τ-mode for a symmetrical spin-spin quartet (74). Using the approach of Gutowsky, McCall, and Slichter (69), they formulated the "four-line" problem having $p_A = P_B = 1/8$ and $p_B = p_C = 3/8$ with $\Delta\omega_A = -\Delta\omega_D = 3\Delta\omega_B = -3\Delta\omega_C$ referred to the average resonance frequency $\gamma H_0 = (\omega_A + \omega_D) / 2 = (\omega_B + \omega_C) / 2$. Their treatment assumed $T_{2A} = T_{2B} = T_{2C} = T_{2D} = T_2$, but it did not necessarily exclude overlap effects. In the region of intermediate rates of exchange they related the rate constants to the ratio of maximum to central minimum intensities. The effects of rates of kinetic processes upon this ratio were calculated numerically for various degrees of overlap. The results of their numerical calculations were presented in graphical form. In the region of fast exchange rates, they related the rate constants to the full line-width at one-half maximum intensity for the coalesced quartet. Numerical calculations, similar to those in the previous case, were made, and these results also were presented in graphical form.

In addition to the "four-line" problem just mentioned, Loewenstein and Meiboom have made similar numerical calculations for spin-spin 1:1 doublets (this is the same as the "two-site" problem discussed earlier) and spin-spin 1:2:1 triplets (the "three-line" problem) (75). The results of these numerical calculations were presented in graphical form. They may be used to account for overlap effects, whereas equation (103), which also applies to the case of a spin-spin 1:1 doublet, is only valid in the event of negligible overlap effects.

In the region of fast exchange rates, another method for evaluating the rate constants for a symmetrical "two-line" (or "two-site") problem has been demonstrated by Takeda and Stejskal (24). These authors have related the rate constants to the ratio of I, the maximum absorption intensity of the coalesced doublet at the exchange rate $1/2\tau$, to I_0, the maximum absorption intensity for the same line when $\tau \longrightarrow 0$. This relationship may be written as

$$\frac{I}{I_0} = \frac{\frac{2}{\tau\delta\omega} + \frac{1}{T_2\delta\omega}}{\frac{2}{\tau\delta\omega} + \frac{1}{T_2\delta\omega} + \frac{T_2\delta\omega}{4}} \quad . \tag{106}$$

This equation is not restricted to cases of negligible overlap, but theoretically it is restricted to cases where $T_{2A} = T_{2B} = T_2$.

In addition to the methods thus far discussed, Piette and Anderson have derived the equation of motion for the RF magnetization, summed over all X nuclei, for a system experiencing effective X nuclear random exchange among any number of magnetic sites (81). This more generalized equation, which may be applied to a spectrum containing any number of lines, may be written as

$$M = -\omega_1 M_0 \frac{\sum_j \left[\frac{p_j}{\frac{1}{T_j'} + i\Delta\omega_j}\right]}{\sum_j \left[p_j \cdot \frac{\frac{1}{T_{2j}} + i\Delta\omega_j}{\frac{1}{T_j'} + i\Delta\omega_j}\right]} \quad , \tag{107}$$

where

$$\frac{1}{T_j'} = \frac{1}{\tau} + \frac{1}{T_{2j}} \quad . \tag{108}$$

Equation (107) is the same as one derived by Arnold (72), only he assumed that all T_{2j} were equal. From equation (107), Piette and Anderson were able to obtain approximate expansions which related the rate constants to the line-widths at one-half maximum intensity.

One expansion is valid in the region of slow exchange rates (i.e., when $| \omega_i - \omega_j | T_j' >> 1$ for any i and j). This expansion may be written as

$$(\pi \Delta \nu) = \frac{1}{T_{2j}} + \frac{(1 - p_j)}{\tau} \quad , \tag{109}$$

where $(\pi \Delta \nu)$ is the measured line-width of the j^{th} resonance line at one-half maximum intensity in units of rps. For cases that may be kinetically represented by equations (48) through (51) with $\tau_A = \tau_B$, equation (109) may conveniently be substituted into the Arrhenius-type rate equation to yield

$$\log_{10}\left[(\pi\Delta\nu) - \frac{1}{T_{2j}} \right] = \log_{10} \left[2A (1 - p_j) \right] - \frac{E_a}{2.303\, RT} \cdot \tag{110}$$

The other expansion derived by Piette and Anderson is valid in the region of fast exchange rates (i.e., when $| \omega_i - \omega_j | T' << 1$, or $| \omega_i - \omega_j | \tau << 1$). This expansion is written as

$$(\pi \Delta \nu) = \frac{1}{T_2} + \nabla \tau \quad , \tag{111}$$

where

$$\nabla = \sum_j p_j \left[\omega_j - \sum_j p_j \omega_j \right]^2 \tag{112}$$

is the <u>second moment</u> (86, 87) of the spectrum in the absence of kinetic exchange processes. In addition to the restrictions mentioned above,

equation (111) also requires that all T_{2_j} are equal and that $\tau \ll T_2$. The equation does not apply to cases where the line-width is large in the absence of exchange (i.e., $\tau \gg T_2$, $T' \approx T_2$, and $|\omega_i - \omega_j| T_2 \ll 1$). As before, when equation (111) is applied to kinetic problems correctly represented by equations (48) through (51) with $\tau_A = \tau_B$, it may be substituted into the Arrhenius-type rate equation to yield

$$\log_{10} [(\pi \Delta \nu) T_2 - 1] = \log_{10} \left(\frac{\nabla T_2}{2A}\right) + \frac{E_a}{2.303\, RT} . \qquad (113)$$

Although the quite general expansions of Piette and Anderson are not valid in the region of intermediate rates of exchange, they should be extremely helpful in the studies of multiple-line spectra.

An earlier statement was made that only systems free of paramagnetic substances would be considered. However, it is pertinent to point out that many of these methods are easily adapted to paramagnetic systems. A very good example of such an adaptation is the treatment of electron exchange reactions as given by McConnell and Berger (85). They used the original formulation of Gutowsky, McCall and Slichter (64) to relate the rate of rapid electron exchange between a diamagnetic site and a paramagnetic site to the line-width for the X nuclear magnetic resonance at the diamagnetic site.

One other important fact should be mentioned. The theory presented in this section really overlooks many minor subtleties that actually exist in any real system. Several very rigorous mathematical considerations have dealt with the effects of kinetic processes upon NMR line shapes (references 84, and 89 through 94). In particular, these works have thoroughly examined the whole general field of nuclear magnetic relaxations. However, there is no cause for alarm. For, although these more profound mathematical treatments have given a better understanding of the true complexities of any real system, they confirm the important general predictions derived in this section from the simple Bloch equations.

EXPERIMENTAL

Spectrometer

The spectra were obtained with a high-resolution nuclear-induction type NMR spectrometer, Varian Associates (VA) Model V-4300-2. A VA Model V-4301C fixed-frequency RF unit and a VA Model V-4331A RF probe were used to obtain NMR spectra at the fixed frequency 40.000 mcs. The frequency was measured with a Collins Type 51J-4 RF receiver against the National Bureau of Standards (NBS) Station WWV. The VA Model V-4301C RF unit utilizes amplitude detection. A VA Model V-4311 fixed-frequency RF unit and a VA modified Model V-4331A RF probe were used to obtain NMR spectra at the fixed frequency 60.000 mcs., also measured with the Collins receiver against NBS Station WWV. The VA Model V-4311 RF unit utilizes phase-sensitive detection. The 60 mcs. probe was modified so that it, and the Model V-4311 RF unit, could be used with or without the simultaneous usage of the VA Model V-4320 spin decoupler. The spin decoupler was capable of transmitting 56.44 or 4.33 mcs. at power levels corresponding to various degrees of NMR saturation.

The static magnetic field was obtained with a VA twelve-inch electromagnet, Model V-4012A-HR, and associated regulated magnet power supply, VA modified Model V-2100A. A field-reversing mechanism was installed in the magnet power supply. This provided a way for cycling the applied large magnetic field to higher homogeneity. A VA model VK-3513 field trimmer was bolted to the yoke of the electro-magnet. This also provided a way for obtaining higher homogeneity in the applied large magnetic field.

Several features were included to insure overall stability for the system. The applied large magnetic field was stabilized with a VA Model VK-3506 magnetic flux stabilizer. Stabilization of the 117 volt A.C. (single-phase) input to the regulated magnet power supply was accomplished with the use of a Raytheon Model VR-6115 voltage stabilizer. The 117 volt A.C. (single-phase) inputs to all other spectrometer and accessory circuits were regulated with a Sorensen Model 1000 S A.C. voltage regulator. Distilled water, used for cooling the electromagnet, was recycled through a refrigerated copper tank. The temperature of the water at the output of this tank was regulated at $18.0 \pm 0.15^{\circ}C$. A commercial air-conditioning unit regulated the ambient room temperature. Air temperature in the region of the magnet was normally stabilized to better than $\pm 2^{\circ}C$. Since overheating of the electromagnet windings may lead to their destruction, two precautionary steps were taken. The usual safety switch in the cooling-water line was set to turn off the current in the electromagnet when the water pressure dropped below a safe value. This switch is of importance in the event of a water-line plug or a malfunction in the recycling pump. In addition, a "thermoregulating" switch was placed in the water tank and wired in series with the pressure switch just mentioned. The "thermoregulating" switch was set so that the current in the electromagnet would be turned off automatically when the water temperature exceeded $95^{\circ}F$. This last precaution is of extreme importance in the event of a malfunction in the refrigeration unit.

Modifications for Observing Spectra at High or Low Temperatures

To use the VA RF probes for observing high-resolution NMR spectra of samples at high or low temperatures, several requirements must be fulfilled. Due to limitations in the homogeneity of the static magnetic

field, spinning samples of small volume must, as usual, be surrounded by a small receiver coil. The temperature of the samples must be regulated precisely at the desired high or low value over long periods of time. Also, the sample must be thermally insulated from the RF probe. This last requirement is necessary because excessive heating or cooling of the RF probes may damage some of their vital components. Heating or cooling of the RF probes may also induce thermal gradients in the nearby magnet pole faces. Such thermal gradients cause undesirable inhomogeneities in the static magnetic field. Therefore, devices were constructed that would enable one to fulfill the above requirements.

Vacuum-jacketed receiver coil inserts -- Two vacuum-jacketed receiver coil inserts were made to plug into the VA Model V-4331A RF probes. Except for the number of turns in the receiver coils, the two inserts were identical. The design for their construction was, in some ways, similar to that used by Shoolery and Roberts (95). One insert had six turns of No. 40 pure copper wire and was used at the RF 40.000 mcs. The other insert had three turns of the same kind of wire and was used at 60.000 mcs.

The vacuum envelope, made of cylindrical Pyrex tubing, provided the necessary thermal insulation between the sample and the RF probe (see Figure 6). A female standard taper, sealed into the top of the envelope, supported a male standard taper sealed to a cylindrical inner tube. This inner tube extended coaxially in the vacuum envelope, down to within about two millimeters from the inner bottom of the envelope. A small Teflon cup was cemented inside the bottom of the inner tube. This cup served as a bearing for spinning sample tubes (about 5 mm. od.). The receiver coil was wound and cemented on the outside of the inner tube, about three-eighths of an inch above the top of the Teflon cup. The receiver coil lead wires were insulated with Teflon and brought out

Figure 6 -- Cross sectional drawing of probe body, vacuum-jacketed receiver coil insert, upper chamber, and mounting plate and tube. Pyrex glass - A = 12 mm. od., B = 24 mm. od., 21 mm. id., C = inner tube, 9 mm. od., 7 mm. id., D = 14 mm. od., 11.6 mm. id., E = 18.6 mm. od., 16.2 mm. id., F = 19 mm. od., G = 8 mm. od., H = sample tube, 0.192 ± .002 in. od., 0.1604 in. id., straight within ± 0.003 in., I = 12/5 ball joints, J = 12/30 standard tapers, K = flared handle; Teflon - L = split rings, M = bearing, N = gasket, O = spinning collet, P = insulator; brass - Q = 4-40 screws, R = 6-32 screws, S = RF coaxial connector; ceramix - T = mounting plug; pure copper - U = receiver coils and leads; V = vacuum envelope; aluminum - W = VA air-driven NMR sample-spinning turbine, X = centering plate for air-driven turbine, 2.5 x 1.5 x 0.25 in., Y = upper chamber, outside 5 x 2.75 x 1.5 in., inside 4.5 x 2.25 x 1.25 in., Z = VA Model V-4331A RF probe body, a = mounting plate, 5.25 x 1.5 x 0.5 in. slotted for b = mounting tube, outside 20 x 0.75 x 0.75 in., c = mounting bolt, 3/8 - 24; filtered air - d = turbine input, e = turbine exit, f = input heating or cooling, g = input heating or cooling, room temperature, h = exit heating and cooling; i = thermocouple junction.

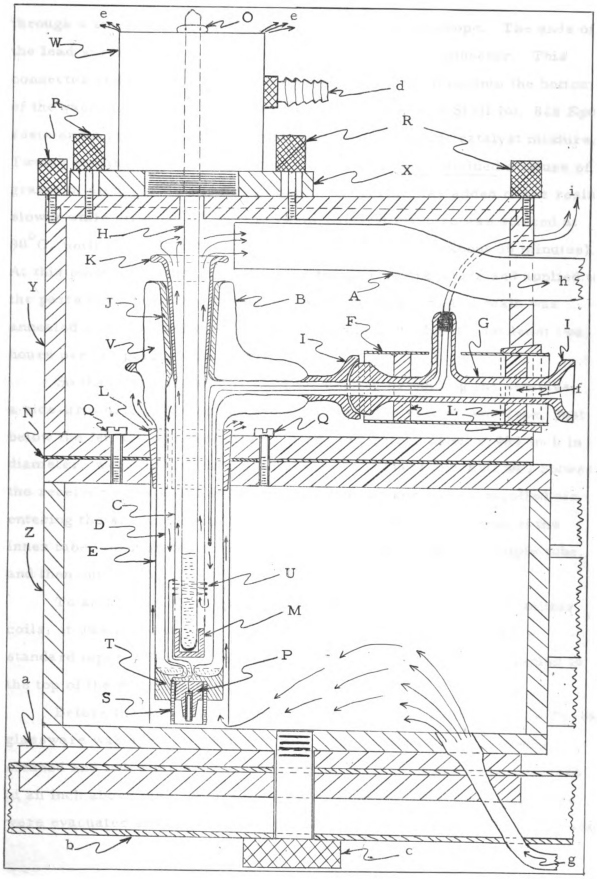
e
O
e
W
d
R
R
X
i
H
K
h
A
Y
J
B
F
G
I
I
V
L
f
L
N
Q
Q
C
D
Z
E
U
M
T
P
a
S
b
c
g

through a small hole in the bottom of the vacuum envelope. The ends of the lead wires were soldered to a brass RF coaxial connector. This connector and its ceramic mounting plug were cemented onto the bottom of the vacuum envelope. All cementing was done with Shell No. 828 Epon resin and a pyromellitic dianhydride-maleic anhydride catalyst mixture. Twenty grams of resin was heated to 70° C., a finely divided mixture of 3.4 grams of dianhydride and 5.6 grams of anhydride was added to the resin slowly while stirring. Then the resin-catalyst mixture was stirred at 90°C. until polymerization just started (this required about 30 minutes). At this point, the mixture was cooled to room temperature and applied to the parts to be cemented together. After application, the resin was annealed at 80°C. and at 20 degree intervals up to 220°C. (at least two hours per temperature interval).

So that dry air could be used for heating or cooling the samples, a side-arm delivery tube was sealed through the vacuum envelope, just below the female standard taper. Also, two holes, about 0.084 inch in diameter, were drilled through the inner tube about one-half way between the receiver coils and the Teflon cup. The temperature controlled air entering the side arm would then flow down around the outside of the inner tube, through the holes at the bottom, up around the sample tube, and then out the top of the insert.

To adjust the RF coupling of the receiver coil to the transmitter coils, it was necessary to be able to turn the inner tube and male standard taper. For this purpose, a flared Pyrex handle was sealed to the top of the male standard taper.

Before the vacuum-jacketed inserts were assembled, all the Pyrex glassware was annealed in a furnace. The jackets were thoroughly cleaned and twice silvered, from the top, down to about three-quarters of an inch above the ultimate levels of the receiver coils. The jackets were evacuated and sealed off at pressures less than 10^{-7} mm. Hg at about

500°C. Each insert was then assembled according to the following procedure. (A) To remove all ferromagnetic surface impurities, all parts were soaked in concentrated hydrochloric acid, rinsed, and then thoroughly dried at 110°C. (B) The receiver coil was wound on the inner tube, clamped firmly in place, cemented, and annealed. (C) The lead wires were insulated with Teflon tape, cemented to the outside of the inner tube, and annealed. (D) A small amount of high-temperature silicon grease was applied to the male standard taper, and the receiver coil lead wires were drawn out through the hole in the bottom of the vacuum envelope while the inner tube was inserted in place. (E) The lead-wire ends were threaded through two small holes in the ceramic mounting plug. (F) This plug was cemented to the bottom of the vacuum envelope, aligned, and then annealed. (G) The coaxial connector was inserted into the ceramic plug with resin. (H) The lead wires were soldered to the connector, the center post of the connector was cemented in place, and then the resin was annealed.

The two vacuum-jacketed receiver coil inserts, assembled in the manner just described, did not break during temperature cycles between -100° and + 220°C. An insert, when placed into the probe, was held firmly in position by means of a Teflon ring around the outside of the vacuum envelope (see Figure 6).

Sample spinning -- An aluminum upper chamber was constructed to fit on the top of each RF probe (see Figure 6). A Teflon gasket was inserted between the probe and upper chamber, and the chamber was made fast with two small brass screws. Among other functions, the upper chamber served as a mounting for a VA air-driven NMR sample-spinning turbine. An aluminum plate on the cover of the upper chamber was threaded to receive the turbine. The plate was fastened to the cover with two brass screws. By using oversized screw holes in the plate,

the turbine could be centered so that sample tubes would spin freely and rapidly. The cover was made to fit the top of the upper chamber closely. This allowed removal and replacement of the cover, plate and turbine as a unit, without disturbing the alignment of the turbine. A hole, 0.25 in. in diameter, was drilled through the cover so that a sample tube could be lowered into the receiver coil insert directly below.

In order to obtain sufficiently free and rapid spinning, the sample tubes had to be extremely straight and well balanced. Therefore, custom-manufactured sample tubes were used (96). These Pyrex glass tubes had the following dimensions--0.192 ± .002 in. od., 0.1604 in. id., straight within 0.003 in., hemispherical bottoms.

A small amount of friction between the spinning sample tube bottom and the Teflon bearing would turn the inner tube in the receiver coil insert. This slight turning was highly undesirable because it caused detuning of the RF coupling between the receiver coil and the transmitter coils. Detuning was prevented by demobilizing the inner tube of the receiver coil insert. This was accomplished by carefully forcing small cork wedges between the side edges of the flared handle at the top of the insert and the walls of the upper chamber.

Probe mounting -- The RF probe was bolted on top of a horizontal mounting plate and tube. The mounting tube was bolted to the probe mounting post. Then the applied field could be mapped, in the usual way, with the RF probe. Also, the RF probe could be moved in and out of the applied field.

With the RF probe located at the center of the applied field gap, one end of the aluminum mounting tube extended well out of the field gap. The out-of-field end of this tube was used for supporting lead wires, cables and other necessary accessories.

Temperature control -- The sample temperature was regulated by passing temperature and flow-rate controlled air through the vacuum jacketed receiver coil insert. At very low or high sample temperatures, the air escaping from the top of the insert caused the upper chamber and RF probe to deviate markedly from room temperature. Thermal conduction through the bottom of the receiver coil insert also caused the RF probe to deviate from room temperature. These difficulties were eliminated by passing room-temperature air into the tuning hole at the bottom of the RF probe whence it flowed through the probe body to the bottom of the insert, up around the outside of the vacuum envelope, through the split Teflon ring and into the upper chamber. This prevented heating or cooling of the probe due to thermal conduction through the bottom of the receiver coil insert. In addition, a Pyrex tube was fitted through the front of the upper chamber. One end of this tube was placed near the top of the receiver coil insert, just below the cover on the upper chamber. The other end was connected to a flexible rubber hose, which led to the intake of an air blower. In this way, the air escaping from the top of the insert, and some room-temperature air, was removed from the upper chamber.

The air which was used for spinning, heating and cooling was taken from a pressure reduction gauge attached to a compressed air line. To prevent contamination of the RF probe and insert the air was filtered. After filtering, the air was split into three flow-rate controlled streams. The flow rate of one stream, used for sample spinning, was controlled with the usual needle valve on the spectrometer. The flow rate of another stream, used for maintaining the probe at room temperature, was controlled with an adjustable gate-type valve. The flow rate of the third air stream, used for regulating the sample temperature, was controlled with a needle valve, a pressure reduction gauge, another needle valve, and a small adjustable leak (series connection in the order

mentioned). For low temperature measurements, this last stream of air was dried with a cold trap and a calcium chloride drying tower. The trap and tower were connected into the line immediately following the series of flow-rate-control valves. Drying was sufficient to prevent harmful frosting at low temperatures. Both the cold trap and drying tower were by-passed for high temperature measurements.

After controlling the flow rate (and drying when necessary), the air for controlling the sample temperature was led into a heat exchanger. For low temperatures, a coil of copper tubing immersed in a liquid air or a dry ice and solvent bath was used as a heat exchanger. In this case, the cooled air was led through silvered and vacuum-jacketed delivery tubes to the input at the front of the upper chamber. For high temperature measurements, a coil of resistance wire, carrying an adjustable current from a powerstat, was used as the heat exchanger. The resistance wire was wound onto an asbestos-covered Pyrex finger which fit into the silvered and vacuum-jacketed delivery tube located at the input to front of the upper chamber (see Figure 7). The sample temperature was controlled at low values by adjusting the flow rate of dry air and the temperature of the bath in which the coil of copper tubing was immersed. The sample temperature was controlled at high values by regulating the flow rate of air and the current flowing through the coil of resistance wire. For sample temperatures above 150°C., a preheater with adjustable dissipation (zero to 500 watts) was placed in the air line just before the coil of resistance wire.

To prevent the receiver coil insert from moving while mapping the field, it was necessary that the delivery tube at the input to the upper chamber be held firmly in place. This was done by clamping the silvered and vacuum-jacketed delivery tube to the aluminum mounting tube (see Figure 7). The delivery tube was clamped so that it exerted a steady inward force against the input to the upper chamber. In this way, the Pyrex ball-joint connections were also held firmly together without the use of clamps.

Figure 7. The RF probe, some accessories for controlling temperature, and the probe mounting. A = sample tube, B = sample-spinning turbine, C = upper chamber, D = RF probe, E = mounting plate, F = mounting tube, G = mounting bolts, H = moveable mounting post, I = vacuum-jacketed heat exchanger and delivery tube, J = lead wires for the heating element, K = armored lead wires for the thermocouple, L = input of air for control of sample temperature, M = input of room-temperature air to the probe body, N = exit of heating and cooling air, O = input of air to the sample-spinning turbine.

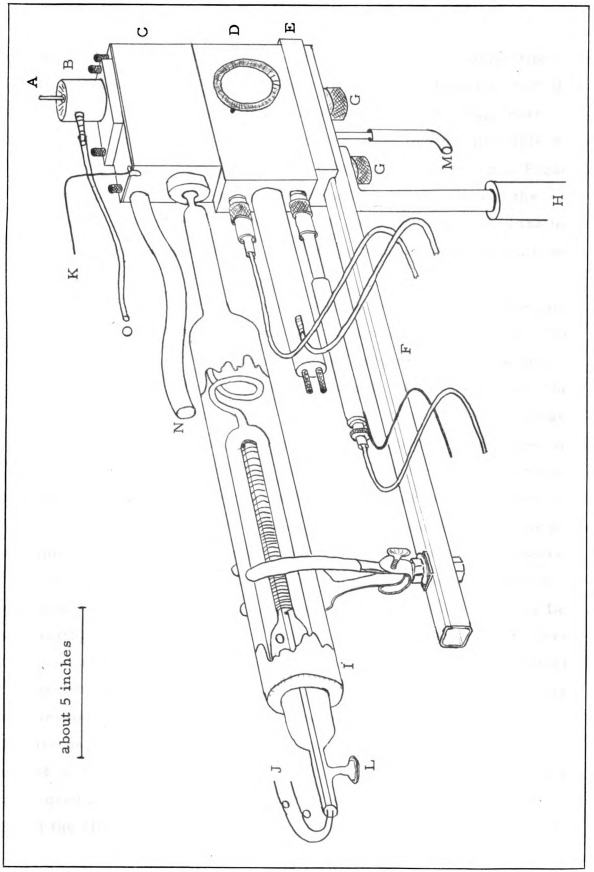
A
B
C
D
E
G
G
M
H
K
O
N
F
I
J
L
about 5 inches

Temperature measurement -- The sample temperature was monitored with a copper-constantan thermocouple (No. 30 wire) in conjunction with an adjustable bucking voltage, a Leeds and Northrup Model 9835-B D.C. microvolt amplifier, and a Brown Model Y153X10V-X6 strip chart recorder. The measuring-junction lead wires of the thermocouple were cemented into a side-arm double-ball-joint adapter as shown in Figure 6. The measuring junction was then threaded into the side arm of the receiver coil insert and down between the vacuum envelope and the inner tube of the insert. The junction was finally located about one-half inch above the receiver coil.

The E.M.F. of the measuring junction, versus a reference junction at 0°C., was monitored with a circuit as diagramed in Figure 8. The pure copper wires from the measuring and reference junctions were connected to the Input I as labelled in Figure 8. With this circuit, the temperature could be measured to $\pm 0.02^{\circ}$C. and monitored to changes of less than $\pm 0.002^{\circ}$C. In practice, the temperature was adjusted to the desired value, measured, and then monitored for deviations from the measured value. The deflection of the linear recorder scale (zero to 12 mv.) was calibrated in microvolts per inch for all setting of the scale multiplier of the D.C. microvolt amplifier. These calibrations were made by applying known microvoltages to Input I. The known microvoltages were obtained from a constant-current controller and two Leeds and Northrup standard resistors, one ohm and one kilohm. The thermocouple was calibrated, while connected to Input I, at the temperatures of the equilibria for carbon dioxide sublimation, melting pure ice, sodium sulfate-sodium sulfate pentahydrate transition, and boiling pure water. The temperature - E.M.F. calibrations were in agreement (within $\pm 0.04^{\circ}$C.) with literature values (111). Therefore, the literature data were used in constructing the working E.M.F. versus temperature curves. From the slopes of these curves, the recorder scale defection was then

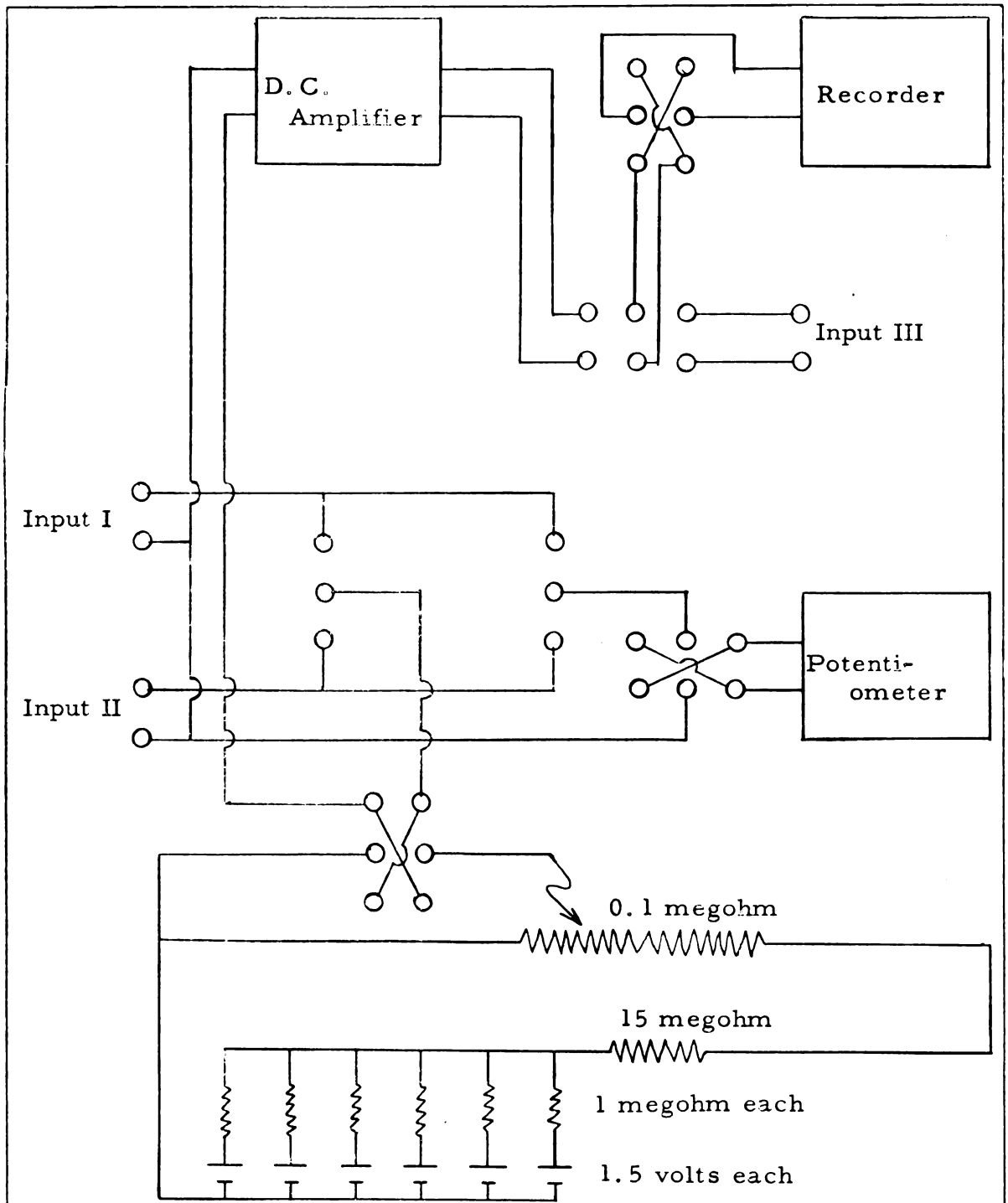

Figure 8. Diagram of circuit used for monitoring and measuring sample temperatures.

calibrated in degrees per inch for each setting of the scale multiplier of the D.C. amplifier. Calibrations were made at ten degree intervals.

Sample temperatures could be controlled for long periods of time to about ± 0.1°C. in the region zero to 100°C. In the regions -100 to zero °C. and 100 to 220° C., sample temperatures could be controlled to about ± 0.5°C.

Current Shims

For a field gap of 1.75 inches between the magnet pole faces, applied fields greater than 15.5 kilogauss could be obtained with the electromagnet and regulated magnet power supply. However, at these higher values of the applied field, properly cycled, "flat," and homogeneous fields could not be obtained. To obtain high-resolution fluorine magnetic resonance spectra at the RF 60.000 mcs. (an applied field of about 14.979 kilogauss), shim coils were constructed to give the necessary homogeneity.

The shim coils consisted of a pair of figure-eight coils and two pairs of concentric circular coils. The diameter of the figure-eight coils was about 2.25 inches. Each pair of circular coils had one coil four inches in diameter and the other coil 1.5 inches in diameter. Each pair of concentric circular coils was fastened with celluloid tape to separate sheets of stiff paper backing. A figure-eight coil was taped over each pair of circular coils so that the center of the figure-eight coil coincided with the common axis of the circular coils. Each figure-eight coil was wound so that D.C. in the two loops would flow in opposite senses (see Figure 9). The loops were made with six turns of No. 40 pure copper wire. Each circular coil was made with ten turns of the same kind of wire.

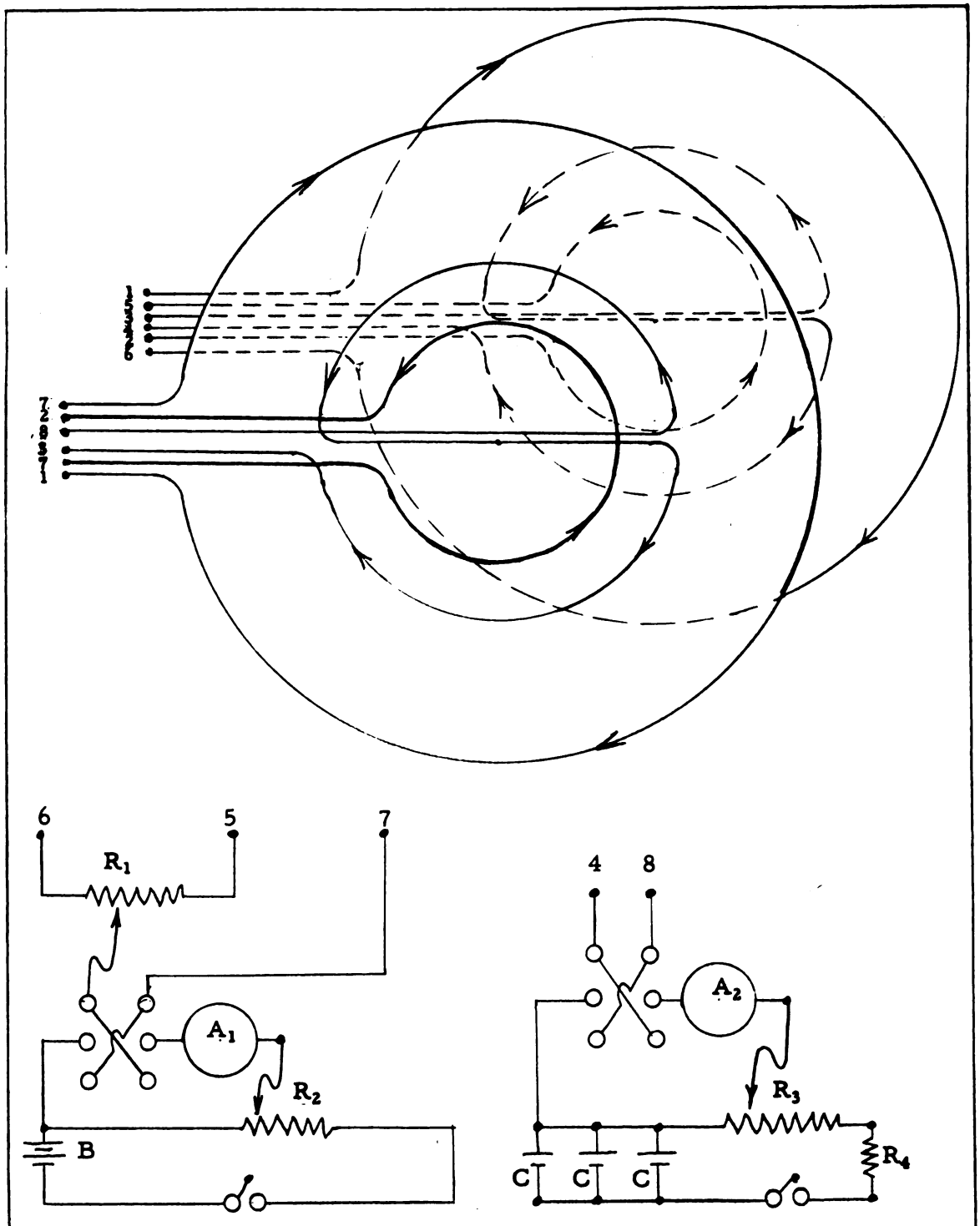

Figure 9. Diagram of shim coils and circuits. Ammeters -A_1 = 0 to 200 ma., A_2 = 0 to 100 ma.; helipots -R_1 = 70 ohms, R_2 = R_3 = 1 kilohm; R_4 = 200 ohms; B = battery of Edison cells, ca. 15 volts; C = dry cells, 1.5 volts. Connections between all points having common numbers are omitted.

The paper-backed coils were taped to either side of the RF probe, figure-eights in a vertical position, so that the axis of the circular coils passed through the center of the receiver coil inside the probe. Since the sides of the RF probe were parallel, the Helmholtz condition was obtained for the two circular coils of large diameter, and for the two of small diameter.

Each pair of circular coils was so connected that D.C. in the coil of large diameter would always flow in the opposite sense to that in the coil of small diameter. The steady voltage for the D.C. in the circular coils was obtained from a battery of Edison cells. The direction of this D.C. could be reversed, and the magnitude of the current was adjustable. The magnitude of the D.C. flowing in the circular coils could also be divided between the coils of large and of small diameters. The steady voltage for the D.C. in the figure-eight coils was obtained from three dry cells connected in parallel. The direction of this current could be reversed, and its magnitude was adjustable.

The shim coils were used only when observing high-resolution fluorine magnetic resonance at the RF 60.000 mcs. The circular coils were used to flatten the undercycled ("dome-shaped") static magnetic field. The flattening was accomplished by choosing the direction of D.C. in the small circular coils such that the magnetic field at the sample produced by these coils would be in opposition to the applied large magnetic field. The magnetic field at the sample produced by the large circular coils would then be in the same direction as the applied large magnetic field. The D.C. was divided between small and large circular coils so that a null field due to all the circular coils was produced at the sample. After the field at the sample due to the circular coils had been nullified, the degree of shaping could easily be adjusted by varying the total amount of current flowing in the circular coils. The effective field at the sample was usually undercycled for currents below about

120 milliamperes. Very "flat" (usually very homogeneous) effective fields at the sample were obtained for current values in the region about 120 to 175 milliamperes. For larger current values, the effective field was usually overcycled ("dish-shaped").

Occasionally the inhomogeneity along the vertical y-axis could be removed more easily by using the figure-eight shim coils than by shimming the electromagnet. Spinning of the sample usually caused sufficient averaging of the inhomogeneity along the horizontal x-axis. The necessary D.C. in the figure-eight coils was only from zero to ten milliamperes. For this reason, the figure-eight coils probably would have been much more useful had each loop contained only one turn of wire. A coil of one turn per loop could have been wound much more symmetrically than the coils having six turns per loop.

Resolution

With the apparatus described above, the limits of resolution at the RF 60.000 mcs. were approximately as follows: protons - 0.2 cps, 0.0033 ppm, or 0.047 milligauss; F^{19} - 0.5 cps, 0.0083 ppm, or 0.124 milligauss. The limits of resolution (but not the intensities) at the RF 40.000 mcs. were slightly better than at 60.000 mcs.

Materials Used

The materials for which data were obtained are tabulated in Table III. Physical constants listed as "observed" in this table are for the materials used in the preparation of samples. The observed values may be compared with the tabulated literature values.

The amide N, N-dimethyltrifluoroacetamide was prepared by allowing trifluoroacetic anhydride to react with anhydrous dimethylamine (the molar ratio of anhydride to amine was 2:1). The anhydride was added

SOME PHYSICAL CONSTANTS FOR MATERIALS USED

TABLE III

SOME PHYSICAL CONSTANTS FOR MATERIALS USED

	Observed			Literature			
	m.p., °C.	b.p., °C.	mm.	m.p., °C.	b.p., °C.	mm.	Reference
$HCON(CH_3)_2$ [c]		151.5	740	-61	153	760	(97)
$CH_3CON(CH_3)_2$ [c]		59.0	9	-20	165	758	(97)
$C_2H_5CON(CH_3)_2$ [c]		58.5	10	-45	175.5	765	(97)
$CF_3CON(CH_3)_2$ [a]		134.3	740		135	760	(98)
$CH_2 = CHCON(CH_3)_2$ [d]		46.0	3		96-104	35	(99)
$ClCON(CH_3)_2$ [d]		58.0	30	-33	167	754	(100)
$C_6H_5CON(CH_3)_2$ [a]	40-41			41-42	273	760	(101)
$CH_3CON(C_6H_5CH_2)_2$ [a]		194.2	1		195	3	(102)
$C_2H_5OCON(CH_3)_2$ [a]		142.0	733		147	760	(8)
$CH_3OCON(CF_3)_2$ [b]		76	760		76	760	(98)
$CF_3CON(CF_3)_2$ [b]		30	760		30	760	(98)
CH_2Br_2 [c]		96.0	740				
CCl_4 [c]		76.0	743				
$CCl_3CON(CH_3)_2$ [a]		85.2	5	Requires: 25.22 C, 3.18 H, 55.85 Cl, and 7.36% N.			
				Found: 25.43 C, 3.25 H, 55.66 Cl, and 7.52% N.			

[a] Prepared in this laboratory.
[b] Prepared in the laboratory of Professor J. A. Young, University of Florida, Gainesville, Florida.
[c] Purchased from Distillation Products Industries, Eastman Organic Chemicals Department, Rochester, N. Y.
[d] Purchased from K. and K. Laboratories, Inc., Jamaica, N. Y.

slowly to an ether solution of the amine. During addition of the anhydride, the reaction vessel was immersed in an ice-hydrochloric acid bath, and the reaction mixture was stirred. After complete addition of the anhydride, the mixture was neutralized with aqueous sodium bicarbonate. The ether layer was separated and dried over anhydrous sodium sulfate and the ether was then removed by distillation. Distillation of the product in vacuo yielded a colorless liquid at a constant boiling point.

The amides N, N-dimethylbenzamide, ethyl-N, N-dimethylcarbamate, N, N-dimethyltrichloroacetamide, and N, N-dibenzylactamide were all prepared by allowing the appropriate acid chloride to react with the appropriate anhydrous amine (the molar ratio of acid chloride to amine was less than one-half). In each case, the acid chloride was added slowly to an ether solution of the amine. During addition of the acid chloride, the reaction vessel was immersed in an ice-hydrochloric acid bath, and the reaction mixture was stirred. The amine hydrochlorides were removed by filtration. Excess dibenzylamine was removed by addition of anhydrous hydrogen chloride prior to filtration. In each case, the filtrate was dried over anhydrous sodium sulfate and the ether removed by distillation. Excess dimethylamine was removed during distillation of the ether. After two recrystallizations from ether-hexane mixtures, N, N-dimethylbenzamide was obtained as colorless crystals with a sharp melting point. The amides N, N-dibenzylacetamide, ethyl-N, N-dimethylcarbamate, and N, N-dimethyltrichloroacetamide were obtained by distillation in vacuo. Each compound was colorless and had a constant boiling point. The amides ethyl-N, N-dimethylcarbamate and N, N-dimethyltrichloroacetamide were liquids of low viscosity, whereas N, N-dibenzylacetamide was a highly viscous oil. No reference to N, N-dimethyltrichloroacetamide could be found in the literature. Therefore, a sample was submitted to carbon, hydrogen, chlorine, and nitrogen analyses (see Table III).

The two amides methyl-N, N-bis-(trifluoromethyl)-carbamate and N, N-bis-(trifluoromethyl)-trifluoroacetamide were prepared and purified in the laboratory of Professor J. A. Young at the University of Florida. The colorless liquids were distilled under reduced pressure directly into sample tubes.

The remaining compounds listed in Table III were obtained from commercial laboratories. Each compound was dried over anhydrous sodium sulfate and then fractionated (usually in vacuo). Only colorless liquids having constant boiling points were used in the preparation of samples.

Preparation of Samples

Data were obtained for the following pure liquid amides: N, N-dimethylformamide; N, N-dimethylacetamide; N, N-dimethylpropionamide, N, N-dimethyltrichloroacetamide; N, N-dimethyltrifluoroacetamide; N, N-dimethylcarbamyl chloride; ethyl-N, N-dimethylcarbamate; methyl-N, N-bis-(trifluoromethyl)-carbamate; and N, N-bis-(trifluoromethyl)-trifluoroacetamide. In addition, data were obtained for the following solutions: 84.7_1, 68.8_8, 58.0_0, 40.5_7, 22.1_7, and 10.1_4 mole per cent N, N-dimethylpropionamide in dibromomethane; 69.3_4, 39.9_4, and 11.0_7 mole per cent N, N-dimethylpropionamide in carbon tetrachloride; 90.0_3, 63.4_4, 40.9_2, and 10.7_2 mole per cent N, N-dimethylcarbamyl chloride in dibromomethane; 71.3_4, 40.0_8, and 10.9_8 mole per cent N, N-dimethylcarbamyl chloride in carbon tetrachloride; 36.3_4 mole per cent N, N-dimethylbenzamide in dibromomethane; 38.0_9 mole per cent N, N-dibenzylacetamide in carbon tetrachloride. The concentrations were determined from the weights of pure components, and care was taken to prevent changes in concentrations due to volatilization. Also, care was taken to prevent contamination of the samples, especially with water.

Each sample, consisting of about one-half a milliliter of liquid, was thoroughly degassed by reducing the pressure over the solid to about 10^{-4} mm. Hg at the boiling point of air. At this pressure and temperature, a vacuum-tight seal was made at the top of each sample tube.

For some high-temperature studies not reported in this thesis, it was necessary to observe spectra for some liquids near and/or above their normal boiling points. In such a case, the liquid would distill from the warmer lower portion of the sample tube to the cooler upper portion of the tube. To prevent distillations of this type, the liquid was confined in the temperature-controlled lower portion of the tube. This was accomplished by drawing the sample tube off to form a vacuum-tight seal just above the degassed and frozen sample. The short sample tube was resealed to the drawn-off end so that a vacuum-tight constriction still remained just above the frozen sample. Then the sample tube was placed in a machine lathe, and straightened with a gas-oxygen flame. One end of the tube was held tightly by a collet-type headstock, and the other end was held loosely in a chuck-type tailstock. The tube was rotated slowly while the glass was softened with the flame. Then the lathe was stopped, and the tube was drawn slightly with the tightened tailstock.

Determination of Energy Barriers for Hindered Internal Rotations

High-resolution NMR absorption spectra were obtained for all the samples at the radiofrequency 60.000 mcs. and for some of the samples at 40.000 mcs. Linear sweep rates in the region from about 0.011 to 0.013 ppm per second were used. Internal frequency separations were determined by the side-band technique. The audio frequencies for producing side bands were derived from a

Hewlett-Packard Model 200 CD wide-range oscillator or a Hewlett-Packard Model 202A low-frequency function generator. The audio frequencies were counted directly with a Hewlett-Packard Model 521A electronic counter, which was calibrated against NBS Station WWV.

Chemical nonequivalence between the protons of one N-substituent and those of the other N-substituent was observed for most of the symmetrically N, N-disubstituted amides studied. The energy barrier for internal rotation about the central C-N bond was determined for each of these compounds. Three methods for obtaining the energy barriers were investigated.

Method I - The first method that was considered was that originally proposed by Piette and Anderson (81). They used the method to estimate the energy barriers for hindered internal rotations about the O-N bond of some alkyl nitrites. At the beginning of this present research, attempts were made to estimate the energy barrier for internal rotation about the central C-N bond of N, N-dimethylpropionamide dissolved in dibromomethane (40.5_7 mole percent amide). In the region of slow rates of internal rotation, the line width at one-half maximum intensity was measured at several temperatures for the proton resonance of each N-methyl group. The proton spectra were obtained at the radio-frequency 60.000 mcs. and at linear sweep rates in the region from about 0.011 to 0.013 ppm per second. The linear sweep scale was calibrated by the side-band technique. The magnitude of the applied RF field H_1 was reduced well below the lowest value giving noticeable saturation. Several spectra were recorded at each temperature with the linear sweep field varying first in the increasing direction, and then in the decreasing direction. The recordings were made with a Sanborn Model 151-100A fast-response graphic recorder in conjunction with a

Sanborn D.C. amplifier. Chart speeds of 10 or 20 mm. per second were used, and the line widths were measured directly from the recordings. The natural line width $2/T_{2j}$ (the line width in the absence of internal rotation) was measured for the proton resonance of each N-methyl group at low temperatures. The two natural line widths were slightly different because of the very weak nonequivalent spin-spin interactions of the protons of each N-methyl group with the methylene protons of the ethyl group. These spin-spin interactions could not be resolved. The natural line width of the proton resonance of the dibromomethane solvent was measured at each temperature. This measurement was made by the "decay-of-wiggles" technique (103). The natural line width of the proton resonance of each N-methyl group was obtained at each temperature from the appropriate measured value at the lowest temperature used, the measured value for dibromomethane at the lowest temperature used, and the measured value for dibromomethane at the temperature in question. The following equation was used:

$$[(1/T_2)^{t_0} - (1/T_2)^{t}]_{N\text{-}CH_3} = [(1/T_2)^{t_0} - (1/T_2)^{t}]_{CH_2Br_2} \qquad (115)$$

In this equation, $(1/T_2)^{t_0}$ represents one-half the natural line width of the proton resonance of the designated group at the lowest temperature t_0 (i.e., in the absence of internal rotation about the central C-N bond of the amide), and $(1/T_2)^{t}$ represents the similar value at the temperature t. At the lowest temperature t_0, all natural line widths were determined from spectra recorded under conditions of identical homogeneity in the applied field H_0. At each higher temperature t, the natural line width for the proton resonance of dibromomethane and the line widths for the proton resonances of the N-methyl groups were also determined from spectra recorded under conditions of identical homogeneity.

Natural line widths for the proton resonances of the N-methyl groups were found to be in the region from about 0.6 to 1.2 cps. The chemical shift between the two peaks in the absence of internal rotation (at lower temperatures) was about 7.5 cps. At higher temperatures, the onset of internal rotation caused the expected broadening and coalescence of the two peaks. Because of the coalescence, the broadening of the two line widths could be measured only in the region from about 0.6 to 2.0 cps. Since the line widths could be measured only to about $\pm$ 0.3 cps, the estimation of the energy barrier E_a from equation (110) was very unreliable.

In the region of fast internal rotation (at higher temperatures), the proton resonance of the two N-methyl groups was coalesced to a single line. The width at one-half maximum intensity of this line was measured at several temperatures above the NMR coalescence temperture T_c (the lowest temperature at which the observed chemical shift between the proton resonances of the N-methyl groups equals zero). The natural line width $(2/T_2)^t$ of the coalesced line at each temperature t was obtained from equation (115) and the following values: (1) the measured value of the natural line width of the coalesced line at the highest temperature used $(2/T_2)^{t_0}_{N(CH_3)_2}$, (2) the measured value of the natural line width for the proton resonance of dibromomethane at the highest temperature used $(2/T_2)^{t_0}_{CH_2Br_2}$, and the measured value for dibromomethane at the temperature in question $(2/T_2)^{t}_{CH_2Br_2}$. The rotational narrowing of the coalesced line width could be measured only in the region from about 3.0 to 0.8 cps. Again, because of the errors in the line-width measurements, the estimation of the energy barrier from equation (113) was very unreliable.

Method II - The second method that was considered was that originally developed by Gutowsky and Holm (5, 6). They used the method

to estimate the energy barriers for internal rotation about the central C-N bond of N, N-dimethylformamide and N, N-dimethylacetamide. Their measurements were made at the radiofrequency 17.735 mcs., whereas the measurements made by their method in the present work were made at the radiofrequency 60.000 msc. Their method was used to determine the energy barrier for internal rotation about the central C-N bond of N, N-dimethylformamide. The method consists of the measurement of the frequency separation of the proton resonances of the N-methyl groups at several temperatures. Linear sweep rates in the region from about 0.011 to 0.013 ppm per second were used, and the magnitude of the applied RF field was reduced well below the lowest value giving noticeable saturation. The sweep scale was calibrated with two narrow reference signals, one on each side of the proton resonance doublet for the N-methyl groups. The coalesced proton resonance of the N-methyl groups of N, N-dimethylcarbamyl chloride was used as the low-field reference signal, and the proton resonance of the methyl group of acetophenone was used as the other reference signal. The reference compounds were sealed in small Pyrex capillaries, which were inserted inside the sealed sample tube. The separation of the two reference peaks was measured at each temperature by the side-band technique. This separation was found to be invariant, within experimental error, with changes in temperature. The separation $\delta\nu_e$ of the proton resonances of the N-methyl groups of N, N-dimethylformamide was measured in terms of the constant separation of the reference peaks in the absence of audio-frequency modulation. Six measurements were made at each temperature. The recordings were made with the Sanborn recorder and D. C. amplifier.

The proton resonance of each N-methyl group was split into a doublet by the spin-spin coupling with the aldehyde proton.

This splitting was resolved under conditions of very slow sweep (about 0.0027 ppm per second) and very high resolution. The splitting of the low-field N-methyl proton resonance was about 0.28 cps, whereas that of the high-field N-methyl proton resonance was about 0.56 cps. Therefore, the effective natural line widths of the proton resonances of the two N-methyl groups were different. The chemical shift $\delta\nu$ between the two peaks in the absence of internal rotation was about fifteen times larger than either effective natural line width. For this reason, no overlap corrections were made. In the region of interest, the observed separations $\delta\nu e$ of the two peaks could be measured only to about ± 0.6 cps.

Equation (97) may be written in units of cps as

$$1/\tau\,\delta\nu = \pi\sqrt{2}\;\sqrt{1-(\delta\nu e/\delta\nu)^2} \qquad (114)$$

From the average of each set of six values of $(\delta\nu e/\delta\nu)$, the rate of internal rotation $1/2\tau$ was calculated as $1/\tau\,\delta\nu$ from equation (114) for each temperature. Using equation (104), the energy barrier E_a and the frequency factor A for the internal rotation were then calculated from the least-squared straight line slope and intercept, respectively, for the plot of $\log_{10}(4\pi^2\tau\,\delta\nu)$ against $1/T$. The NMR coalescence temperature T_c and the rate of internal rotation $1/2\tau$ at 298.2° K. were calculated from the least-squared data. Somewhat naively assuming the validity of the absolute rate equation, the free energy of activation for the internal rotation at 298.2°K., $\Delta F^{\dagger}_{298.2}$, was calculated from equation (105).

Method III - The third method consisted of the measurement of the ratio r of maximum to central minimum intensities of the resonances due to the α - protons of the two N-substituents of the particular symmetrically N, N-disubstituted amide in question. The ratios were measured at several temperatures. Most of the amides used in this

research were studied by this method. Of the three methods considered, this last one yielded the most reliable energy barriers for internal rotation. All spectra were observed at the radiofrequency 60.000 mcs. The procedure used for all the compounds is described in the following paragraphs.

The chemical shift $\delta\nu$ between the two resonance peaks due to the α-protons of the two N-substituents in the absence of internal rotation was determined by the side-band technique. The Sanborn recorder and D.C. amplifier were used for making these measurements. The value of $\delta\nu$ was taken as the largest measureable value of the separation $\delta\nu_e$ between the two resonance peaks. As expected, this value was always observed at the lower temperatures used for a given amide.

The ratios r were calculated from spectral intensities taken directly from the records of the spectra. In each case, the value of r was calculated as the ratio of the average of the maximum intensities for the two resonance peaks to the intensity of the central minimum. The average of the base lines on either side of the doublet was used for obtaining the spectral intensities. All measurements of the ratio r were taken from spectra recorded with a VA Model G-10 graphic recorder in conjunction with the Sanborn D.C. amplifier. These spectra were all recorded at about the same linear sweep rate (from about 0.011 to 0.013 ppm per second). Also, the spectra were all recorded at the same magnitude of the applied RF field H_1, which in every case was well below the lowest value giving noticeable saturation. Each spectrum was observed with the damping of the RF receiver set at maximum. The gain of the D.C. amplifier and/or recorder were adjusted so that the base line of each spectrum would fall at the lower edge of the chart paper, and so that the maxima in each spectrum would fall at the upper edge of the chart paper. This adjustment gave spectral intensities corresponding to deflections from about 100 to

120 mm. on the chart paper. The base line was adjusted to fall, as closely as possible, at a common level on both sides of the spectrum. This adjustment was made with the adjustable RF reference phase of the phase-sensitive detector, and the adjustment always provided the best observable approximation to Lorentzian line shapes. The base lines on either side of the spectrum seldom disagreed by more than two millimeters. Before recording the spectrum at each temperature, a region of high homogeneity in the applied field H_0 was found by mapping the field with the RF probe and a standard sample. At low temperatures, thoroughly degassed acetaldehyde was used as the standard sample; the ringing of the narrow lines of the quartet due to the resonance of the aldehyde proton was used as the criterion for homogeneity. At higher temperatures, thoroughly degassed pentachloroethane was used as the standard sample; the ringing of the proton resonance was used as the criterion for homogeneity. From eight to twelve spectra of the amide doublet were then recorded at each temperature. The spectra were obtained in pairs. The first spectrum of each pair was recorded with the linear sweep field varying in the increasing direction, whereas the second spectrum was recorded with the linear sweep field varying in the decreasing direction. Between each pair of observations, the RF probe was moved slightly in the applied field H_0. The reason for each slight movement of the probe was to attempt to find a region of higher homogeneity in the applied field.

For each substituted amide studied in this work, the chemical shift $\delta\nu$ between the resonance peaks due to the α-protons of the N-substituents in the absence of internal rotation was much larger than either of the two effective natural line widths. Therefore, no overlap corrections were made. The average of the five highest values

of the ratio r obtained at each temperature (the average of the five values corresponding to highest homogeneity in the applied field at each temperature) were used to obtain the rate of internal rotation at each temperature. The rates $1/2\tau$ were obtained as $\log_{10}(4\pi^2\tau\delta\nu)$ from a plot of $\log_{10}(4\pi^2\tau\delta\nu)$ against the ratio r (see Figure 10). The curve was calculated with the use of equation (103). Also shown in Figure 10, is a plot of $\log_{10}(4\pi^2\tau\delta\nu)$ against the quantity $(\delta\nu_e/\delta\nu)$, as calculated from equation (114). The values of E_a, A, T_c, and $\Delta F^{\dagger}_{298.2}$ were calculated by the methods previously described in Method II.

Of the N, N-dimethyl amides studied, ethyl-N, N-dimethylcarbamate was the only one for which the energy barrier for internal rotation was not determined. This compound showed only one narrow resonance peak for the protons of the N methyl groups from room temperature down to the freezing point of the compound. Energy barriers for internal rotation could not be determined for methyl-N, N-bis-(trifluoromethyl)-carbamate and N, N-bis-(trifluoromethyl)-trifluoroacetamide. The fluorine resonance for the N-trifluoromethyl groups of the former compound consisted of one narrow resonance line from room temperature down to the freezing point. The fluorine resonance for the N-trifluoromethyl groups of the latter compound consisted of a symmetrical 1:3:3:1 quartet from room temperature down to the freezing point. The quartet arises from the spin- spin coupling of the fluorine nuclei of the two equivalent N-trifluoromethyl groups with the three fluorine nuclei of the C-trifluoromethyl group.

The protons of each phenyl group of N, N-dibenzylacetamide were found to be essentially equivalent, whereas the protons of one methylene group were chemically nonequivalent from those of the other methylene group. The proton resonance doublet for the methylene groups was used for obtaining the energy barrier for internal rotation about the central C-N bond of this compound.

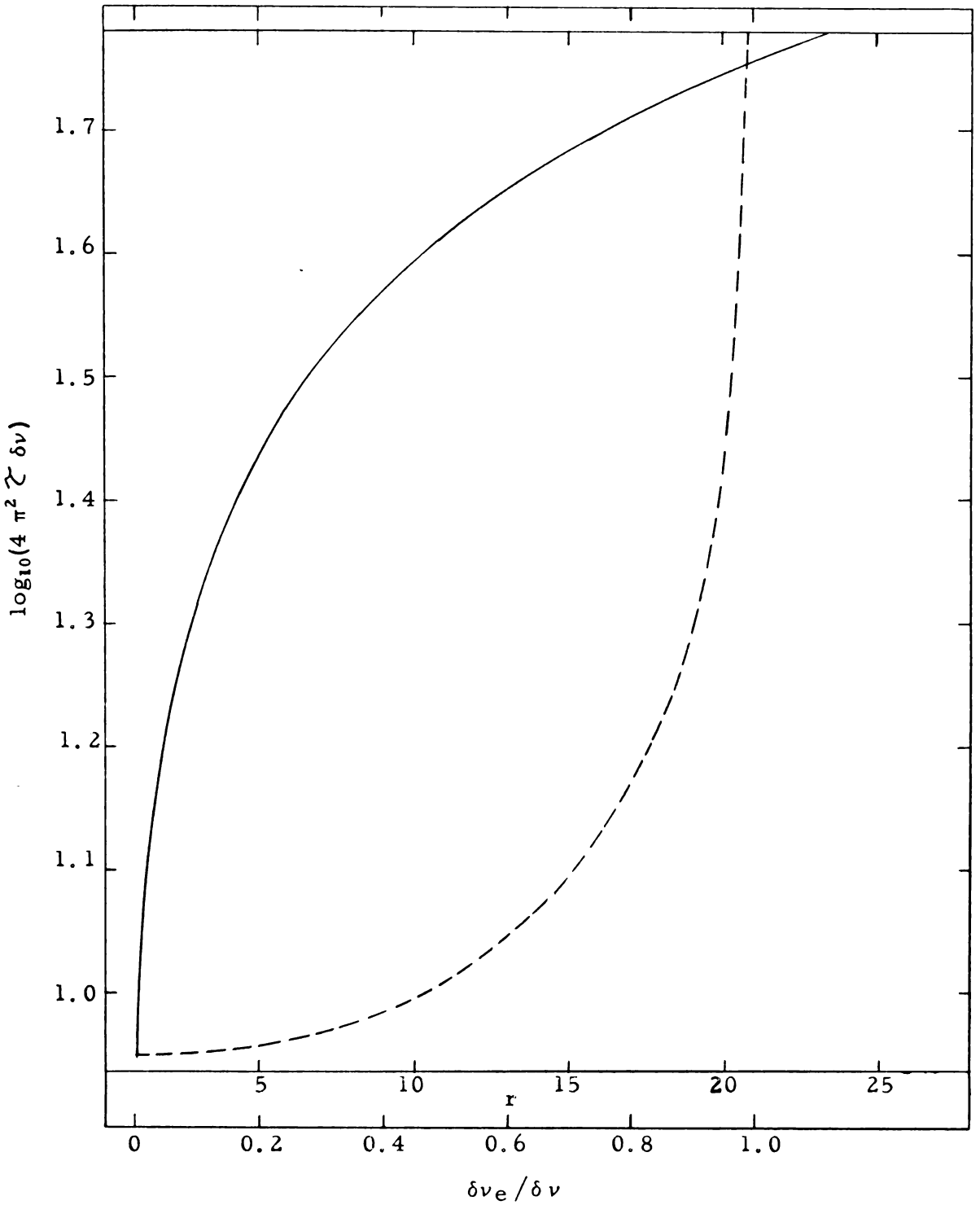

Figure 10. Solid curve: ratio of maximum to central minimum intensities, r, for two equally intense absorption lines as a function of exchange rate $1/2\tau$. Dashed curve: observed separation $\delta\nu_e$ of two equally intense absorption lines, relative to the observed separation in the absence of exchange $\delta\nu$, as a function of exchange rate. Each curve applies only when overlap effects are negligible.

The proton resonance of N, N-dimethyltrifluoroacetamide consisted of two symmetrical 1:3:3:1 quartets. The splitting in the low-field quartet was exactly twice that in the high-field quartet. The quartets arise from the nonequivalent spin-spin interactions of the protons in each N-methyl group with the three fluorine nuclei of the trifluoromethyl group. When the fluorine resonance of the trifluoromethyl group was saturated (at a radiofrequency of about 56.452_5 mcs.) the proton resonance of the N-methyl groups consisted of two narrow resonance lines. The fluorine resonance was saturated with a VA Model V-4320 spin decoupler and the appropriate probe adapter. The energy barrier for internal rotation about the central C-N bond of N, N-dimethyltrifluoroacetamide was, therefore, obtained from spectra of the proton resonance doublet while the fluorine resonance was being saturated.

External Chemical Shifts

After all the studies of internal rotation were completed, the external chemical shifts of the resonance lines of the spectrum of each sample were determined. The external reference material was sealed inside a small Pyrex capillary, which was inserted inside the sample tube. The frequency separations were determined by the side-band technique. External chemical shifts for all proton resonance lines were determined relative to the resonance peak due to the ring protons of toluene. The external chemical shifts for all fluorine resonance lines were determined relative to the resonance peak due to the fluorine nuclei of 1, 2-dibromo-1, 1, 2, 2-tetrafluoroethane.

Calculation of Errors in the Energy Barriers and Frequency Factors

For each set of data, the errors in the energy barrier E_a and the frequency factor A were calculated from the least-squared data for the straight-line plot of $\log_{10}(4\pi^2 \gamma \delta \nu) = y$ against $(10^3/T) = x$.

The calculated errors cover the region of 90 percent confidence (104). The limits of 90 percent confidence in E_a are given by

$$2.303\, R\, [\, b \pm t\sigma / (\, \sum_i |\, x_i - \bar{x}\,|^2)^{\frac{1}{2}}\,] , \qquad (116)$$

where b is the least-squared slope, $\bar{x}$ is the average value of the n values of 1/T, t is a constant for converting the standard error in the slope to the region of 90 percent confidence (the value of t depends upon the number of points n), and σ is given by

$$\sigma^2 \cong [\, \sum_i y_i^2 - a \sum_i y_i - b \sum_i x_i y_i\,] / n-2 . \qquad (117)$$

In equation (117), a is the least-squared intercept.

The limits of 90 percent confidence in A were calculated from

$$(\delta\nu/2)10^{-a \pm t\sigma [\sum_i x_i^2 / n \sum_i |\, x_i - \bar{x}\,|^2]^{\frac{1}{2}}} . \qquad (118)$$

This function assumes that the error in A due to the error in the measurement of $\delta\nu$ is small compared to the error in A introduced by the error in a. This assumption was valid in every case.

RESULTS

High-resolution Spectra

All the spectra shown in this thesis were obtained at the radio-frequency 60.000 mcs. and with the linear sweep field increasing from left to right. Positions of proton magnetic resonance lines are given with respect to the resonance position of the ring protons of toluene which was used as an external reference. Positions of fluorine magnetic resonance lines are given with respect to the resonance position of the fluorine nuclei of 1, 1-dibromo-1, 1, 2, 2-tetrafluoroethane which was used as an external reference. Frequency displacements to the right (the high-field side) of the reference positions are arbitrarily taken as positive, whereas those to the left (the low-field side) are taken as negative.

N, N-Dimethylformamide - The high-resolution proton resonance spectrum of pure N, N-dimethylformamide is shown in Figure 11. The magnetic resonance of the aldehyde proton consists of an unresolved multiplet centered at -71.4 cps. Theoretically this multiplet consists of ten equally-spaced (0.28 cps) lines with relative intensities 3:10:20:33:40:40:33:20:10:3. The doublet centered at 232.3 cps is due to the magnetic resonance of the protons of one N-methyl group, whereas the doublet centered at 241.7 cps is due to the proton resonance of the other N-methyl group. The splitting of the low-field doublet is 0.28 cps, and that of the high-field doublet is 0.56 cps. The shift between the two doublets is very large compared to the effective natural line width of either partially resolved doublet. The gain used while recording the low-field multiplet was much larger than that used while recording the high-field doublets.

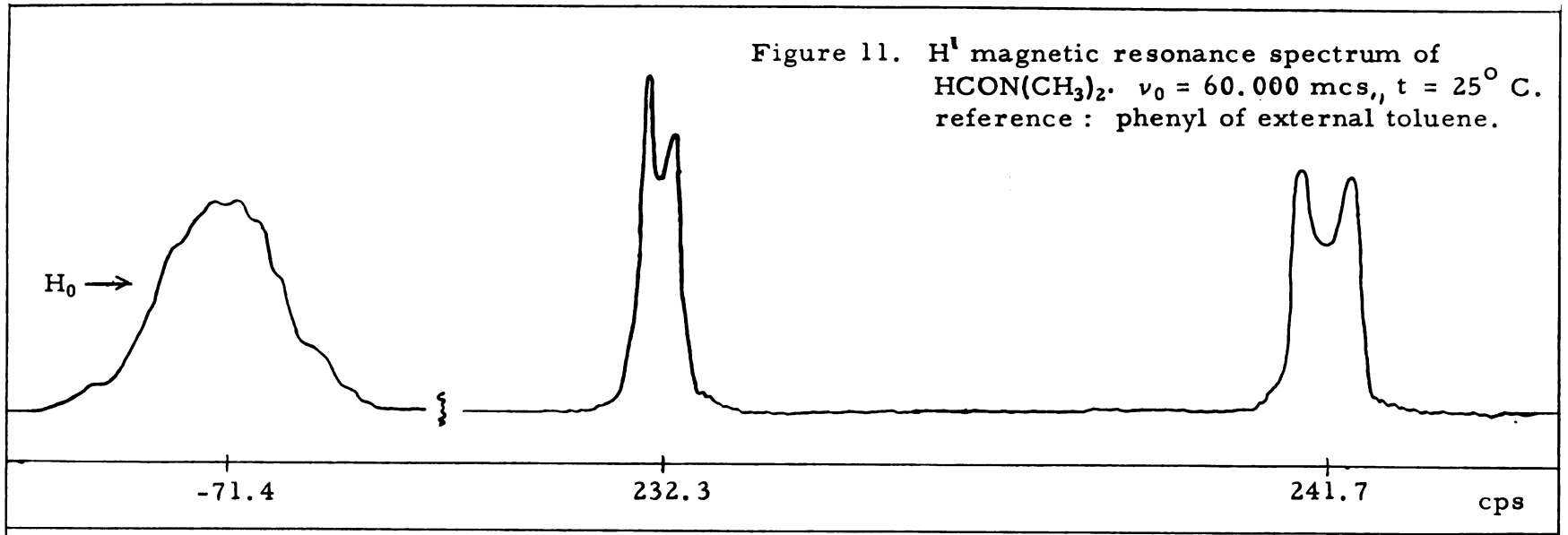

Figure 11. H^1 magnetic resonance spectrum of $HCON(CH_3)_2$. ν_0 = 60.000 mcs., t = 25° C. reference : phenyl of external toluene.

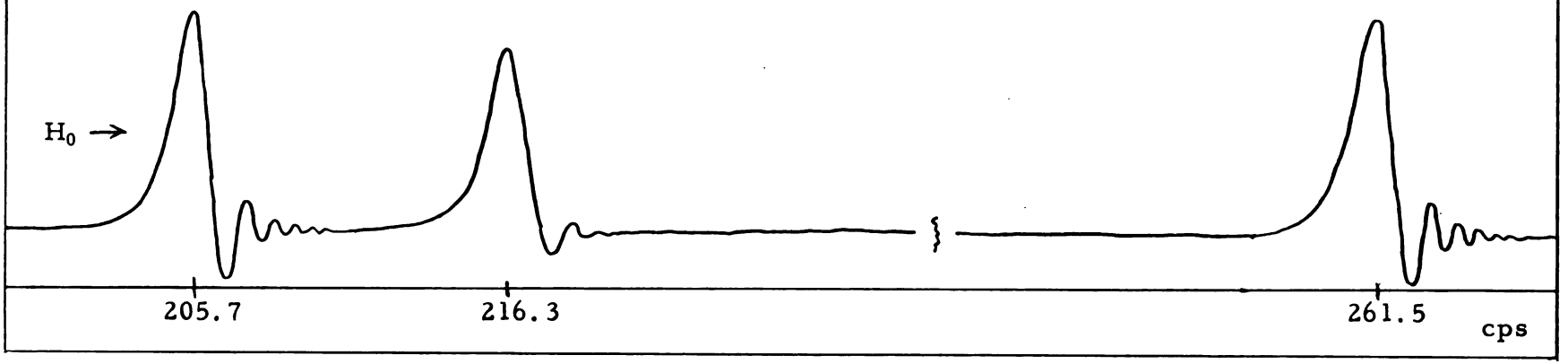

Figure 12. H^1 magnetic resonance spectrum of $CH_3CON(CH_3)_2$. ν_0 = 60.000 msc., t =-27.6°C. reference: phenyl of external toluene.

N, N-Dimethylacetamide - The proton magnetic resonance spectrum of pure N, N-dimethylacetamide is shown in Figure 12. The lines at 205.7 and 216.3 cps are due to the proton resonance of the two nonequivalent N-methyl groups. The resonance of the protons of the C-methyl group is located at 261.5 cps. Very weak and nonequivalent spin-spin coupling of the protons of the C-methyl group with the protons of each N-methyl group causes the effective natural line width of the high-field N-methyl proton resonance to be slightly broader than that of the low-field N-methyl proton resonance line.

N, N-Dimethylpropionamide - The proton magnetic resonance spectrum of pure N, N-dimethylpropionamide is shown in Figure 13. The proton resonance due to one N-methyl group is located at 225.2 cps, whereas that of the other N-methyl group is located at 234.4 cps. The effective natural line width of the high-field N-methyl proton resonance is slightly broader than that of the low-field N-methyl proton resonance. The difference is caused by the very weak and nonequivalent spin-spin coupling of the methylene protons with the protons of each N-methyl group. The effective natural line width of each N-methyl proton resonance is small compared to the chemical shift between the lines.

The quartet between 250.9 and 272.5 cps arises from the resonance of the methylene protons, whereas the triplet between 338.8 and 348.3 cps is due to the resonance of the methyl protons of the ethyl group. The triplet and quartet structures are the result of spin-spin coupling between the methylene and methyl protons of the ethyl group. Each component of the quartet and triplet is split into a multiplet. These small splittings also result from the spin-spin coupling between the methylene and methyl protons of the ethyl group. At lower applied fields, where $J_{CH_3CH_2}$ becomes comparable in magnitude to $\nu_{CH_3} - \nu_{CH_2}$, the true complexity of the "ethyl spectrum" would become much more apparent than that revealed in Figure 13.

Figure 13. H^1 magnetic resonance spectrum of $CH_3CH_2CON(CH_3)_2$. ν_0 = 60.000 msc., t = -27.5° C., reference: phenyl of external toluene.

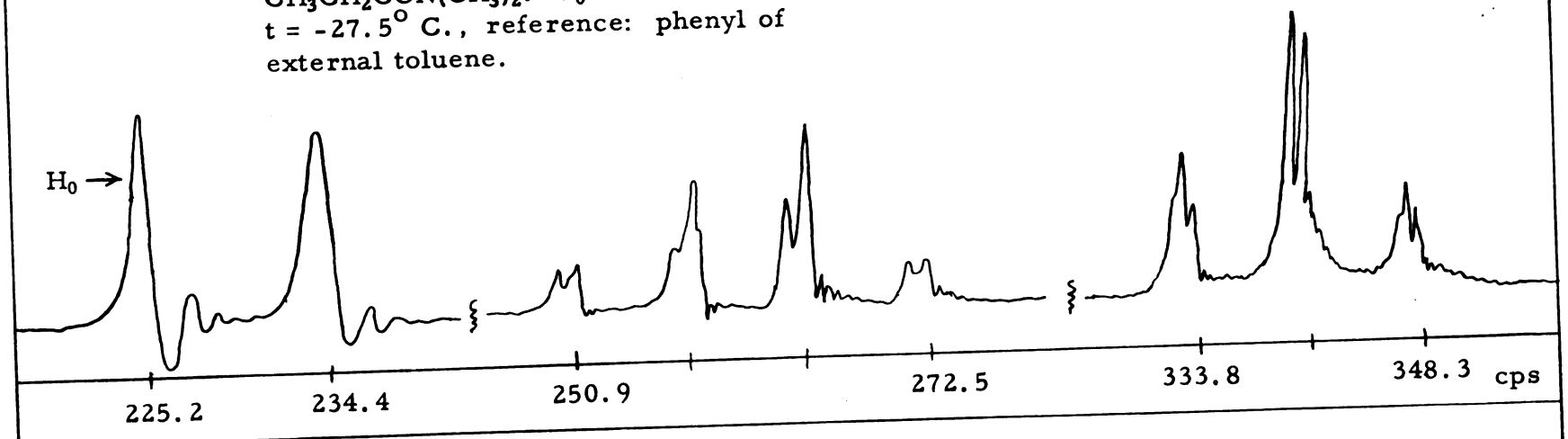

Figure 14. H^1 magnetic resonance spectrum of $CCl_3CON(CH_3)_2$ ν_0 = 60.000 msc., t = -26.8° C., reference: phenyl of external toluene.

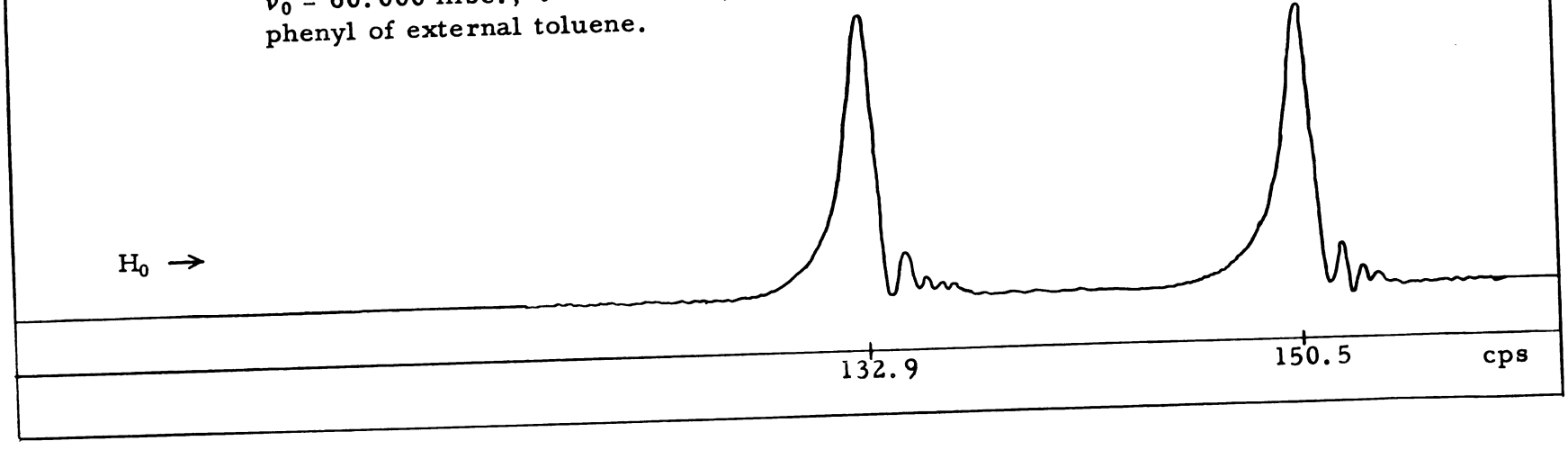

The doublet, quartet and triplet shown in Figure 13 were each recorded at slightly different gains. The proton resonance spectra of the solutions of N, N-dimethylpropionamide in dibromomethane and in carbon tetrachloride were all essentially the same as that shown in Figure 13. The pertinent NMR data for these solutions are tabulated in Table IV.

N, N-Dimethyltrichloroacetamide - The proton magnetic resonance spectrum of pure N, N-dimethyltrichloroacetamide is shown in Figure 14. The line at 132.9 cps is due to the proton resonance of one N-methyl group, and the line at 150.5 cps arises from the proton resonance of the other N-methyl group. The natural line widths of both lines are about the same, and these widths are negligible compared to the chemical shift between the lines.

N, N-Dimethyltrifluoroacetamide - The high-resolution fluorine magnetic resonance spectrum of pure N, N-dimethyltrifluoroacetamide is shown in Figure 15. The multiplet structure arises from the non-equivalent spin-spin coupling of the three fluorine nuclei with the protons of each N-methyl group. Theoretically this spectrum consists of ten equally-spaced (0.7 cps) lines with relative intensities 3:10:20:33:40:40:33:20:10:3. The observed spectrum is in agreement with the theoretical one.

The high-resolution proton magnetic resonance spectrum of pure N, N-dimethyltrifluoroacetamide is shown in Figure 16. The quartet between 215.2 and 219.4 cps is due to the resonance of the protons of one N-methyl group, whereas the quartet between 223.7 and 225.8 cps is due to the proton resonance of the other N-methyl group. The quartet structures are the result of nonequivalent spin-spin coupling of the three fluorine nuclei with the protons of each N-methyl group. The splitting in the low-field quartet is 1.4 cps, and that in the high-field quartet is 0.7 cps.

TABLE IV

PROTON CHEMICAL SHIFTS FOR SOME SOLUTIONS OF N, N-DIMETHYLPROPIONAMIDE*

Mole Percent Amide	Solvent	δ solvent, ppm	δ $N(CH_3)_2$', ppm		δ CH_2', ppm	δ CH_3', ppm	t, °C.
100			3.75_4	3.90_7	4.36_2	5.68_3	-27.5
84.7_1	CH_2Br_2	1.21_3	3.64_3	3.79_1	4.31_7	5.60_0	-26.8
68.8_8	CH_2Br_2	1.19_7	3.46_2	3.60_5	4.21_7	5.49_2	-26.8
58.0_9	CH_2Br_2	1.17_5	3.44_0	3.57_7	4.15_8	5.42_7	-23.4
40.5_7	CH_2Br_2	1.09_7	3.26_5	3.38_9	3.99_5	5.23_8	-26.4
22.1_7	CH_2Br_2	$.98_0$	3.11_0	3.21_7	3.79_3	5.04_7	-24.0
10.1_4	CH_2Br_2	$.91_3$	2.99_9	3.09_4	3.66_7	4.92_5	-23.8
69.3_4	CCl_4		3.67_0	3.83_0	4.31_8	5.59_2	-24.0
39.9_4	CCl_4		3.52_6	3.68_7	4.20_8	5.48_3	-24.0
11.0_7	CCl_4		3.43_6	3.59_7	4.17_5	5.40_0	-23.8

*Chemical shifts are relative to the ring protons of external toluene. The value of $J_{CH_3CH_2}$ was about 7.2 cps in each case.

Figure 15. F^{19} magnetic resonance spectrum of $CF_3CON(CH_3)_2$. ν_0 = 60.000 mcs., t = 25°C., reference: external CF_2BrCF_2Br.

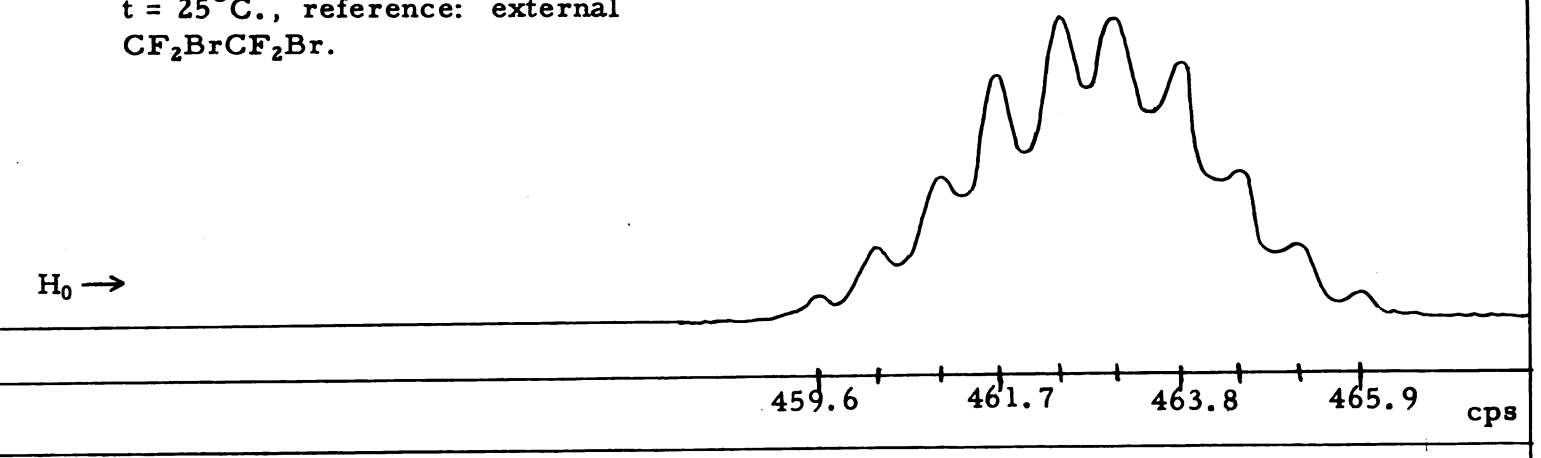

Figure 16. H^1 magnetic resonance spectrum of $CF_3CON(CH_3)_2$. ν_0 = 60.000 mcs., t = 25°C., reference: phenyl of external toluene.

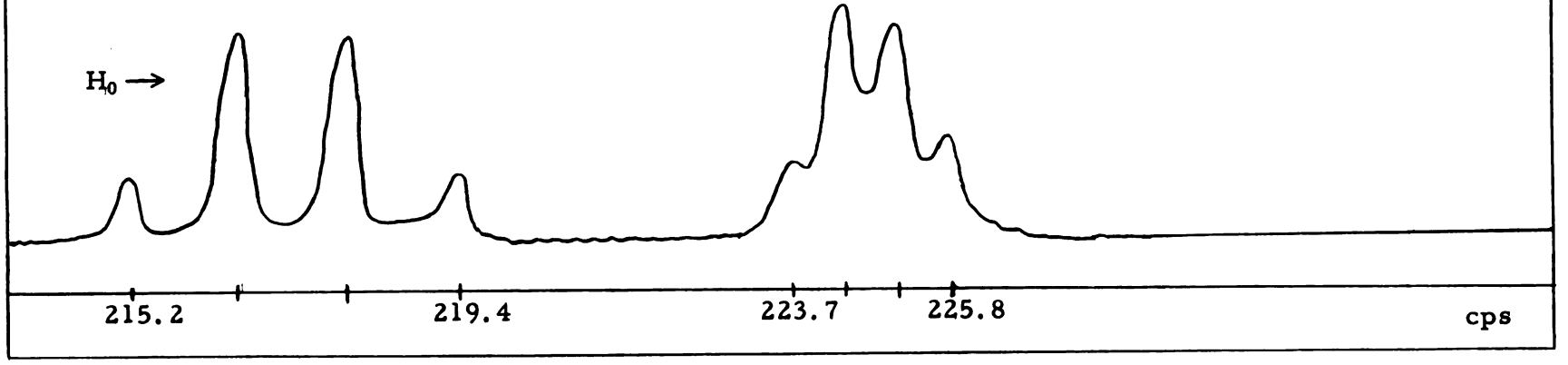

N, N-Dimethylacrylamide - The high resolution proton magnetic resonance spectrum of pure N, N-dimethylacrylamide is shown in Figure 17. The resonance line at 215.3 cps is due to the proton resonance of one N-methyl group, whereas the line at 224.8 cps is due to the proton resonance of the other N-methyl group. The effective natural line widths of these two lines are about the same. This indicates that the spin of the tertiary proton of the vinyl group is coupled very weakly and equivalently with the spins of the protons of each N-methyl group. The effective natural line widths of the two N-methyl proton resonance lines are small compared to the chemical shift between the lines.

The proton resonance of the vinyl group is located between -25.7 and 68.6 cps. The gain used while recording this portion of the spectrum was much higher than that used while recording the proton resonance of the two N-methyl groups. The proton resonance of the vinyl group shown in Figure 17 is indicative of the complexity of NMR spectra when the magnitudes of spin-spin coupling constants are comparable to the corresponding internal chemical shifts. The "vinyl spectrum" is of the type (ABC),* and although the complete solutions for the analysis of such a spectrum may, in principle, be given in closed form, the solutions are more simply arrived at by numerical calculations. The "vinyl spectrum" of N, N-dimethylacrylamide is similar to the "vinyl spectrum" of styrene (105).

N, N-Dimethylbenzamide - The proton magnetic resonance spectrum of 36.3$_4$ mole percent N, N-dimethylbenzamide in dibromomethane is shown in Figure 18. The peak at -60.7 cps is due to the proton resonance of the phenyl group, and the peak at 81.6 cps is due to the proton resonance of the solvent dibromomethane. The line at 202.9 cps arises from one

*An ABC-type spectrum is the spectrum of a system having three non-equivalent nuclear spins, the three internal chemical shifts and the three coupling constants being of the same order of magnitude.

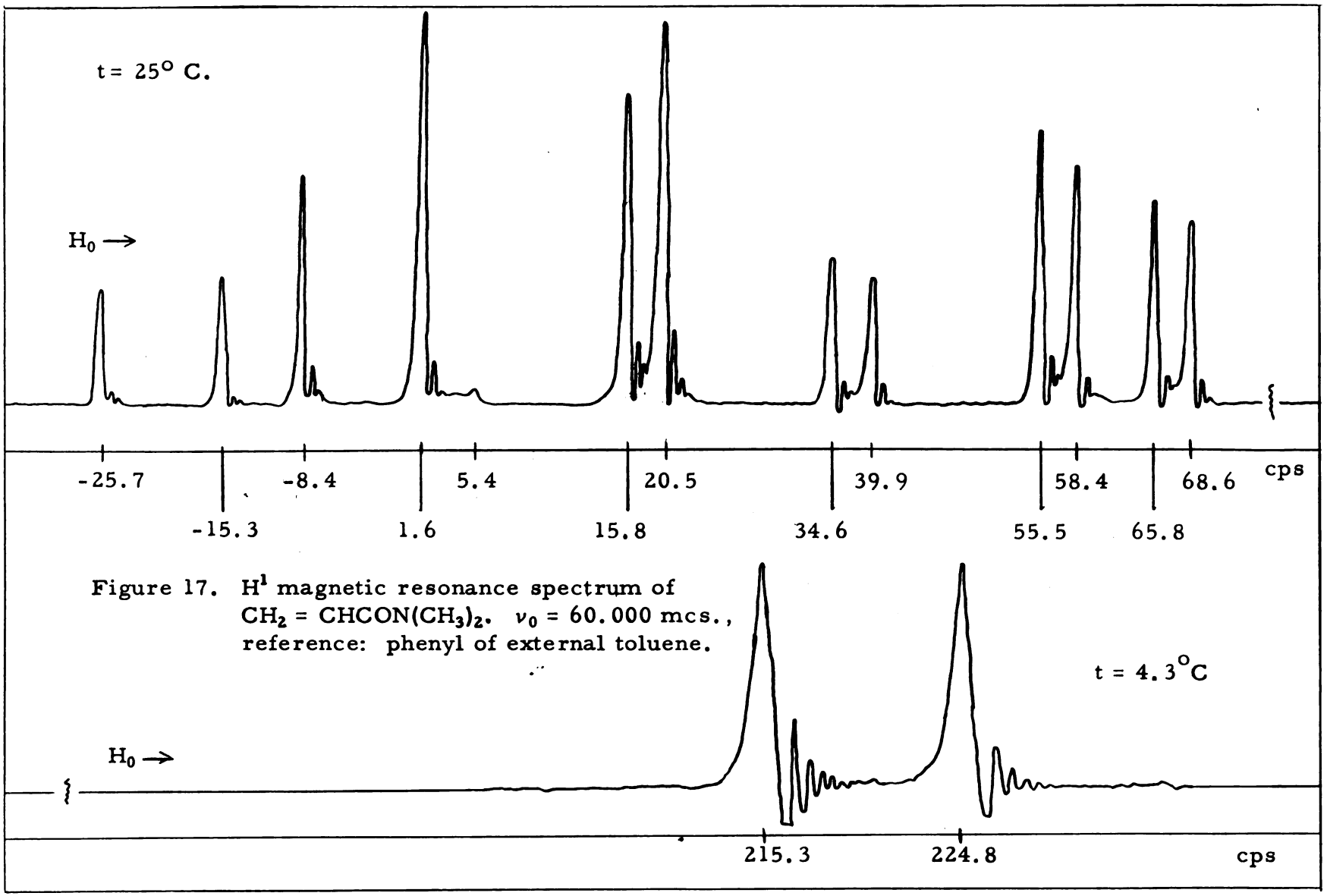

Figure 17. H^1 magnetic resonance spectrum of $CH_2 = CHCON(CH_3)_2$. ν_0 = 60.000 mcs., reference: phenyl of external toluene.

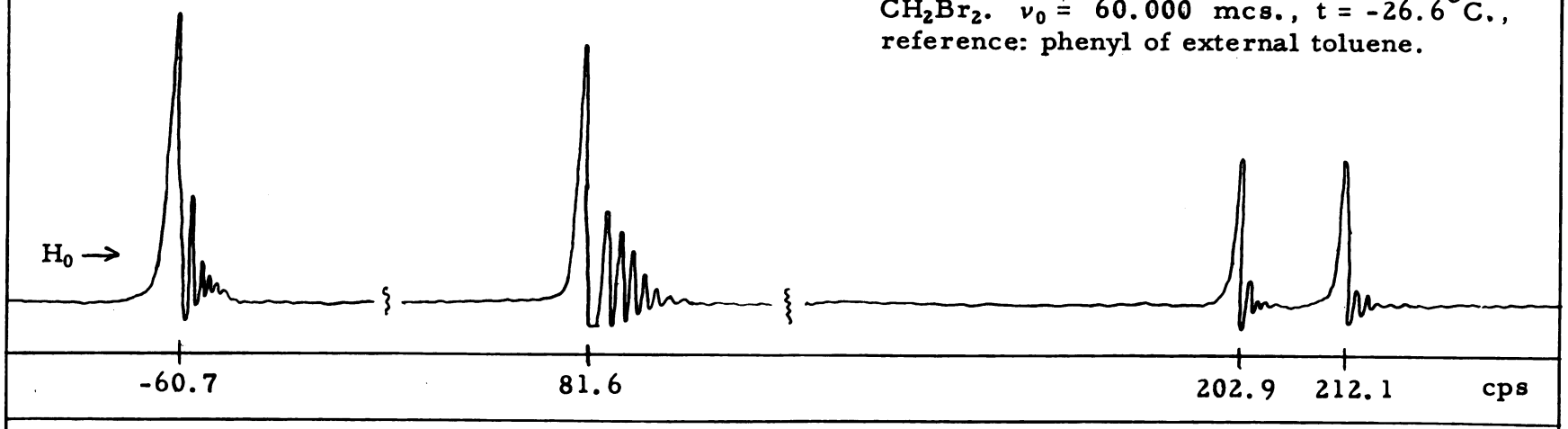

Figure 18. H^1 magnetic resonance spectrum of 36.3$_4$ mole percent $C_6H_5CON(CH_3)_2$ in CH_2Br_2. ν_0 = 60.000 mcs., t = -26.6°C., reference: phenyl of external toluene.

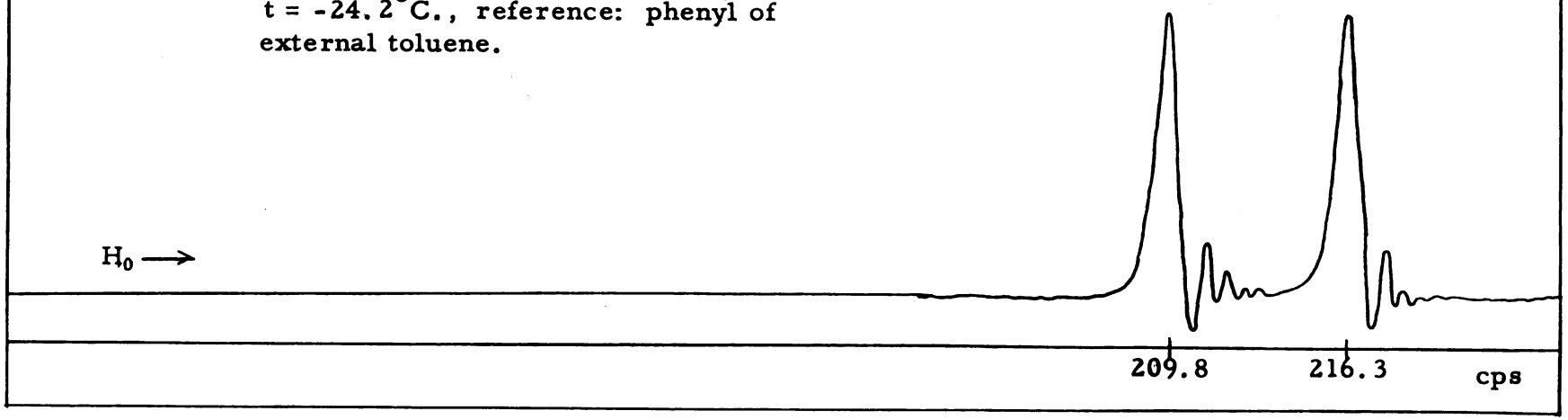

Figure 19. H^1 magnetic resonance spectrum of $ClCON(CH_3)_2$. ν_0 = 60.000 mcs., t = -24.2°C., reference: phenyl of external toluene.

N-methyl proton resonance, whereas the line at 212.1 cps is due to the other N-methyl proton resonance. The natural line widths of the two N-methyl proton resonances are small compared to the chemical shift between the two lines.

N, N-Dimethylcarbamyl chloride - The proton magnetic resonance spectrum of pure N, N-dimethylcarbamyl chloride is shown in Figure 19. One line is due to the proton resonance of one N-methyl group, and the other line is due to the proton resonance of the other N-methyl group. The natural line widths of the two lines are small compared to the chemical shift between the two lines.

The proton resonance spectra of the solutions of N, N-dimethylcarbamyl chloride in dibromomethane and in carbon tetrachloride were all essentially the same as that shown in Figure 19. The pertinent NMR data for these solutions are tabulated in Table V.

N, N-Dibenzylacetamide - The proton magnetic resonance spectrum of 38.0_9 mole percent N, N-dibenzylacetamide is shown in Figure 20. The large peak at -42.3 cps is due to the proton resonance of the two phenyl groups, and the peak at 100.1 cps is due to the proton resonance of the solvent dibromomethane. The peak at 266.4 cps arises from the proton resonance of the methyl group. The line at 117.0 cps is due to the proton resonance of one methylene group, and the line at 129.0 cps is due to the proton resonance of the other N-methyl group. Due to very weak spin-spin coupling between the ring and the methylene protons of each benzyl group, the proton resonance lines for each methylene group are broadened slightly. However, the effective natural line widths of these lines are still small compared to the chemical shift between the two lines.

The proton resonance spectrum of 38.2_9 mole percent N, N-dibenzylacetamide in carbon tetrachloride is shown in Figure 21. This spectrum is essentially the same as the one shown in Figure 20.

TABLE V

PROTON CHEMICAL SHIFTS FOR SOME SOLUTIONS OF N, N-DIMETHYLCARBAMYL CHLORIDE

Mole Per cent Amide	Solvent	δ solvent, ppm	δ $N(CH_3)_2$, ppm		t, °C.
100			3.49_6	3.60_3	-24.2
90.0_3	CH_2Br_2	1.38_8	3.41_5	3.52_2	-24.5
63.4_4	CH_2Br_2	1.25_3	3.20_9	3.31_4	-24.5
40.9_2	CH_2Br_2	1.10_7	3.04_8	3.15_2	-23.7
10.7_2	CH_2Br_2	$.90_3$	2.80_4	2.90_6	-22.2
71.3_5	CCl_4		3.49_9	3.51_8	-20.2
40.0_8	CCl_4		3.32_2	3.44_4	-20.2
10.9_8	CCl_4		3.21_9	3.34_1	-19.7

*Chemical shifts are relative to the ring protons of external toluene.

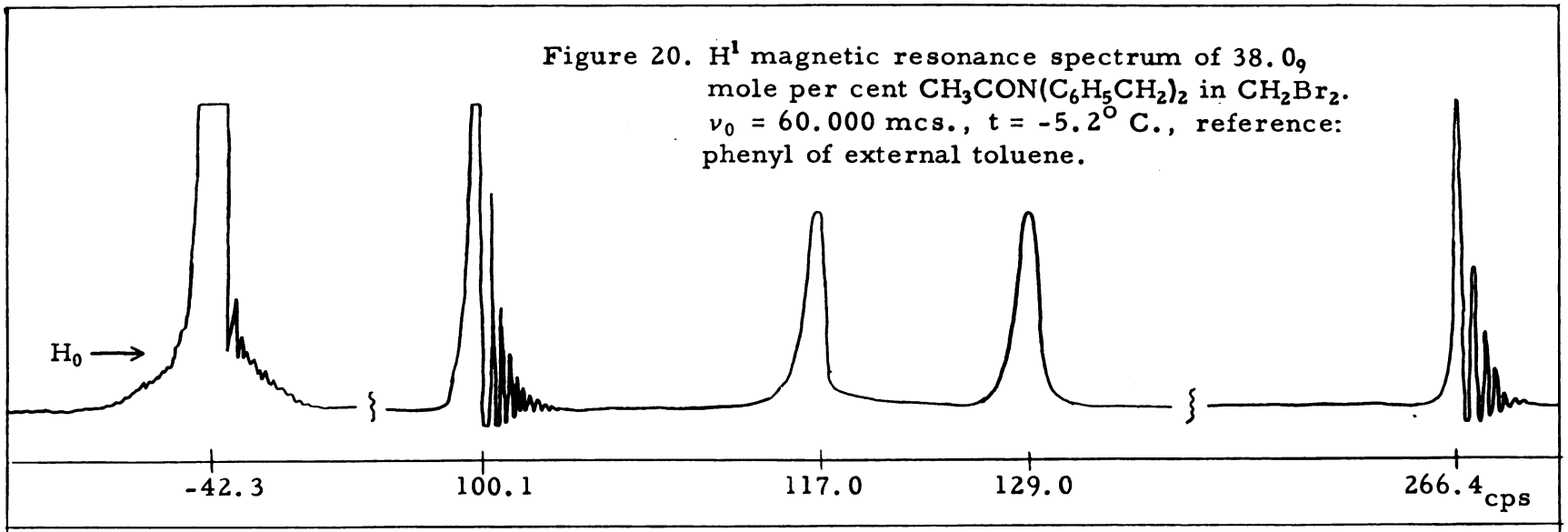

Figure 20. H^1 magnetic resonance spectrum of 38.0$_9$ mole per cent $CH_3CON(C_6H_5CH_2)_2$ in CH_2Br_2. ν_0 = 60.000 mcs., t = -5.2° C., reference: phenyl of external toluene.

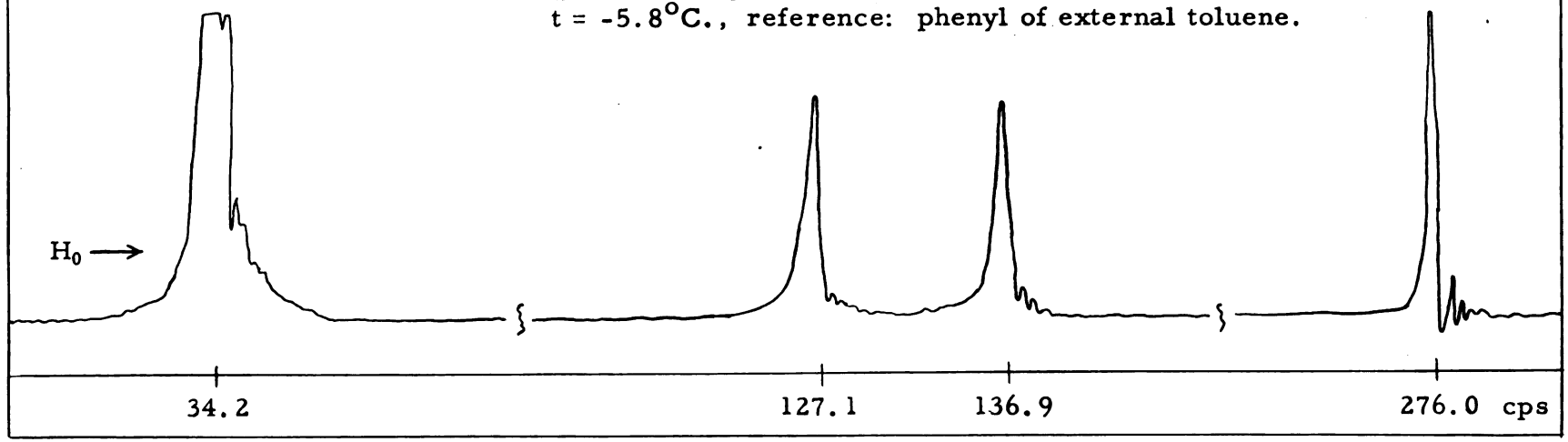

Figure 21. H^1 magnetic resonance spectrum of 38.2$_9$ mole per cent $CH_3CON(C_6H_5CH_2)_2$ in CCl_4. ν_0 = 60.000 mcs., t = -5.8°C., reference: phenyl of external toluene.

Ethyl-N, N-dimethylcarbamate - The proton magnetic resonance spectrum of pure ethyl-N, N-dimethylcarbamate is shown in Figure 22. The quartet between 148.3 and 168.7 cps and the triplet between 325.2 and 338.8 cps are due to the proton resonance of the ethyl group. The narrow line at 229.5 cps is due to the proton resonance of the two equivalent N-methyl groups. The gain used while recording this line was less than that used while recording the quartet and triplet. The proton resonance of the two N-methyl groups was observed to be a single narrow line in the temperature region from room temperature down to the freezing point.

N, N-Bis-(trifluoromethyl)-trifluoroacetamide - The fluorine magnetic resonance spectrum of pure N, N-bis-(trifluoromethyl)-trifluoroacetamide is shown in Figure 23. The quartet between -323.7 and -306.7 cps arises from the fluorine resonance of the two equivalent N-trifluoromethyl groups, whereas the septet between 685.0 and 718.6 cps arises from the fluorine resonance of the C-trifluoromethyl group. The gain used while recording the septet was much greater than that used while recording the quartet. The splittings in the quartet and septet are about 5.6 cps. The spectrum for the septet consists of seven equally spaced lines with relative intensities 1:6:15:20:15:6:1. The observed septet is in agreement with the theoretical one. The spectrum of the quartet did not change in the temperature region from room temperature down to the freezing point.

Methyl-N, N-bis-(trifluoromethyl)-carbamate - The proton magnetic resonance spectrum of pure methyl-N, N-bis-(trifluoromethyl)-carbamate consists of a single narrow line. The external chemical shift, relative to the proton resonance of the ring protons of toluene, is 2.84_8 ppm. The fluorine resonance was observed to be a single narrow line in the temperature region from room temperature down to the freezing point. The external chemical shift, relative to the fluorine resonance of 1, 1-dibromo-1, 1, 2, 2, -tetrafluoroethane, is -5.26_0 ppm.

Figure 22. H^1 magnetic resonance spectrum of $C_2H_5OCON(CH_3)_2$. ν_0 = 60.000 mcs., t = 25° C., reference: phenyl of external toluene.

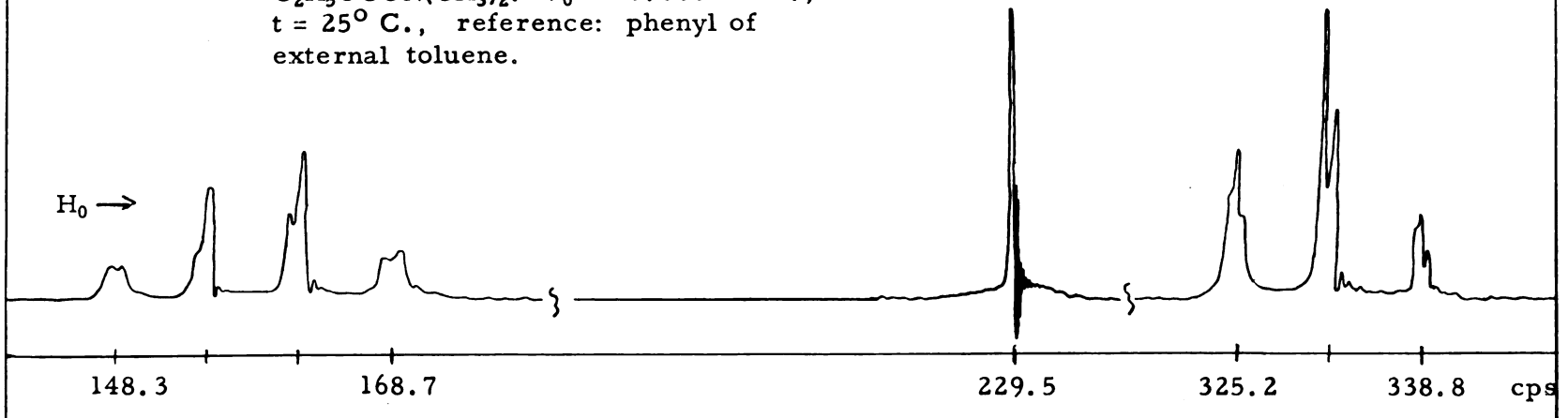

Figure 23. F^{19} magnetic resonance spectrum of $CF_3CON(CF_3)_2$. ν_0 = 60.000 mcs., t = 25° C., reference: external CF_2BrCF_2Br.

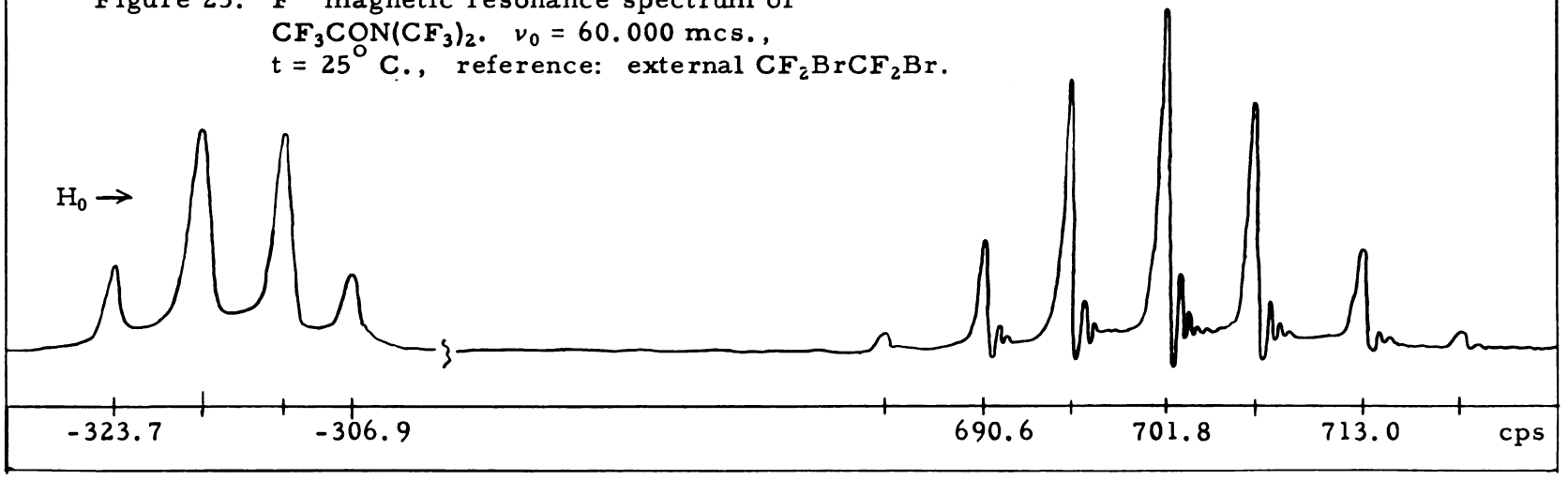

Hindered Internal Rotation

N, N-Dimethylformamide - The hindered internal rotation about the central C-N bond of N, N-dimethylformamide was studied by Methods II and III. Some of the spectra, from which data were obtained by Method III, are shown in Figure 24. The experimental data obtained by Method III are tabulated in Table VI, and the experimental data obtained by Method II are tabulated in Table VII. For comparison, the data obtained by Gutowsky and Holm (5, 6), who studied the internal rotation in this compound by Method II, are tabulated in Table VIII. The data obtained by Method III are plotted as $\log_{10}(4\pi^2\tau\,\delta\nu)$ against $10^3/T$ in Figure 25, and a similar plot for the data obtained by Method II is shown in Figure 26. For comparison, a somewhat similar plot of the data obtained by Gutowsky and Holm is shown in Figure 27.

N, N-Dimethylacetamide - The hindered internal rotation of pure N, N-dimethylacetamide was studied by Method III. Some of the spectra, from which data were obtained, are shown in Figure 28. The experimental data are tabulated in Table IX and plotted as $\log_{10}(4\pi^2\tau\,\delta\nu)$ against $10^3/T$ in Figure 29. For comparison the data obtained by Gutowsky and Holm (5, 6), who studied this compound by Method II, are tabulated in Table X and plotted in Figure 30.

N, N-Dimethylpropionamide - The hindered internal rotation about the central C-N bond of pure N, N-dimethylpropionamide was studied by Method III. In addition, the phenomenon was also studied for the following concentrations (mole per cent) of amide (a) in dibromomethane: 84.7_1, 68.8_8, 58.0_0, 40.5_7, 22.1_7, and 10.1_4; and (b) in carbon tetrachloride: 69.3_4, 39.9_4, and 11.0_7. The experimental data for the pure liquid amide, the solutions of amide and dibromomethane, and the solutions of amide and carbon tetrachloride are tabulated in Tables XI, XII, and XIII, respectively. These data are plotted as $\log_{10}(4\pi^2\tau\,\delta\nu)$

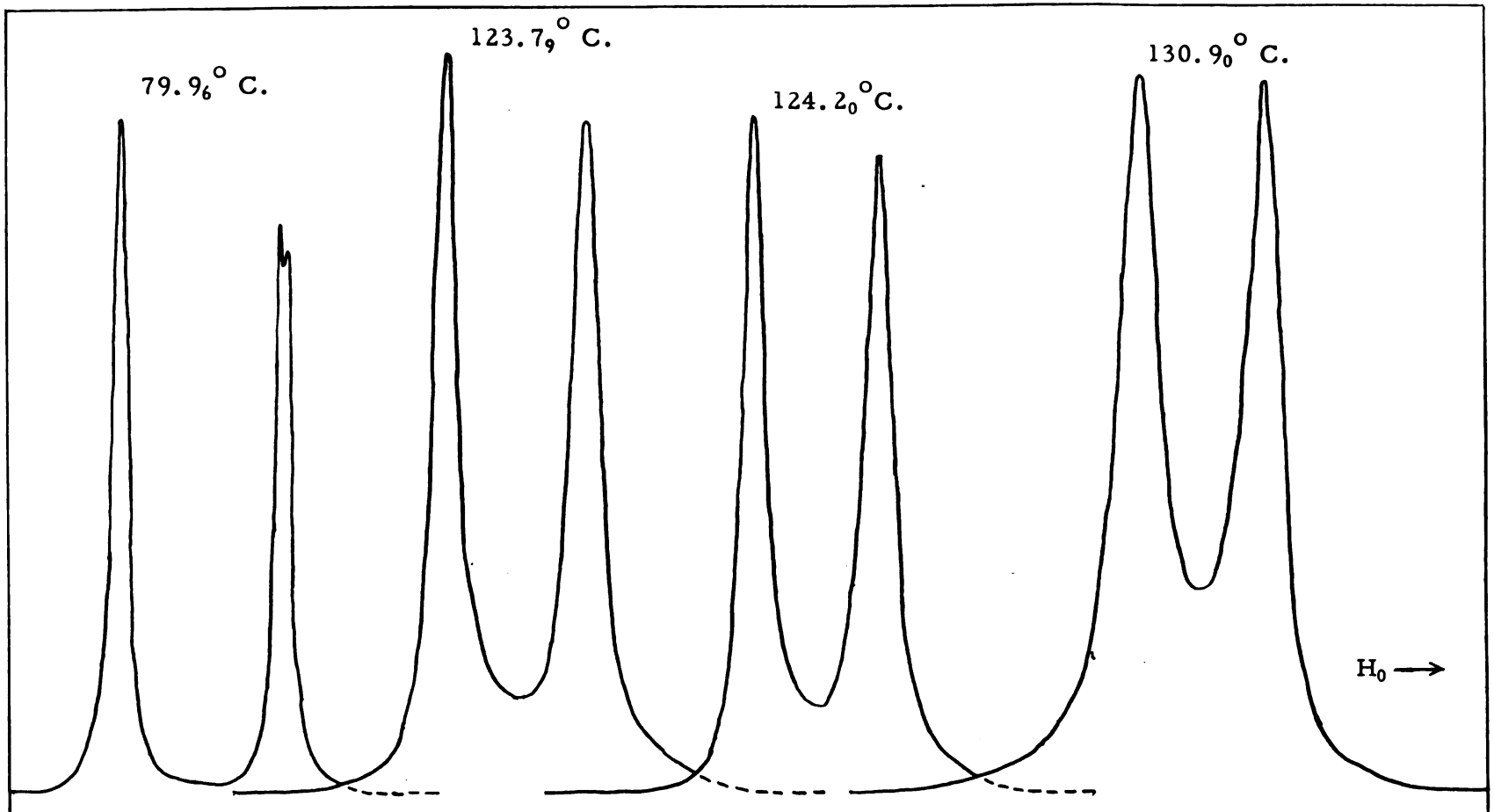

Figure 24. Proton magnetic resonance spectra of the methyl groups in N, N-dimethylformamide at various temperatures, ν_0 = 60.000 mcs. The sweep rates and recorder gains were not exactly the same at every temperature.

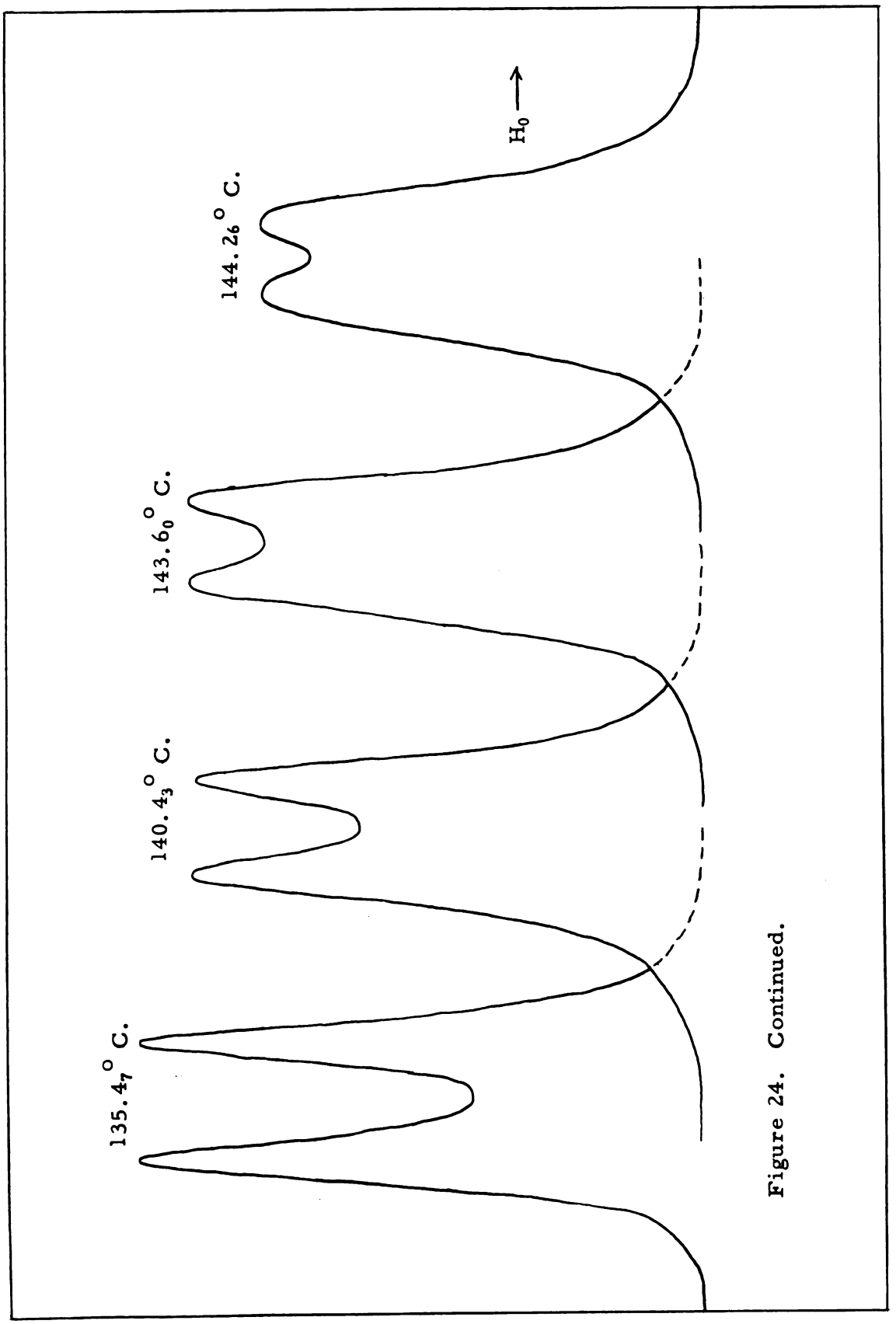

Figure 24. Continued.

TABLE VI

TEMPERATURE DEPENDENCE OF THE RATE OF INTERNAL ROTATION ABOUT THE CENTRAL C-N BOND OF $HCON(CH_3)_2$, METHOD III

ν_0 = 60.000 mcs., $\delta\nu$ = 9.43 ± .20 cps at 25°C.

t, °C.	$10^3/T$, (°K.)	r	$\log_{10}(4\pi^2\tau\delta\nu)$
144.26 ± .10*	2.3957	1.141 ± .002*	1.0425 ± .0005*
143.60 ± .01	2.3994	1.166 ± .017	1.0515 ± .0060
140.43 ± .10	2.4178	1.474 ± .036	1.1305 ± .0060
135.47 ± .08	2.4472	2.451 ± .030	1.2675 ± .0030
130.90 ± .13	2.4749	3.528 ± .060	1.3552 ± .0040
124.20 ± .40	2.5166	7.562 ± .071	1.5310 ± .0023
123.79 ± .40	2.5192	7.507 ± .060	1.5295 ± .0020

*The error given is the average deviation from the average of five measurements.

TABLE VII

TEMPERATURE DEPENDENCE OF THE RATE OF INTERNAL ROTATION ABOUT THE CENTRAL C-N BOND OF $HCON(CH_3)_2$, METHOD II

ν_0 = 60.000 mcs., $\delta\nu$ = 9.43 ± .20 cps at 25°C.

t, °C.	$10^3/T$, (°K.)	r	$\log_{10}(4\pi^2\tau\delta\nu)$
131.76 ± .12*	2.4696	5.49 ± .92*	1.0395 ± .0443*
128.72 ± .10	2.4883	7.41 ± .60	1.1557 ± .0713
122.81 ± .21	2.5254	8.07 ± .97	1.2350 ± .1280
121.48 ± .12	2.5340	8.24 ± .38	1.2620 ± .0790
115.86 ± .16	2.5706	8.58 ± .36	1.3295 ± .1145
113.12 ± .18	2.5888	9.00 ± .69	1.4665 ± .1915
107.18 ± .10	2.6292	9.16 ± .27	1.5615 ± .1393

*The error given is the average deviation from the average of six measurements.

TABLE VIII

TEMPERATURE DEPENDENCE OF THE RATE OF INTERNAL ROTATION ABOUT THE CENTRAL C-N BOND OF $HCON(CH_3)_2$, ACCORDING TO GUTOWSKY AND HOLM(5, 6), METHOD II

ν_0 = 17.735 mcs., $\delta\nu$ = 3.24 ± .05 cps at -37.2°C., T_2 = 0.88 ± .19 cps

t, °C.	$10^3/T$, (°K.)	$\delta\nu_e$, cps	$\log_{10}(\tau\,\delta\nu)$
95.8 ± 1*	2.7100	1.90 ± .10*	-.3166 ± .0130*
93.8 ± 1	2.7248	2.01 ± .10	-.3034 ± .0134
89.3 ± 1	2.7586	2.10 ± .05	-.2753 ± .0143
87.3 ± 1	2.7739	2.45 ± .10	-.1784 ± .0303
85.8 ± 1	2.7855	2.20 ± .10	-.2606 ± .0147
81.3 ± 1	2.8209	2.45 ± .10	-.1784 ± .0303
74.0 ± 1	2.8818	2.64 ± .19	-.0993 ± .0605
70.8 ± 1	2.9070	2.75 ± .10	-.0286 ± .0704
51.8 ± 1	3.0769	2.94 ± .19	.1605 ± .1457
49.3 ± 1	3.1008	3.06 ± .14	.2984 ± .1758
-37.2 ± 1		3.20 ± .05	

*The error given is the standard deviation from the average of about ten measurements.

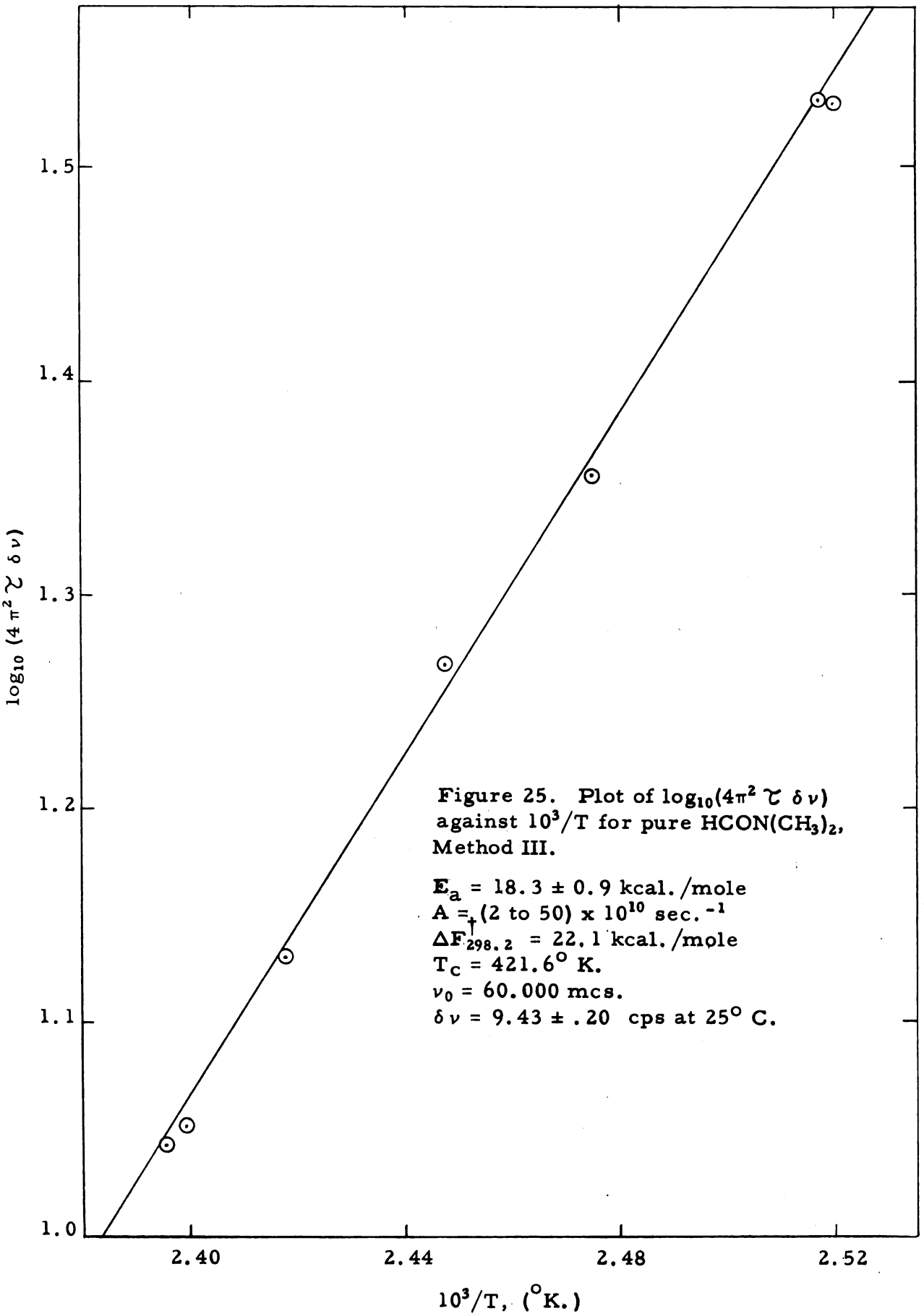

Figure 25. Plot of $\log_{10}(4\pi^2 \tau \delta\nu)$ against $10^3/T$ for pure $HCON(CH_3)_2$, Method III.

E_a = 18.3 ± 0.9 kcal./mole
$A = \dagger$ (2 to 50) x 10^{10} sec.$^{-1}$
$\Delta F^{\dagger}_{298.2}$ = 22.1 kcal./mole
T_C = 421.6° K.
ν_0 = 60.000 mcs.
$\delta\nu$ = 9.43 ± .20 cps at 25° C.

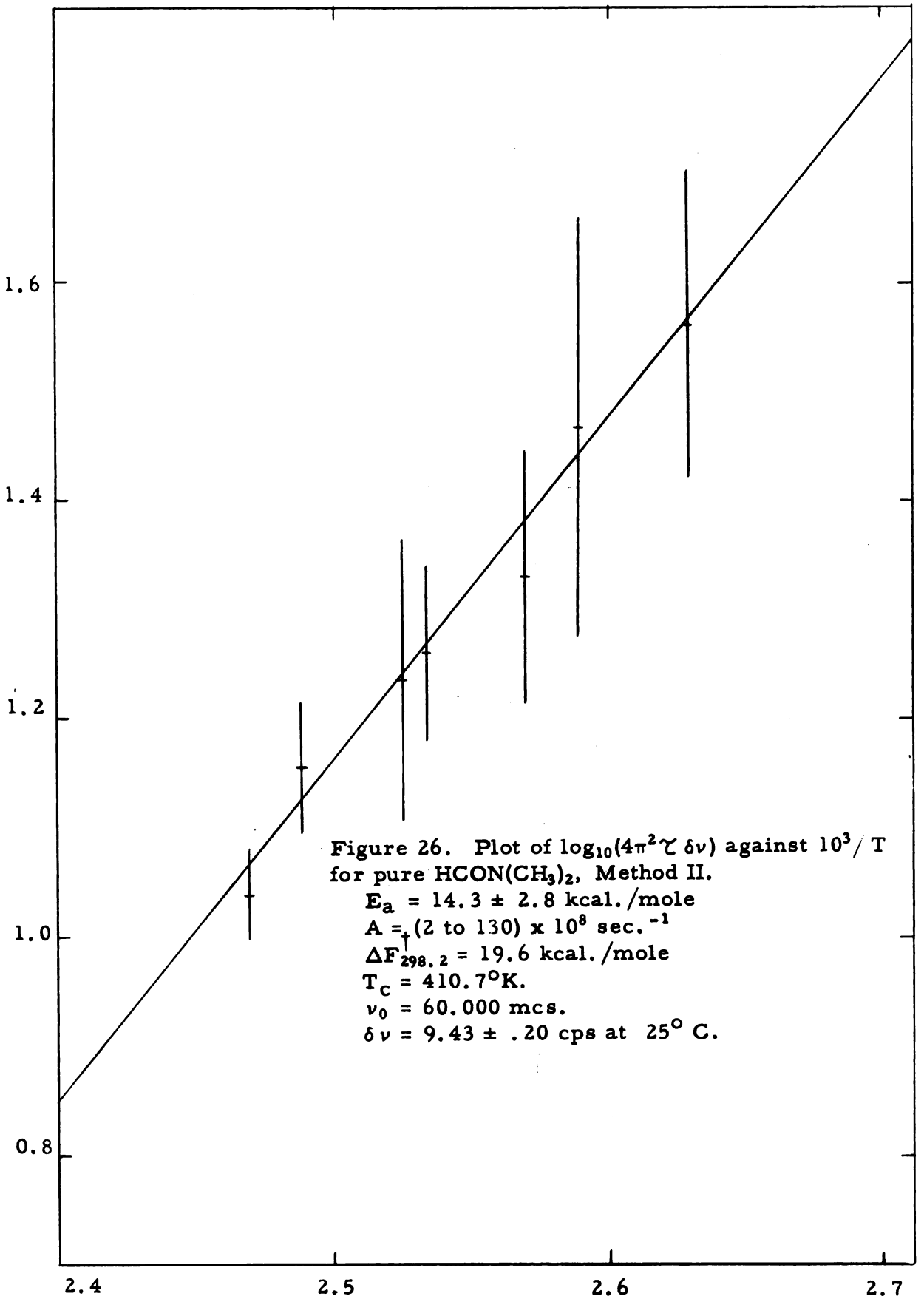

Figure 26. Plot of $\log_{10}(4\pi^2 \tau \delta\nu)$ against $10^3/T$ for pure $HCON(CH_3)_2$, Method II.

E_a = 14.3 ± 2.8 kcal./mole

$A = \pm$(2 to 130) x 10^8 sec.$^{-1}$

$\Delta F_{298.2}$ = 19.6 kcal./mole

T_c = 410.7°K.

ν_0 = 60.000 mcs.

$\delta\nu$ = 9.43 ± .20 cps at 25° C.

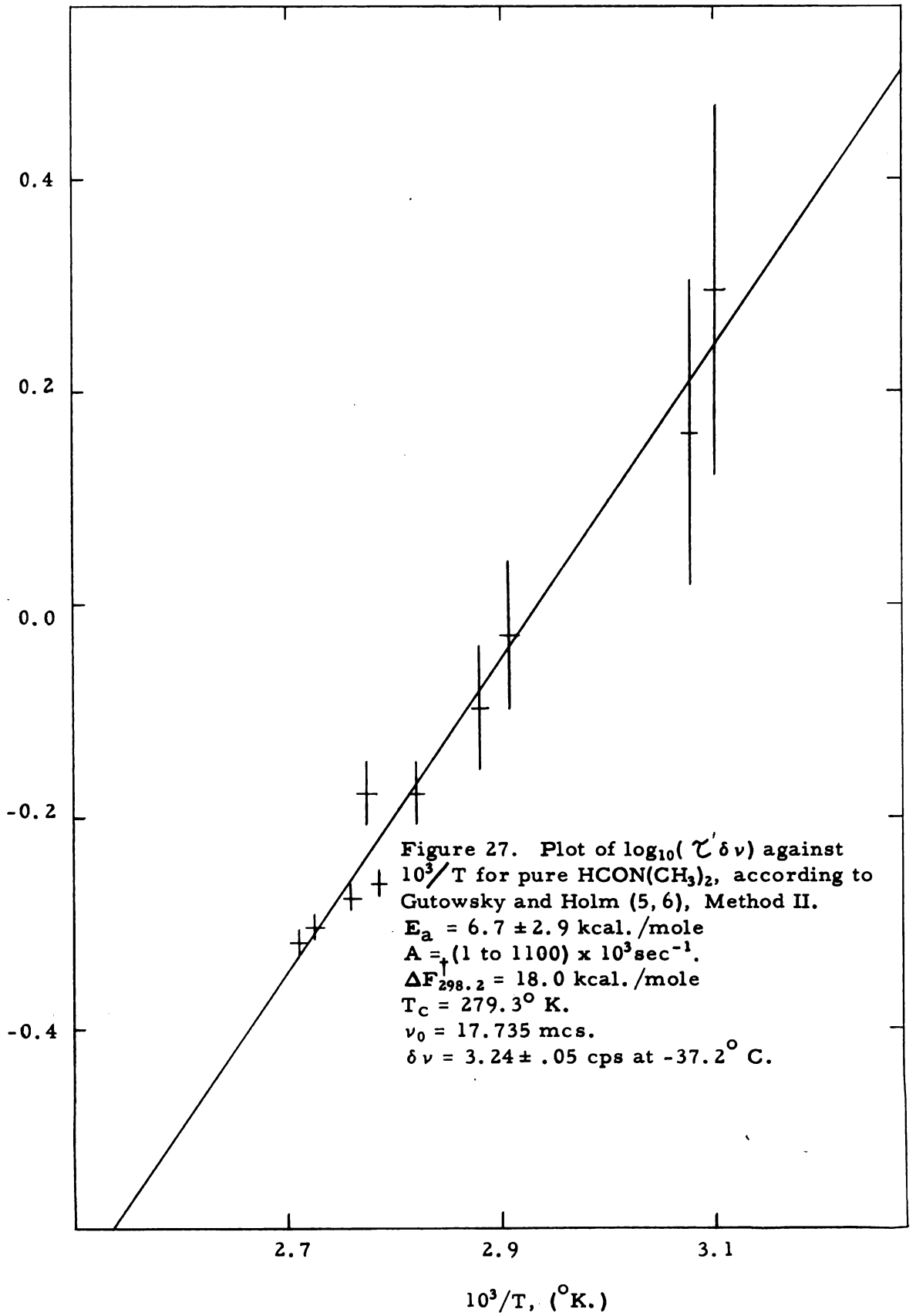

Figure 27. Plot of $\log_{10}(\tau' \delta\nu)$ against $10^3/T$ for pure $HCON(CH_3)_2$, according to Gutowsky and Holm (5, 6), Method II.
$E_a = 6.7 \pm 2.9$ kcal./mole
$A = \dagger$ (1 to 1100) x $10^3 sec^{-1}$.
$\Delta F^{\dagger}_{298.2} = 18.0$ kcal./mole
$T_C = 279.3°$ K.
$\nu_0 = 17.735$ mcs.
$\delta\nu = 3.24 \pm .05$ cps at -37.2° C.

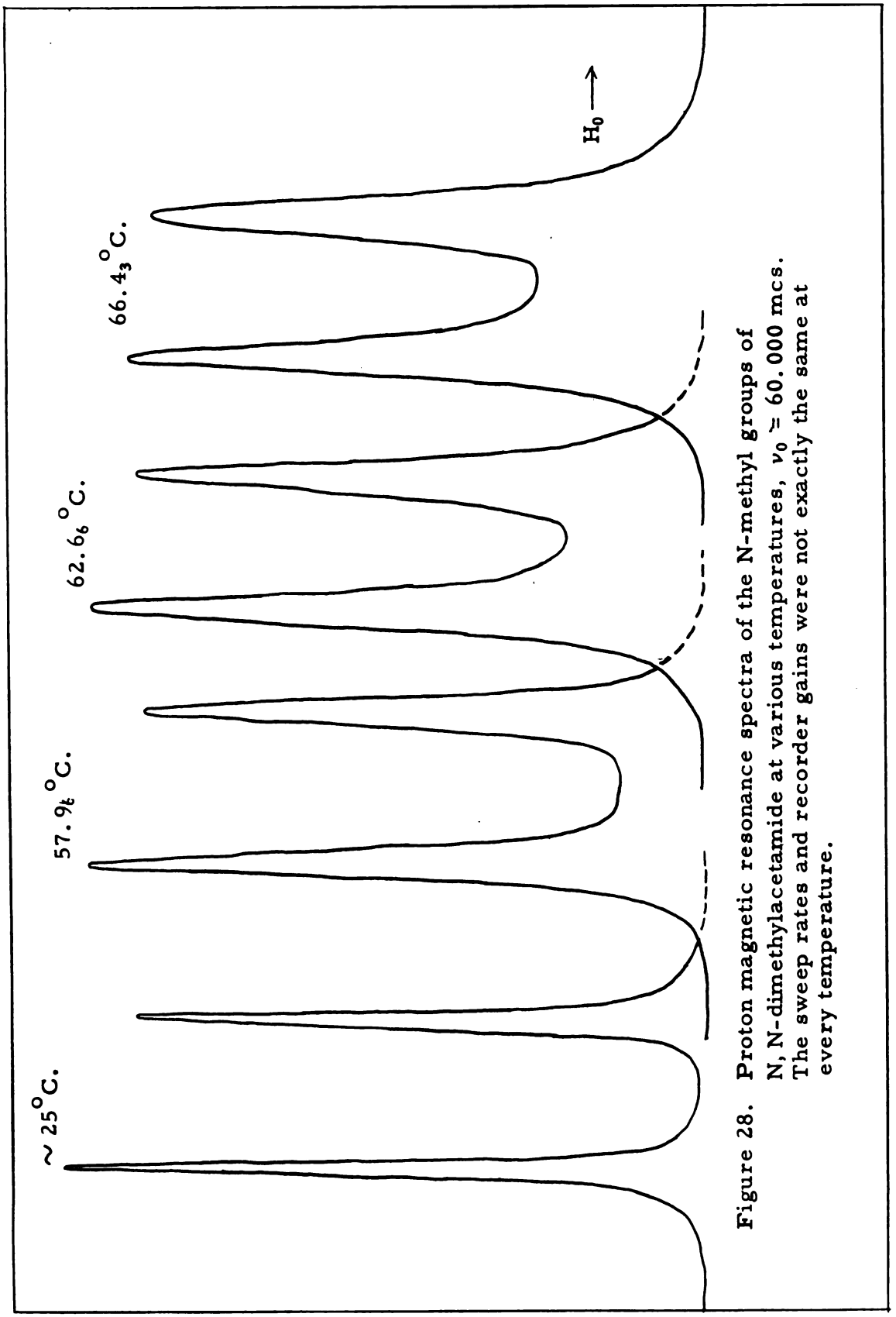

Figure 28. Proton magnetic resonance spectra of the N-methyl groups of N, N-dimethylacetamide at various temperatures, $\nu_0 \simeq 60.000$ mcs. The sweep rates and recorder gains were not exactly the same at every temperature.

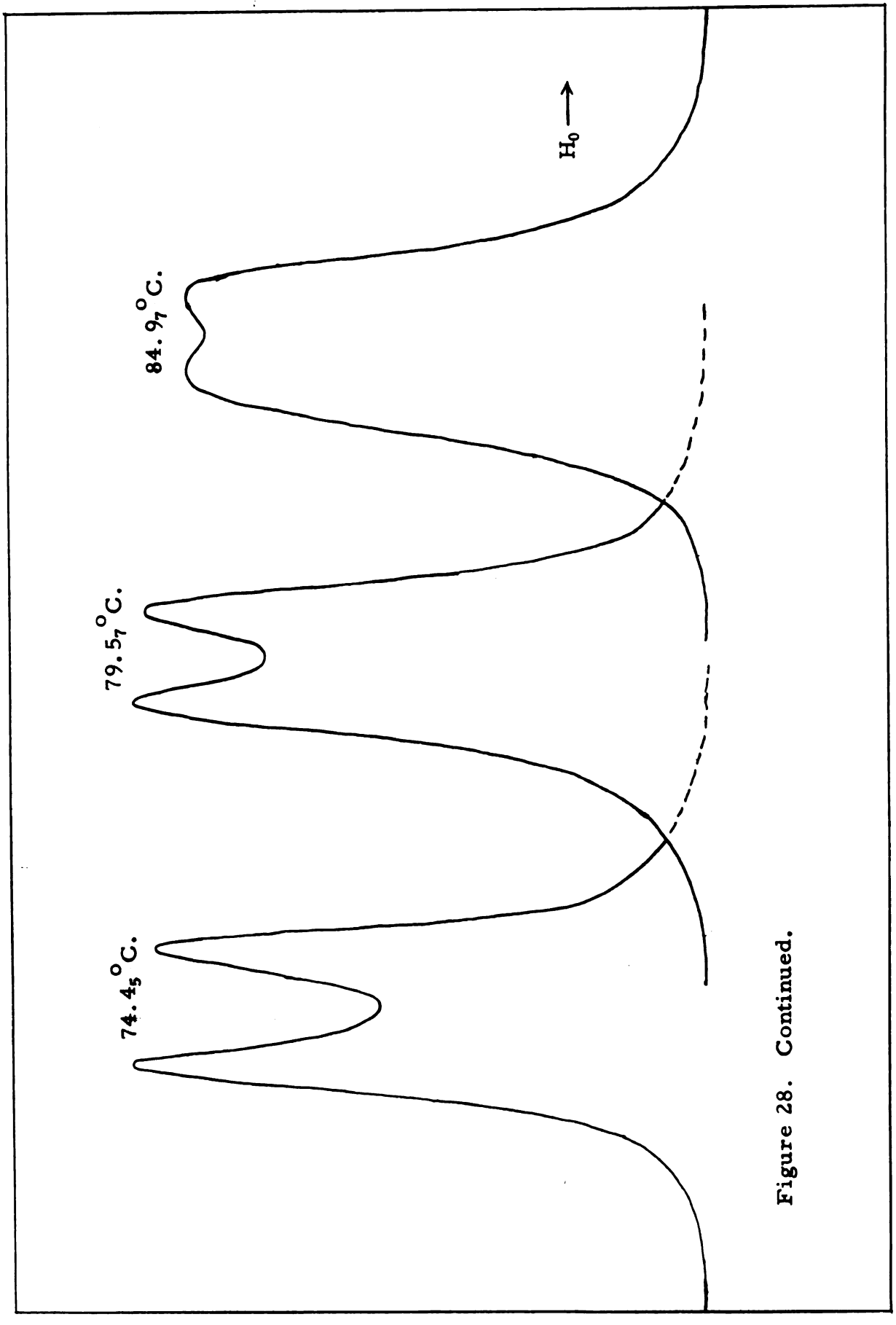

Figure 28. Continued.

TABLE IX

TEMPERATURE DEPENDENCE OF THE RATE OF INTERNAL ROTATION ABOUT THE CENTRAL C-N BOND OF $CH_3CON(CH_3)_2$, METHOD III

ν_0 = 60.000 mcs., $\delta\nu$ = 10.55 ± .34 cps at -27.6°C.

t, °C.	$10^3/T$, (°K.)	r	$\log_{10}(4\pi^2\tau\,\delta\nu)$
84.97 ± .33*	2.7923	1.029 ± .005*	.9890 ± .0035*
79.57 ± .10	2.8350	1.287 ± .023	1.0880 ± .0033
74.45 ± .01	2.8768	1.743 ± .023	1.1787 ± .0015
66.43 ± .09	2.9447	3.401 ± .025	1.3467 ± .0014
62.66 ± .09	2.9778	4.361 ± .027	1.4053 ± .0065
57.96 ± .04	3.0201	7.145 ± .238	1.5180 ± .0055

*The error given is the average deviation from the average of five measurements.

TABLE X

TEMPERATURE DEPENDENCE OF THE RATE OF INTERNAL ROTATION ABOUT THE CENTRAL C-N BOND OF $CH_3CON(CH_3)_2$, ACCORDING TO GUTOWSKY AND HOLM (5, 6), METHOD II

ν_0 = 17.735 mcs., $\delta\nu$ = 3.91 ± .14 cps at -24.2°C., T_2 = 1.13 ± .25 cps

t, °C.	$10^3/T$, (°K.)	$\delta\nu_e$, cps	$\log_{10}(\tau\,\delta\nu)$
49.3 ± 1*	3.1008	1.56 ± .11*	-.4794 ± .0090*
48.0 ± 1	3.1133	2.14 ± .21	-.4317 ± .0292
46.5 ± 1	3.1279	2.45 ± .14	-.3892 ± .0321
43.3 ± 1	3.1596	2.78 ± .11	-.3296 ± .0366
39.8 ± 1	3.1949	3.25 ± .14	-.1962 ± .0644
37.3 ± 1	3.2206	3.45 ± .14	-.0993 ± .1140
33.8 ± 1	3.2573	3.48 ± .18	-.0770 ± .1363
29.8 ± 1	3.3003	3.63 ± .14	-.0555 ± .3010
19.8 ± 1	3.4130	3.77 ± .11	+.2980 ± .2757
-24.2 ± 1	4.0161	3.89 ± .14	

*The error given is the standard deviation from the average of about ten measurements.

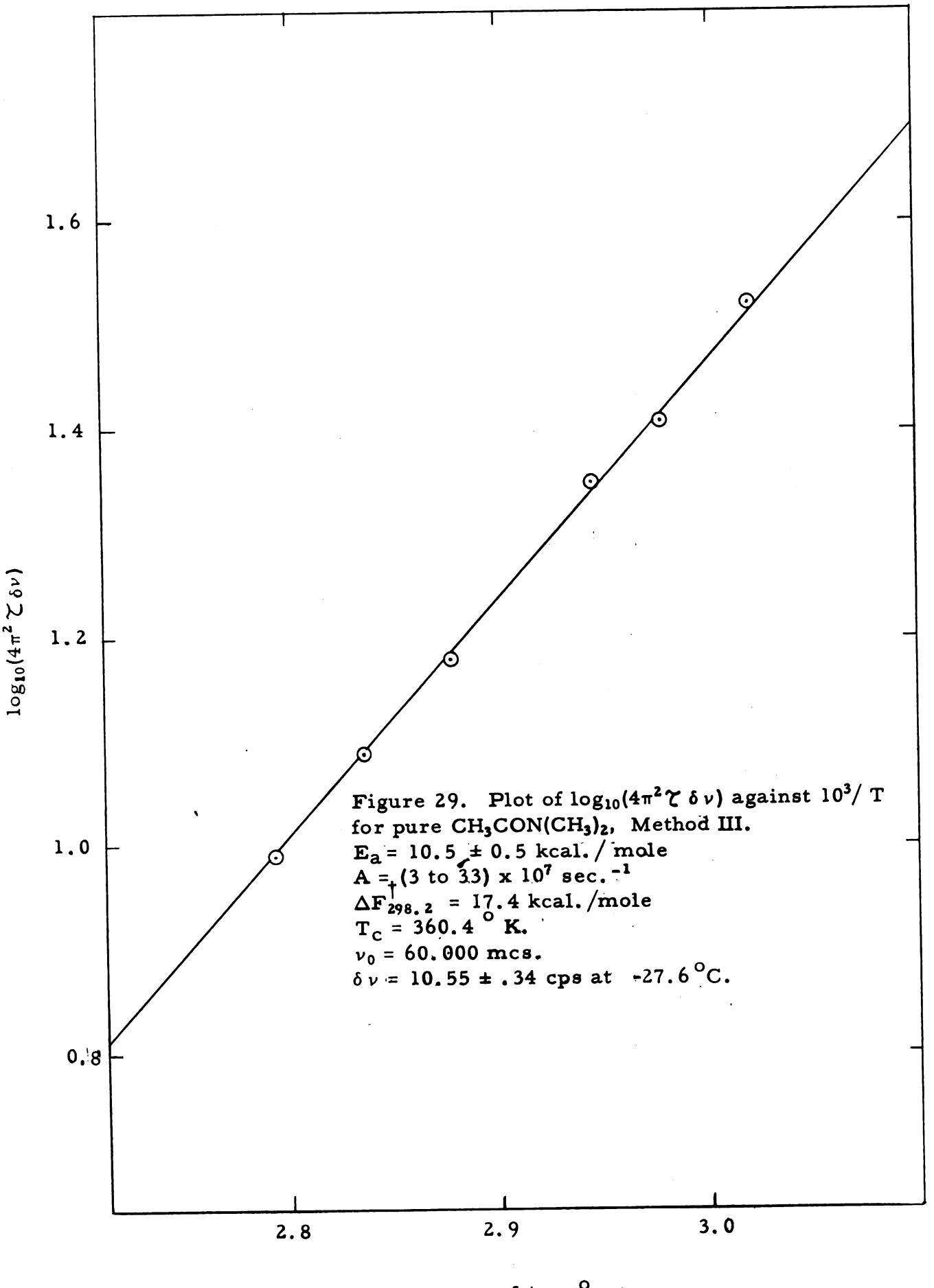

Figure 29. Plot of $\log_{10}(4\pi^2 \tau \delta\nu)$ against $10^3/T$ for pure $CH_3CON(CH_3)_2$, Method III.
E_a = 10.5 ± 0.5 kcal./mole
$A = \pm$(3 to 33) x 10^7 sec.$^{-1}$
$\Delta F_{298.2}$ = 17.4 kcal./mole
T_c = 360.4 $^\circ$K.
ν_0 = 60.000 mcs.
$\delta\nu$ = 10.55 ± .34 cps at -27.6 $^\circ$C.

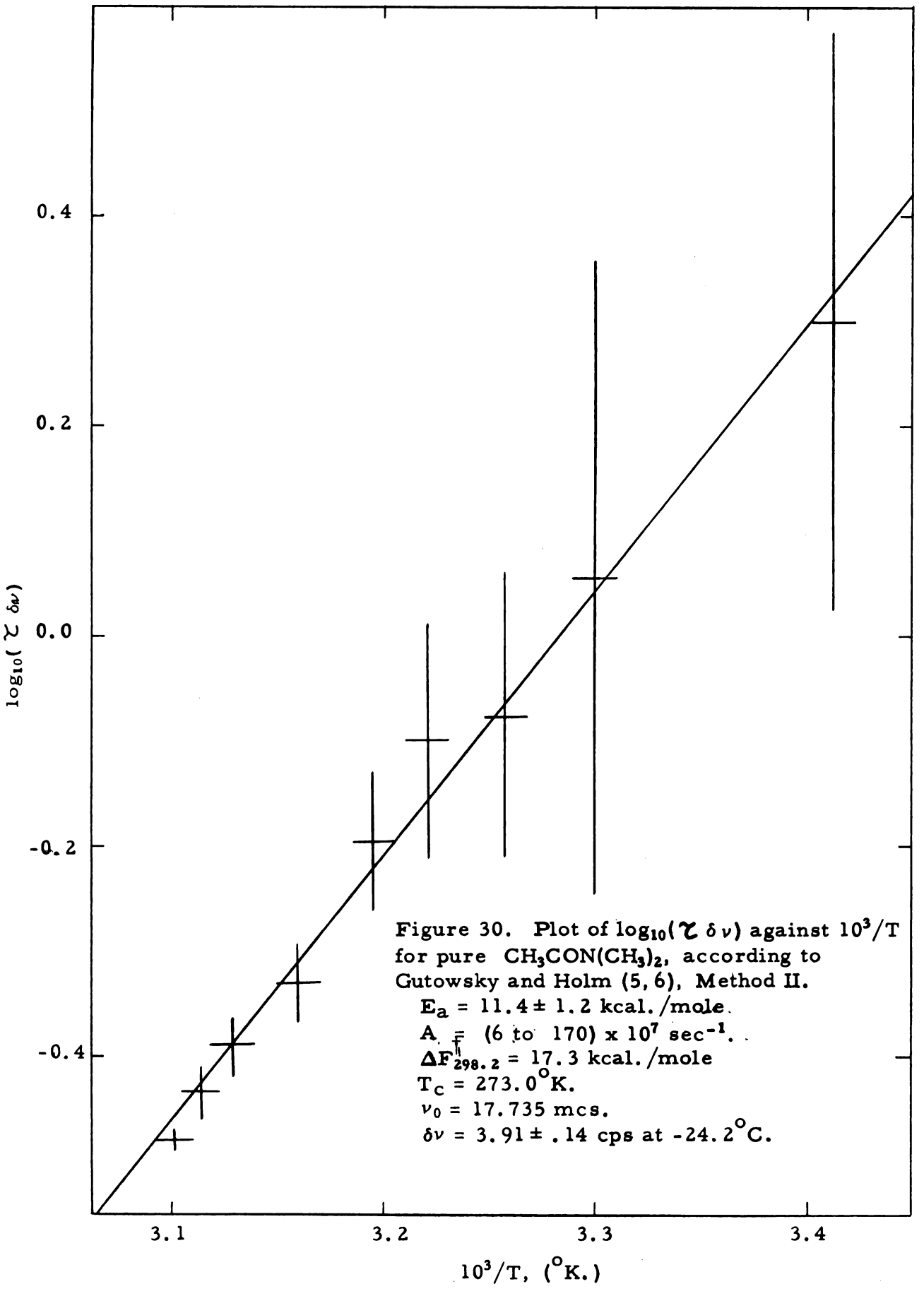

Figure 30. Plot of $\log_{10}(\tau\,\delta\nu)$ against $10^3/T$ for pure $CH_3CON(CH_3)_2$, according to Gutowsky and Holm (5, 6), Method II.

$E_a = 11.4 \pm 1.2$ kcal./mole.

$A = (6 \text{ to } 170) \times 10^7$ sec^{-1}.

$\Delta F^{\ddagger}_{298.2} = 17.3$ kcal./mole

$T_c = 273.0^\circ$K.

$\nu_0 = 17.735$ mcs.

$\delta\nu = 3.91 \pm .14$ cps at -24.2°C.

against $10^3/T$ in Figures 31 through 40. The concentration dependencies of the energy barrier E_a, for the solutions of amide in dibromomethane and for the solutions of amide in carbon tetrachloride, are shown in Figure 41.

N, N-Dimethyltrichloroacetamide - The hindered internal rotation about the central C-N bond of pure N, N-dimethyltrichloroacetamide was studied by Method III. The experimental data are tabulated in Table XIV and plotted as $\log_{10}(4\pi^2\gamma\delta\nu)$ against $10^3/T$ in Figure 42.

N, N-Dimethyltrifluoroacetamide - The hindered interval rotation about the central C-N bond of pure N, N-dimethyltrifluoroacetamide was studied by Method III. The proton-fluorine spin-spin interactions were decoupled by the double irradiation technique. Some of the spectra, from which data were obtained, are shown in Figure 43. The experimental data are tabulated in Table XV and plotted as $\log_{10}(4\pi^2\gamma\delta\nu)$ against $10^3/T$ in Figure 44.

N, N-Dimethylacrylamide - The internal rotation about the central C-N bond of N, N-dimethylacrylamide was studied by Method III. The experimental data are tabulated in Table XVI and plotted as $\log_{10}(4\pi^2\gamma\delta\nu)$ against $10^3/T$ in Figure 45.

N, N-Dimethylbenzamide - The hindered internal about the central C-N bond of N, N-dimethylbenzamide (36.3_4 mole per cent in dibromomethane) was studied by Method III. The experimental data are tabulated in Table XVII and plotted as $\log_{10}(4\pi^2\gamma\delta\nu)$ against $10^3/T$ in Figure 46.

N, N-Dimethylcarbamyl chloride - The hindered internal rotation about the central C-N bond of pure N, N-dimethylcarbamyl chloride was studied by Method III. In addition, the phenomenon was studied for the following concentrations (mole per cent) of amide (a) in dibromomethane: 90.0_3, 63.4_4, 40.9_3, and 10.7_2; and (b) in carbon tetrachloride: 71.3_5,

TABLE XI

TEMPERATURE DEPENDENCE OF THE RATE OF INTERNAL ROTATION ABOUT THE CENTRAL C-N BOND OF N, N-DIMETHYLPROPIONAMIDE, METHOD III

ν_0 = 60.000 mcs., $\delta\nu$ = 9.18 ± .17 cps at -27.5°C.

t, °C.	$10^3/T$, (°K.)	r	$\log_{10}(4\pi^2\tau\,\delta\nu)$
56.26 ± .05*	3.0356	1.094 ± .004*	1.0244 ± .0019*
55.83 ± .05	3.0396	1.095 ± .006	1.0248 ± .0025
52.44 ± .16	3.0713	1.410 ± .014	1.1165 ± .0027
50.48 ± .08	3.0899	1.623 ± .020	1.1589 ± .0038
50.44 ± .09	3.0902	1.702 ± .025	1.1720 ± .0040
47.26 ± .04	3.1209	2.163 ± .027	1.2362 ± .0035
44.65 ± .14	3.1465	2.495 ± .111	1.2720 ± .0116
39.27 ± .14	3.2007	3.597 ± .185	1.3600 ± .0126
34.01 ± .16	3.2555	5.896 ± .134	1.4745 ± .0053

*The error given is the average deviation from the average of five measurements.

TABLE XII

TEMPERATURE DEPENDENCIES OF THE RATE OF INTERNAL ROTATION ABOUT THE CENTRAL C-N BOND OF N, N-DIMETHYLPROPIONAMIDE IN DIBROMOMETHANE SOLUTIONS, METHOD III

ν_0 = 60.000 mcs.

(a) 84.7_1 mole per cent amide, $\delta\nu$ = 8.88 ± .20 cps at -26.8°C.

t, °C.	$10^3/T$, (°K.)	r	$\log_{10}(4\pi^2\tau\,\delta\nu)$
56.04 ± .11*	3.0395	1.081 ± .006*	1.0172 ± .0005*
55.13 ± .06	3.0461	1.041 ± .005	1.0285 ± .0347
52.59 ± .23	3.0698	1.321 ± .038	1.0957 ± .0089
49.94 ± .13	3.0950	1.591 ± .008	1.1530 ± .0012
49.86 ± .14	3.0958	1.635 ± .012	1.1608 ± .0019
46.78 ± .05	3.1256	2.282 ± .073	1.2491 ± .0078
44.72 ± .26	3.1458	2.644 ± .073	1.2862 ± .0068
39.29 ± .09	3.2005	4.143 ± .251	1.3933 ± .0149
34.14 ± .06	3.2541	6.024 ± .177	1.4794 ± .0063
(b) 68.8_8 mole per cent amide, $\delta\nu$ = 8.55 ± .21 cps at -26.8°C.			
56.07 ± .05	3.0374	1.083 ± .009	1.0191 ± .0034
54.95 ± .13	3.0478	1.102 ± .002	1.0271 ± .0003
52.51 ± .11	3.0706	1.348 ± .019	1.1022 ± .0040
50.59 ± .07	3.0888	1.620 ± .008	1.1580 ± .0012
50.04 ± .14	3.0941	1.643 ± .017	1.1622 ± .0029
47.04 ± .04	3.1230	2.254 ± .073	1.2463 ± .0081
44.83 ± .06	3.1448	2.480 ± .054	1.2704 ± .0057
39.81 ± .11	3.1952	4.088 ± .060	1.3903 ± .0035
33.98 ± .09	3.2558	6.538 ± .308	1.4981 ± .0112

Continued

TABLE XII - Continued

t, °C.	$10^3/T$, (°K.)	r	$\log_{10}(4\pi^2\tau\delta\nu)$
(c) 58.0$_0$ mole per cent amide, $\delta\nu$ = 8.24 ± .19 cps at -23.4°C.			
56.20 ± .09	3.0356	1.079 ± .008	1.0180 ± .0042
55.90 ± .05	3.0390	1.075 ± .004	1.0159 ± .0021
52.91 ± .11	3.0668	1.356 ± .005	1.1040 ± .0012
50.55 ± .06	3.0892	1.598 ± .009	1.1545 ± .0017
50.36 ± .11	3.0910	1.605 ± .018	1.1555 ± .0034
47.41 ± .07	3.1194	2.136 ± .065	1.2327 ± .0081
45.59 ± .12	3.1373	2.467 ± .046	1.2692 ± .0044
39.67 ± .05	3.1966	3.997 ± .140	1.3847 ± .0028
39.64 ± .24	3.1969	3.671 ± .127	1.3647 ± .0082
36.44 ± .07	3.2300	6.147 ± .009	1.4840 ± .0005
34.18 ± .24	3.2537	6.451 ± .280	1.4950 ± .0102
(d) 40.5$_7$ mole per cent amide, $\delta\nu$ = 7.45 ± .25 cps at -26.4°C.			
56.61 ± .09	3.0324	1.029 ± .005	.9890 ± .0045
55.97 ± .10	3.0383	1.059 ± .004	1.0078 ± .0026
55.90 ± .08	3.0389	1.059 ± .004	1.0078 ± .0026
52.47 ± .07	3.0710	1.286 ± .020	1.0872 ± .0051
50.19 ± .13	3.0926	1.505 ± .008	1.1370 ± .0016
50.16 ± .08	3.0929	1.551 ± .010	1.1456 ± .0017
47.65 ± .09	3.1171	2.077 ± .035	1.2253 ± .0045
46.12 ± .06	3.1320	2.155 ± .018	1.2350 ± .0022
39.90 ± .09	3.1943	3.519 ± .082	1.3547 ± .0057
35.00 ± .21	3.2451	5.133 ± .253	1.4427 ± .0107

Continued

TABLE XII - Continued

t, °C.	$10^3/T$, (°K.)	r	$\log_{10}(4\pi^2\tau\delta\nu)$
(e) 22.1$_7$ mole per cent amide, $\delta\nu$ = 6.42 ± .13 cps at -24.0°C.			
57.30 ± .09	3.0261	1.000 ± .004	.9856 ± .0039
52.33 ± .05	3.0723	1.241 ± .012	1.0755 ± .0035
50.82 ± .18	3.0866	1.334 ± .012	1.0988 ± .0019
49.47 ± .09	3.0995	1.491 ± .023	1.1342 ± .0052
47.17 ± .14	3.1218	1.691 ± .056	1.1702 ± .0097
45.71 ± .12	3.1361	1.879 ± .023	1.1990 ± .0035
39.91 ± .08	3.1942	3.017 ± .063	1.3182 ± .0054
34.96 ± .06	3.2455	4.685 ± .065	1.4215 ± .0031
(f) 10.1$_4$ mole per cent amide, $\delta\nu$ = 5.77 ± .26 cps at -23.8°C.			
51.28 ± .06	3.0822	1.516 ± .007	1.1395 ± .0007
46.99 ± .07	3.1235	2.005 ± .003	1.2160 ± .0005
42.45 ± .05	3.1685	2.328 ± .048	1.2542 ± .0050
39.25 ± .05	3.2009	2.772 ± .063	1.2977 ± .0038
36.55 ± .02	3.2288	3.501 ± .024	1.3538 ± .0015
36.32 ± .11	3.2312	3.395 ± .072	1.3462 ± .0050
34.23 ± .02	3.2532	3.881 ± .013	1.3780 ± .0007
30.08 ± .04	3.2977	4.738 ± .065	1.4242 ± .0033

*The error given is the average deviation from the average of five measurements.

TABLE XIII

TEMPERATURE DEPENDENCIES OF THE RATE OF INTERNAL ROTATION ABOUT THE CENTRAL C-N BOND OF N, N-DIMETHYLPROPIONAMIDE IN CARBON TETRACHLORIDE SOLUTIONS, METHOD III

ν_0 = 60.000 mcs.

(a) 69.3$_4$ mole per cent amide, $\delta\nu$ = 9.59 ± .18 cps at -24.0°C.

t, °C.	$10^3/T$, (°K.)	r	$\log_{10}(4\pi^2\tau\delta\nu)$
51.38 ± .05*	3.0813	1.140 ± .003*	1.0420 ± .0015*
47.02 ± .07	3.1232	1.531 ± .016	1.1420 ± .0030
42.47 ± .05	3.1683	1.964 ± .019	1.2105 ± .0037
39.56 ± .02	3.1978	2.527 ± .026	1.2752 ± .0025
36.76 ± .04	3.2260	3.138 ± .027	1.3277 ± .0020
34.84 ± .05	3.2468	3.544 ± .037	1.3565 ± .0035
(b) 39.9$_4$ mole per cent amide, $\delta\nu$ = 9.69 ± .13 cps at -24.0°C.			
34.27 ± .05	3.2528	1.061 ± .005	1.0090 ± .0025
29.94 ± .02	3.2992	1.310 ± .009	1.0935 ± .0025
26.10 ± .05	3.3416	1.696 ± .007	1.1710 ± .0015
24.47 ± .24	3.3599	1.780 ± .008	1.1845 ± .0010
18.68 ± .02	3.4265	2.744 ± .045	1.2952 ± .0032
14.07 ± .15	3.4815	4.056 ± .028	1.3882 ± .0018
(c) 11.0$_7$ mole per cent amide, $\delta\nu$ = 9.65 ± .15 cps at -23.8°C.			
36.69 ± .03	3.2274	1.108 ± .027	1.0303 ± .0097
34.94 ± .09	3.2457	1.209 ± .008	1.0655 ± .0030
29.97 ± .05	3.2989	1.544 ± .011	1.1445 ± .0020
26.54 ± .12	3.3367	1.913 ± .026	1.2035 ± .0035
18.66 ± .25	3.4269	3.052 ± .062	1.3210 ± .0047
12.73 ± .12	3.4978	4.385 ± .177	1.4065 ± .0090

*The error given is the average deviation from the average of five measurements.

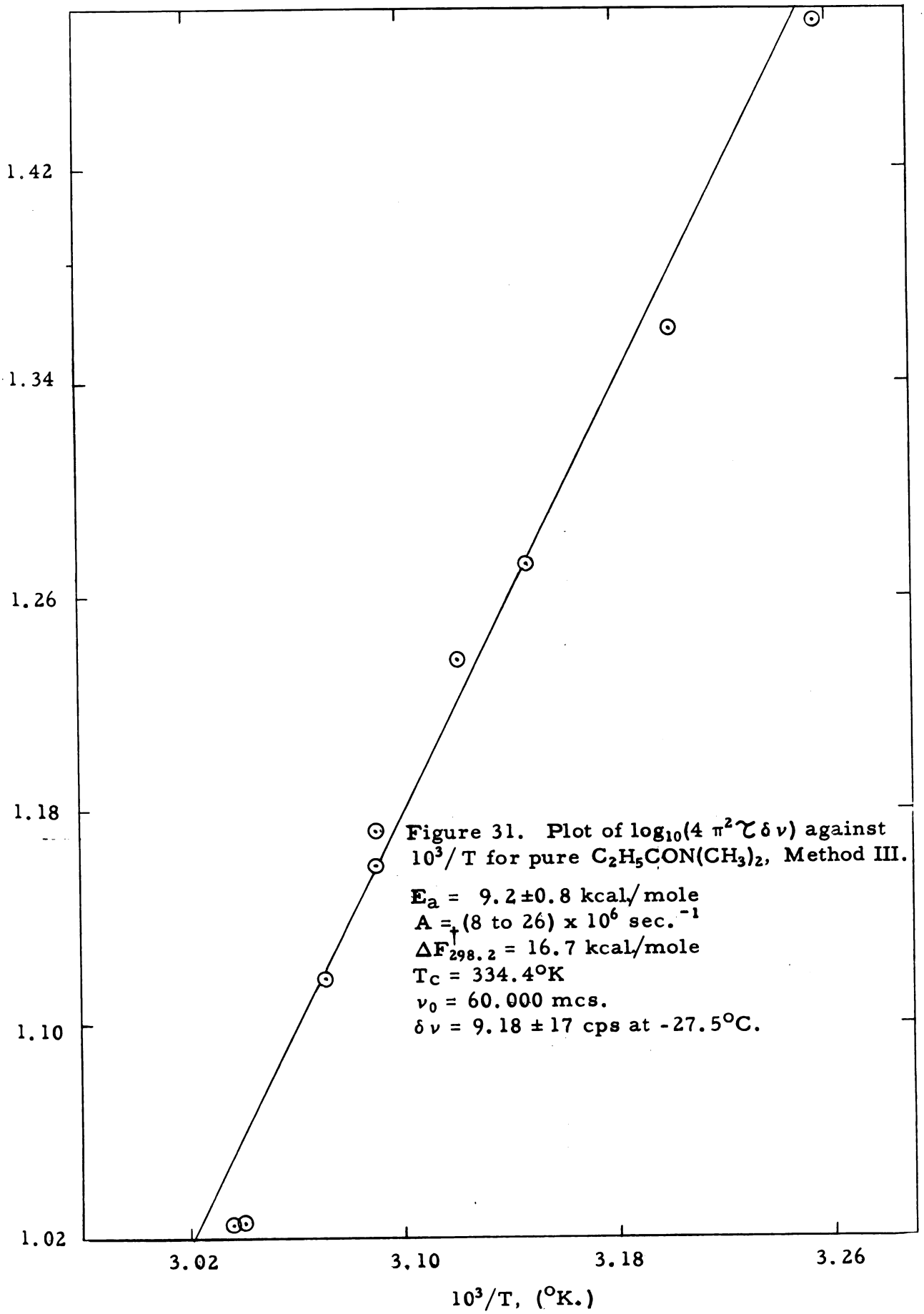

Figure 31. Plot of $\log_{10}(4\pi^2\tau\delta\nu)$ against $10^3/T$ for pure $C_2H_5CON(CH_3)_2$, Method III.

E_a = 9.2 ±0.8 kcal/mole
$A = \pm$(8 to 26) x 10^6 sec.$^{-1}$
$\Delta F^{\dagger}_{298.2}$ = 16.7 kcal/mole
T_C = 334.4°K
ν_0 = 60.000 mcs.
$\delta\nu$ = 9.18 ± 17 cps at -27.5°C.

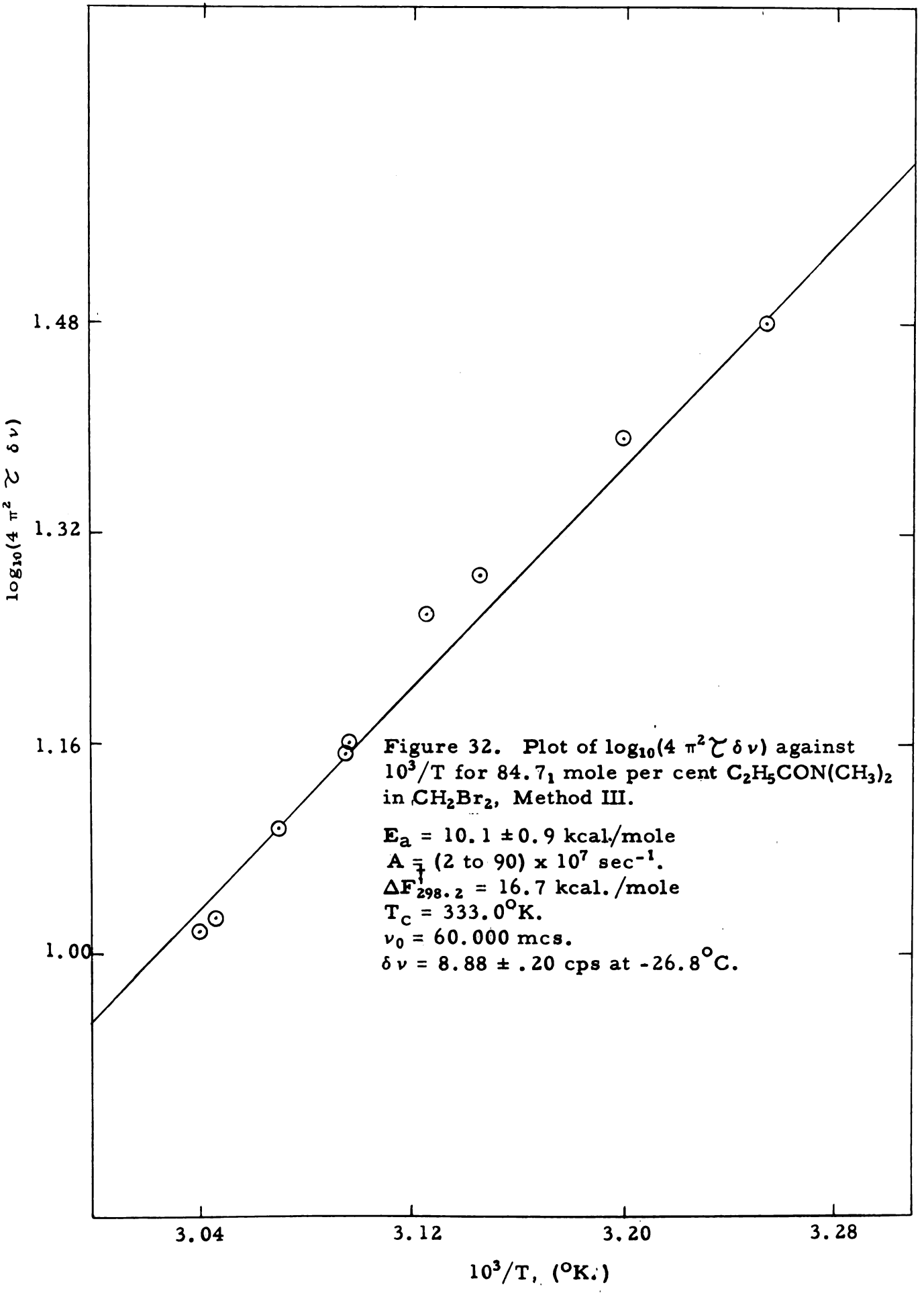

Figure 32. Plot of $\log_{10}(4\pi^2\tau\delta\nu)$ against $10^3/T$ for 84.7$_1$ mole per cent $C_2H_5CON(CH_3)_2$ in CH_2Br_2, Method III.

E_a = 10.1 ± 0.9 kcal./mole
$A = \frac{1}{\tau}$ (2 to 90) x 10^7 sec^{-1}.
$\Delta F^{\ddagger}_{298.2}$ = 16.7 kcal./mole
T_c = 333.0°K.
ν_0 = 60.000 mcs.
$\delta\nu$ = 8.88 ± .20 cps at -26.8°C.

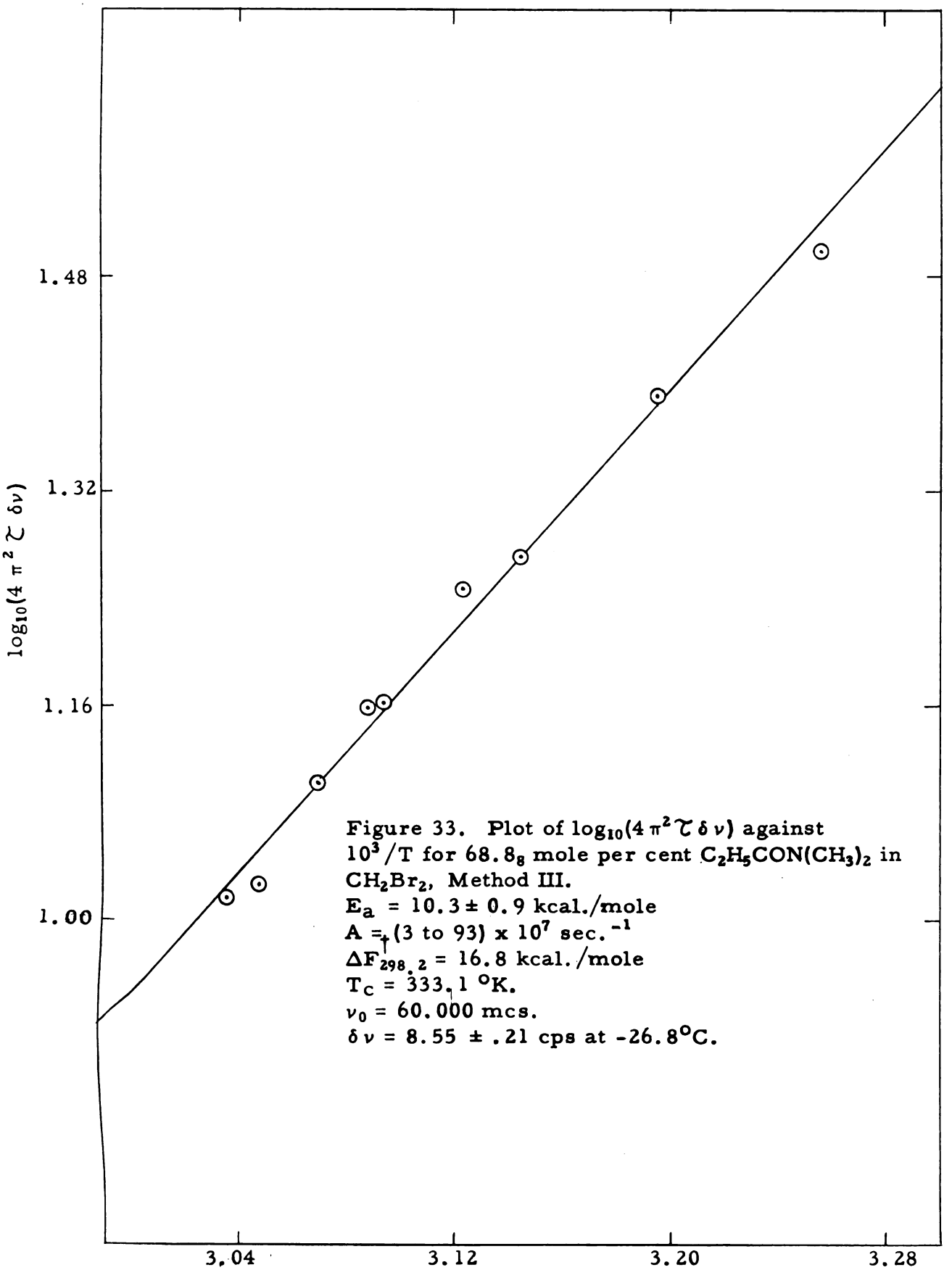

Figure 33. Plot of $\log_{10}(4\pi^2\tau\delta\nu)$ against $10^3/T$ for 68.8$_8$ mole per cent $C_2H_5CON(CH_3)_2$ in CH_2Br_2, Method III.
E_a = 10.3 ± 0.9 kcal./mole
A = (3 to 93) x 10^7 sec.$^{-1}$
$\Delta F_{298.2}$ = 16.8 kcal./mole
T_c = 333.1 °K.
ν_0 = 60.000 mcs.
$\delta\nu$ = 8.55 ± .21 cps at -26.8°C.

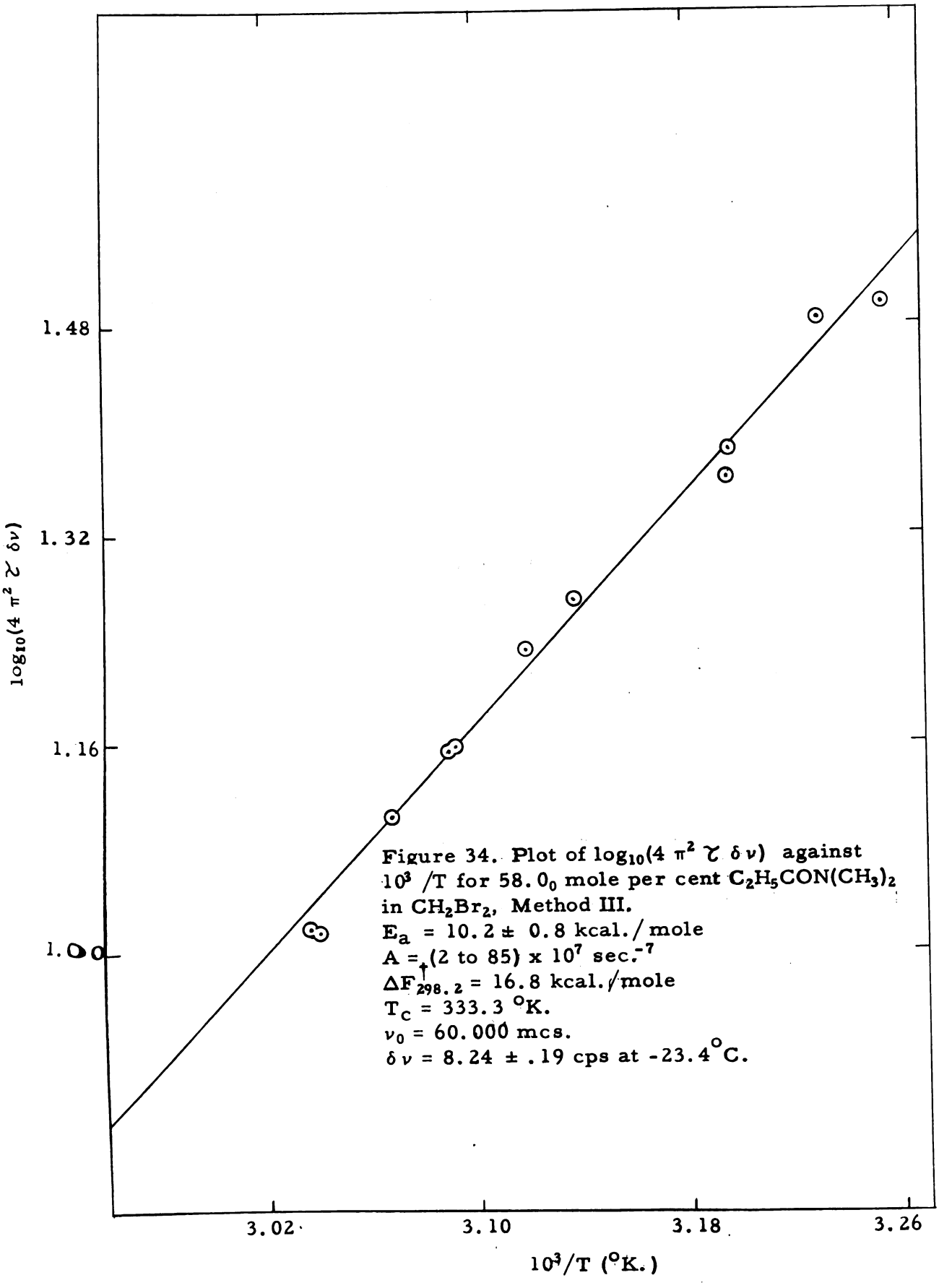

Figure 34. Plot of $\log_{10}(4\pi^2 \gamma \delta\nu)$ against $10^3/T$ for 58.0$_0$ mole per cent $C_2H_5CON(CH_3)_2$ in CH_2Br_2, Method III.
E_a = 10.2 ± 0.8 kcal./mole
$A = (2 \text{ to } 85) \times 10^7$ sec.$^{-7}$
$\Delta F^{\dagger}_{298.2}$ = 16.8 kcal./mole
T_c = 333.3 °K.
ν_0 = 60.000 mcs.
$\delta\nu$ = 8.24 ± .19 cps at -23.4°C.

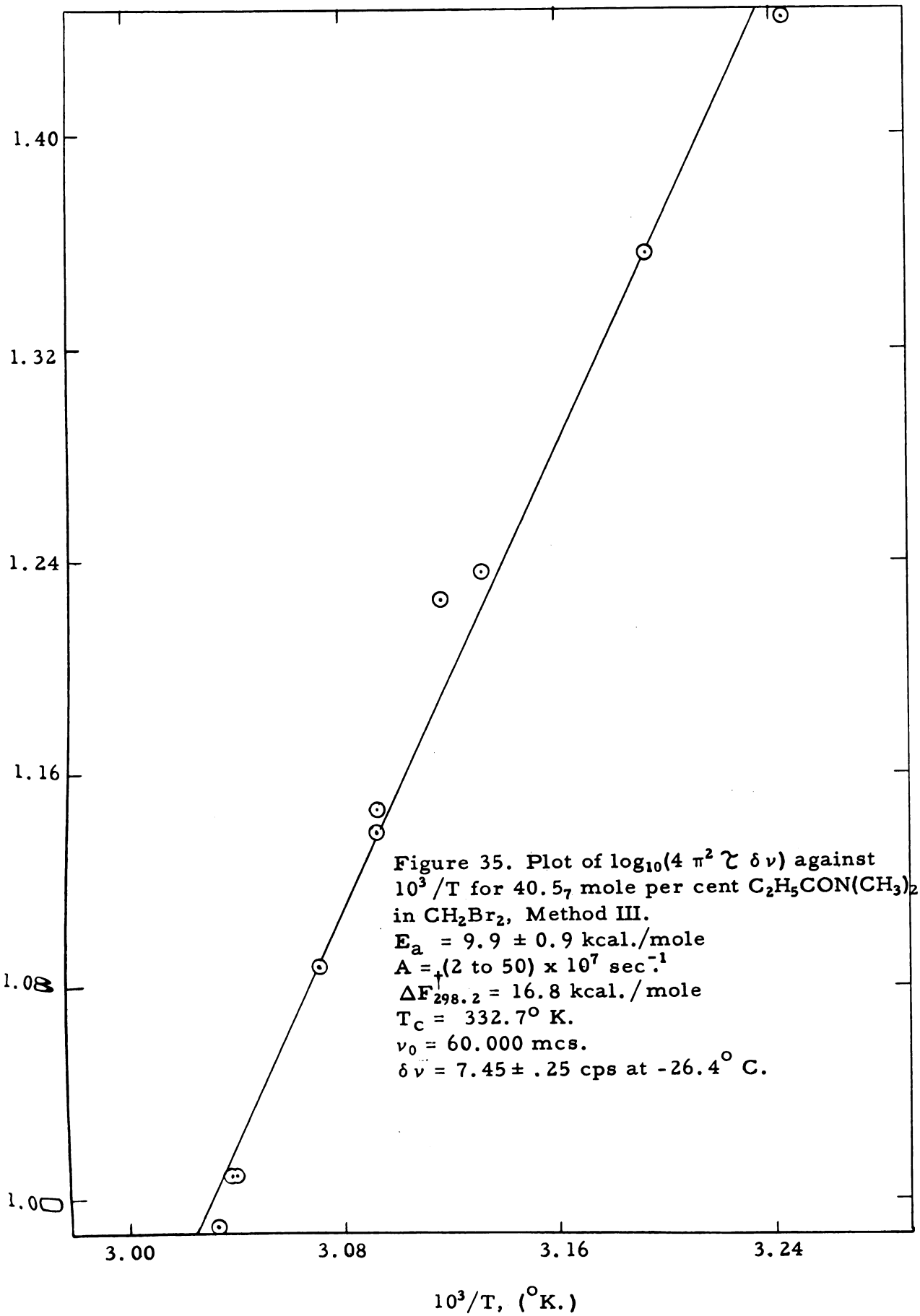

Figure 35. Plot of $\log_{10}(4\pi^2\tau\delta\nu)$ against $10^3/T$ for 40.5$_7$ mole per cent $C_2H_5CON(CH_3)_2$ in CH_2Br_2, Method III.
E_a = 9.9 ± 0.9 kcal./mole
$A = \dagger$(2 to 50) x 10^7 $sec.^{-1}$
$\Delta F^{\dagger}_{298.2}$ = 16.8 kcal./mole
T_c = 332.7° K.
ν_0 = 60.000 mcs.
$\delta\nu$ = 7.45 ± .25 cps at -26.4° C.

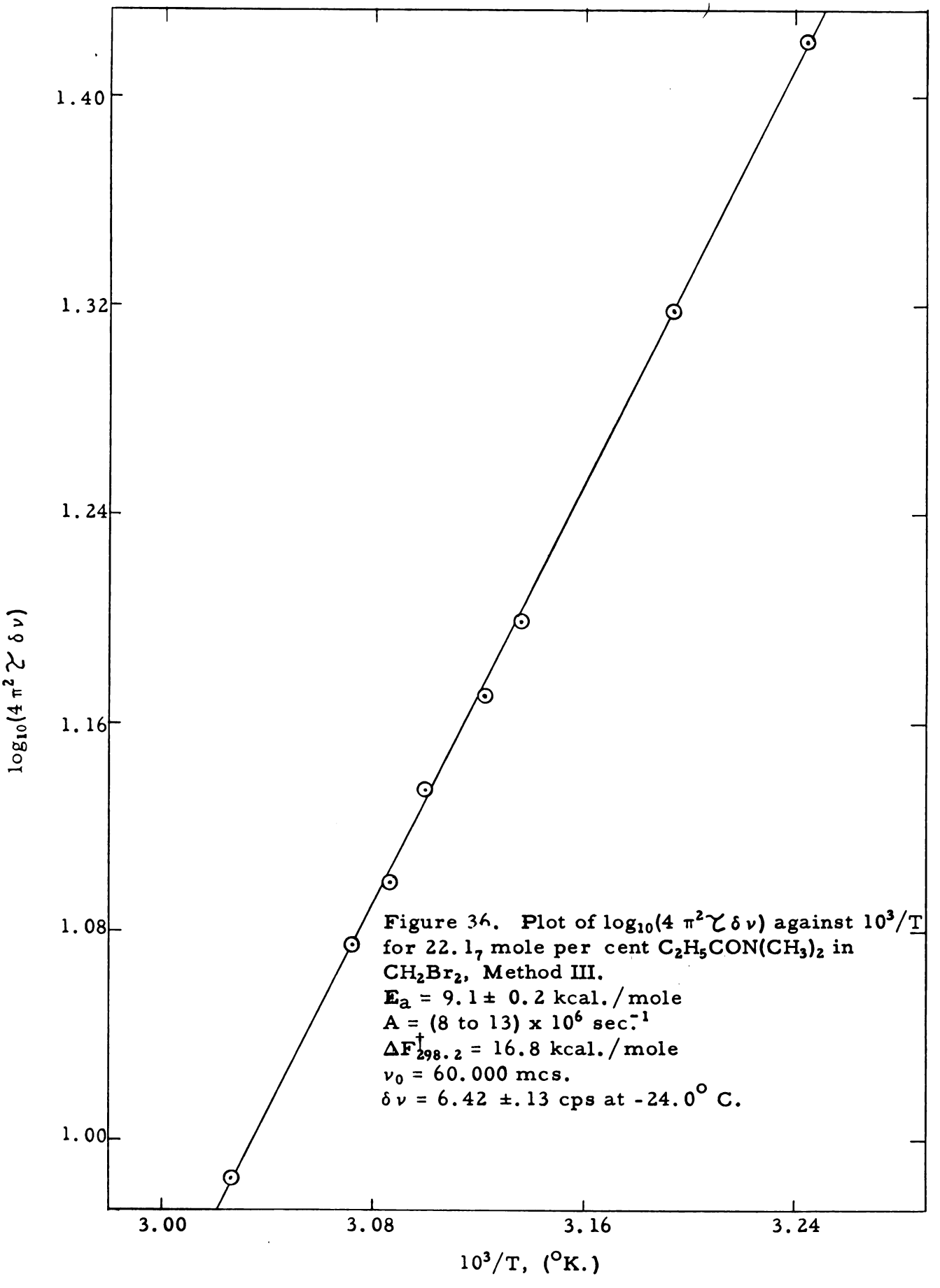

Figure 36. Plot of $\log_{10}(4\pi^2\gamma\delta\nu)$ against $10^3/T$ for 22.1$_7$ mole per cent $C_2H_5CON(CH_3)_2$ in CH_2Br_2, Method III.
E_a = 9.1 ± 0.2 kcal./mole
A = (8 to 13) x 10^6 $sec.^{-1}$
$\Delta F^{\dagger}_{298.2}$ = 16.8 kcal./mole
ν_0 = 60.000 mcs.
$\delta\nu$ = 6.42 ±.13 cps at -24.0° C.

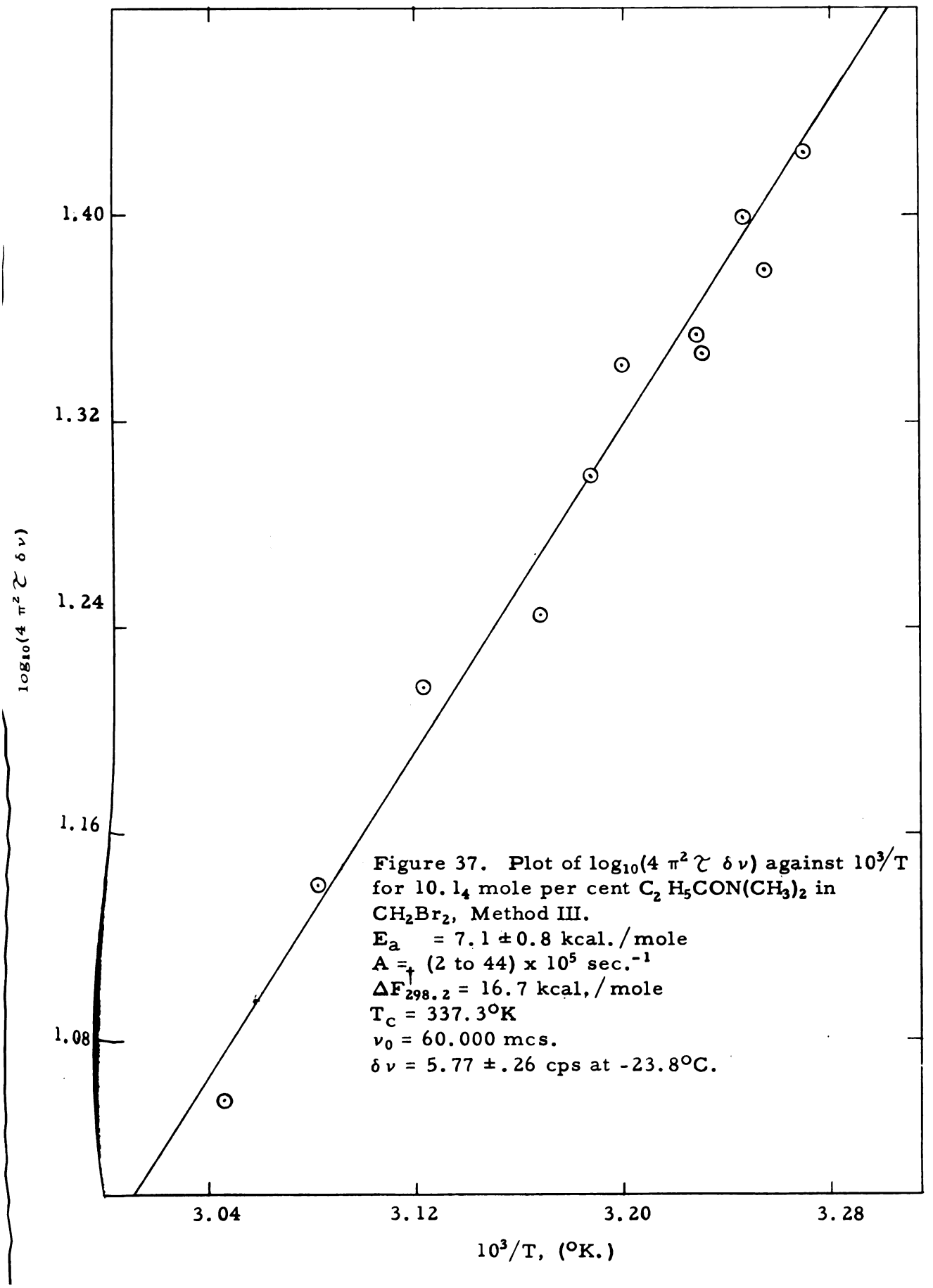

Figure 37. Plot of $\log_{10}(4\pi^2\tau\,\delta\nu)$ against $10^3/T$ for 10.1$_4$ mole per cent $C_2H_5CON(CH_3)_2$ in CH_2Br_2, Method III.
E_a = 7.1 ± 0.8 kcal./mole
$A = \dagger$ (2 to 44) x 10^5 sec.$^{-1}$
$\Delta F_{298.2}$ = 16.7 kcal./mole
T_c = 337.3°K
ν_0 = 60.000 mcs.
$\delta\nu$ = 5.77 ± .26 cps at -23.8°C.

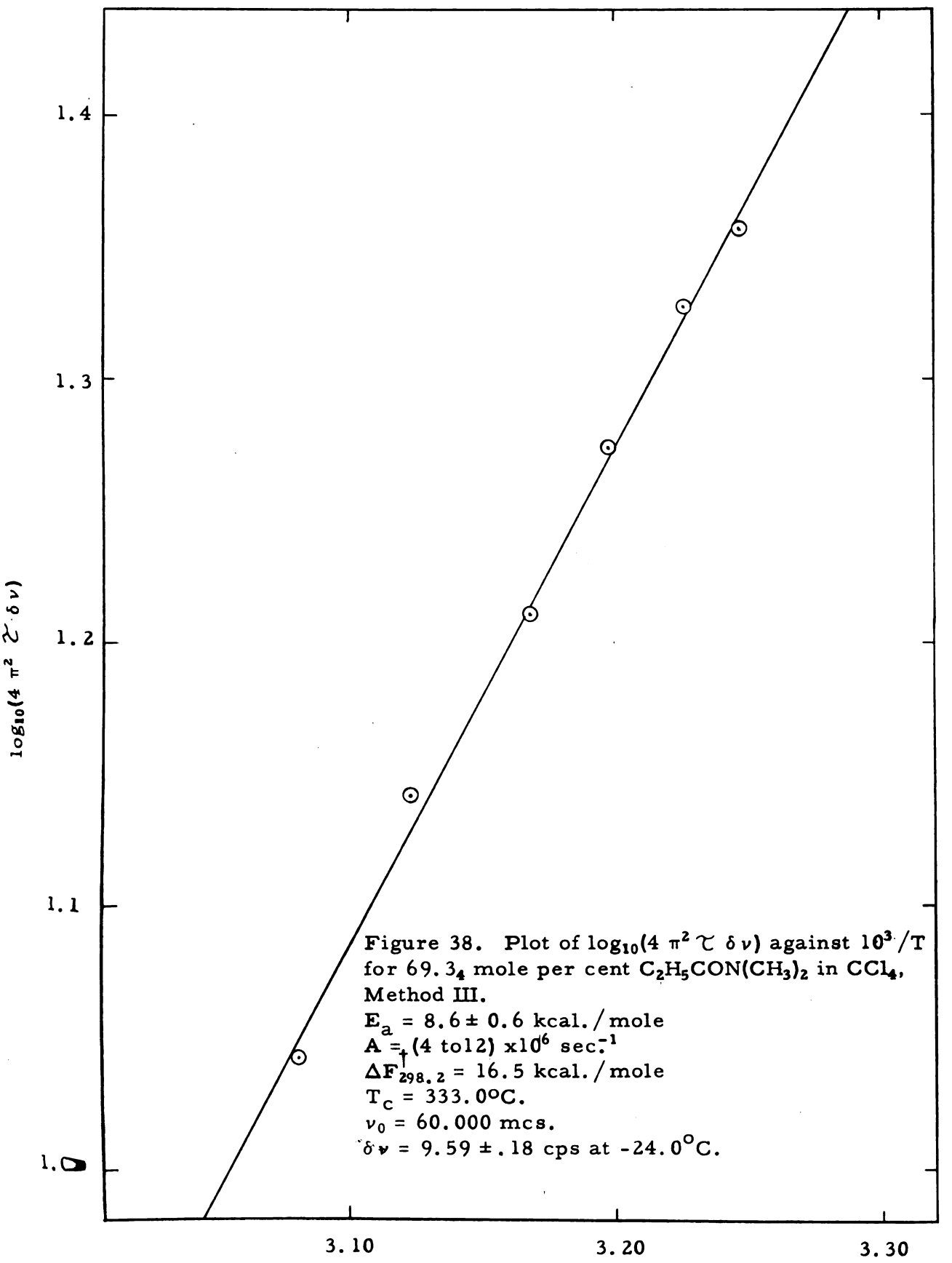

Figure 38. Plot of $\log_{10}(4\pi^2 \tau \delta\nu)$ against $10^3/T$ for 69.3$_4$ mole per cent $C_2H_5CON(CH_3)_2$ in CCl_4, Method III.
E_a = 8.6 ± 0.6 kcal./mole
A = (4 to12) x10^6 sec.$^{-1}$
$\Delta F^{\dagger}_{298.2}$ = 16.5 kcal./mole
T_c = 333.0°C.
ν_0 = 60.000 mcs.
$\delta\nu$ = 9.59 ± .18 cps at -24.0°C.

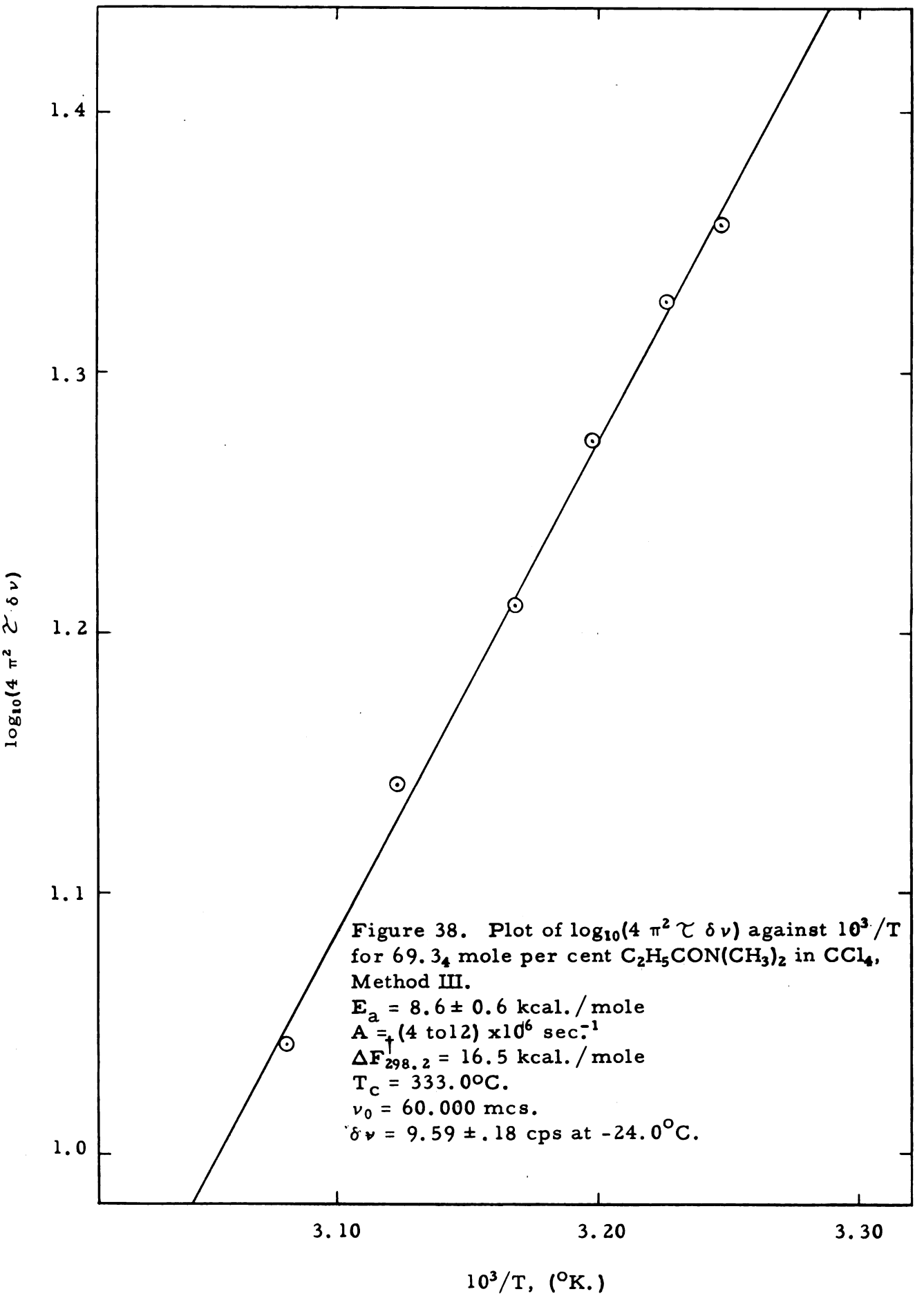

Figure 38. Plot of $\log_{10}(4\pi^2 \tau \delta\nu)$ against $10^3/T$ for 69.3$_4$ mole per cent $C_2H_5CON(CH_3)_2$ in CCl_4, Method III.
E_a = 8.6 ± 0.6 kcal./mole
$A = \dagger$(4 to12) x10^6 $sec.^{-1}$
$\Delta F^{\dagger}_{298.2}$ = 16.5 kcal./mole
T_c = 333.0°C.
ν_0 = 60.000 mcs.
$\delta\nu$ = 9.59 ± .18 cps at -24.0°C.


.40
.32
.24
.16
.08
.00

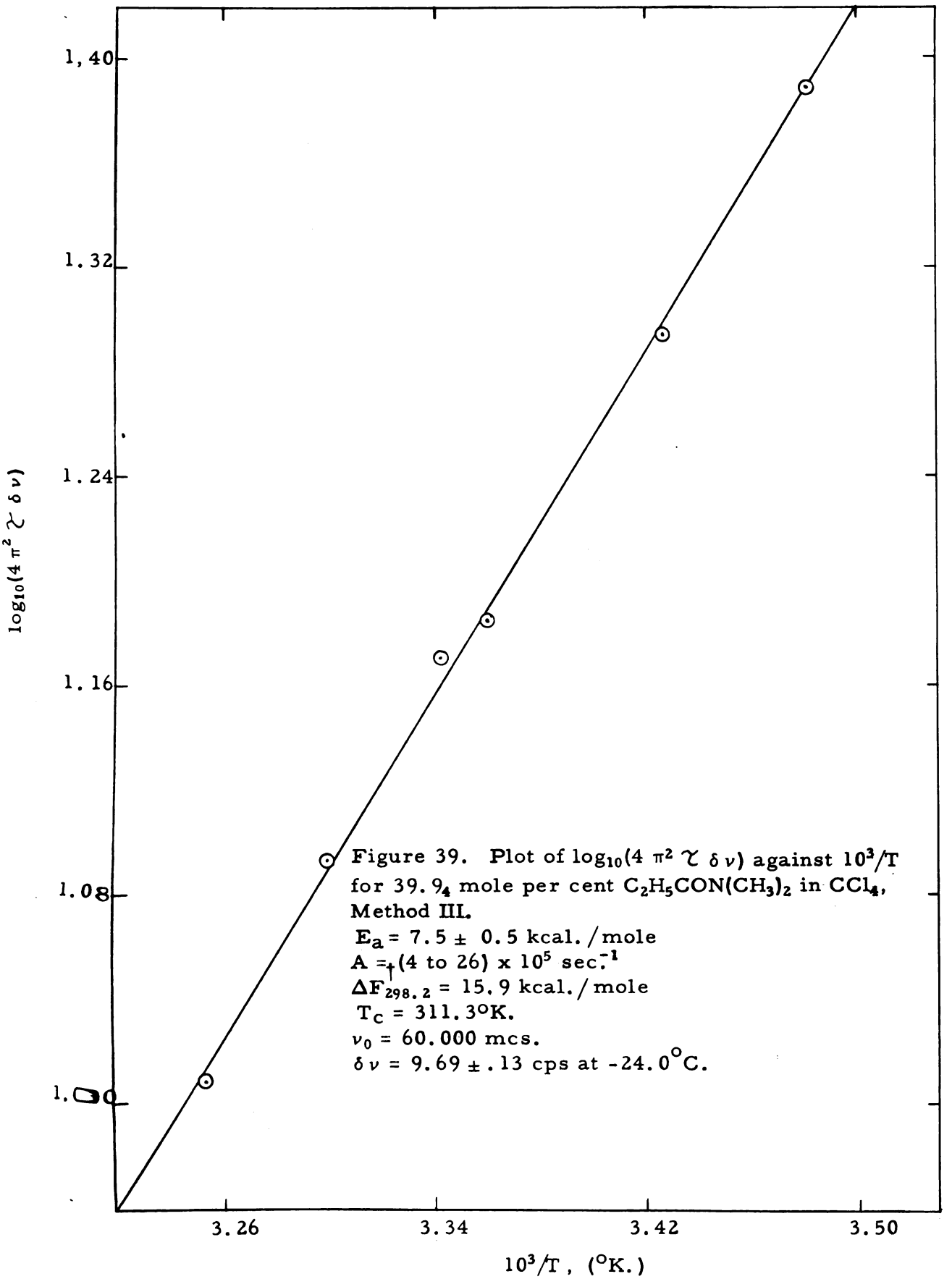

Figure 39. Plot of $\log_{10}(4\pi^2 \tau \delta\nu)$ against $10^3/T$ for 39.9$_4$ mole per cent $C_2H_5CON(CH_3)_2$ in CCl_4, Method III.
$E_a = 7.5 \pm 0.5$ kcal./mole
$A = \uparrow$(4 to 26) x 10^5 sec.$^{-1}$
$\Delta F_{298.2} = 15.9$ kcal./mole
$T_c = 311.3$°K.
$\nu_0 = 60.000$ mcs.
$\delta\nu = 9.69 \pm .13$ cps at -24.0°C.

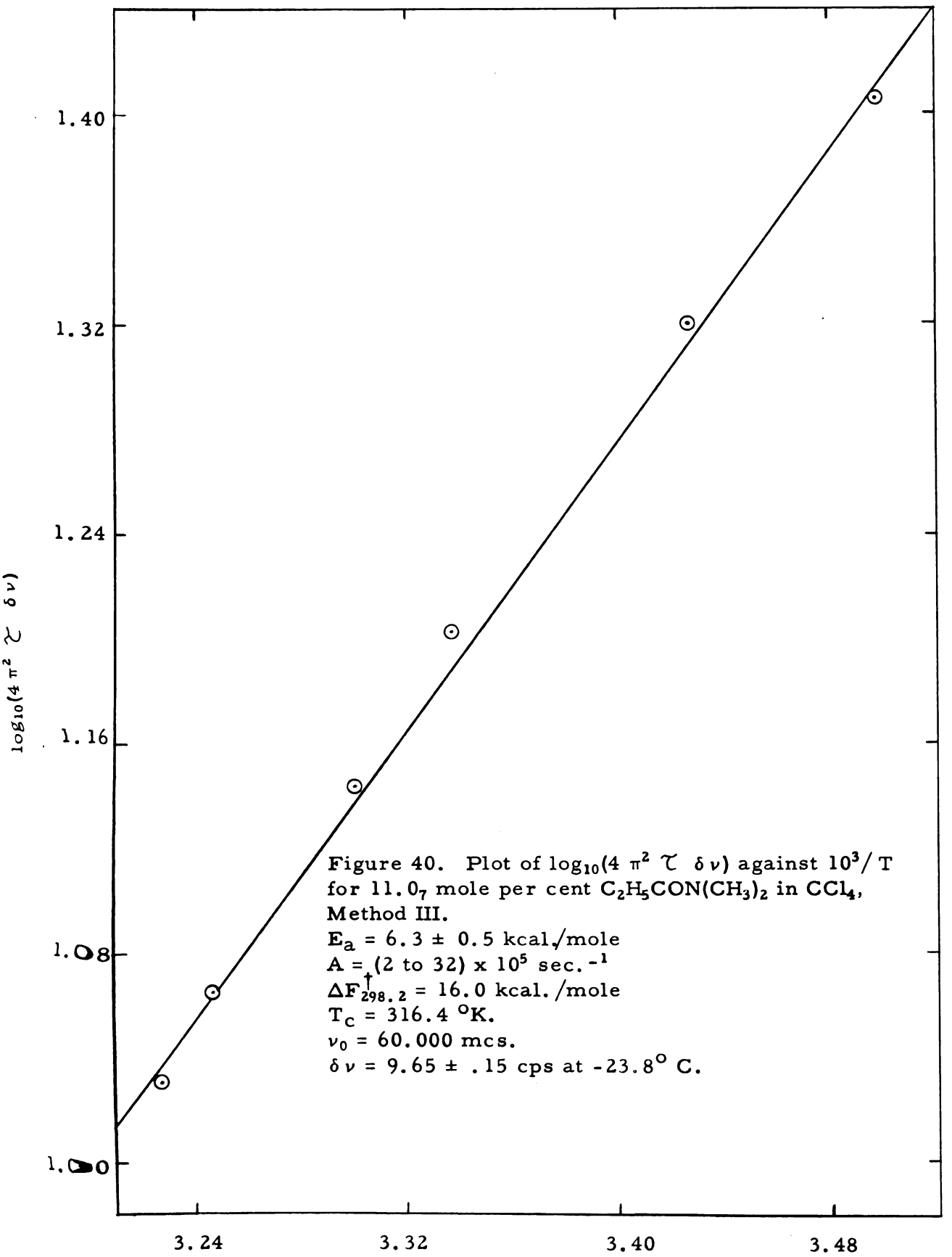

Figure 40. Plot of $\log_{10}(4\pi^2 \tau \delta\nu)$ against $10^3/T$ for 11.0$_7$ mole per cent $C_2H_5CON(CH_3)_2$ in CCl_4, Method III.
E_a = 6.3 ± 0.5 kcal./mole
A = (2 to 32) x 10^5 sec.$^{-1}$
$\Delta F^{\dagger}_{298.2}$ = 16.0 kcal./mole
T_c = 316.4 °K.
ν_0 = 60.000 mcs.
$\delta\nu$ = 9.65 ± .15 cps at -23.8° C.

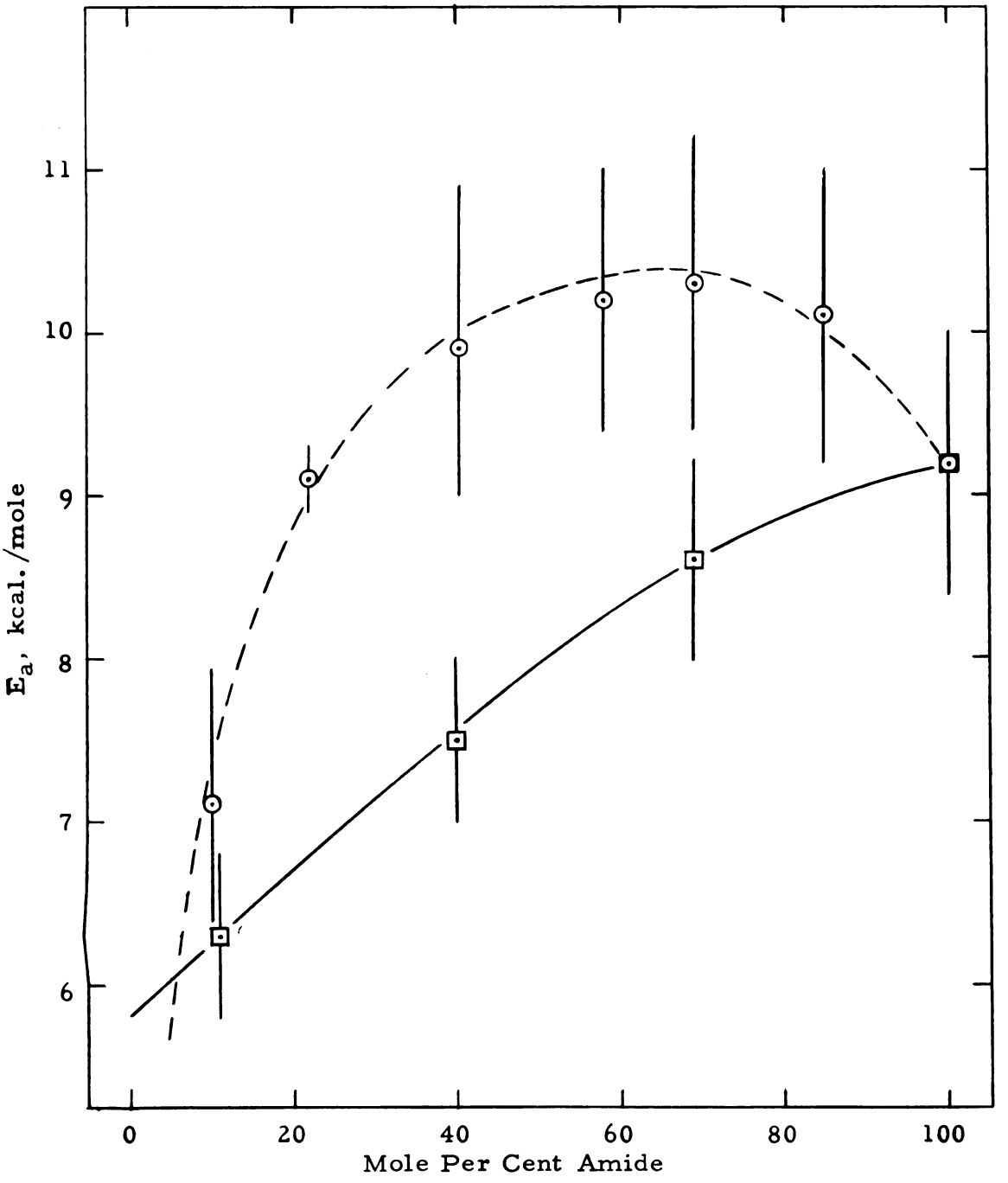

Figure 41. Concentration dependencies of the energy barrier E_a for internal rotation about the central C-N bond of N, N-dimethylpropionamide in: (a) dibromomethane solutions - -⊙- - -⊙- -, and (b) carbon tetrachloride solutions —⊡——⊡——.

TABLE XIV

TEMPERATURE DEPENDENCE OF THE RATE OF INTERNAL ROTATION ABOUT THE CENTRAL C-N BOND OF N, N-DIMETHYLTRICHLOROACETAMIDE, METHOD III

ν_0 = 60.000 mcs., $\delta\nu$ = 17.51 ± .22 cps at -26.8°C.

t, °C.	$10^3/T$, (°K.)	r	$\log_{10}(4\pi^2\gamma\,\delta\nu)$
10.28 ± .24*	3.5306	1.149 ± .013*	1.0450 ± .0050*
8.60 ± .03	3.5491	1.308 ± .005	1.0932 ± .0010
5.95 ± .05	3.5828	1.641 ± .009	1.1620 ± .0014
3.43 ± .45	3.6155	2.239 ± .032	1.2447 ± .0035
-0.45 ± .05	3.6669	3.394 ± .031	1.3467 ± .0016
-4.07 ± .05	3.7162	5.377 ± .108	1.4532 ± .0048

* The error given is the average deviation from the average of five measurements.

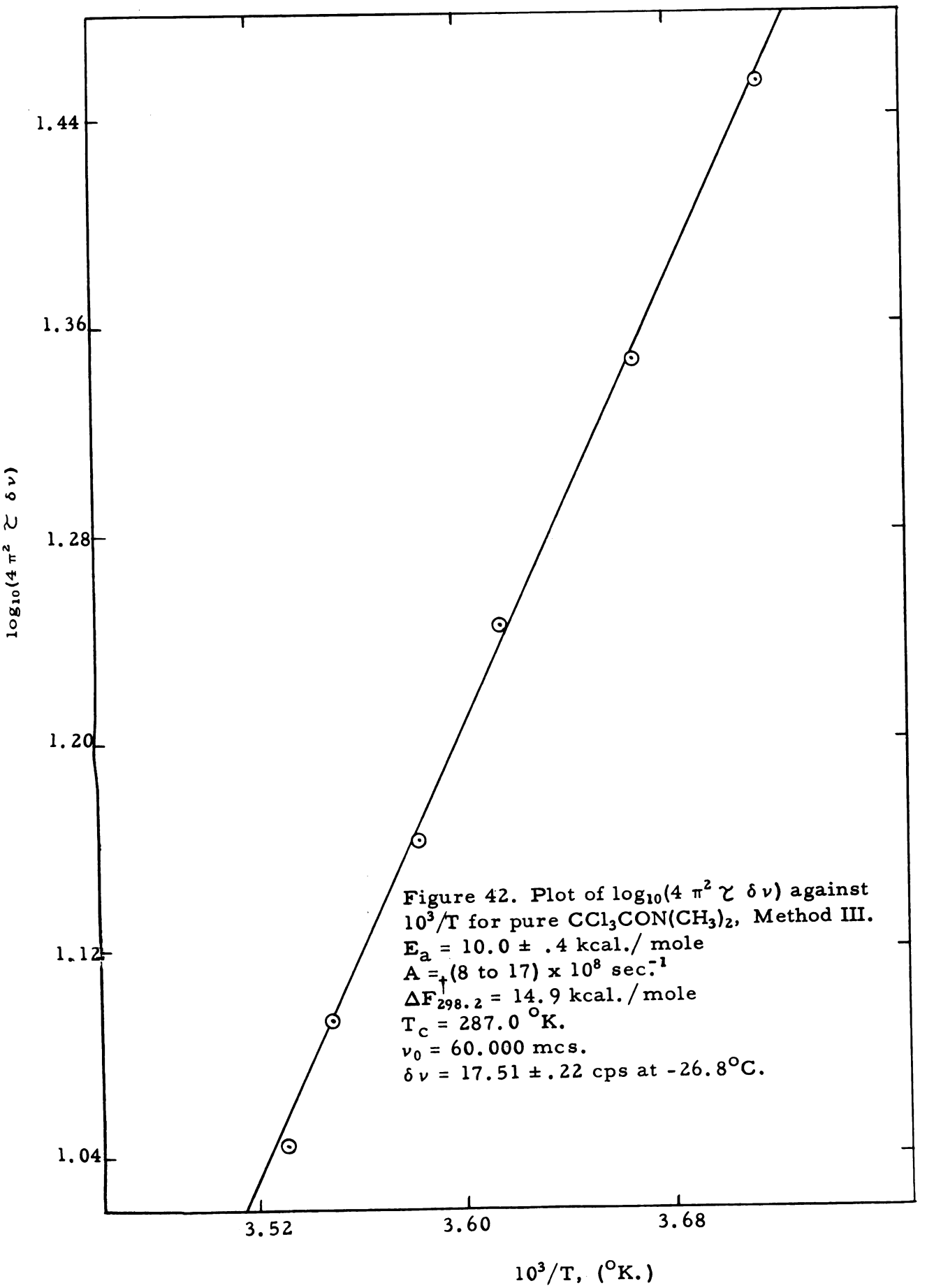

Figure 42. Plot of $\log_{10}(4\pi^2 \tau \delta\nu)$ against $10^3/T$ for pure $CCl_3CON(CH_3)_2$, Method III.
E_a = 10.0 ± .4 kcal./ mole
$A = \dagger$(8 to 17) x 10^8 $sec.^{-1}$
$\Delta F_{298.2}$ = 14.9 kcal./ mole
T_c = 287.0 $^oK.$
ν_0 = 60.000 mcs.
$\delta\nu$ = 17.51 ± .22 cps at -26.8$^oC.$

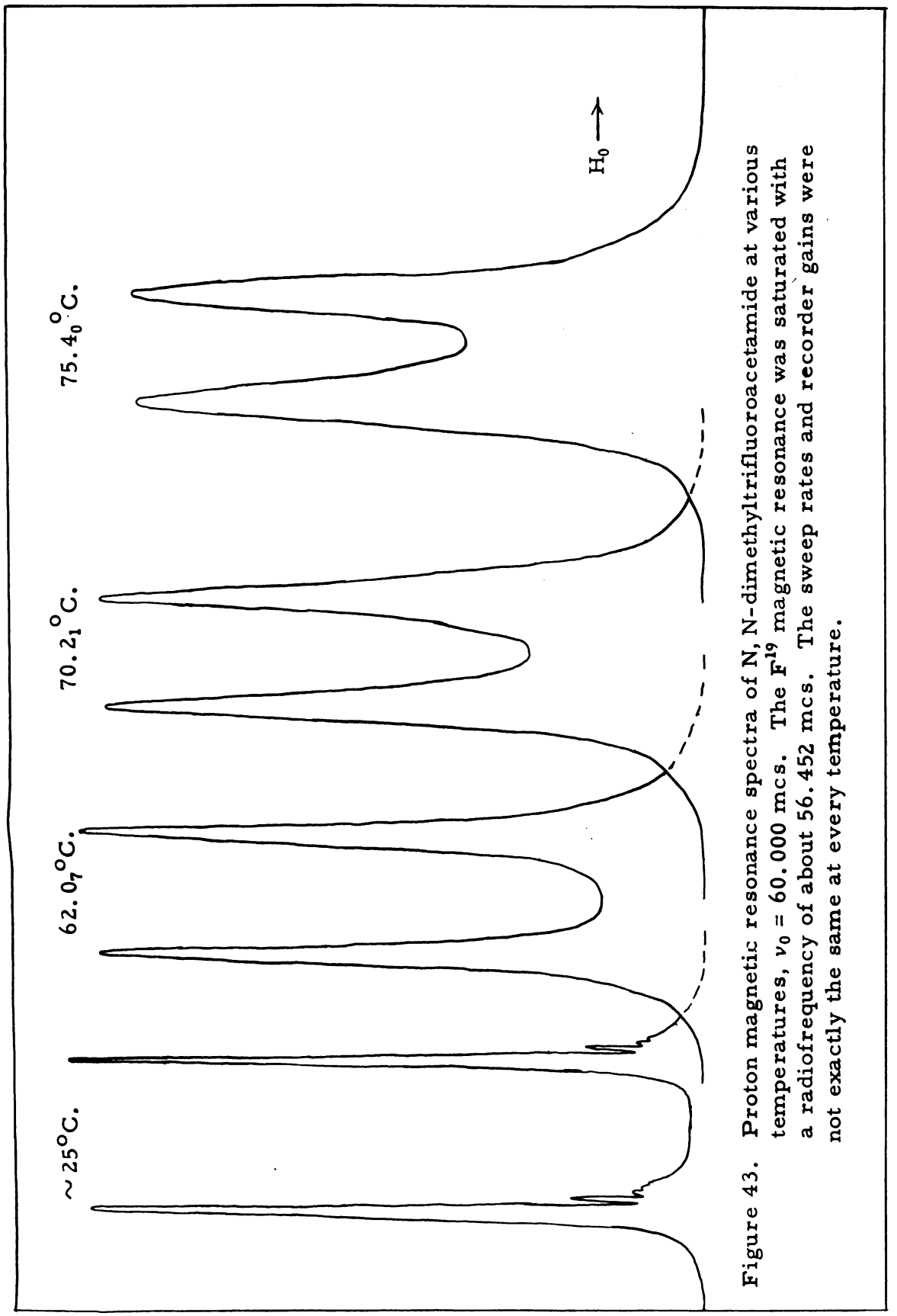

Figure 43. Proton magnetic resonance spectra of N, N-dimethyltrifluoroacetamide at various temperatures, ν_0 = 60.000 mcs. The F^{19} magnetic resonance was saturated with a radiofrequency of about 56.452 mcs. The sweep rates and recorder gains were not exactly the same at every temperature.

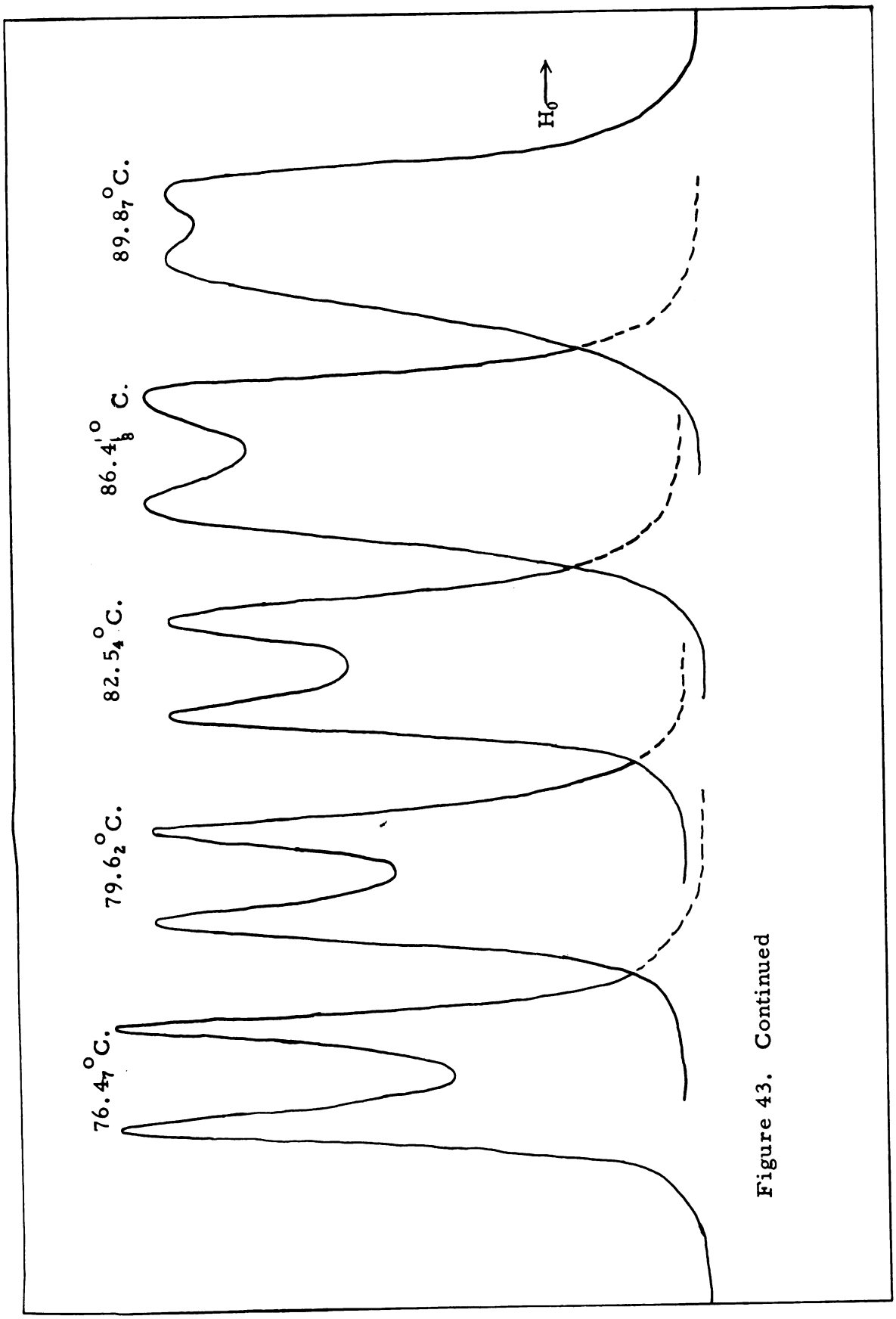

Figure 43. Continued

TABLE XV

TEMPERATURE DEPENDENCE OF THE RATE OF INTERNAL ROTATION ABOUT THE CENTRAL C-N BOND OF N, N-DIMETHYLTRIFLUOROACETAMIDE, METHOD III

ν_0 = 60.000 mcs., $\delta\nu$ = 7.48 ± .30 cps at 21.4°C.

t, °C.	$10^3/T$, (°K.)	r	$\log_{10}(4\pi^2 \tau\, \delta\nu)$
89.87 ± .11*	2.7546	1.066 ± .008*	1.0115 ± .0040*
86.48 ± .06	2.7806	1.221 ± .014	1.0695 ± .0043
82.54 ± .07	2.8113	1.527 ± .023	1.1414 ± .0041
79.62 ± .07	2.8346	1.843 ± .011	1.1932 ± .0018
76.47 ± .04	2.8602	2.324 ± .012	1.2622 ± .0030
75.40 ± .04	2.8689	2.426 ± .041	1.2648 ± .0042
70.21 ± .15	2.9123	3.513 ± .069	1.3542 ± .0048
62.07 ± .11	2.9830	5.822 ± .185	1.4805 ± .0020

*The error given is the average deviation from the average of five measurements.

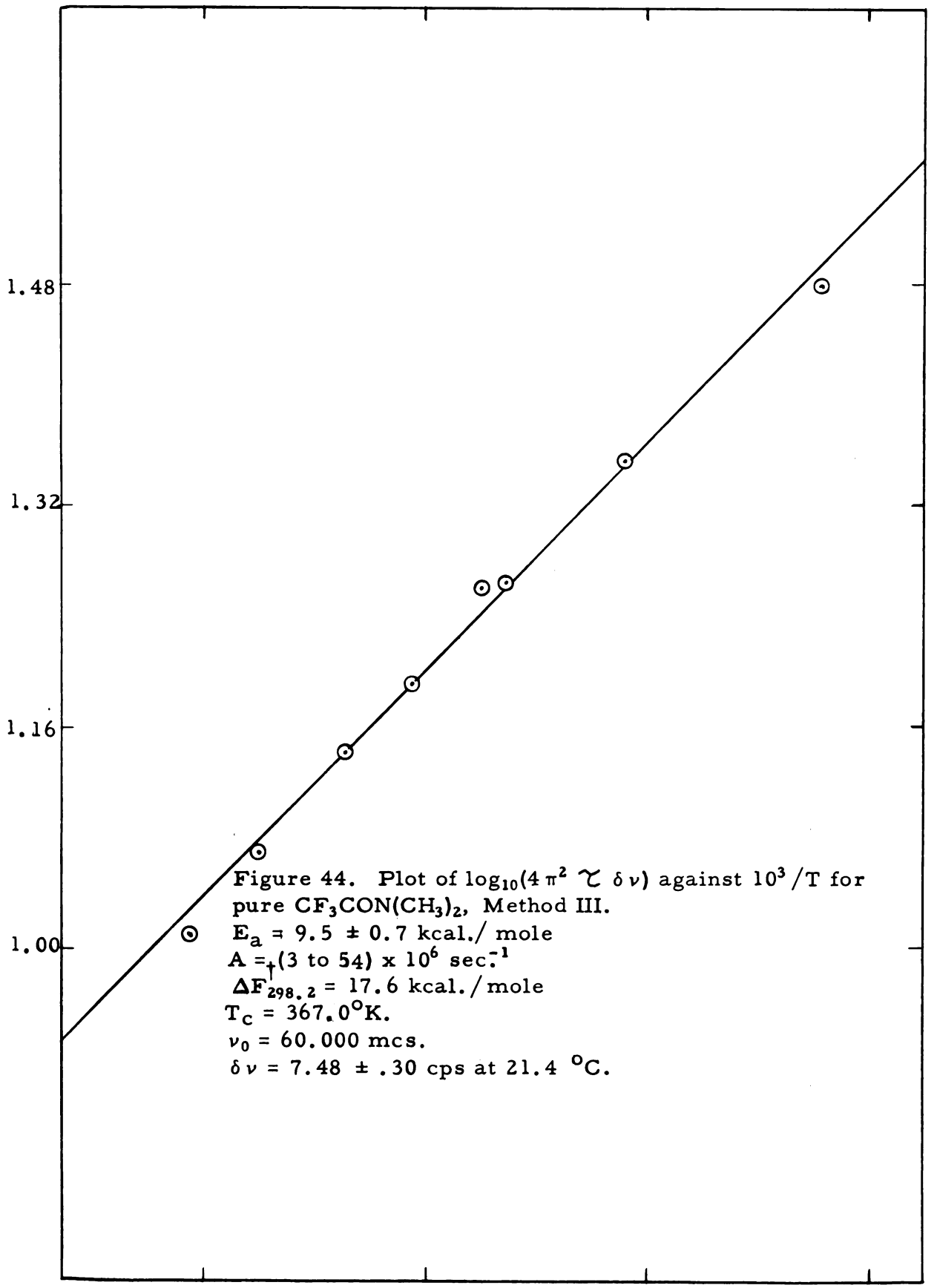

Figure 44. Plot of $\log_{10}(4\pi^2 \tau \delta\nu)$ against $10^3/T$ for pure $CF_3CON(CH_3)_2$, Method III.
$E_a = 9.5 \pm 0.7$ kcal./ mole
$A = \pm$(3 to 54) x 10^6 $sec.^{-1}$
$\Delta F_{298.2} = 17.6$ kcal./ mole
$T_c = 367.0^oK.$
$\nu_0 = 60.000$ mcs.
$\delta\nu = 7.48 \pm .30$ cps at 21.4 $^oC.$

TABLE XVI

TEMPERATURE DEPENDENCE OF THE RATE OF INTERNAL ROTATION ABOUT THE CENTRAL C-N BOND OF N, N-DIMETHYLACRYLAMIDE, METHOD III

ν_0 = 60.000 mcs., $\delta\nu$ = 9.46 ± .21 cps at 4.3°C.

t, °C.	$10^3/T$, (°K.)	r	$\log_{10}(4\pi^2 \tau \delta\nu)$
39.20 ± .07*	3.2014	1.180 ±.006*	1.0560 ± .0020*
38.33 ± .04	3.2104	1.199 ± .004	1.0625 ± .0009
35.93 ± .02	3.2353	1.313 ± .001	1.0946 ± .0002
33.90 ± .02	3.2567	1.571 ± .006	1.1495 ± .0005
27.21 ± .12	3.3292	2.285 ± .039	1.2497 ± .0038
25.04 ± .02	3.3535	2.499 ± .016	1.2728 ± .0002

*The error given is the average deviation from the average of five measurements.

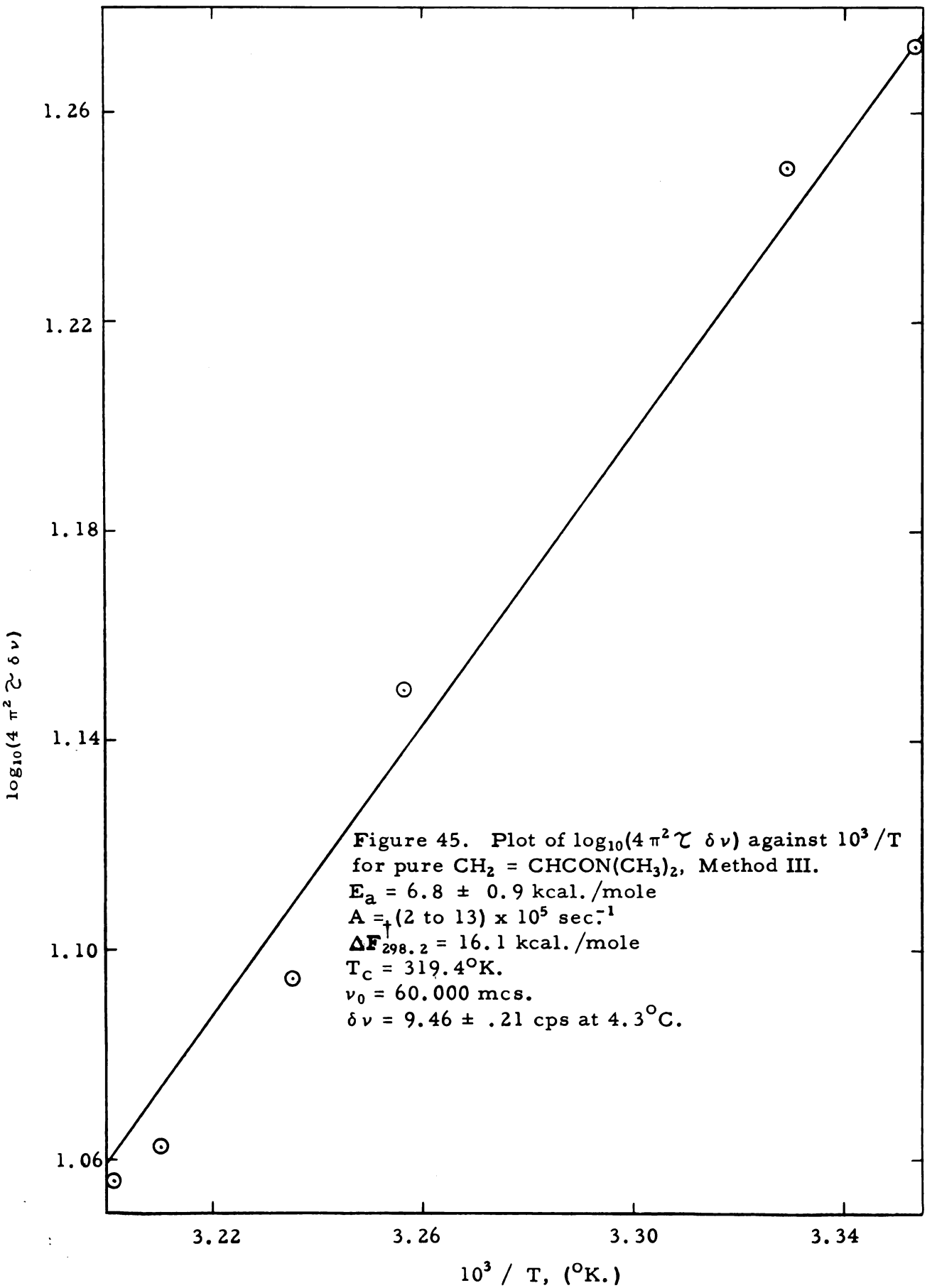

Figure 45. Plot of $\log_{10}(4\pi^2\tau\ \delta\nu)$ against $10^3/T$ for pure $CH_2 = CHCON(CH_3)_2$, Method III.
E_a = 6.8 ± 0.9 kcal./mole
A = (2 to 13) x 10^5 $sec.^{-1}$
$\Delta F^{\dagger}_{298.2}$ = 16.1 kcal./mole
T_c = 319.4°K.
ν_0 = 60.000 mcs.
$\delta\nu$ = 9.46 ± .21 cps at 4.3°C.

TABLE XVII

TEMPERATURE DEPENDENCE OF THE RATE OF INTERNAL ROTATION ABOUT THE CENTRAL C-N BOND OF N, N-DIMETHYLBENZAMIDE (36.3$_4$ MOLE PER CENT IN DIBROMOMETHANE), METHOD III

ν_0 = 60.000 mcs., $\delta\nu$ = 9.22 ± .18 cps at -26.6°C.

t, °C.	10^3 / T, (°K.)	r	$\log_{10}(4\pi^2 \tau \delta\nu)$
9.91 ± .02*	3.5327	1.010 ± .003*	.9720 ± .0035*
9.15 ± .15	3.5422	1.040 ± .004	.9965 ± .0027
6.66 ± .05	3.5737	1.206 ± .009	1.0650 ± .0027
5.80 ± .05	3.5847	1.289 ± .012	1.0883 ± .0034
2.81 ± .45	3.6236	1.505 ± .006	1.1368 ± .0012
-2.04 ± .16	3.6884	2.369 ± .071	1.2586 ± .0076
-3.97 ± .10	3.7148	2.944 ± .025	1.3122 ± .0020
-11.76 ± .11	3.8256	5.651 ± .096	1.4652 ± .0035

*The error given is the average deviation from the average of five measurements.

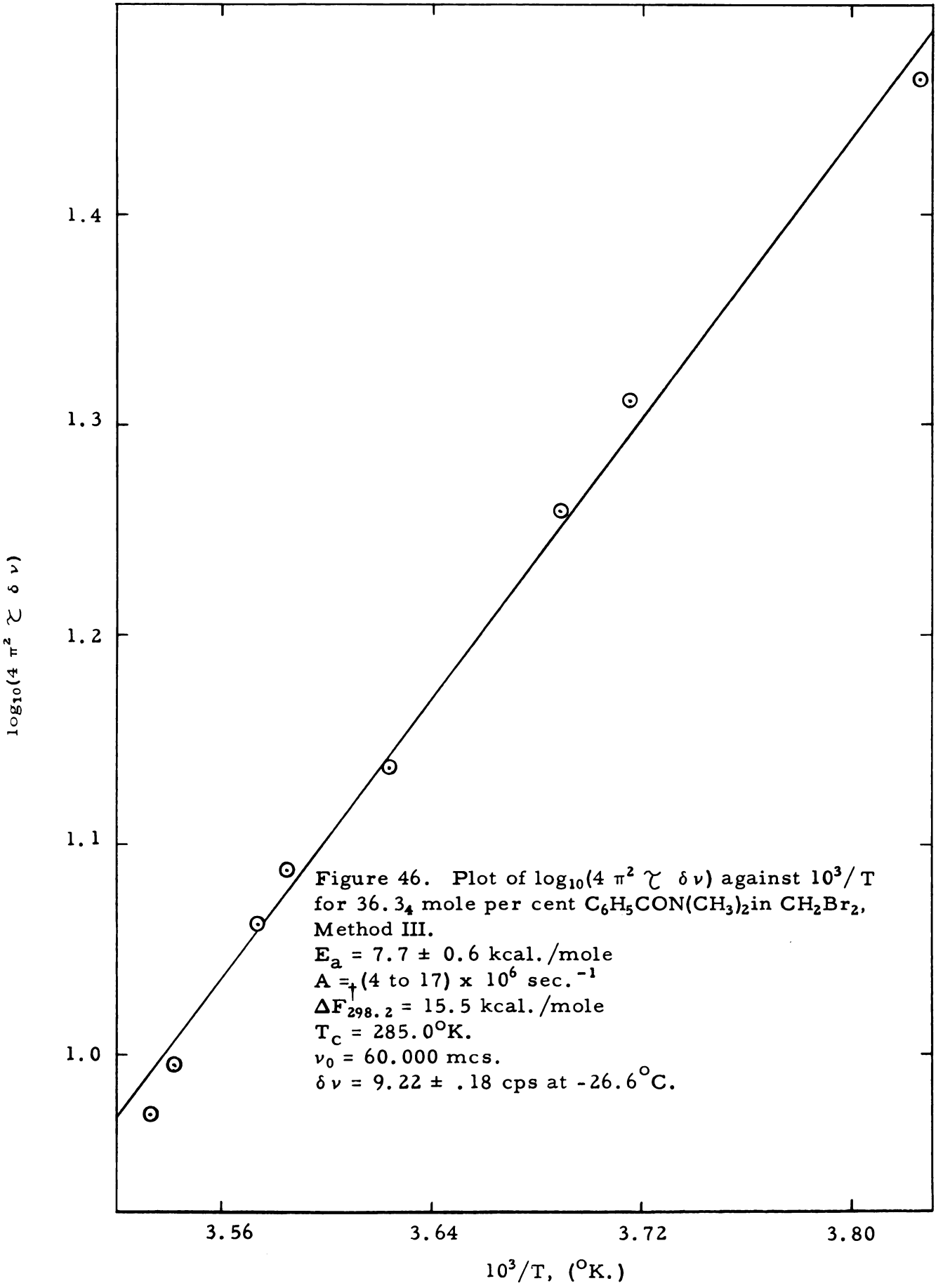

Figure 46. Plot of $\log_{10}(4\pi^2 \tau \delta\nu)$ against $10^3/T$ for 36.3$_4$ mole per cent $C_6H_5CON(CH_3)_2$ in CH_2Br_2, Method III.
E_a = 7.7 ± 0.6 kcal./mole
$A = \dagger$(4 to 17) x 10^6 sec.$^{-1}$
$\Delta F^{\dagger}_{298.2}$ = 15.5 kcal./mole
T_c = 285.0^{o}K.
ν_0 = 60.000 mcs.
$\delta\nu$ = 9.22 ± .18 cps at -26.6^{o}C.

40.0_8, and 10.9_8. The experimental data for the pure liquid amide, the solutions of amide and dibromomethane, and the solutions of amide and carbon tetrachloride are tabulated in Tables XVIII, XIX, and XX, respectively. These data are plotted as $\log_{10}(4\pi^2 \tau \delta\nu)$ against $10^3/T$ in Figures 47 through 54. The concentration dependencies of the energy barrier E_a, for the solutions of amide in dibromomethane and for the solutions of amide in carbon tetrachloride, are shown in Figure 55.

N, N-Dibenzylacetamide - The hindered internal rotation about the central C-N bond of N, N-dibenzylacetamide (38.0_9 mole per cent in dibromomethane) was studied by Method III. The experimental data are tabulated in Table XXI and plotted as $\log_{10}(4\pi^2 \tau \delta\nu)$ against $10^3/T$ in Figure 56.

In addition, the phenomenon was studied for the amide in carbon tetrachloride solution (38.2_9 mole per cent amide). These data are tabulated in Table XXII and plotted as $\log_{10}(4\pi^2 \tau \delta\nu)$ against $10^3/T$ in Figure 57.

The values of E_a, A, $\Delta F^{\dagger}_{298.2}$ and T_c for hindered internal rotation, about the central C-N bond of the amides studied, are tabulated in Table XXIII.

TABLE XVIII

TEMPERATURE DEPENDENCE OF THE RATE OF INTERNAL ROTATION ABOUT THE CENTRAL C-N BOND OF N, N-DIMETHYLCARBAMYL CHLORIDE, METHOD III

ν_0 = 60.000 mcs., $\delta\nu$ = 6.46 ± .13 cps at -24.2°C.

t, °C.	10^3 T, (°K.)	r	$\log_{10}(4\pi^2\tau\,\delta\nu)$
47.13 ± .06*	3.1222	1.103 ± .003*	1.0383 ± .0009*
42.40 ± .07	3.1690	1.406 ± .017	1.1155 ± .0040
39.94 ± .20	3.1939	1.586 ± .014	1.1523 ± .0022
33.21 ± .06	3.2640	2.566 ± .025	1.2788 ± .0024
29.94 ± .02	3.2992	2.953 ± .029	1.3130 ± .0023
24.18 ± .10	3.3632	4.580 ± .069	1.4162 ± .0035

*The error given is the average deviation from the average of five measurements.

TABLE XIX

TEMPERATURE DEPENDENCE OF THE RATE OF INTERNAL ROTATION ABOUT THE CENTRAL C-N BOND OF N, N-DIMETHYLCARBAMYL CHLORIDE IN DIBROMOMETHANE SOLUTIONS, METHOD III

ν_0 = 60.000 mcs.

(a) 90.0_3 mole per cent amide, $\delta\nu$ = 6.45 ± .29 cps at -24.5°C.

t, °C.	10^3 T, (°K.)	r	$\log_{10}(4\pi^2\tau\,\delta\nu)$
47.27 ± .04*	3.1208	1.124 ± .003*	1.0362 ± .0008*
42.33 ± .09	3.1697	1.448 ± .008	1.1252 ± .0016
38.65 ± .05	3.2071	1.810 ± .010	1.1889 ± .0013
34.56 ± .02	3.2497	2.486 ± .018	1.2710 ± .0017
32.07 ± .02	3.2762	2.070 ± .062	1.3224 ± .0048
26.03 ± .05	3.3424	4.820 ± .050	1.4285 ± .0025
(b) 63.4_4 mole per cent amide, $\delta\nu$ = 6.27 ± .20 at -24.5°C.			
47.37 ± .09	3.1198	1.149 ± .002	1.0450 ± .0010
42.31 ± .02	3.1700	1.511 ± .007	1.1480 ± .0015
38.65 ± .05	3.2071	1.905 ± .017	1.2022 ± .0025
34.60 ± .04	3.2493	2.605 ± .029	1.2825 ± .0027
33.14 ± .10	3.2648	3.157 ± .036	1.3290 ± .0030
28.42 ± .02	3.3159	4.959± .040	1.4351 ± .0016
(c) 40.9_2 mole per cent amide, $\delta\nu$ = 6.25 ± .20 cps at -23.7°C.			
47.24 ± .05	3.1211	1.147 ± .004	1.0445 ± .0015
42.22 ± .02	3.1708	1.451 ± .006	1.1260 ± .0010
38.65 ± .05	3.2071	1.909 ± .006	1.2028 ± .0007
34.64 ± .05	3.2499	2.771 ± .033	1.2977 ± .0022
32.51 ± .05	3.2715	2.995 ± .056	1.3165 ± .0045
26.49 ± .05	3.3372	5.238 ± .150	1.4472 ± .0055

Continued

TABLE XIX - Continued

t, °C.	$10^3/T$, (°K.)	r	$\log_{10}(4\pi^2\gamma\ \delta\nu)$
(d) 10.7_2 mole per cent amide, $\delta\nu = 6.08 \pm .15$ cps at -22.2°C.			
47.03 ± .05	3.1231	1.130 ± .012	1.0380 ± .0050
42.26 ± .07	3.1704	1.372 ± .009	1.1078 ± .0032
38.69 ± .05	3.2067	1.632 ± .012	1.1602 ± .0021
32.30 ± .02	3.3005	3.289 ± .045	1.3393 ± .0034
29.82 ± .02	3.3005	3.289 ± .045	1.3393 ± .0034
24.35 ± .02	3.3612	4.332 ± .088	1.4042 ± .0040

*The error given is the average deviation from the average of five measurements.

TABLE XX

TEMPERATURE DEPENDENCIES OF THE RATE OF INTERNAL ROTATION ABOUT THE CENTRAL C-N BOND OF N, N-DIMETHYLCARBAMYL CHLORIDE IN CARBON TETRACHLORIDE SOLUTIONS, METHOD III

ν_0 = 60.000 mcs.

(a) 71.3_4 mole per cent amide, $\delta\nu$ = 7.18 ± .20 cps at -20.2°C.

t, °C.	$10^3/T$, (°K.)	r	$\log_{10}(4\pi^2\tau\delta\nu)$
47.04 ± .09*	3.1231	1.107 ± .002*	1.0292 ± .0010*
42.37 ± .06	3.1693	1.388 ± .006	1.1115 ± .0013
38.50 ± .05	3.2086	1.719 ± .013	1.1748 ± .0022
33.12 ± .02	3.2650	2.416 ± .032	1.2637 ± .0033
29.84 ± .02	3.3003	2.739 ± .033	1.2947 ± .0030
25.85 ± .02	3.3444	3.719 ± .031	1.3679 ± .0020
(b) 40.0_8 mole per cent amide, $\delta\nu$ = 7.34 ± .20 cps at -20.2°C.			
47.19 ± .09	3.1216	1.024 ± .002	.9850 ± .0010
42.19 ± .05	3.1711	1.255 ± .009	1.0795 ± .0022
37.24 ± .05	3.2217	1.569 ± .017	1.1490 ± .0030
30.96 ± .07	3.2882	2.106 ± .034	1.2290 ± .0042
27.51 ± .05	3.3259	2.780 ± .018	1.2985 ± .0015
25.01 ± .02	3.3538	3.081 ± .028	1.3232 ± .0022
(c) 10.9_8 mole per cent amide, $\delta\nu$ = 7.33 ± .25 cps at -19.7°C.			
38.60 ± .02	3.2076	1.111 ± .003	1.0312 ± .0012
36.64 ± .05	3.2279	1.206 ± .020	1.065 ± .0055
34.76 ± .04	3.2476	1.308 ± .011	1.9032 ± .0025
29.87 ± .05	3.3000	1.731 ± .026	1.1768 ± .0042
25.20 ± .02	3.3517	2.206 ± .079	1.2410 ± .0085
16.21 ± .03	3.4558	4.343 ± .033	1.4043 ± .0017

*The error given is the average deviation from the average of five measurements.

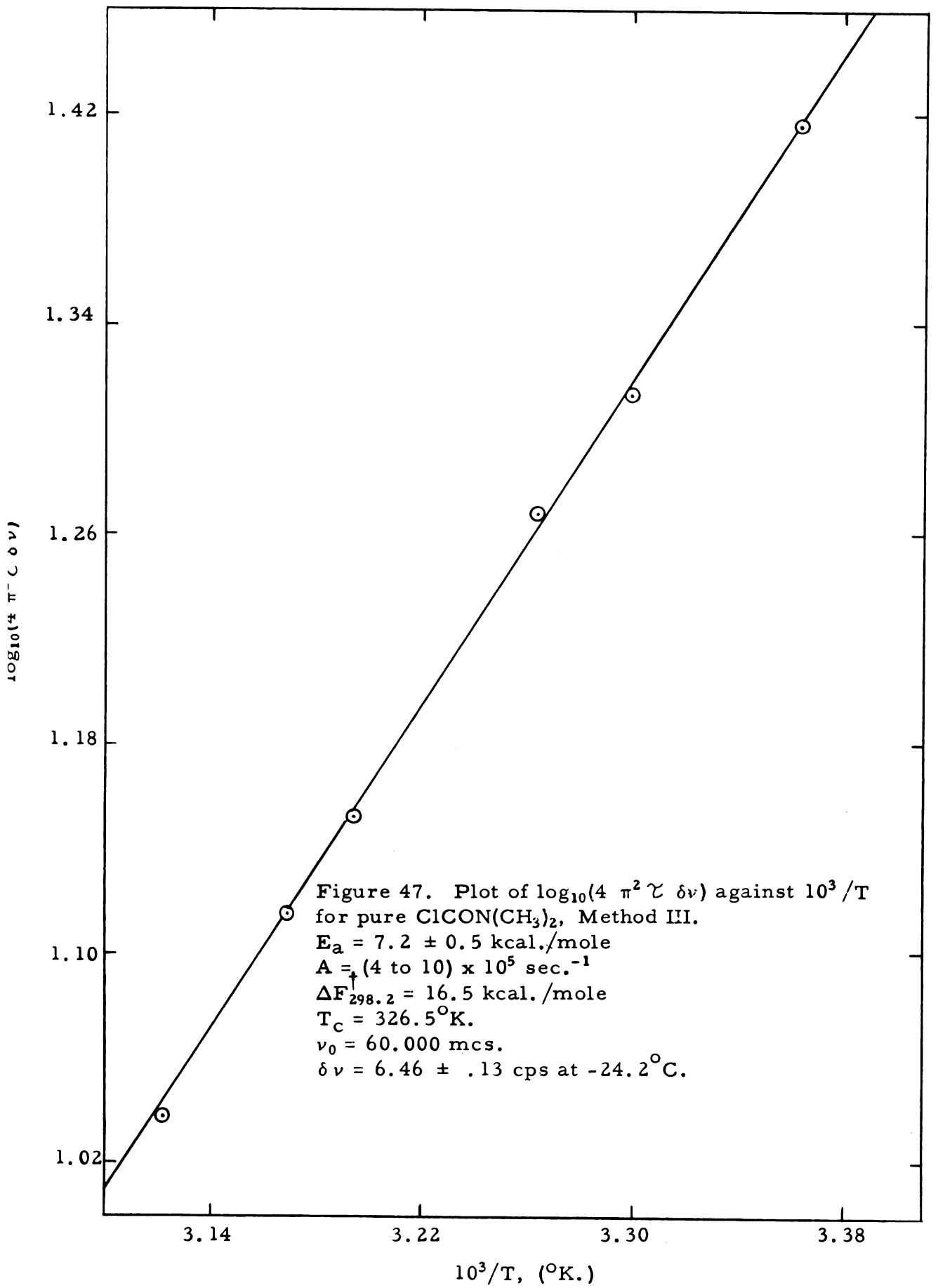

Figure 47. Plot of $\log_{10}(4\ \pi^2\ \tau\ \delta\nu)$ against $10^3/T$ for pure $ClCON(CH_3)_2$, Method III.
E_a = 7.2 ± 0.5 kcal./mole
A = (4 to 10) x 10^5 sec.$^{-1}$
$\Delta F^{\dagger}_{298.2}$ = 16.5 kcal./mole
T_c = 326.5°K.
ν_0 = 60.000 mcs.
$\delta\nu$ = 6.46 ± .13 cps at -24.2°C.

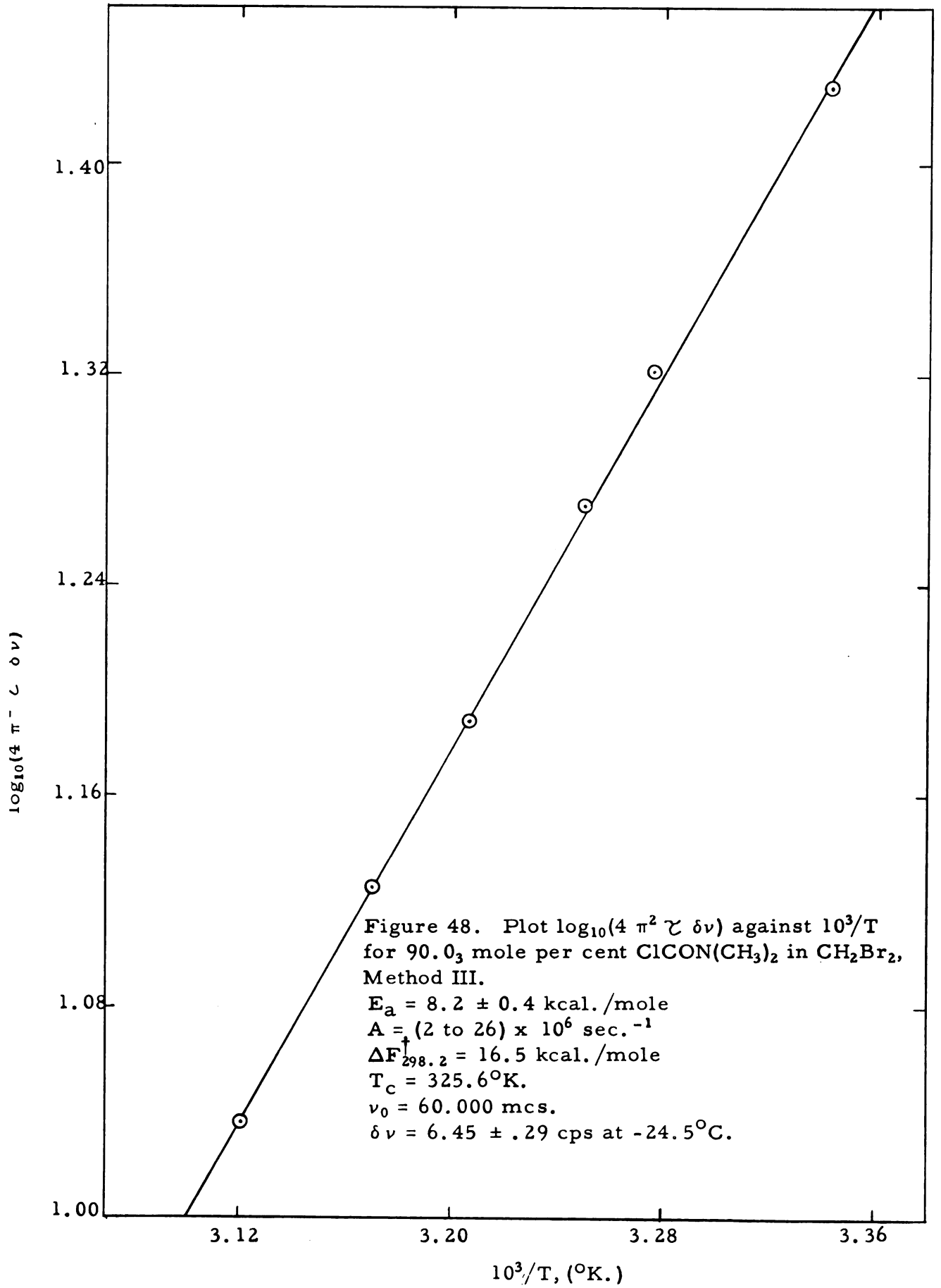

Figure 48. Plot $\log_{10}(4\pi^2 \gamma \delta\nu)$ against $10^3/T$ for 90.0$_3$ mole per cent $ClCON(CH_3)_2$ in CH_2Br_2, Method III.
E_a = 8.2 ± 0.4 kcal./mole
A = (2 to 26) x 10^6 sec.$^{-1}$
$\Delta F^{\ddagger}_{298.2}$ = 16.5 kcal./mole
T_c = 325.6°K.
ν_0 = 60.000 mcs.
$\delta\nu$ = 6.45 ± .29 cps at -24.5°C.

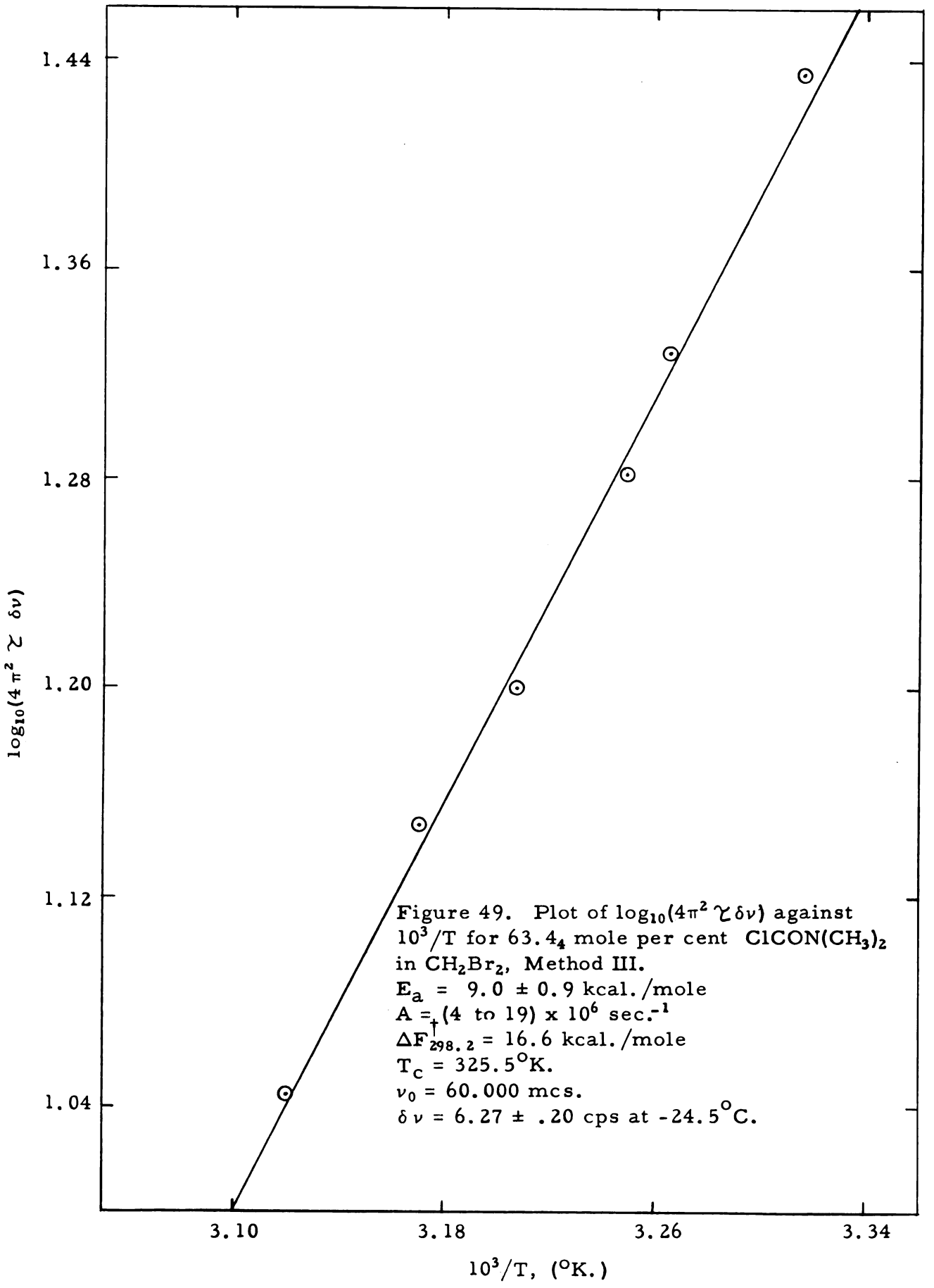

Figure 49. Plot of $\log_{10}(4\pi^2 \tau \delta\nu)$ against $10^3/T$ for 63.4_4 mole per cent $ClCON(CH_3)_2$ in CH_2Br_2, Method III.
E_a = 9.0 ± 0.9 kcal./mole
$A = \pm$ (4 to 19) x 10^6 sec.$^{-1}$
$\Delta F^{\dagger}_{298.2}$ = 16.6 kcal./mole
T_c = 325.5^oK.
ν_0 = 60.000 mcs.
$\delta\nu$ = 6.27 ± .20 cps at -24.5^oC.

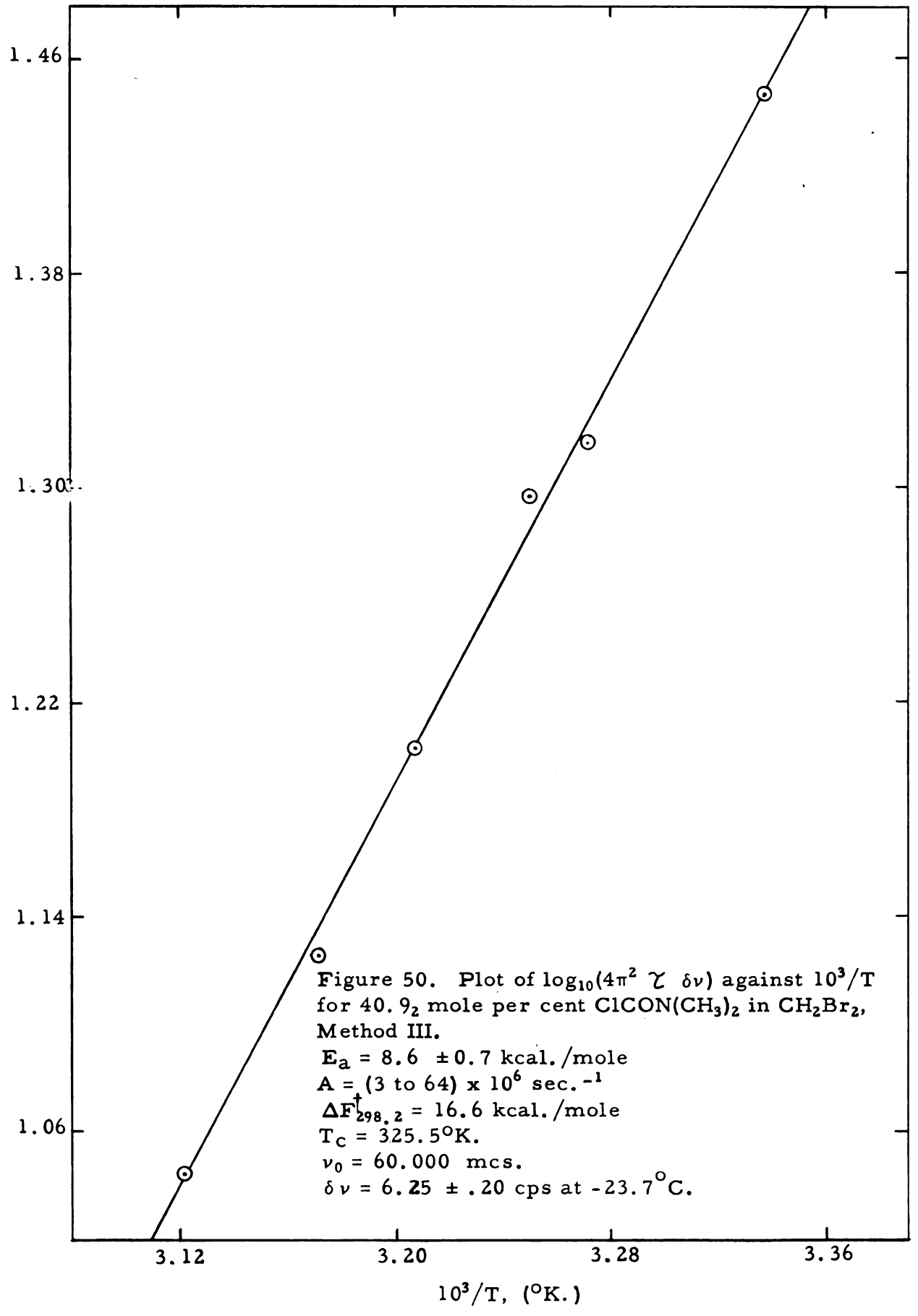

Figure 50. Plot of $\log_{10}(4\pi^2 \gamma \delta\nu)$ against $10^3/T$ for 40.9_2 mole per cent $ClCON(CH_3)_2$ in CH_2Br_2, Method III.
E_a = 8.6 ± 0.7 kcal./mole
A = (3 to 64) x 10^6 sec.$^{-1}$
$\Delta F^{\ddagger}_{298.2}$ = 16.6 kcal./mole
T_C = 325.5°K.
ν_0 = 60.000 mcs.
$\delta\nu$ = 6.25 ± .20 cps at -23.7°C.

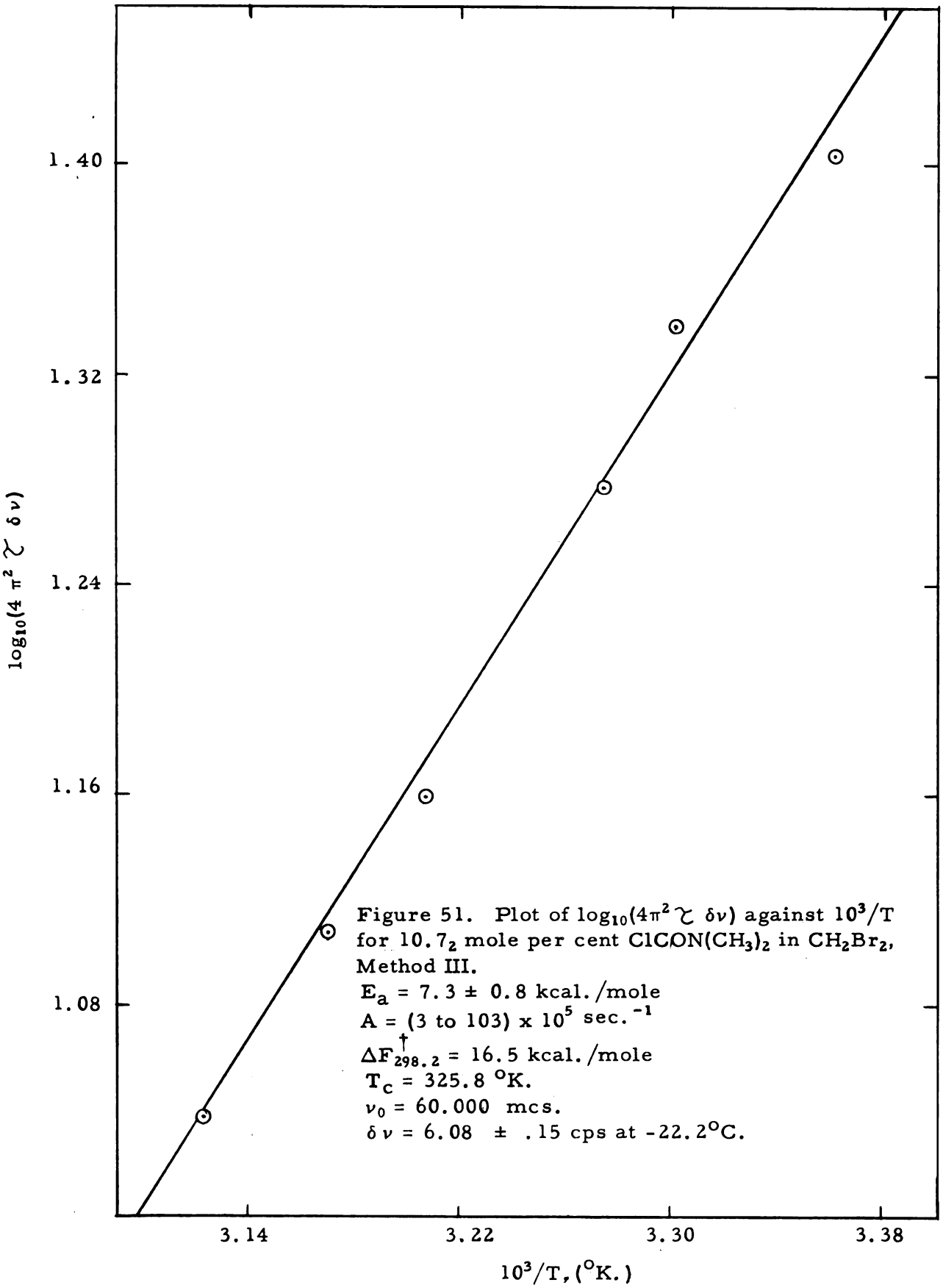

Figure 51. Plot of $\log_{10}(4\pi^2 \tau \delta\nu)$ against $10^3/T$ for 10.7$_2$ mole per cent $ClCON(CH_3)_2$ in CH_2Br_2, Method III.
E_a = 7.3 ± 0.8 kcal./mole
A = (3 to 103) x 10^5 sec.$^{-1}$
$\Delta F^{\dagger}_{298.2}$ = 16.5 kcal./mole
T_c = 325.8 ^oK.
ν_0 = 60.000 mcs.
$\delta\nu$ = 6.08 ± .15 cps at -22.2^oC.

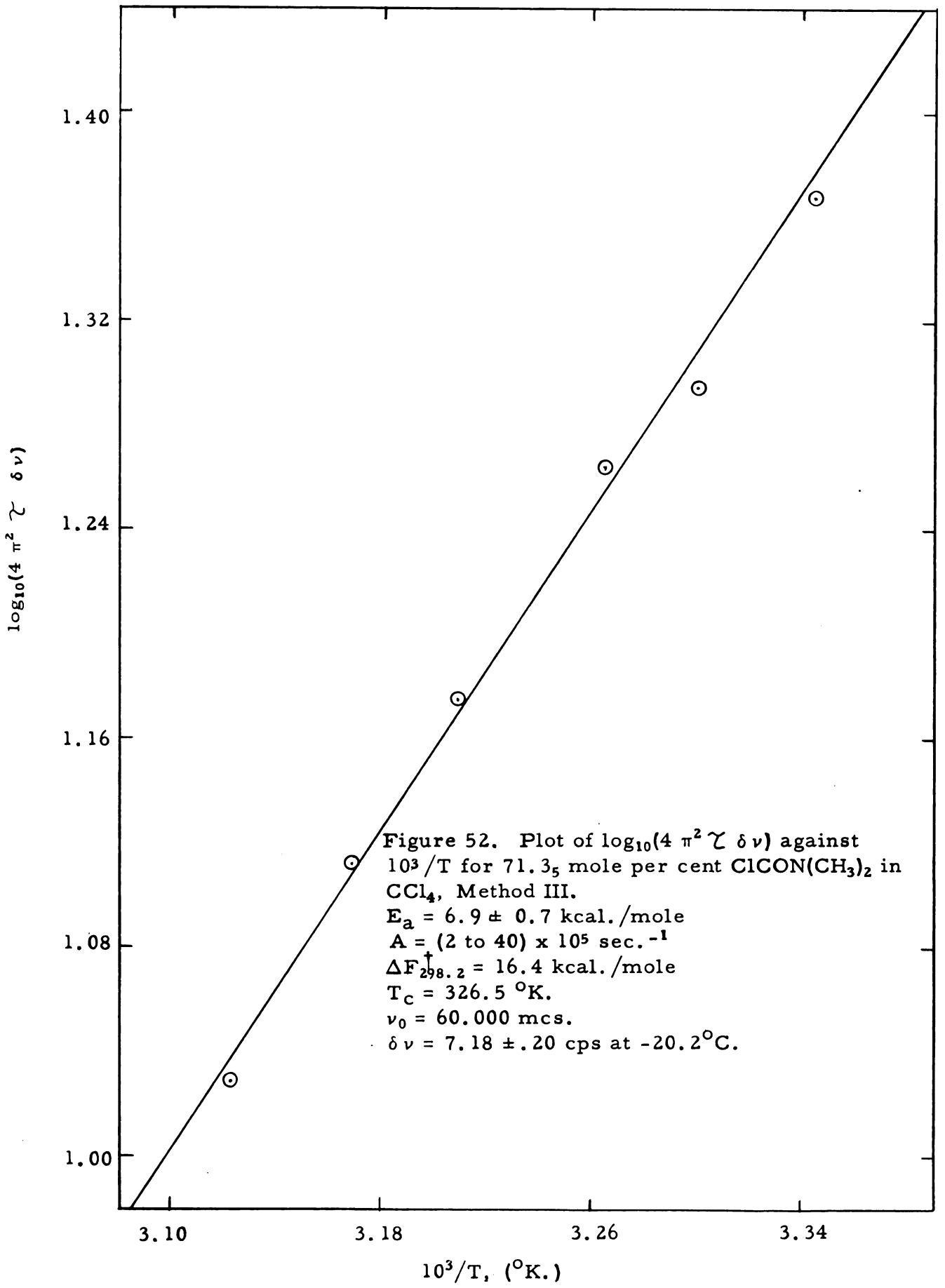

Figure 52. Plot of $\log_{10}(4\pi^2 \tau \delta\nu)$ against $10^3/T$ for 71.3$_5$ mole per cent $ClCON(CH_3)_2$ in CCl_4, Method III.
E_a = 6.9 ± 0.7 kcal./mole
A = (2 to 40) x 10^5 sec.$^{-1}$
$\Delta F^{\dagger}_{298.2}$ = 16.4 kcal./mole
T_c = 326.5 °K.
ν_0 = 60.000 mcs.
$\delta\nu$ = 7.18 ± .20 cps at -20.2°C.

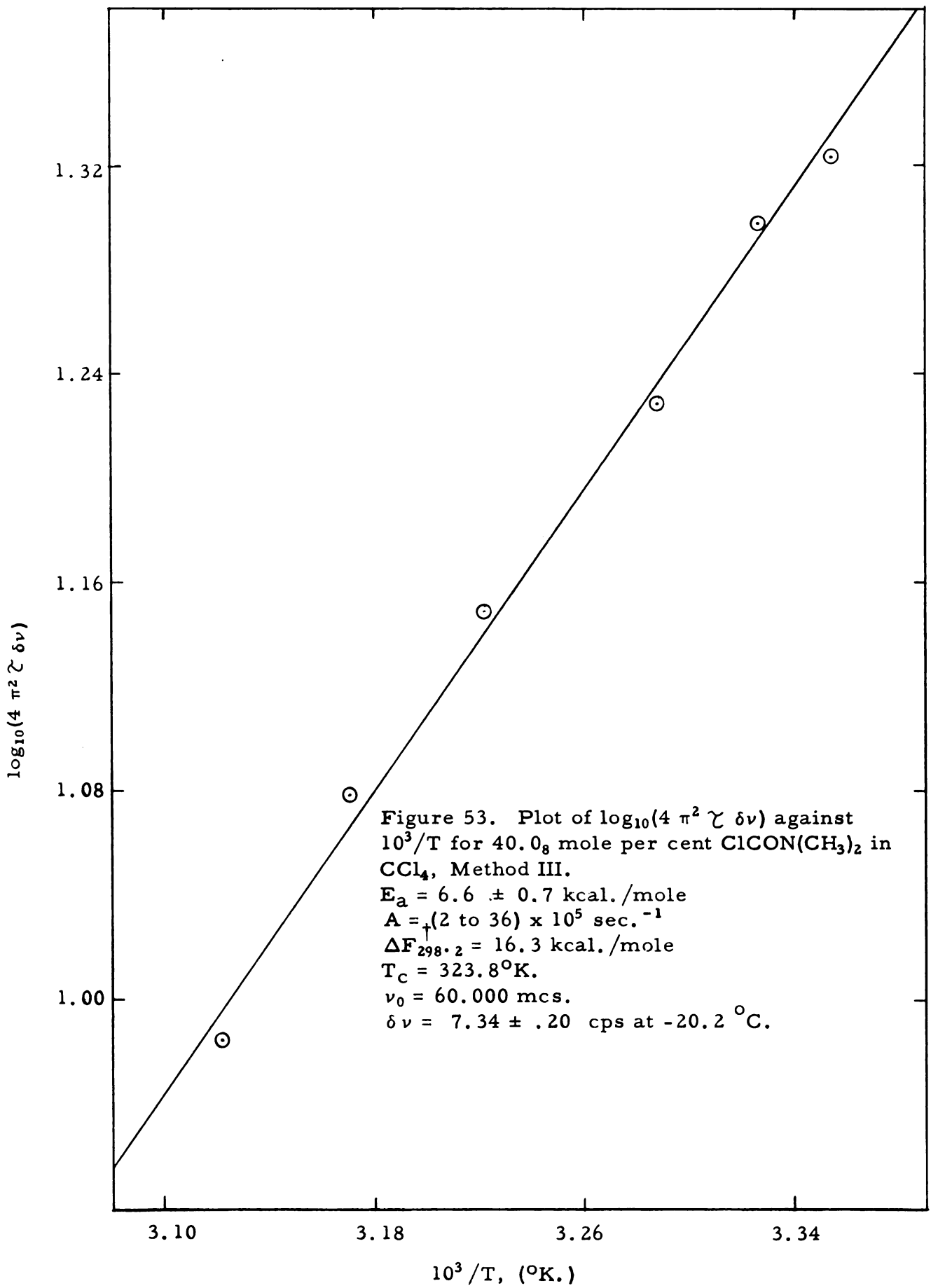

Figure 53. Plot of $\log_{10}(4\pi^2 \gamma \delta\nu)$ against $10^3/T$ for 40.0$_8$ mole per cent $ClCON(CH_3)_2$ in CCl_4, Method III.
E_a = 6.6 ± 0.7 kcal./mole
$A = {}^{\dagger}$(2 to 36) x 10^5 sec.$^{-1}$
$\Delta F^{\dagger}_{298.2}$ = 16.3 kcal./mole
T_c = 323.8°K.
ν_0 = 60.000 mcs.
$\delta\nu$ = 7.34 ± .20 cps at -20.2 °C.

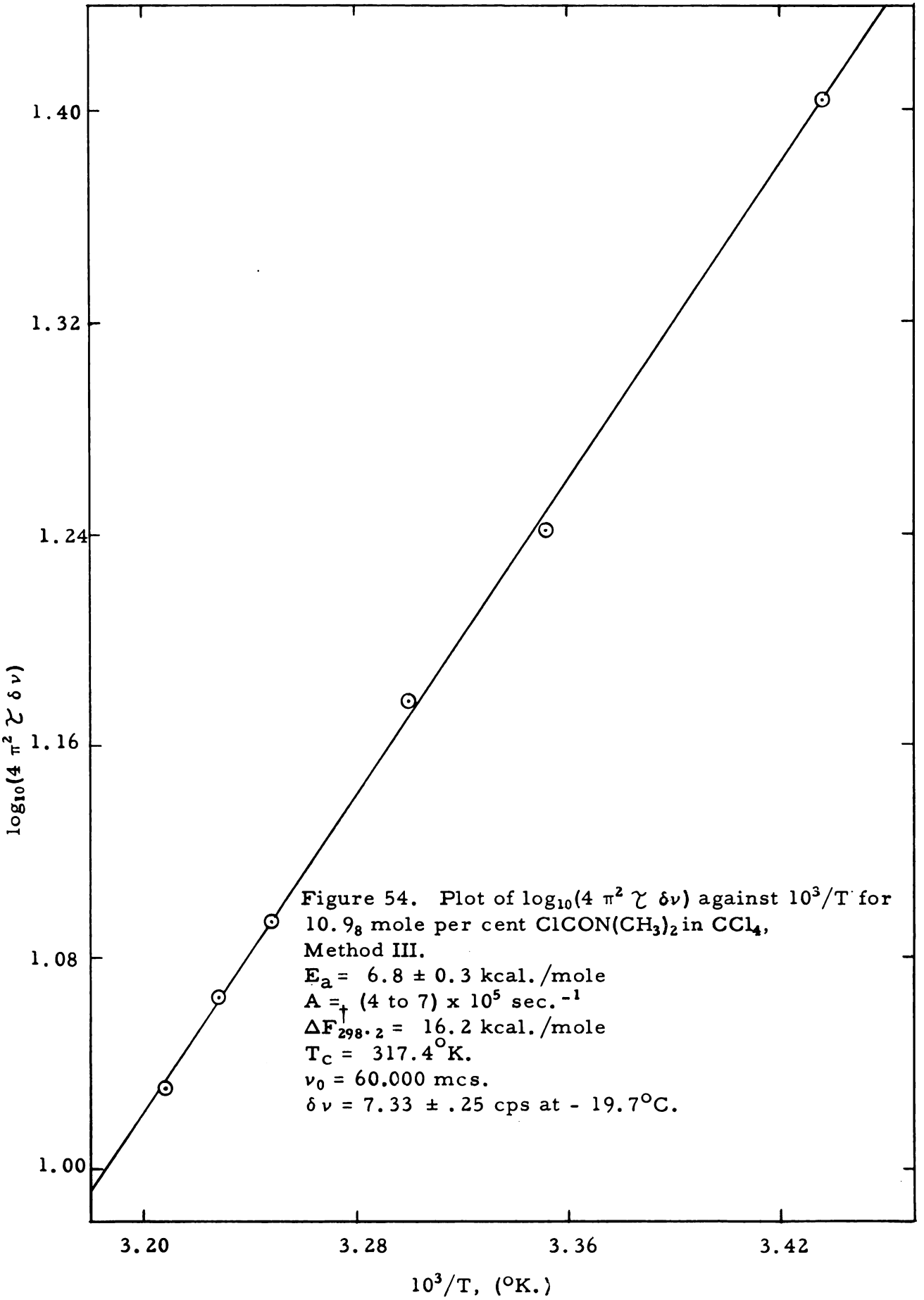

Figure 54. Plot of $\log_{10}(4\pi^2 \gamma \delta\nu)$ against $10^3/T$ for 10.9_8 mole per cent $ClCON(CH_3)_2$ in CCl_4, Method III.
E_a = 6.8 ± 0.3 kcal./mole
$A = \dagger$ (4 to 7) x 10^5 sec.$^{-1}$
$\Delta F_{298.2}$ = 16.2 kcal./mole
T_c = 317.4°K.
ν_0 = 60.000 mcs.
$\delta\nu$ = 7.33 ± .25 cps at - 19.7°C.

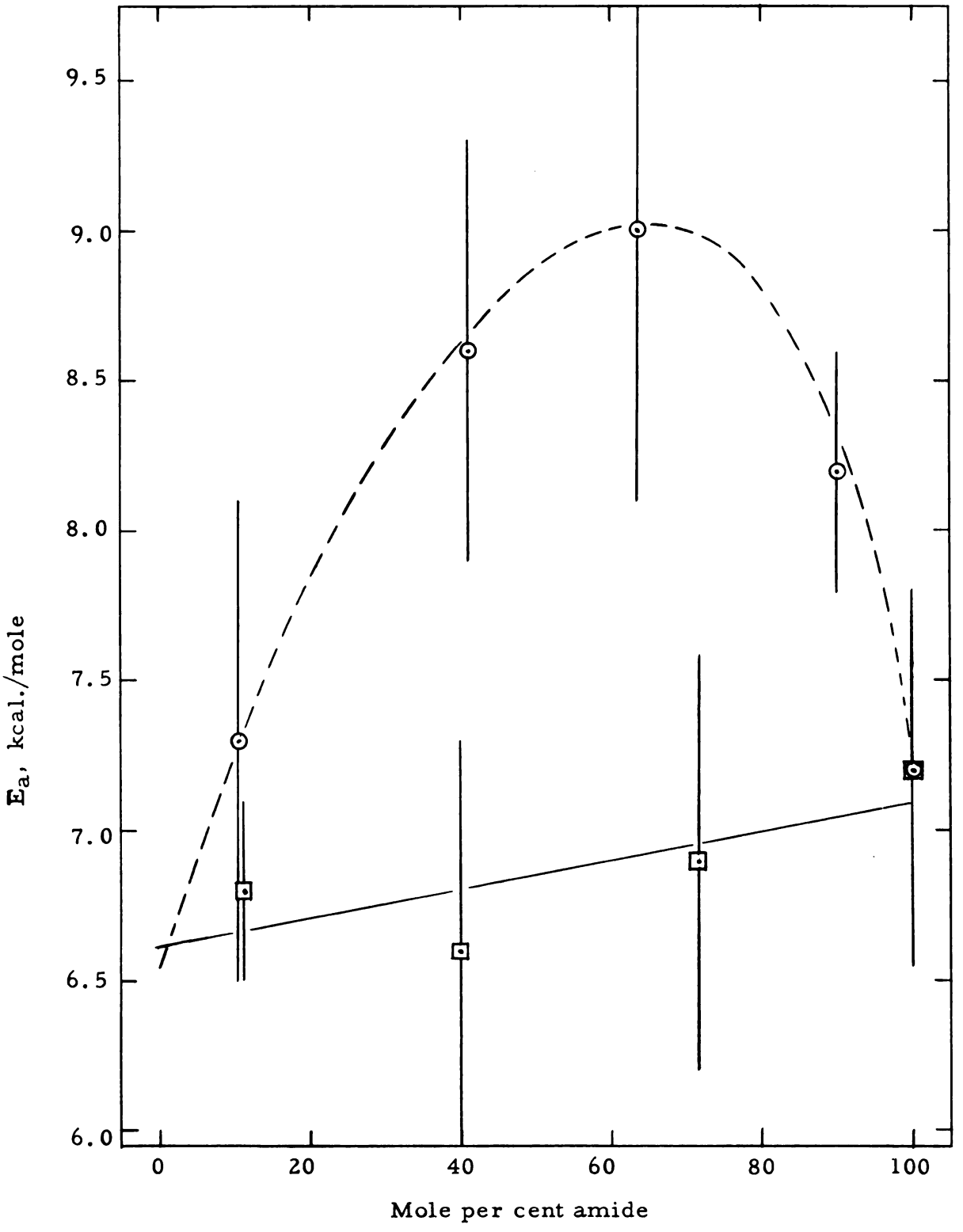

Figure 55. Concentration dependencies of the energy barrier E_a for internal rotation about the central C-N bond of N, N-dimethylcarbamyl chloride in: (a) dibromomethane solutions - - -⊙- - -⊙----, and (b) carbon tetrachloride solutions ——⊡——⊡——.

TABLE XXI

TEMPERATURE DEPENDENCE OF THE RATE OF INTERNAL ROTATION ABOUT THE CENTRAL C-N BOND OF N, N-DIBENZYLACETAMIDE (38.0$_9$ MOLE PER CENT IN DIBROMOMETHANE), METHOD III

ν_0 = 60.000 mcs., $\delta\nu$ = 12.02 ± .14 cps at -5.2°C.

t, °C.	$10^3/T$, (°K.)	r	$\log_{10}(4\pi\,\tau\,\delta\nu)$
65.54 ± .09*	2.9525	1.068 ± .005*	1.0125 ± .0035*
58.59 ± .07	3.0143	1.403 ± .008	1.1150 ± .0018
51.96 ± .06	3.0758	1.995 ± .014	1.2146 ± .0019
47.10 ± .04	3.1225	2.976 ± .029	1.3147 ± .0025
44.27 ± .05	3.1503	3.128 ± .039	1.3268 ± .0032
40.97 ± .02	3.1834	3.986 ± .030	1.3842 ± .0018
37.94 ± .04	3.2144	4.835 ± .131	1.4292 ± .0060

*The error given is the average deviation from the average of five measurements.

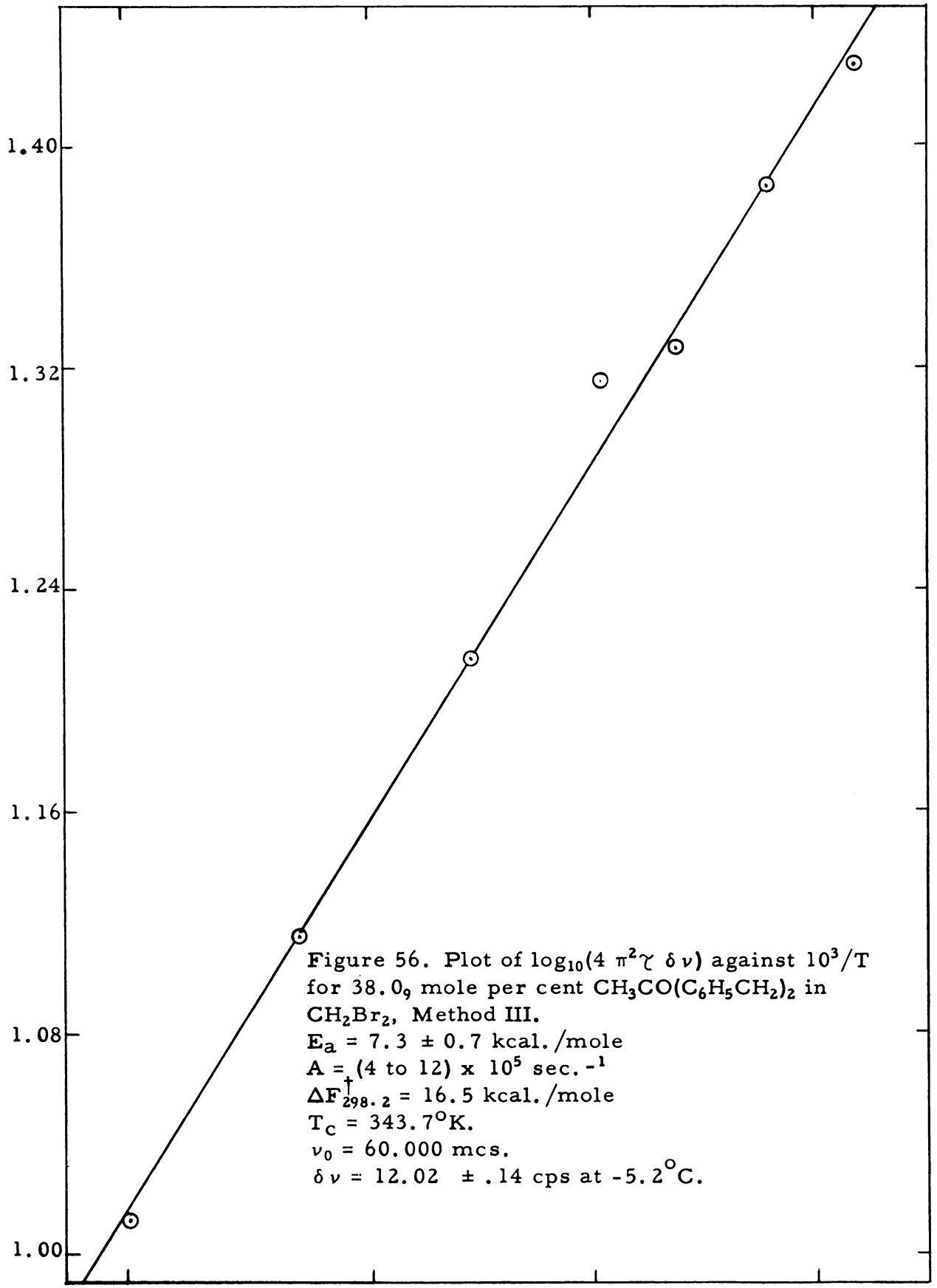

Figure 56. Plot of $\log_{10}(4\pi^2\gamma\,\delta\nu)$ against $10^3/T$ for 38.0$_9$ mole per cent $CH_3CO(C_6H_5CH_2)_2$ in CH_2Br_2, Method III.
E_a = 7.3 ± 0.7 kcal./mole
A = (4 to 12) x 10^5 sec.$^{-1}$
$\Delta F^{\dagger}_{298.2}$ = 16.5 kcal./mole
T_c = 343.7°K.
ν_0 = 60.000 mcs.
$\delta\nu$ = 12.02 ± .14 cps at -5.2°C.

TABLE XXII

TEMPERATURE DEPENDENCE OF THE RATE OF INTERNAL ROTATION ABOUT THE CENTRAL C-N BOND OF N, N-DIBENZYLACETAMIDE (38.2$_9$ MOLE PER CENT IN CARBON TETRACHLORIDE), METHOD III

ν_0 = 60.000 mcs., $\delta\nu$ = 9.79 ± .22 cps at -5.8°C.

t, °C.	$10^3/T$, (°K.)	r	$\log_{10}(4\pi^2\tau\,\delta\nu)$
55.72 ± .10*	3.0406	1.077 ± .009*	1.0169 ± .0036*
52.13 ± .05	3.0742	1.185 ± .012	1.0580 ± .0034
47.11 ± .07	3.1224	1.565 ± .017	1.1482 ± .0030
42.54 ± .02	3.1676	1.989 ± .030	1.2138 ± .0037
36.83 ± .07	3.2259	2.416 ± .012	1.2638 ± .0010
34.34 ± .02	3.2520	3.164 ± .010	1.3297 ± .0008
31.87 ± .37	3.2784	3.393 ± .056	1.3475 ± .0042

*The error given is the average deviation from the average of five measurements.

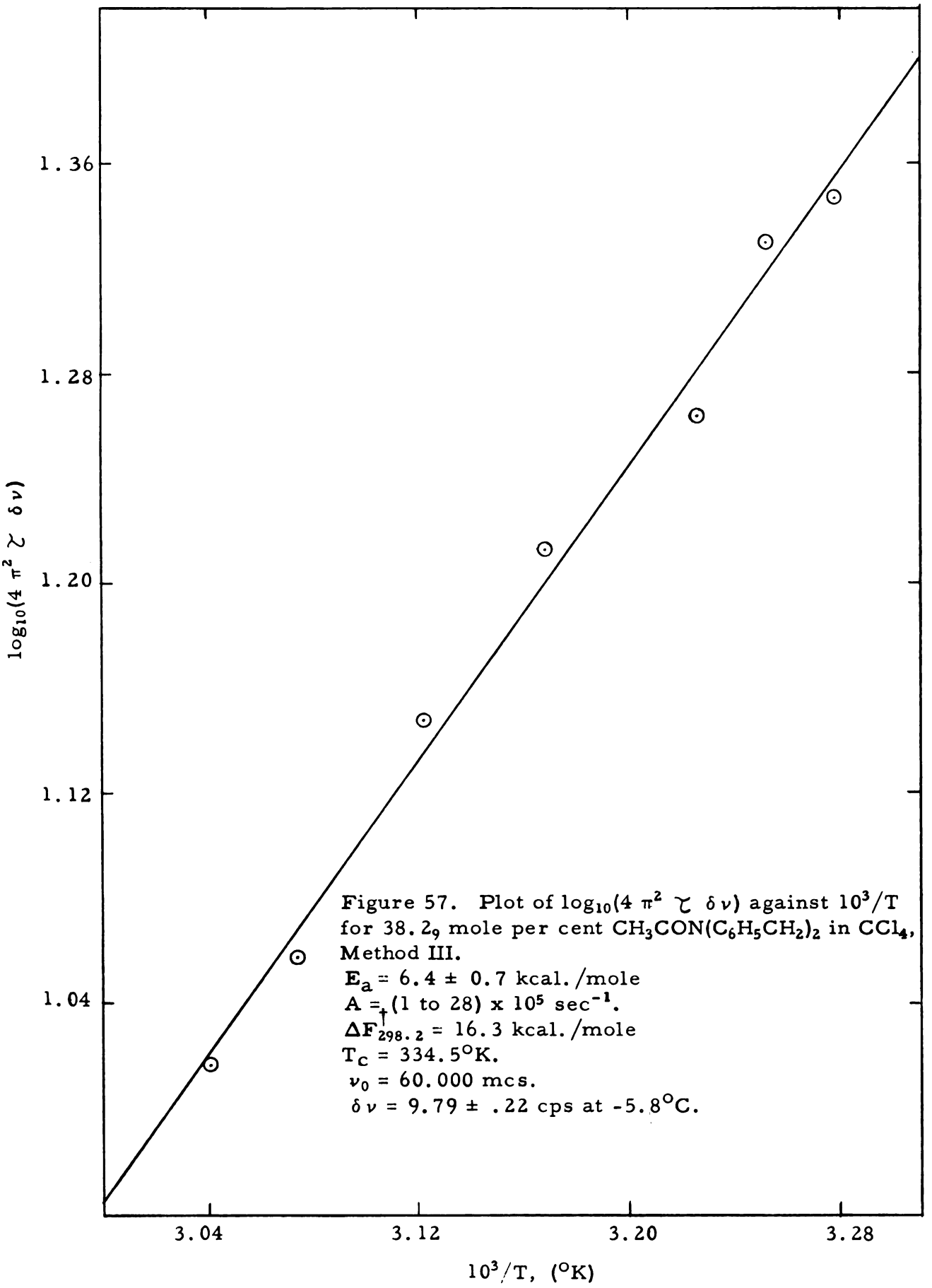

Figure 57. Plot of $\log_{10}(4\pi^2 \tau \delta\nu)$ against $10^3/T$ for 38.2$_9$ mole per cent $CH_3CON(C_6H_5CH_2)_2$ in CCl_4, Method III.
E_a = 6.4 ± 0.7 kcal./mole
$A = \dagger$ (1 to 28) x 10^5 sec^{-1}.
$\Delta F^{\dagger}_{298.2}$ = 16.3 kcal./mole
T_c = 334.5°K.
ν_0 = 60.000 mcs.
$\delta\nu$ = 9.79 ± .22 cps at -5.8°C.

TABLE XXIII

VALUES OF E_a, A, $\Delta F^{\dagger}_{298.2}$ and T_c FOR HINDERED INTERNAL ROTATION ABOUT THE CENTRAL C-N BOND OF SOME SYMMETRICALLY N, N-DISUBSTITUTED AMIDES AS DETERMINED BY PROTON MAGNETIC RESONANCE SPECTROSCOPY, $\nu_0 \approx 60.000$ mcs.

Amide	Mole per cent amide	Solvent	E_a kcal./mole	A,* sec^{-1}	$\Delta F^{\dagger}_{298.2}$ kcal./mole	T_c, °K.
$HCON(CH_3)_2$	100		18.3 ±0.9**	(2 to 50) x 10^{10}	22.1	421.6
$HCON(CH_3)_2$	100		14.3 ± 2.8***	(2 to 130) x 10^{8}***	19.6***	410.7***
$CH_3CON(CH_3)_2$	100		10.5 ± 0.5	(3 to 33) x 10^{7}	17.4	360.4
$C_2H_5CON(CH_3)_2$	100		9.2 ± 0.8	(8 to 26) x 10^{6}	16.7	334.4
$C_2H_5CON(CH_3)_2$	84.7_1	CH_2Br_2	10.1 ± 0.9	(2 to 90) x 10^{7}	16.7	330.0
$C_2H_5CON(CH_3)_2$	68.8_8	CH_2Br_2	10.3 ± 0.9	(3 to 93) x 10^{7}	16.8	333.1
$C_2H_5CON(CH_3)_2$	58.0_0	CH_2Br_2	10.2 ± 0.8	(2 to 85) x 10^{7}	16.8	333.3
$C_2H_5CON(CH_3)_2$	40.5_7	CH_2Br_2	9.9 ± 0.9	(2 to 50) x 10^{7}	16.8	332.7
$C_2H_5CON(CH_3)_2$	22.1_7	CH_2Br_2	9.1 ± 0.2	(8 to 13) x 10^{6}	16.8	332.2
$C_2H_5CON(CH_3)_2$	10.1_4	CH_2Br_2	7.1 ± 0.8	(2 to 44) x 10^{5}	16.7	337.3
$C_2H_5CON(CH_3)_2$	69.34	CCl_4	8.6 ± 0.6	(4 to 12) x 10^{6}	16.5	333.0
$C_2H_5CON(CH_3)_2$	39.9_4	CCl_4	7.5 ± 0.5	(4 to 26) x 10^{5}	15.9	311.3
$C_2H_5CON(CH_3)_2$	11.0_7	CCl_4	6.3 ± 0.5	(2 to 32) x 10^{5}	16.0	316.0
$CCl_3CON(CH_3)_2$	100		10.0 ± 0.5	(8 to 17) x 10^{8}	14.9	287.0
$CF_3CON(CH_3)_2$	100		9.5 ± 0.7	(3 to 54) x 10^{6}	17.6	367.0
$CH_2FCHCON(CH_3)_2$	100		6.8 = 0.9	(2 to 13) x 10^{5}	16.1	319.4

Continued

TABLE XXIII - Continued

Amide	Mole per cent amide	Solvent	E_a kcal./mole	A_1* sec^{-1}	$\Delta F^{\dagger}_{298.2}$ kcal./mole	T_c, °K
$C_6H_5CON(CH_3)_2$	36.3_4	CH_2Br_2	7.7 ± 0.6	(4 to 17) x 10^6	15.5	285.0
$ClCON(CH_3)_2$	100		7.2 ± 0.5	(4 to 10) x 10^5	16.5	326.5
$ClCON(CH_3)_2$	90.0_3	CH_2Br_2	8.2 ± 0.4	(2 to 22) x 10^6	16.5	325.6
$ClCON(CH_3)_2$	63.4_4	CH_2Br_2	9.0 ± 0.9	(4 to 19) x 10^6	16.6	325.5
$ClCON(CH_3)_2$	40.9_3	CH_2Br_2	8.6 ± 0.7	(3 to 64) x 10^6	16.6	325.5
$ClCON(CH_3)_2$	10.7_2	CH_2Br_2	7.3 ± 0.8	(3 to 103) x 10^5	16.5	325.8
$ClCON(CH_3)_2$	71.3_5	CCl_4	6.9 ± 0.7	(2 to 40) x 10^5	16.4	326.5
$ClCON(CH_3)_2$	40.0_8	CCl_4	6.6± 0.7	(2 to 36) x 10^5	16.3	323.8
$ClCON(CH_3)_2$	10.9_8	CCl_4	6.8 ± 0.3	(4 to 7) x 10^5	16.2	317.4
$CH_3CO(C_6H_5CH_2)_2$	38.0_9	CH_2Br_2	7.3 ± 0.7	(4 to 12) x 10^5	16.5	343.7
$CH_3CO(C_6H_5CH_2)_2$	38.2_9	CCl_4	6.4 ± 0.7	(1 to 28) x 10^5	16.3	334.5

*The limits shown are for 90 per cent confidence in A.
**The value and error given cover the limits of 90 per cent confidence.
***These values were obtained by Method II, whereas all other values were obtained by Method III.

DISCUSSION

Methods for Obtaining Energy Barriers and Frequency Factors for Hindered Internal Molecular Rotations by High-resolution Nuclear Magnetic Resonance

In the Theoretical Background of this thesis, several NMR methods for obtaining energy barriers and frequency factors for hindered internal molecular rotations were introduced. Attempts were made to use three of these methods to study the phenomenon of hindered internal rotation about the central C-N bond of some symmetrically N, N-disubstituted amides. The first method used, Method I, was not well suited to the study of hindered internal rotation about the central C-N bond of N, N-dimethylpropionamide. This method relates changes in resonance line widths to the rate of the kinetic process being studied. For N, N-dimethylpropionamide, the magnitudes of the changes in the line widths of the two N-methyl proton resonances with the rate of internal rotation are determined by the chemical shift between the N-methyl proton resonances in the absence of internal rotation. For N, N-dimethylpropionamide, this chemical shift is only about 7.5 cps (at ν_0 = 60.000 mcs.).

One equation of Method I, equation (110), is valid only in the region of slow rate processes. This equation relates the kinetic broadening of resonance line widths to the rate of the process. For N, N-dimethylpropionamide the region over which equation (110) is valid corresponds to changes in the N-methyl proton resonance line widths from about 0.6 to 2.0 cps. Since the line widths were measurable only to an accuracy of about ± 0.3 cps, the rates calculated from equation (110) were very unreliable.

The other equation of Method I, equation (113), is valid only in the region of very fast rate processes. This equation relates the kinetic

narrowing of the line width of the coalesced resonance peak to the rate of the process. For N, N-dimethylpropionamide the region over which equation (113) is valid corresponds to changes in the coalesced N-methyl proton resonance line width from about 3 to 0.8 cps. Again, because of the inherent errors in line-width measurements, the rates calculated from equation (113) were very unreliable.

Similar errors should be expected when Method I is applied to most of the other symmetrically N, N-disubstituted amides. Since the chemical shift in the absence of internal rotation about the central C-N bond of N, N-dimethyltrichloroacetamide is about 17.5 cps (at ν_0 = 60.000 mcs.), Method I would probably yield fairly reliable rates of internal rotation for this compound. Piettle and Anderson used Method I for studying the hindered internal rotation about the O-N bond of some alkyl nitrites (81). For these compounds, the chemical shift between the resonances of the α-protons of the cis and trans alkyl nitrites, in the absence of internal rotation, was about 43 cps (at ν_0 = 40 mcs). Therefore, for the alkyl nitrites the regions over which equations (110) and (113) were valid corresponded to changes in line widths that were very large compared to the experimental error in the line-width measurements. For such systems, one should expect Method I to yield quite accurate values for the rates of internal rotations. Piette and Anderson found that in the region of slow rates of internal rotation about the O-N bond of the alkyl nitrites, equation (110) yielded unreliable values for the energy barriers. However, in the region of very fast internal rotations, they found that equation (113) yielded values for the energy barriers having errors of about 2 kcal./mole. More accurate values for the energy barriers to hindered internal rotations about the O-N bond of alkyl nitrites would probably be obtained by using Method I and an applied

radiofrequency of 60.000 mcs. At this higher frequency, the chemical shift between the resonances of the α-protons of the cis and trans isomers, in the absence of internal rotation, would be about 22 cps larger than the chemical shift which was observed at 40 mcs. This larger chemical shift would correspond to more pronounced changes in line widths due to rotational averaging.

A second method, Method II, was used to obtain the energy barrier and frequency factor for hindered internal rotation about the central C-N bond of N, N-dimethylformamide. For this compound, Method II relates the observed frequency separation of the two N-methyl proton resonances to the rate of the internal rotation. The chemical shift between these resonances in the absence of internal rotation is about 9.4 cps (at ν_0 = 60.000 mcs.). Since effective natural line widths from about 0.3 to 0.6 cps were observed for the two resonance lines, corrections due to the effect of overlap on the apparent separation of the two peaks were much smaller than the experimental errors in the measurements of the peak separations (see Figure 5). Therefore, the overlap corrections were neglected.

Method II was originally proposed by Gutowsky and Holm (5, 6), who used it to study hindered internal rotation about the central C-N bond of N, N-dimethylformamide and N, N-dimethylacetamide. Their measurements were made at the applied radiofrequency 17.735 mcs., where the chemical shift between the N-methyl proton resonances of N, N-dimethylformamide in the absence of internal rotation was about 3.2 cps. Since effective natural line widths of about 2.3 cps were observed, corrections due to the effect of overlap on the apparent separation of the two peaks were very important (see Figure 5). For N, N-dimethylformamide, Gutowsky and Holm obtained 7 ± 3 kcal./mole and from 10^3 to 10^7 $sec.^{-1}$ for the energy barrier and frequency factor, respectively. These authors suggested that more

precise values should be obtained by using higher applied radiofrequencies. At higher frequencies, the chemical shift between the N-methyl proton resonances in the absence of internal rotation would be proportionately larger, and providing that the experimental errors would be no worse, more precise results would be obtained.

The use of Method II in this present work yielded 14.3 ± 2.8 kcal./mole and (2 to 130) x 10^8 $sec.^{-1}$ for the energy barrier and frequency factor, respectively, for hindered internal rotation about the central C-N bond of N, N-dimethylformamide. Although the data were obtained at the radiofrequency 60.000 mcs., these results are not significantly more precise than those obtained by Gutowsky and Holm. Just as the chemical shift between the two N-methyl proton resonances in the absence of internal rotation is about 3.4 times greater at 60.000 mcs. than at 17.735 mcs., the errors in the measurements of the separations between the two peaks in the presence of internal rotation are also greater. The increased chemical shift leads to increased broadening due to rotational averaging. Since the tops of broad absorption peaks are quite flat, the frequency positions of the maxima of such absorption peaks are difficult to determine precisely. This difficulty seriously effects results obtained from the use of Method II. In the region of very slow rotational rates, where the broadening of the resonance lines due to rotational averaging is small, the change in the separation between resonance peaks is very insensitive to large changes in rotational rates. Therefore, in the region where the separation between resonance peaks can be measured most accurately, the dependence of the separation upon rotational rate is too small for accurately determining changes in rate. This dependence of the separation of resonance peaks upon the rate of rotation is clearly shown in Figure 10. In the region of faster rotational rates, where broadening of the resonance

lines is large, the separation between peaks is very sensitive to changes in rate. So, in the region where the separation between resonance peaks is very sensitive to changes in rate, the measurements of frequency separations are subject to large error.

Frequency positions of broad NMR lines are best determined by use of the dispersion u-mode, which is very sensitive to changes in the slope of the absorption v-mode. However, the effects of overlap on the apparent separation of dispersion modes may be extremely important (see Figure 5). Because of errors in the measurements of effective natural line widths, overlap corrections are, in general, subject to large errors. Therefore, no serious attempts were made to measure the separations of the N-methyl proton dispersion lines for N, N-dimethylformamide.

The third method, Method III, was used to study the hindered internal rotation about the central C-N bond of most of the symmetrically N, N-disubstituted amides used in this work. For an N, N-dimethyl amide, this method relates the ratio of maximum to central minimum intensities for the chemical-shift doublet of the two N-methyl proton resonances, to the rate of internal rotation about the central C-N bond of the amide. For all the amides studied by Method III, the effects of overlap upon the ratios of maximum to central minimum intensities were estimated, from equations (74), (91), and (93), to be negligible compared to the errors in the measurements of the intensity ratios. Therefore, no overlap corrections were made.

Since changes in the intensity ratios were more pronounced than changes in line widths and frequency separations, and since the ratios could be measured quite precisely, the results obtained from the use of Method III were more accurate than those obtained by either Method I or II. The dependence of the intensity ratio upon the rate

of internal rotation is clearly shown in Figure 10. The ratios could be measured most accurately in the region of fast internal rotations, (i.e., in the region of small ratios). In this region, large changes in the rate correspond to small changes in the ratio. The errors in the ratio measurements were largest in the region of slow internal rotations (i.e., in the region of large ratios). In this region, small fluctuations in the base line have pronounced effects upon the observed ratios. However, large changes in the intensity ratios in this region correspond to only small changes in rate (see Figure 10).

For the hindered internal rotations studied in this work, Method III had the disadvantage that it was applicable only over temperature ranges of about 25 degrees. As mentioned in the theoretical background of this thesis, Takeda and Stejskal (24) have recently developed an NMR method for measuring the rates of exchange reactions in the region of very fast exchange rates. Their method should be applicable to the study of hindered internal rotation about the central C-N bond of most of the amides used in this present work. By using Method III and the method recently proposed by Takeda and Stejskal, one should be able to obtain experimental rates for the internal rotation over temperature ranges of about 50 degrees. Providing the errors in the rates as determined by the method of Takeda and Stejskal were no worse than those in the rates determined by Method III, the larger temperature range would markedly decrease the errors in the energy barriers and frequency factors.

Results

The energy barrier hindering internal rotation about the central C-N bond of pure N, N-dimethylformamide is 18.3 ± 0.9 kcal./mole in height. This value was obtained by Method III. The actual error in the value 14.3 kcal./mole, as obtained by Method II, is probably much larger than the estimated error of 2.8 kcal./mole given in Figure 26 and Table XXIII. As described in the Experimental section of this thesis, the errors were calculated from the set of points obtained when several measurements were averaged at each of several temperatures. The deviations from these averages were not considered when the errors were calculated. Figure 26 shows that such deviations are very large for data obtained by Method II. In view of such large deviations, the linearity of the resultant averages is quite surprising. The error in the energy barrier obtained by Method II would probably be much larger than 2.8 kcal./mole, if one included the deviations from average values in the error calculations. Figures 27 and 30 show that the data obtained by Gutowsky and Holm (5, 6) contain similar errors. These authors reported the value 7 ± 3 kcal./mole for the energy barrier hindering internal rotation about the central C-N bond of N, N-dimethylformamide. Their estimated error was confirmed when calculated from their data by the method described in the Experimental section of this thesis. Therefore, an estimated error of ± 3 kcal./mole for the measurements of Gutowsky and Holm on N, N-dimethylformamide does not include the large deviations from average values and should, therefore, be regarded as too optimistic.

The high value 18.3 ± 0.9 kcal./mole, obtained by Method III, is supported by the high value (about 20 kcal./mole) reported earlier (41).

It is supported also by the high value (about 18 kcal./mole)* for the energy barrier hindering internal rotation about the C-N bond of formamide. Assuming that the central C-N bond of N, N-dimethylformamide contains about 40 per cent C=N character (29), a barrier height of 18.2 kcal./mole may be estimated from the difference between the C=N bond energy, 94 kcal./mole (113), and the C-N bond energy, 48.6 kcal./mole (113).

The energy barrier hindering internal rotation about the central C-N bond of N, N-dimethylacetamide is 10.5 ± 5 kcal./mole. This value was obtained by Method III, and it is in agreement with the value 12 ± 2 kcal./mole reported by Gutowsky and Holm (5, 6). It should be noted that the barrier for N, N-dimethylacetamide is about 7.8 kcal./mole lower than that for N, N-dimethylformamide. Usually, N, N-dialkyl amides are considered to be only very slightly associated (18, 22, 36). However, a small amount of association, involving the slightly acidic aldehyde hydrogen atom of N, N-dimethylformamide, may be responsible for the higher barrier for this compound. Determination of the barrier for N, N-dimethylformamide as a function of concentration in several solvents would probably give definitive information concerning the effects due to association. Barriers for rotation about the C-N bond

---

*This value was obtained by W. G. Schneider from NMR measurements on N^{15} labelled formamide. His estimate of the energy barrier was revealed in a footnote of a recent article by Costain and Dowling (112). These authors have re-examined the microwave spectrum of formamide. Their results show that the dihedral angle between the H'NC plane and the NCO plane, and between the H"NC plane and the NCH plane are 7 ± 5°, and 12 ± 5°, respectively. The hydrogen designated in H' is cis to the oxygen atom, and the one designated as H" is cis to the aldehyde hydrogen atom. Although these angles are small, they show significant non-planarity at the nitrogen atom. Previous to the work of Costain and Dowling, the microwave spectrum of formamide had been interpreted on the basis of a completely planar structure for the molecule (28, 29).

in amides are much larger than observed barriers for internal rotations in ethane, amines, alcohols, and ketones, which are about one to three kcal./mole (3). The extra height of the barrier for rotation about the C-N bond in amides is attributed to partial double bond character of the C-N bond. Resonance between structures I and II have been shown to be important (27, 28, 29, 112).

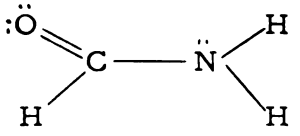

I

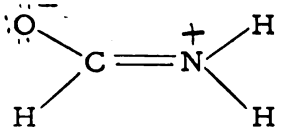

II

The contribution of II has been estimated as about 40 per cent (29). In acetamide, where additional structures such as III (hyperconjugation) may contribute (106), the double bond character of the central C-N bond would be somewhat reduced.

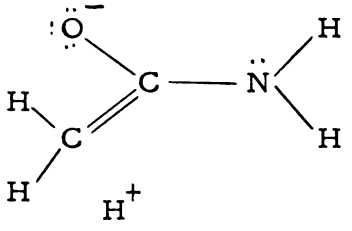

III

An alternative explanation of the large difference between the barriers for N, N-dimethylformamide and N, N-dimethylacetamide may be that the transition state for internal rotation about the central C-N bond of the latter molecule involves an excited electronic state of the molecule. If the energy surface of an excited state crosses that for the normal state, the barrier and frequency factor for internal rotation may be markedly suppressed (107, 108). Such an explanation for the

large difference between the barriers for these apparently similar molecules seems somewhat doubtful. However, this explanation, as it pertains to the large differences among the barriers and frequency factors for internal rotation about the C=C bond of ethylene and its derivatives, seems to be fairly well accepted (107, 108, 109).

The energy barrier hindering internal rotation about the central C-N bond of pure N, N-dimethylpropionamide is 9.2 ± 0.8 kcal./mole. The small difference between this value and that for N, N-dimethylacetamide is equal to the sum of the experimental errors involved. Since the reported errors are those for 90 per cent confidence, the small difference between the two barriers may be regarded as significant with probably at least 50 per cent confidence. The magnitude of the difference (1.3 kcal./mole) is about what one would predict on the basis of the additional suppression of the energy barrier due to the difference between the hyperconjugative resonance of the C-methyl group of N, N-dimethylacetamide and that of the ethyl group of N, N-dimethylpropionamide.

The values of the barriers hindering internal rotation about the central C-N bond of N, N-dimethyltrichloroacetamide and N, N-dimethyltrifluoroacetamide are 10.0 ± 0.5 kcal./mole and 9.5 ± 0.7 kcal./mole, respectively. As expected, these values are about the same as that for N, N-dimethylacetamide. If there is any significant difference among the three values it is probably due to inductive effects of the more electronegative halogen atoms, which would be expected to increase the barrier height.

The barrier hindering internal rotation about the central C-N bond of N, N-dimethylacrylamide is 6.8 ± 0.9 kcal./mole. This value is significantly lower than that for N, N-dimethylacetamide. The difference (about 3.7 kcal./mole) between these two barrier heights is attributed to the contribution of the resonance structure,

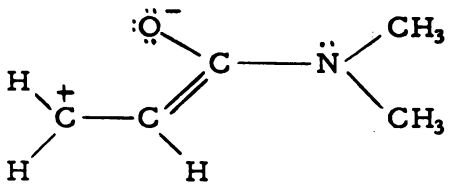

IV

which is in competition with the contribution of the structure similar to II above. The low value, 7.2 ± 0.5 kcal./mole, for the barrier hindering internal rotation about the central C-N bond of N, N-dimethylcarbamyl chloride is attributed to the contribution of the resonance structure V.

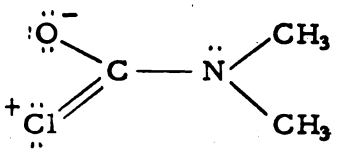

V

Similarly, the low barrier height, 7.7 ± 0.6 kcal./mole, for N, N-dimethylbenzamide (36.3$_4$ mole per cent in dibromomethane) is attributed to the contributions of the resonance structures VI, VII, and VIII.

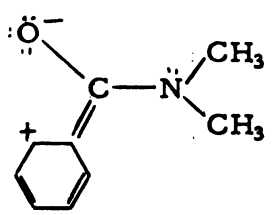

VI

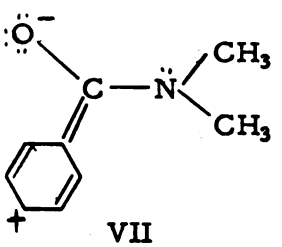

VII

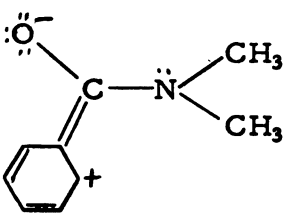

VIII

It should be noted, however, that the energy barrier was obtained for this compound dissolved in dibromomethane solution. The effect of the solvent upon the barrier height may be significant.

The proton resonances due to the two N-methyl groups of ethyl-N, N-dimethylcarbamate were observed to consist of a single narrow line, even at quite low temperatures. This observation is explained in terms of one phenomenon, which plays a dual role in causing the coalescence of the two resonances. For the protons of the two N-methyl groups to have different chemical shifts, the environmental shielding of the protons of each N-methyl group must be different. For ethyl-N, N-dimethylcarbamate, such differences in shielding would have to result from differences in the electron densities around the two oxygen atoms. However, resonance between the two structures IX and X

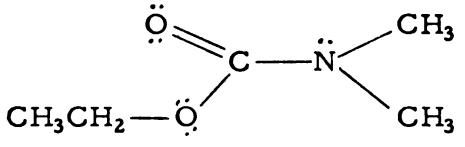

IX

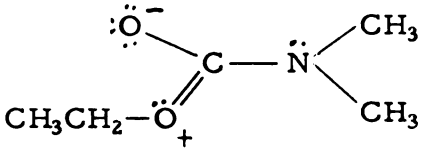

X

tends to make the electron densities around the two oxygen atoms about the same. The importance of this resonance should be apparent from the estimated large resonance energy, 24 kcal./mole (110), associated with it. Therefore, one role of the above resonance is to cause the protons of each N-methyl group to have similar chemical shifts. The second effect would be to suppress the contribution of the resonance structure analogous to II. This effect reduces the barrier to internal rotation about the central C-N bond so that the rate of rotation would be too large to "see" on the NMR time scale. Similar arguments explain the failure to detect hindered internal rotation about the central C-N bond of methyl-N, N-bis-(trifluoromethyl)-carbamate. The failure to detect hindered internal rotation about the central C-N bond of N, N-bis-(trifluoromethyl)-trifluoroacetamide is quite surprising. Since the barrier for this molecule would be

expected to be at least as large as that for N, N-dimethyltrifluoracetamide, one is led to conclude that the chemical shift between the two N-trifluoromethyl groups in the absence of internal rotation is very small.

The barrier to internal rotation about the central C-N bond of N, N-dimethylpropionamide was observed to decrease from 9.2 ± 0.8 kcal./mole for the pure liquid to a low value of 6.3 ± 0.5 kcal./mole for 11.0_7 mole per cent amide in carbon tetrachloride solution (see Figure 41). This decrease in the barrier is probably due to dissociation of the slightly associated pure liquid amide when diluted, and to the change in the dielectric constant of the solution upon dilution. Figure 41 shows that most of the observed changes in the barrier, when the amide was diluted with dibromomethane, were within the experimental errors involved. However, the values obtained suggest that when the amide is diluted with dibromomethane, the barrier rises to a maximum of about 10.3 kcal./mole at about 66 mole per cent amide, and then falls to the low value of about 7.1 kcal./mole at about 10 mole per cent amide. These effects are attributed to a specific interaction, which involves two molecules of amide and one molecule of solvent. The actual existence of these effects are supported to some degree by the similar results observed for solutions of N, N-dimethylcarbamyl chloride in carbon tetrachloride and in dibromomethane (see Figure 55). Although these results should not, of course, be regarded as conclusive evidence for specific solvent-solute interactions, they certainly serve as an incentive to search for more pronounced effects in solutions of substituted amides in other solvents.

The following energy barriers for hindered internal rotation about the central C-N bond of N, N-dibenzylacetamide were obtained:

38.0_9 mole per cent amide in dibromomethane, 7.3 ± 0.7 kcal./mole; 38.2_9 mole per cent amide in carbon tetrachloride, 6.4 ± 0.7 kcal./mole. These values probably contain significant contributions due to solvent effects.

The experimental frequency factors for the internal rotations studied vary from very low values of about 10^5 $sec.^{-1}$ to higher values of about 10^7 $sec.^{-1}$ The highest frequency factor, about 10^{10} $sec.^{-1}$, was obtained for N, N-dimethylformamide. It should be noticed that the experimental frequency factors, obtained from the Arrhenius-type rate equation, are much lower than the normal value kT/h predicted by the simple theory of absolute reaction rates. It is not surprising, therefore, that the calculated free-energies of activation, shown in Table XXIII, do not agree with the experimental energies of activation. Since small entropies of activation are expected for internal rotations (108), the low experimental frequency factors may be explained in terms of the more general theory of absolute reaction rates; i.e., in terms of low transmission coefficients.

SUMMARY

A Varian high-resolution nuclear magnetic resonance spectrometer was used for observing proton and fluorine magnetic resonance spectra of several symmetrically N, N-disubstituted amides over a wide range of temperatures. Apparatus for controlling sample temperatures at high or low values was constructed. Also, coils for electrically shimming the applied magnetic field were constructed. The use of these coils was essential to the observation of high-resolution fluorine magnetic resonance spectra at the applied radio-frequency 60.000 mcs.

Theoretical methods for relating the rate of internal rotation about the central C-N bond of the substituted amides to various components of resonance line shapes were considered. Three of these methods were applied experimentally to the study of the phenomenon of hindered internal rotation. Of the three methods used, only one was well adapted to the study of hindered internal rotation about the central C-N bond of the symmetrically N, N-disubstituted amides used in this work. This method relates the ratio of maximum to central minimum absorption intensities of a symmetrical resonance doublet to the rate of internal rotation. The energy barrier and frequency factor, for each internal rotation studied, were calculated from the experimental temperature dependence of the rate of internal rotation. The experimental errors were much lower than those previously reported for similar studies.

The phenomenon of hindered internal rotation about the central C-N bond of the following pure liquid amides was studied: N, N-dimethylformamide; N, N-dimethylacetamide; N, N-dimethylpropionamide;

N, N-dimethyltrichloroacetamide; N, N-dimethyltrifluoroacetamide; N, N-dimethylacrylamide; and N, N-dimethylcarbamyl chloride. The internal rotation about the C-N bond of N, N-dimethylbenzamide was studied for a solution of the amide in dibromomethane. Similar studies were made for a solution of N, N-dibenzylacetamide in dibromomethane, and for a solution of this amide in carbon tetrachloride.

The apparent rates of internal rotation about the central C-N bond of ethyl-N, N-dimethylcarbamate, and about the central C-N bond of methyl-N, N-bis-(trifluoromethyl)-carbamate, were too fast to be detected, even at quite low temperatures. In addition, the presence of hindered internal rotation about the central C-N bond of N, N-bis-(trifluoromethyl)-trifluoroacetamide could not be detected.

The origin of the barrier to internal rotation about the C-N bond of the amide group is attributed to the existence of partial C=N bond character, which arises from resonance between valence bond structures. Some possible explanations for the exceptionally high barrier observed for N, N-dimethylformamide are the following: a small amount of intermolecular association of the pure liquid, the nonexistence of contributing resonance structures that would suppress the partial double bond character of the central C-N bond, and the possibility of the barriers for all the other amides being suppressed by transition states which involve excited electronic states. The low-barrier compounds were compared with N, N-dimethylactamide. The values of the energy barriers for these compounds were explained in terms of contributing resonance structures which suppress the double bond character of the central C-N bond.

For most of the internal rotations studied, the experimental frequency factors were from about 10^5 to 10^7 $sec.^{-1}$ These low values were attributed to low transmission coefficients.

The phenomenon of hindered internal rotation about the central C-N bond of N, N-dimethylpropionamide was studied for several solutions of the amide in dibromomethane and in carbon tetrachloride. The concentration dependence of the barrier to internal rotation for the amide in dibromomethane solutions suggests the possible existence of a specific solvent-solute interaction. When the amide was diluted with carbon tetrachloride, the barrier was observed to decrease markedly. This decrease is attributed to the dissociation of the slightly associated pure liquid amide upon dilution. Similar effects were observed for solutions of N, N-dimethylcarbamyl chloride in dibromomethane and in carbon tetrachloride.

The apparent very rapid internal rotations about the central C-N bond of ethyl-N, N-dimethylcarbamate, and about the central C-N bond of methyl-N, N-bis-(trifluoromethyl)-carbamate, are attributed to a low energy barrier for the internal rotations. These compounds have important resonance structures which tend to suppress the double bond character of the central C-N bond.

BIBLIOGRAPHY

1. Mizushima, S., "Structure of Molecules and Internal Rotation," Academic Press Inc., New York, N. Y., 1954.

2. Phillips, W. D., Ann. N. Y. Acad. Sci. 70, 817 (1958).

3. Lin, C. C. and J. D. Swalen, Rev. Mod. Phys. 31, 841.

4. Glassstone, S., K. J. Laidler, and H. Eyring, "The Theory of Rate Processes," pp. 1-2, McGraw-Hill Book Co., Inc., New York, N. Y., 1941.

5. Gutowsky, H. S. and C. H. Holm, J. Chem. Phys. 25, 1228 (1956).

6. Holm, C. H., Doctoral Thesis, Univ. of Illinois, 1955.

7. Pauling, L., "The Nature of the Chemical Bond," 2nd ed., pp. 133, 207-208, Cornell Univ. Press, Ithaca, N. Y., 1940.

8. Kohlrausch, K. W. F. and A. Pongratz, Monatsh. 70, 226 (1937).

9. Chaplin, H. O. and L. Hunter, J. Chem. Soc., 1114 (1937).

10. Buswell, A. M., W. H. Rodebush, and M. F. Roy, J. Am. Chem. Soc. 60, 2444 (1938).

11. Kohlrausch, K. W. F. and R. Seka, Z. physik. Chem. B43, 355 (1939).

12. Dawson, L. R., P. G. Sears, and R. H. Graves, J. Am. Chem. Soc. 77, 1986 (1955).

13. Davies, M., J. C. Evans, and R. L. Jones, Trans. Faraday Soc. 51, 761 (1955).

14. Bello, J., J. Phys. Chem. 60, 1341 (1956).

15. O'Brien, J. L. and C. Niemann, J. Am. Chem. Soc. 79, 1386 (1957).

16. Mizushima, S., et al., ibid. 72, 3490 (1950).

17. Mizushima, S., op. cit., pp. 139-152; "Advances in Protein Chem.," 9, 299 (1954).

18. Cannon, C. G., Mickrochim. Acta, 555 (1955).

19. Davies, M. and L. Hopkins, Trans. Faraday Soc. 53, 1563 (1957).

20. Spinner, E., Spectrochim. Acta, 95 (1959).

21. Goldfarb, A. R., A. Mele, and N. Gutstein, J. Am. Chem. Soc. 77, 6194 (1955).

22. Fraenkel, G. and C. Niemann, Proc. Natl. Acad. Sci. 44, 688 (1958).

23. Berger, A., A. Loewenstein, and S. Meiboom, J. Am. Chem. Soc. 81, 62 (1959).

24. Takeda, M. and E. O. Stejskal, ibid. 82, 25 (1960).

25. Spinner, E., J. Phys. Chem. 64, 275 (1960).

26. Corey, R. B. and J. Donahue, J. Am. Chem. Soc. 72, 2899 (1952); R. B. Corey and L. Pauling, Proc. Roy. Soc. London B141, 10 (1953); R. B. Corey, Fortschr. Chem. org. Naturstoffe 8, 310 (1951); R. B. Corey and L. Pauling, ibid. 11, 18 (1954).

27. Pauling, L., "The Nature of the Chemical Bond," 3rd ed., p. 282, Cornell Univ. Press, Ithaca, N. Y., 1960.

28. Kurland, R. J., J. Chem. Phys. 23, 2202 (1955).

29. Kurland, R. J. and E. B. Wilson, Jr., ibid. 27, 585 (1957).

30. Pauling, L., in "Symposium on Proton Structure," ed. by A. Neuberger, John Wiley and Sons, New York, N. Y., 1958.

31. Bates, W. W. and M. E. Hobbs, J. Am. Chem. Soc. 73, 2151 (1951).

32. Zahn, C. T., Physik. Z. 33, 515 (1932).

33. Devoto, G., Gazz. chim. ital. 63, 495 (1933).

34. Kumler, W. D. and C. W. Porter, J. Am. Chem. Soc. 56, (1934).

35. Leader, G. R., ibid. 73, 856 (1951).

36. Leader, G. R. and J. F. Gormely, ibid., 5731.

37. Kumler, W. D., ibid. 74, 261 (1952).

38. Longster, G. F. and E. E. Walker, Trans. Faraday Soc. 49, 229 (1953).

39. Phillips, W. D., J. Chem. Phys. 23, 1363 (1955).

40. Phillips, W. D., C. E. Looney, and C. P. Spaeth, J. Molecular Spectroscopy 1, 35 (1957).

41. "This is NMR at Work," Technical Information Bulletin from the Radiofrequency Spectroscopy Laboratory of Varian Associates, Instruments Division, Palo Alto, California, Vol. 2. of series A, No. 28, 1957.

42. Piette, L. H., J. D. Ray and R. A. Ogg, J. Molecular Spectroscopy 2, 66 (1958).

43. Lauterbur, P. C., J. Chem. Phys. 26, 217 (1957).

44. Holder, B. E. and M. P. Klein, ibid. 23, 1956 (1955).

45. Van Vleck, J. H., "The Theory of Electric and Magnetic Susceptibilities," pp. 89-104, Oxford University Press, New York, 1932.

46. Pauli, W., Naturwiss. 12, 741 (1924).

47. Andrew, E. R., "Nuclear Magnetic Resonance," pp. 1-3, 7-8, Cambridge Univ. Press, New York, N. Y., 1955.

48. Pople, J. A., W. G. Schneider, and H. J. Bernstein, "High-resolution Nuclear Magnetic Resonance," pp. 22-23, McGraw-Hill Book Company, Inc., New York, N. Y., 1959.

49. Schiff, L. I., "Quantum Mechanics," pp. 254-263, 399-400, McGraw-Hill Book Company, Inc., New York, 1955.

50. Bloembergen, N. E., E. M. Purcell, and R. V. Pound, Phys. Rev. 73, 679 (1948).

51. Bloch, F., Phys. Rev. 70, 460 (1946).

52. Knight, W. D., ibid. 76, 1259 (1949).

53. Proctor, W. G. and F. C. Yu, ibid., 77, 717 (1950).

54. Dickinson, W. C., ibid. 736.

55. Linstrom, G., ibid. 78, 817 (1950).

56. Thomas, H. A., ibid. 80, 901 (1950).

57. Arnold, J. T., and M. E. Packard, J. Chem. Phys. 19, 1608 (1951).

58. Bene, G. J., P. M. Denis, and R. C. Exterman, Physica 17, 308 (1951).

59. Glick, R. E., and A. A. Bothner-By, J. Chem. Phys. 22, 1143 (1954).

60. Reilly, C. A., ibid. 25, 604 (1956).

61. Proctor, W. G., and F. C. Yu, Phys. Rev. 78, 471 (1950).

62. Gutowsky, H. S., and D. W. McCall, ibid. 82, 748 (1951).

63. Hahn, E. L. and D. E. Maxwell, ibid. 84, 1246 (1951).

64. Gutowsky, H. S., D. W. McCall, and C. P. Slichter, ibid. 84, 589 (1951).

65. Hahn, E. L., and D. E. Maxwell, ibid. 84, 1286 (1951).

66. Bloch, F., ibid. 93, 944 (1954).

67. Bloom, A. L. and J. N. Shoolery, ibid. 97, 1261 (1955).

68. Anderson, W. A., ibid. 102, 151 (1956).

69. Gutowsky, H. S., D. W. McCall, and C. P. Slichter, J. Chem. Phys. 21, 279 (1953).

70. Gutowsky, H. S. and A. Saika, ibid. 1688.

71. Weinberg, I. and J. R. Zimmerman, ibid. 23, 748 (1955).

72. Arnold, J. T., Phys. Rev. 102, 136 (1956).

73. Drysdale, J. J. and W. D. Phillips, J. Am. Chem. Soc. 79, 319 (1957).

74. Grunwald, E., A. Loewenstein, and S. Meiboon, J. Chem. Phys. 27, 630 (1957).

75. Loewenstein, A. and S. Meiboom, ibid. 1067.

76. Muetterlies, E. L. and W. D. Phillips, J. Am. Chem. Soc. 79, 322 (1957).

77. Looney, C. E., W. D. Phillips, and E. L. Reilly, ibid. 6136.

78. Anbar, M., A. Loewenstein, and S. Meiboom, ibid. 80, 2630 (1958).

79. Cotton, F. A., J. W. George, and J. S. Waugh, J. Chem. Phys. 28, 994 (1958).

80. Muetterties, E. L. and W. D. Phillips, op. cit. 81, 1084 (1959).

81. Piette, L. H. and W. A. Anderson, J. Chem. Phys. 30, 899 (1959).

82. McConnell, H. M., ibid. 28, 430 (1958).

83. McConnell, H. M. and D. D. Thompson, ibid. 26, 958 (1957).

84. Anderson, P. W., J. Phys. Soc. Japan 9, 316 (1954).

85. Glasstone, S., K. J. Laidler, and H. Eyring, op. cit., p. 195.

86. Van Vleck, J. H., Phys. Rev. 74, 1168 (1948).

87. Anderson, W. A. and H. M. McConnell, J. Chem. Phys. 26, 1496 (1957).

88. McConnell, H. M. and S. B. Berger, ibid. 27, 230 (1957).

89. Kubo, R. and K. Tomita, J. Phys. Soc. Japan 9, 888 (1954).

90. Kubo, R., ibid., 935.

91. Bloch, F., Phys. Rev. 102, 104 (1956).

92. Kubo, R., Nuovo Cimento 6, 1063 (1957).

93. Bloch, F., op. cit. 105, 1206 (1957).

94. Kaplan, J. I., J. Chem. Phys. 28, 278 (1958); ibid. 29, 462 (1958).

95. Shoolery, J. N. and J. D. Roberts, Rev. Sci. Instruments 28, 61 (1957).

96. Wilmad Glass Co., Inc., Buena, New Jersey.

97. Ruhoff, J. R. and E. E. Reid, J. Am. Chem. Soc. 59, 401 (1937).

98. Young, J. A., T. C. Simmons, and F. W. Hoffmann, ibid. 78, 5637 (1956).

99. Erickson, J. G., ibid. 74, 6281 (1952).

100. Bruhl, J. W., Z. Physik, Chem. 22, 388 (1897).

101. von Braun, J., Ber. 36, 3525 (1903); ibid. 37, 2814 (1904).

102. Holmes, E. L. and C. K. Ingold, J. Chem. Soc. 127, 1800 (1925).

103. Jacobsohn, B. A. and R. K. Wangsness, Phys. Rev. 73, 842 (1948).

104. Kenney, J. F. and E. S. Keeping, "Mathematics of Statistics," part two, 2nd ed., pp. 207-211, 416-417, D. Van Nostrand Co., Inc., New York, N. Y., 1951.

105. Fessenden, R. W. and J. S. Waugh, J. Chem. Phys. 31, 996 (1959).

106. Pauling, L., "The Nature of the Chemical Bond," 3rd ed., p. 282, Cornell Univ. Press, Ithaca, N. Y., 1960.

107. Magee, J. L., W. Shand, and H. Eyring, J. Am. Chem. Soc. 63, 677 (1941).

108. Laidler, K. J., "Chemical Kinetics," pp. 105-108, 382-387, McGraw-Hill Book Co., Inc., New York, N. Y., 1950.

109. Douglas, J. E., B. S. Rabinovitch, and F. S. Looney, J. Chem. Phys. 23, 315 (1955).

110. Pauling, L., op. cit., 2nd ed., p. 138.

111. Minneapolis-Honeywell Regulator Co., Brown Instruments Division, Instruction No. 2128, Issue 5, Section 1137, p. 15.

112. Costain, C. C. and J. M. Dowling, J. Chem. Phys. 32, 158 (1960).

113. Pauling, L., op. cit., 2nd ed., pp. 53, 131.